In vivo application of CRISPR/Cas9 mediated gene re-expression in the failing mouse and human myocardium

Dissertation

For the award of the degree

"Doctor rerum naturalium (Dr. rer. nat.)"

Medical Faculty

of the Georg-August University Göttingen

within the doctoral program **Molecular Medicine**

of the **Georg-August University Göttingen School of Science (GAUSS)**

Submitted by **Eric Schoger**

born in Berlin, Germany

Göttingen 2021

I. Examination Board

PD Dr. rer. nat. Laura C. Zelarayán (Supervisor and 1st Referee)
Institute of Pharmacology and Toxicology
University Medical Center Göttingen
Robert-Koch-Straße 40
37075 Göttingen, Germany

Prof. Dr. rer. nat. Blanche Schwappach (2nd Referee)
Dean of the Medical Faculty
University Medical Center Hamburg-Eppendorf
Martinistraße 52
20246 Hamburg, Germany

Prof. Dr. rer. nat. Rüdiger Behr (3rd Referee)
German Primate Center
Leibniz Institute for Primate Research
Kellnerweg 4
37077 Göttingen, Germany

Prof. Dr. mult. Thomas Meyer
Department of Psychosomatic Medicine and Psychotherapy
University of Medical Center Göttingen
Von-Siebold-Straße 5
37075 Göttingen, Germany

Prof. Dr. rer. nat. Susanne Lutz
Institute of Pharmacology and Toxicology
University Medical Center Göttingen
Robert-Koch-Straße 40
37075 Göttingen, Germany

Prof. Dr. rer. nat. Katrin Streckfuß-Bömeke
Institute of Pharmacology and Toxicology
Julius-Maximilians-Universität Würzburg
Versbacher Straße 9
97078 Würzburg, Germany

Date of disputation: 19th of November 2021

II. Affidavit

Here, I declare that my doctoral thesis entitled "*In vivo application of CRISPR/Cas9 mediated gene re-expression in the failing mouse and human myocardium*" has been written independently with no other sources and aids than quoted.

Eric Schoger

Göttingen, 30th of September 2021

III Acknowledgements

First of all, I would like to thank PD Dr. rer. nat. Laura C. Zelarayán for the opportunity to work on a variety of projects and to join her research group for the completion of my doctoral thesis. You gave me the chance to embrace my enthusiasm for science to the fullest possible extent. Beyond measure, I appreciate your trust and motivation that allowed me to grow as a researcher. I enjoyed our discussions about science, mechanisms, novel tools, projects, and project management as well as career choices, all embedded in a caring and supportive atmosphere. Thank you for the past years and I am looking forward to future discoveries.

I deeply appreciate the commitment of Prof. Dr. rer. nat. Blanche Schwappach and Prof. Dr. rer. nat. Rüdiger Behr for their support and scientific advice as well as for having an open ear for career plan discussions, whenever and wherever I needed them.

I would like to thank the Extended Thesis Committee Members Prof. Dr. mult. Thomas Meyer, Prof. Dr. rer. nat. Susanne Lutz and Prof. Dr. rer. nat. Katrin Streckfuß-Bömeke for their time to review and discuss this work.

I would like to express my gratitude towards Prof. Dr. med. Wolfram-H. Zimmermann for scientific and career related advice. I always had an enjoyable time in the Institute of Pharmacology and Toxicology, an institute with extraordinary possibilities and with the necessary ties to connect with the experts in the world. Thank you for this opportunity and trust, early in my studies and later during my time as a member of the Institute of Pharmacology and Toxicology likewise.

I would like to thank Dr. Eric Olson and Dr. Rhonda Bassel-Duby for welcoming me in their team as a visiting student at the University of Texas Southwestern Medical Center and for critical discussions helping me to shape this project especially during the initial steps of this project.

I had the chance to learn and to work with past and present members of the Zelarayán Lab. I would like to especially thank Dr. Lavanya M. Iyer, Dr. rer. nat. Claudia Noack, Dr. rer. nat. Elena Chebbok, Dr. rer. nat. Maria Patapia Zafeiriou, Dr. Cheila Rocha, Laura Priesmeier, Rosa Kim, Petra Tucholla, Christina Weber, Federico Bleckwedel, Kamal Hazzouri, Janek Fischer, Silvia Bierkamp, Mareike Jassyk, Lena Wieland and Patrizia Kühne. You made this experience an enjoyable and successful adventure.

I would like to thank Jutta Schröder, Andreas Wolf and Dr. med. vet. Anette Wiese for taking greatest care of the mouse colony and logistics associated with it.

The past and current members of the Institute of Pharmacology Sebastian Nagel, Dr. Gabriela L. Santos, Branimir Berečić, Pierre-Luc Satin, Alisa DeGrave, Lennart Schneider, Kea Schmoll, Angeliki Koufali, Paul Kunath, Dr. med. Malte Tiburcy, Dr. rer. nat. Tim Meyer, and Dr. Norman Liaw deserve my greatest appreciation for scientific discussion, fun in- and outside of the lab and for a superb working environment.

I would like to thank all current and former members of the Department of Molecular Biology at the University of Texas Southwestern Medical Center especially Dr. Kelli Carroll, Dr. Catherine Makarewich, Dr. Hisayuki Hashimoto, Dr. James Papizan, Dr. Jessica Cannavino, Dr. Glynnis Gary, Dr. Leonela Amoasii, Dr. Miao Cui, John McAnally, Dr. Wei Tan, Dr. Ning Liu, Daniel Caballero, Dr. Yu Zhang, Dr. Zhaoning Wang, Dr. Andres Ramirez-Martinez, and Akansha Shah. Thank you for making my time in Dallas a fun and exciting experience.

My gratitude and greetings go out to our collaboration partners: Dr. Shirin Doroudgar, University of Arizona, Dr. rer. nat. Lukas Cyganek and his team from the Stem Cell Unit Göttingen, to Dr. rer. nat.

Johnny Kim, Max-Planck Institute for Heart and Lung Research, Dr. rer. nat. Christof Lenz and his team from the mass spectrometry laboratory at the University Medical Center in Göttingen, Prof. Dr. rer. nat. Christoph Dieterich and Prof. Dr. med. Lorenz Lehmann, both University Medical Center Heidelberg.

I would like to thank the Molecular Medicine Study Program Office, especially PD Dr. rer. nat. Werner Albig and Dr. forest. Erik Meskauskas, for their support regarding administrative questions and for welcoming me in the ever-growing family of Molecular Medicine students in Göttingen.

I would like to express my deepest gratitude to my family and friends for their love and support over the past years.

Table of Contents

Declaration **9**

List of non-standard abbreviations **10**

1. Abstract **12**

2. General Introduction **14**

2.1 Heart Failure and Lack of an Endogenous Regenerative Potential of the Adult Mammalian Heart 14

2.2 Inactive WNT/CTNNB1 Signaling is a Pre-requisite for Normal Adult Heart Function 16

2.3 The Krüppel-like Factor Family of DNA Binding Proteins in the Heart 18

2.4 Synthetic Gene Expression Modulation 19

References (General Introduction) 20

3. Summary of Aims **28**

4. Author Contributions **30**

5. Chapter 1: Identification of BZW2 interaction interfaces with KLF15 and CTNNB1 ..... **34**

5.1 Abstract 34

5.2 Introduction 34

5.3 Material and Methods 35

5.4 Results 37

5.4.1 Protein-protein interactions of BZW2 with KLF15 and CTNNB1 *in vitro* 37

5.4.2 Loss of BZW2 leads to a late onset cardiomyopathy 40

5.5 Discussion 42

References (Chapter 1) 42

6. Chapter 2: Establishment of a mouse model for cardiomyocyte-specific gene activation **45**

6.1 Abstract 46

6.2 Introduction 47

6.3 Methods 48

6.4 Results 49

6.4.1 Generation of cardiomyocyte-specific CRISPRa mice 49

6.4.2 Validation of gRNAs for dCas9VPR-mediated transcriptional activation 49

6.4.3 Validation of CRISPRa with multiple gRNAs *in vitro* 51

6.4.4 CRISPRa-mediated endogenous activation of *Mef2d* and *Klf15 in vivo* 52

6.4.5 Specificity of the CRISPRa-mediated gene activation *in vivo* 54

6.5 Discussion 55
6.6 Acknowledgements 58
6.7 Disclosure 58
6.8 Source of Funding 58
References 58
6.9 Supplemental Material 76
6.10 Section I - Detailed methods 76
6.11 Section II - Tables 89
References (Supplemental Material) 92
6.12 Section III - Supplemental figures and figure legends 93
7. Chapter 3: Human induced pluripotent stem cells for CRISPR based gene activation 111
7.1 Abstract 111
7.2 Resource utility 113
7.3 Resource details 113
7.4 Materials and Methods 116
7.5 Acknowledgements 118
References 118
7.6 Additional files 123
8. Chapter 4: Human induced pluripotent stem cells for CRISPR based gene repression 125
8.1 Abstract 125
8.2 Resource utility 127
8.3 Resource details 127
8.4 Materials and Methods 130
8.5 Acknowledgements 133
References 133
8.6 Additional files 138
9. Chapter 5: Enhanced endogenous gene activation in human induced pluripotent stem cells 140
9.1 Abstract 140
9.2 Resource utility 142
9.3 Resource details 142
9.4 Materials and Methods 145
9.5 Acknowledgements 147

References 147

9.6 Additional files 152

10. Chapter 6: Fine-tuning guide RNA targeting rules for endogenous gene activation 154

10.1 Abstract 154

10.2 Introduction 154

10.3 Material and Methods 154

10.4 Results 158

10.4.1Targeting of gRNAs determines endogenous gene activation potential 158

10.5 Discussion 160

References (Chapter 6) 160

11. Chapter 7: Re-activation of *Krüppel-like Factor 15* in stressed mouse and human cardiomyocytes 162

11.1 Abstract 162

11.2 Introduction 162

11.3 Material and Methods 163

11.4 Results 170

11.4.1 Guide RNA delivery for activation of *Krüppel-like factor 15* in the adult mouse heart 170

11.4.2 Restoration of *KLF15* transcription prevents cardiomyocyte hypertrophy upon pressure overload 172

11.4.3 Endogenous gene activation in engineered human myocardium 177

11.4.4 Restoration of *KLF15* levels in engineered human myocardium upon mechanical stress 179

11.4.5 TGFβ signaling mediates *KLF15* transcriptional repression in hiPSC-cardiomyocytes 185

11.5 Discussion 187

References (Chapter 7) 189

12. General Discussion 192

12.1 Transcriptional modulation by CRISPR gene activation in the heart *in vivo* 192

12.2 Specificity of CRISPR-based transcriptional modulation 195

12.3 Efficiency of transcriptional modulation 195

12.4 The role of *Krüppel-like factor 15* in heart failure 197

12.5 Re-establishment of *KLF15* and the nuclear WNT/CTNNB1 protein complex 198

12.6 Conclusions 200

References (General Discussion) 201

List of Figures

2. General Introduction

Introduction figure 1: Strategies for cellular reprogramming and replacement in the heart 16

Introduction figure 2: A multiprotein complex regulating WNT-transcriptional activity in the heart 17

Introduction figure 3: Enzymatically dead Cas9 platforms for transcription modulation 20

5. Chapter 1

Figure 1.1: BZW2 interacts via the W2 protein domain with KLF15 and CTNNB1 38

Figure 1.2: CTNNB1 and KLF15 bind to amino acid sequences within the W2 protein domain of BZW2 39

Figure 1.3: Lack of BZW2 results in modest late onset cardiomyopathy 41

6. Chapter 2

Figure 1: Cardiomyocyte-specific expression of dCas9VPR-2A-tdTomato and validation of gRNAs for efficient transcriptional activation induction of *Klf15* and *Mef2d in vitro* 62

Figure 2: Endogenous activation of *Klf15* and *Mef2d* by selected gRNAs *in vitro* 64

Figure 3: The CRISPRa (dCas9VPR/TRISPR) system induces endogenous gene activation in cardiomyocytes *in vitro* 66

Figure 4: CRISPRa-mediated endogenous activation of *Mef2d* in the postnatal heart 68

Figure 5: CRISPRa-mediated endogenous activation of *Mef2d* exhibits a cardiac hypertrophic phenotype 70

Figure 6: Endogenous activation of *Klf15* in the neonatal heart 72

Figure 7: Assessment of on- and off-target activity by chromatin immunoprecipitation (ChIP) of dCas9VPR *in vivo* 74

Figure 8: Double activation of *Mef2d* and *Klf15* in the neonatal heart and *Mef2d* activation at single cell resolution 75

Online figure I: Identified Myh6-dCas9VPR mouse lines 93

Online figure II: Online figure II: Heart function in dCas9VPR expressing mice 94

Online figure III: Evaluation of single cell CRISPRa potential *in vitro* 95

Online figure IV: Titration of CRISPRa components *in vitro* 96

Online figure V: Quantification of *in vitro* titration of CRISPRa components 97

Online figure VI: Transfection of isolated postnatal cardiomyocytes with *in vitro* transcribed gRNAs and phenotypic consequences of *Mef2d* activation in the postnatal heart 98

Online figure VII: *Mef2d* activation and consequences for heart failure parameters expression 100

Online figure VIII: RNA sequencing of Myh6-dCas9VPR hearts and CRISPRa mediated *Mef2d* activated hearts....101

Online figure IX: Mef2d activation *in vivo* and dCas9VPR off-target prediction analyses....103

Online figure X: Endogenous *Klf15* expression, *Klf15* promoter region H3K27ac status and ChIP qPCR validation *in vitro*....104

Online figure XI: Specificity of *Mef2d* activation....106

Online figure XII: Specificity of *Klf15* activation and *Mef2d* activation at single cell resolution 108

Online figure XIII: Full unedited gels and Immunoblots....110

7. Chapter 3

Figure 1 115

Supplementary figure 1 124

8. Chapter 4

Figure 1 129

Supplementary figure 1 139

9. Chapter 5

Figure 1 144

Supplementary figure 1 153

10. Chapter 6

Figure 6.1: Endogenous gene expression efficiency is dependent on gRNA target site upstream of the transcriptional start site 159

11. Chapter 7

Figure 7.1: CRISPRa for transcriptional activity control in the adult mouse heart....171

Figure 7.2: Transcriptional restoration of *Krüppel-like factor 15* in the stressed murine heart 173

Figure 7.3: Heart function decline was reduced in *Klf15* restored animals....175

Figure 7.4: Single cell isolations from CRISPRa *Klf15* hearts 176

Figure 7.5: Endogenous gene activation of *Krüppel-like factor 15* in hiPSC-derived cardiomyocytes....178

Figure 7.6: CRISPRa in engineered human myocardium 179

Figure 7.7: Myocardial stress modeling in engineered human myocardium 181

Figure 7.8: Cardiomyocyte remodeling in stressed EHM is reduced upon *KLF15* transcriptional restoration....183

Figure 7.9: Functional assessment of stressed EHM upon putative *KLF15* restoration....184

Figure 7.10: The *KLF15* transcriptional repression can be mimicked in hiPSC-cardiomyocytes with TGFB1 stimulation resulting in increased ACTA2 protein levels 186

Figure 7.11: *KLF15* restoration limits ACTA2 expression upon TGFB1 stimulus in hiPSC-cardiomyocytes.....187

12. General Discussion

Discussion figure 1: Perspective for single cell transcriptomics and cell type-specific transcriptome editing with CRISPR/dCas9 200

List of Tables

5. Chapter 1

Table 1.1: Primary and secondary antibodies chapter 1 37

6 Chapter 2

Table 1: Checklist animal studies 89

Table 2: Primers 89

Table 3: gRNAs 90

Table 4: qPCR primers 91

7. Chapter 3

Resource Table 112

Table 1 119

Table 2 120

8. Chapter 4

Resource Table 126

Table 1 133

Table 2 135

9. Chapter 5

Resource Table 141

Table 1 148

Table 2 149

10. Chapter 6

Table 6.1: Primer sequences in chapter 6 155

Table 6.2: Guide RNA sequences in chapter 6 156

11. Chapter 7

Table 7.1: Guide RNA sequences in chapter 7 164

Table 7.2: Primer sequences in chapter 7 165

Table 7.3: Primary and secondary antibodies chapter 7 166

Declaration

I, Eric Schoger, declare that the following thesis is organized into seven chapters of original research including four peer-reviewed and published manuscripts (final peer-reviewed manuscripts), a general abstract, introduction, summary of aims, discussion, and conclusion. For reasons of clarity and comprehensibility, references for each chapter as well as for the general introduction and discussion are kept separate within each individual part of the thesis.

List of non-standard abbreviations

aa	amino acids
AAV	Adeno-associated virus
ATACseq	Assay for Transposase-Accessible Chromatin using sequencing
AWThd	anterior wall thickness in diastole
BW	body weight
CM	cardiomyocytes
Cre	Cre recombinase
CRISPR	Clustered regularly interspaced palindromic repeats
CRISPRa	CRISPR-based gene activation
CRISPRi	CRISPR-based gene inhibition
crRNA	CRISPR RNA
CSA	cross sectional area
ctrl	control
dCas9	catalytically inactive Cas9
EHM	engineered human myocardium
fix	non-flexible metal poles
flex	flexible silicone poles
flp	flippase
gRNA	guide RNA
hiPSC	human induced pluripotent stem cells
hiPSC-CM	human induced pluripotent stem cell derived cardiomyocytes
HW	heart weight
IB	immunoblot
IF	immunofluorescence
i.p.	intraperitoneal
ITR	inverted terminal repeats
KRAB	Krüppel-associated box
lncRNA	long non-coding RNA
LNP	lipid nanoparticle
LTR	long-terminal-repeat-region
LVIDd	left ventricular inner diameter in diastole
N/A	not applicable
NT	non-targeted
(q)PCR	(quantitative) polymerase chain reaction
PWThd	posterior wall thickness in diastole
RNP	ribonucleoprotein
RT	reverse transcriptase
SAM	synergistic activation mediator
SEM	standard error of the mean
TAC	transverse aortic constriction
TL	tibia length
tracrRNA	trans-activating CRISPR RNA
TRISPR	triple gRNA expression cassette
TSS	transcriptional start site
VPR	VP64, p65, RTA tripartite transactivation domain
WPRE	Woodchuck hepatitis virus posttranscriptional regulatory element
WT	wild-type

Gene names and products are presented based on the International Committee on Standardized Genetic Nomenclature for Mice (as of August 2018) and HUGO Gene Nomenclature Committee guidelines (as of August 2020).

1. Abstract

Transcriptional adaptation in cardiomyocytes precedes cellular deterioration and functional decline upon myocardial stress and damage resulting in heart failure progression. The re-activation of WNT/β-catenin (CTNNB1) signaling, an evolutionary conserved developmental cascade, was identified as a driver of disease progression in the hypertrophic myocardium. In the homeostatic adult heart, WNT/CTNNB1 signaling is inhibited by the transcription factor *Krüppel-like factor 15* (*KLF15*). Consequently, transcriptional loss of *KLF15*, which is occurring upon disease progression, leads to the activation of WNT/CTNNB1 signaling concomitant with cardiomyocyte hypertrophy and pathological remodeling. Aiming to identify cardiac-specific regulators of the ubiquitously involved WNT/CTNNB1 pathway, a nuclear, cardiomyocyte-specific, multimeric protein complex consisting of CTNNB1, TCF7L2, KLF15 and BZW2 was elucidated and characterized. Upon improved understanding of the molecular determinants of WNT/CTNNB1 modulation in heart tissue, I aimed to investigate mechanisms for re-establishment of gene regulatory networks by restoration of transcription-controlling homeostatic protein-complexes. Although therapeutically desired, the implementation of this concept is technically challenging. To tackle this problem, CRISPR/Cas9 based gene activity modulation with catalytically inactive Cas9 (dCas9) targeted to gene regulatory regions by guide RNAs (gRNA) in combination with transcriptional activators (VPR) or repressors (KRAB) were repurposed as a platform for synthetic gene activation (CRISPRa) and inactivation (CRISPRi). In this work, a mouse model for endogenous, dCas9VPR-mediated gene activation was established, which efficiently and safely expressed dCas9VPR exclusively in cardiomyocytes. As a proof-of-concept for control over endogenous gene activity *in vivo*, I demonstrated induced expression of *Myocyte enhancer factor 2 D* (*Mef2d*) to recapitulate a hypertrophic cardiomyopathy phenotype within eight weeks after gRNA delivery. Furthermore, titratable, endogenous activation of epigenetically silenced *Klf15* was achieved in neonatal mice. Furthermore, I aimed to re-activate *Klf15* expression in murine hearts upon pressure overload using the established model to achieve transcriptional re-establishment of *Klf15* levels in stressed cardiomyocytes. This resulted in blunted cardiac hypertrophy and reduced organ deterioration. To study the relevance of this approach in human cells, CRISPR/dCas9 systems were introduced into human induced pluripotent stem cell (hiPSC) derived cardiomyocytes. I generated hiPSC expressing dCas9VPR (CRISPRa) or dCas9KRAB (CRISPRi) for full control over endogenous gene activity by targeted transgene integration at the *AAVS1* locus using CRISPR/Cas9 gene editing and homology directed repair. Pluripotency and differentiation potential of these hiPSC lines was not affected by transgene integration or constitutive dCas9VPR or dCas9KRAB expression. These cells were differentiated into spontaneously beating hiPSC-derived cardiomyocytes (hiPSC-cardiomyocytes). Expression of *KLF15* was inducible or repressible, respectively, as well as titratable by applying single or multiple gRNA lentivirally administered or by using cells with distinct dCas9 expression levels. With these cells, engineered human myocardium (EHM) was generated to test transcriptional enhancement of *KLF15* in a 3D model of surrogate human heart tissue. I modelled myocardial stress in EHM by forcing tissues to isometric contractions and confirmed a molecular stress response including a transcriptional loss of *KLF15* reminiscent of the *in vivo* disease condition which was mimicked by TGFB1 stimulation in hiPSC-cardiomyocytes *in vitro*. Moreover, the validation of multiple gRNAs targeted to a total of 10 mouse and 5 human genes allowed to re-define the selection criteria for suitable gRNA design. This was related to the gRNA target site relative to the transcriptional start site (TSS) for dCas9VPR gene activation purposes. Altogether, I contributed to the investigation of potential regulatory target gene expression modulation including *KLF15*. I showed that CRISPR/dCas9 based transcriptional activation is a suitable tool for titratable, endogenous gene activation in both human and mouse cardiomyocytes. The transcriptional loss was rescued by synthetic gene activation, restoring *KLF15* mRNA levels comparable to non-stressed conditions *in vivo* and *in vitro*. This was accompanied by reduced maladaptive cardiomyocyte remodeling and a reduced cellular response to myocardial stress,

which validated the approach. Overall, this work integrated knowledge of fundamental biology to generate tools, that allowed precise and efficient gene activity modulation to prevent heart failure progression and provided a new platform for the identification and validation of potential therapeutic targets.

2. General Introduction

The heart beats approximately 3 billion times in the average human lifetime to maintain the energy demands of the whole body. In mammals, the four chambered organ pumps blood through two individual vascular circuits in rhythmically repeating cycles of heart muscle contraction (systole) and relaxation (diastole). Cardiomyocytes are at the functional center of each heartbeat integrating ion mediated voltage changes and molecular movements (electromechanical coupling) in subunits of a multiprotein complex, the sarcomere.[1] Cardiomyocyte stress along with transcriptional landscape changes are ultimately leading to heart failure. Heart failure is defined as an insufficient cardiac supply of nutrients and oxygen to maintain normal organismal function.[2] The underlying cardiovascular diseases are a major socio-economic burden with a predicted tendency to increase in the upcoming decades despite major advances in treatment and prevention strategies.[3] The understanding of the complex interplay within and between cell-types as well as inter- and intracellular pathways is mandatory for the development of therapeutic options fulfilling requirements regarding safety, specificity, and efficacy. Precise genome and transcriptome modifiers are attractive novel tools to dissect critical pathways and regulators for the identification of potential targets able to counteract heart failure progression and can be used in a cell type-specific manner.

2.1 Heart Failure and Lack of an Endogenous Regenerative Potential of the Adult Mammalian Heart

The heart adapts to acute hemodynamic changes by controlling force (inotropy) and frequency (chronotropy) by neurohumoral mechanisms.[4] Sympathetic and parasympathetic signals mediate contractility of cardiomyocytes directly. Adrenergic signaling via G-protein coupled receptors mediate contraction as well as affect peripheral resistance by vasoconstriction and dilation.[5] The Renin-Angiotensin-Aldosterone System as well as the secretion of natriuretic peptides from cardiomyocytes under mechanical stress regulates ion and volume adaptation, functionally linking the cardiovascular system with the kidney-controlled absolute volume homeostasis.[6] Long-term activation of these systems are a hallmark of an insufficient cardiac output and are currently used as targets for symptomatic heart failure management.[7–11] Persistent, increased hemodynamic preload or afterload, myocardial damage caused by ischemic events or inflammation, arrhythmias and genetic cardiomyopathies are direct causes of chronic cardiac stress and heart failure development.[12] The myocardium reacts to these underlying challenges initially with compensatory mechanisms involving a multicellular crosstalk response and activation of molecular cascades, which normally play a role during development, in an attempt to regenerate.[13]

The disbalance of altered energy demands and supply results in cardiomyocyte hypertrophy and subsequently in cardiomyocyte apoptosis ultimately leading to an overall loss of myocardial contractility.[14] The energy demand of the myocardium, mainly covered by fatty acid consumption in adult cardiomyocytes, increases and switches to a glycolytic metabolism as well as lactate consumption as heart failure is advancing.[15–17] These gradually proceeding events are reflected in a dynamically altered transcriptome profile of cardiomyocytes.[18,19]

This response is the result of an insignificant and inefficient, endogenous regenerative capacity with little proportions of proliferative activity in existing cardiomyocytes within the adult mammalian heart.[20] Instead, the increased demand of contractility is primarily compensated by cardiomyocyte growth governed by a pro-hypertrophic signaling network culminating in Calcineurin/NFAT and MEF2 transcriptional activity in cardiomyocytes, which are both critical downstream transcriptional effectors of the cardiac hypertrophic response.[21] As a central integrator of extracellular signals, PKB/AKT

activates GSK3B which in turn phosphorylates and activates the phosphatase Calcineurin.[22] Calcineurin dephosphorylates NFAT allowing its translocation into the nucleus to drive expression of contractile apparatus components such as *MYH7*.[23] Additionally, the TGFβ signaling cascade triggers MEF2 transcriptional activity via MAPK/P38 signaling.[24] MEF2 transcription factors in turn control the expression of the natriuretic peptides.[25] The maladaptive remodeling gene program resembles partially the transcriptional profile during heart development and is therefore also referred to as *re-activation of a fetal gene program*. Transcription factor expression of *TBX3*, *TBX5*, *GATA4*, *NKX2.5*, and *HAND2* is commonly observed in transcript analyses of failing heart tissue samples, all playing major roles in heart development and determining cardiac lineage cell fates.[26] Activation of fetal gene programs in an environment lacking developmental plasticity however compromise adult organ function and ultimately resulted in maladaptation and failure.[27]

Strategies to replace non-functional or lost myocardial tissue therefore focuses on endogenous regenerative strategies by prevention of further cardiomyocyte loss with re-establishment of homeostatic processes and re-activation of cardiomyocyte cell division or on exogenous cardiomyocyte replacement.[28] Introduction figure 1 summarizes the concepts of cardiomyocyte replacement and loss prevention.

Stem cell technologies promised the possibility to *de novo* generate any cell type by directed *in vitro* recapitulation of developmental programs.[29] Pluripotent cells can be differentiated into all three germ layers including myocardial lineages first by mesodermal and mesenchymal commitment and subsequent inhibition of WNT/CTNNB1 signaling for cardiomyogenic differentiation.[30] This strategy permits autologous cardiomyocyte replacement, however individualized reprogramming of somatic cells into pluripotent cells and differentiation on demand remained time consuming and resource intensive. Intramyocardial injection or vascular perfusion of stem cell derived cardiomyocytes was successfully tested to remuscularize lost myocardial tissue however concerns regarding little retention rate of exogenously delivered cardiomyocytes as well as arrhythmogenicity persisted.[31–33] Therefore, hydrogel embedded cardiomyocytes in combination with non-myocyte fractions cast into 3D tissues were developed to locally cover damaged tissue and improved cardiac contractility *in vivo*.[34–36]

The reprogramming of non-myocytes in the damaged myocardium into functional cardiomyocytes was proposed as an alternative strategy to offer a source for *de novo* cardiomyocytes by inducing a cardiogenesis-reminiscent transcription factor profile. Ectopic expression of *GATA4*, *HAND2*, *MEF2C* and *TBX5* in fibroblasts trans-differentiated these cells into TNNT2 and ACTN2 positive cells. This was improved by addition of *MYOCD* to the trans-differentiation mix indicating successful reprogramming into cardiomyogenic cells.[37,38] Moreover, gene-delivery free trans-differentiation with small molecules was described.[39] However, reprogramming efficiencies were low and on-going efforts aim to improve our understanding of the fibroblast-to-cardiomyocyte conversion as well as the overall reprogramming efficiency by identification of gene regulatory circuits.[40]

The capability of cardiomyocytes in lower vertebrates and neonatal Mammalia to undergo cell division after tissue damage[41] led to the investigation of how cardiomyocyte mitosis, karyokinesis and cytokinesis is controlled and what determines its postmitotic state in adult Mammalia. The regenerative capacity was observed in teleost fish, urodele amphibia, neonatal mice and rats[42] as well as in reported cases of human neonates with myocardial infarction events early after birth.[43] Cell cycle activity in postnatal cardiomyocytes is restricted to DNA synthesis resulting in polynucleated cardiomyocytes without completion of cytokinesis. The fraction of polynucleated postnatal cardiomyocytes was 90% in the mouse and 30% in the human heart, respectively.[44] The regulation of cell division by the intricate interplay of cyclin and cyclin dependent kinases was investigated to harness the root of cellular proliferation.[45–48] *CCND2* transgenic mice showed cell cycle activity in postnatal hearts and prevented decline of cardiac function upon ischemic insult, pressure overload and Doxycycline induced

cardiotoxicity suggesting functional replacement of cardiomyocyte loss.[49,50] Additionally, *CCND2* overexpressing human induced pluripotent stem cells improved the muscular replacement in mouse and swine models upon myocardial infarction.[51,52] Evolutionary conserved molecular pathways such as WNT/CTNNB1 and HIPPO signaling were identified to control cardiomyocyte cell cycle activity in early life.[53] Inactivation of HIPPO signaling in the mouse heart resulted in cardiomyocyte proliferation improving myocardial function post infarction.[54] WNT/CTNNB1 activity in immature cardiomyocytes is generally associated with induction of proliferation. For instance, human induced pluripotent stem cell derived cardiomyocytes underwent cell cycle activation and cell division by inhibition of GSK3B and de-repression of WNT/CTNNB1 signaling consequently.[55] However, despite active WNT/CTNNB1 in adult cardiomyocytes was associated with cell cycle activation, the incapability to complete cytokinesis resulted in cardiomyocyte polyploidy and hypertrophy with negative impact on overall cardiac function underlining the missing link to fully return to a proliferative state.[56]

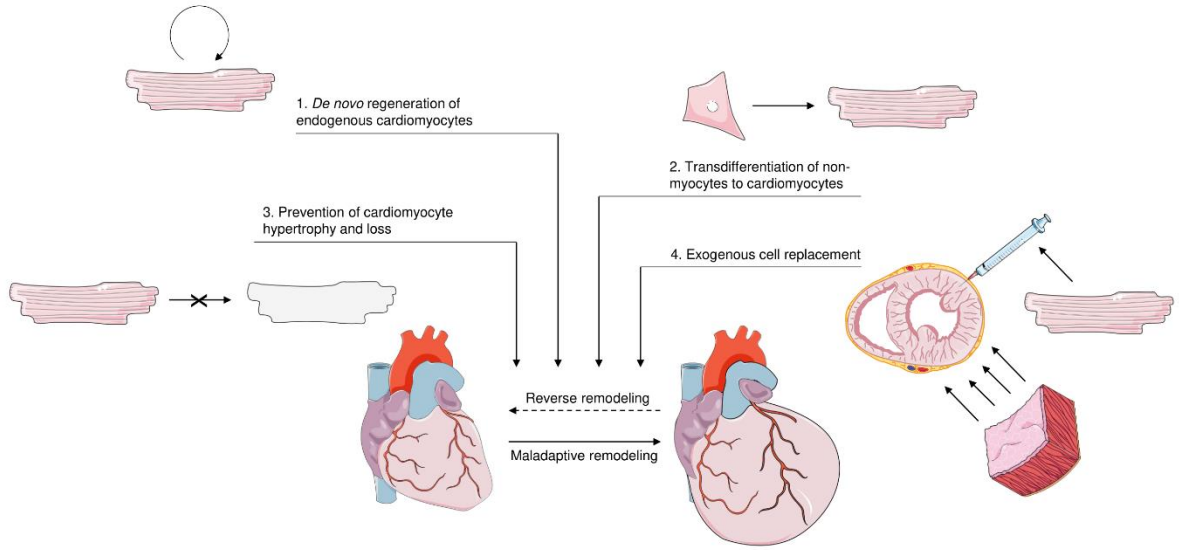

Introduction figure 1. Strategies for cellular reprogramming and replacement in the heart. Cardiomyocyte remodeling and loss drives heart failure progression. Strategies to rescue or replace lost, contractile myocardial tissue include 1. Reprogramming of existing cardiomyocytes to stimulate cardiomyocyte proliferation, 2. Transdifferentiation of non-cardiomyocytes (i.e. fibroblasts) to cardiac myocytes by induction of cardiomyogenic factors, 3. Prevention of further cardiomyocyte loss or 4. Exogenous cardiomyocyte replacement by stem cell derived cardiomyocytes and tissue engineering approaches. Illustration was made with Servier Medical Art.

2.2 Inactive WNT/CTNNB1 Signaling is a Pre-requisite for Normal Adult Heart Function

Cardiac homeostasis is achieved by a complex interplay of molecular signaling pathways controlling cellular function, integrity, metabolism, growth, and motility.[57] The identification of gene regulatory networks and master regulators which can be targeted to control tissue remodeling have been the focus in a myriad of studies.[58] The evolutionary conserved WNT/CTNNB1 pathway has major implications in tissue homeostasis, cell growth, cardiac development, and remodelling.[59] The canonical WNT pathway is kept inactive by CTNNB1 phosphorylation of Serine-45 by CKI followed by phosphorylation of Threonine-41, Serine-37 and Serine-33 by GSK3B. The kinases CKI and GSK3B are part of the CTNNB1-destruction complex consisting of AXIN2 and APC mediating the

ubiquitination by TRCP and degradation of CTNNB1 by the proteasome. Upon WNT ligand - FZD receptor and LRP co-receptor activation, the destruction complex is inactivated and recruited to the cell plasma membrane resulting in PKA mediated Serin-675 phosphorylation of CTNNB1 leading to accumulation in the cytosol and translocation into the nucleus.[60] In the nucleus, CTNNB1 interacts with DNA-binding TCF/LEF family members to control gene expression.[61] In cardiomyocytes, resident CTNNB1 forms a complex with TCF7L2 and *Krüppel-like factor 15* (KLF15) inhibiting WNT/CTNNB1 transcriptional activity in healthy adult hearts.[56,62] Genetic loss of *KLF15* resulted in the development of heart failure in mouse hearts and functional decline in engineered human myocardium (EHM).[63] This phenotypic outcome was accompanied by de-repression of WNT/CTNNB1 activity and molecular and tissue remodelling.[62,64] Aberrantly active WNT/CTNNB1 signaling is associated with cardiac remodeling and cardiac disease conditions. For instance, chronic WNT/CTNNB1 activity signaling by deletion of exon three in the CTNNB1 open reading frame encoding for the Serine-33/37/45 and Threonine-41 phosphorylation sites resulted in the development of cardiomyocyte hypertrophy.[56,61,65] Transcriptional signals, triggered by TCF7L2, were induced and in line with its recruitment to distinct regions of the genome in these mouse hearts as well as in wild-type hearts upon pressure overload when compared to neonatal hearts and liver tissue suggesting a tissue- and condition-specific gene program modulation.[56] Importantly, induced cardiomyocyte-specific deletion of CTNNB1 (deletion of exon 2-6), prevented cardiac hypertrophy and failure upon pressure overload and increased survival in a murine myocardial infarct model.[66,67] In line with this, TCF7L2 expression and transcriptional activity was elevated in the heart of a desmin-cardiomyopathy mouse model as well as in ischemic cardiomyopathy and dilated cardiomyopathy patient's cardiac tissue resulting in aberrant MYC expression.[68] These findings indicated a role of CTNNB1/TCF7L2 transcriptional activity in the diseased heart which is kept under multilateral control in normal cardiac homeostasis. Our current picture of the nuclear WNT complex in cardiomyocytes is summarized in Introduction figure 2. Besides its role in cardiomyocytes, stabilization of CTNNB1 expression in POSTN positive cardiac myofibroblasts were shown to induced fibrosis and heart failure development.[69] Altogether, this suggests a cell type-specific role of WNT/CTNNB1 signaling in the normal heart and in disease conditions. Due to its ubiquitous role in a multitude of tissues, cell type specific regulators of the pathway are potentially attractive therapeutic targets for interventional purposes and deserve further investigation.

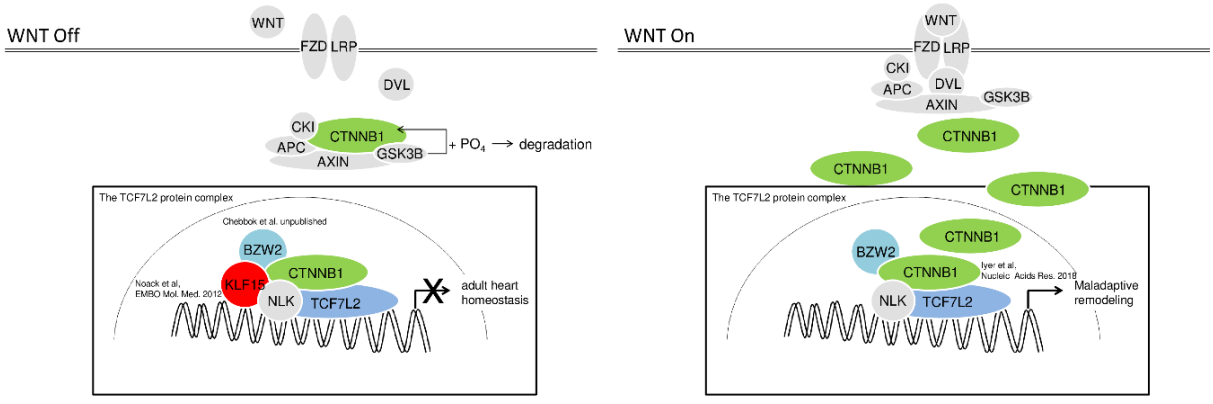

Introduction figure 2. A multiprotein complex regulating WNT-transcriptional activity in the heart. The nuclear WNT downstream transcriptional activity controlling complex consisting of CTNNB1 (green), KLF15 (red), Nemo-like kinase (NLK, grey), Basic leucine zipper and W2 domain containing protein 2 (BZW2, light blue) and TCF7L2 (dark blue) maintains a homeostatic gene

expression profile in adult cardiomyocytes (left panel - WNT Off state). The loss of KLF15 and the accumulation of activated CTNNB1 leads to aberrant gene expression and concomitant cardiac remodeling (right panel - WNT On state).

2.3 The Krüppel-like Factor Family of DNA Binding Proteins in the Heart

The family of Krüppel-like factors (KLFs) contains 18 evolutionary conserved Cys2/His2 zinc-finger protein members with a (G/A)(G/A)GG(T/C)G consensus DNA binding motif.[70,71] These transcription factors were subdivided into transcriptionally activating and inactivating KLFs. These transcription-modulating functions were exerted by interaction with several epigenetic modifiers including P300, SIN3A and HATs.[72,73] In the cardiovascular system, the KLF members *KLF4*, *KLF5*, *KLF10*, *KLF13* and *KLF15* were described. The role of *KLF4* as an original component of the somatic cell reprogramming cocktail into induced pluripotent stem cells was described before.[74] In the postnatal heart, *KLF4* regulated mitochondrial biogenesis via Estrogen related receptor/PPARγ coactivator 1 signaling. In this study, *Klf4* null mice exhibited reduced postnatal survival with impaired mitochondrial functions implicating a major role in controlling myocardial energetics.[75] *KLF5* was first described in cardiac fibroblasts and identified as a driver of cardiovascular stress conditions, activating early stress response signaling pathways and growth factor expression.[76] *Klf10* regulated *Pttg* activity in a TGFβ dependent fashion and male *KLF10* knockout mice developed hypertrophic cardiomyopathy.[77] The loss of *KLF13* was linked to congenital heart defects mediated by GATA4 interactions in the developing heart.[78] *KLF15* is a non-classical KLF which was not clearly classified into overall gene activating or repressing functions based on interaction partner categorization.[72] *KLF15* is expressed in the liver, the kidney and in muscle tissue, including the heart.[79] Within the heart, *KLF15* was expressed in cardiomyocytes, fibroblasts, and smooth muscle cells.[80] Subcellular localization of KLF15 was observed in the nucleus which was mediated by Zinc-finger domains at the C-terminus of the protein harboring a nuclear localization signal.[81] *KLF15* expression was low in the developing heart and increased with maturity.[64] Mechanistically, KLF15 and MEF2 cooperatively stimulated expression of GLUT4 to modulate cardiomyocyte insulin-dependent glucose influx.[82] Moreover, KLF15 and PPARα cooperatively controlled lipid metabolism controlling gene expression further highlighting a central role in cardiac energetics.[83] KLF15 additionally inhibited mTOR/AKT signaling resulting in reduced isoproterenol induced cardiac hypertrophy therefore hinting towards an anti-apoptotic function.[84] *KLF15* sensitivity to cardiac stress triggers, such as Angiotensin II, was investigated and induced cardiomyocyte remodeling characterized by reduced *KLF15* expression levels.[85] Ectopic overexpression of *KLF15* reduced fibrosis in Angiotensin II induced cardiac remodeling by repression of MRTF-A, MRTF-B, and MYOCD blunting pro-hypertrophic MEF2 signaling *in vivo*.[81] This was prevented by Estrogen receptor β signaling upon *KLF15* loss upon Angiotensin II treatment.[86] Overall cell-type and context specific functions of KLF family members in the developing heart and in postnatal myocardial homeostasis seem to be an overarching theme. Focusing on *KLF15*, this factor appears to maintain cardiomyocyte homeostasis by regulating the hypertrophic response and metabolism in the heart while its transcriptional down regulation in cardiac remodeling is in part responsible for pathophysiological processes leading to disease progression. Gene expression re-establishment of *KLF15* back to levels normally found in the healthy heart upon myocardial stress is therefore an attractive target to reinstate cardiomyocyte homeostasis. However, our understanding of the specific role of *KLF15*, especially in WNT/CTNNB1 signaling modulation possibly co-mediated by interactions with cell-type specific partners in the diseased heart, is incomplete.

2.4 Synthetic Gene Expression Modulation

To identify regulatory, functional sequences in the genome and to decipher their individual roles within the complex interplay of molecular pathways, genetic knock-out, knock-in, epigenetic knock-down and overexpression models such as transgenic organisms became indispensable tools for biomedical research.[87,88] Classical overexpression models relied on the integration of coding sequences in the framework of expression cassettes including tissue-specific and inducible promoter sequences as well as additional exogenous sequences ensuring proper transgene expression. These transgenes were integrated into the genome of model organisms during early embryogenesis to guarantee germline propagation or via postnatal viral transduction into somatic cells. However, these approaches typically resulted in supraphysiological expression levels of their gene products.[89] Most transgenic models were additionally restricted to single isoforms and did not reflect the complexity of gene products normally encoded within the endogenous genomic locus. Size limitations particularly existed especially for Adeno-associated viruses (AAV) with a maximum packaging capacity of ~4.7 kbp for open reading frame and expression regulatory sequences framed within inverted terminal repeats (ITRs) limiting gene transfer approaches for larger target gene candidates.[90] Therefore, interest in endogenous gene activity modulation grew in biomedical research. Transcription activator-like effector nucleases (TALEN) and zinc-finger transcription factor engineering were employed to design gene editing tools and artificial transcription factors, however laborious (re-) design and empirical testing of synthetic transcription factors lowered feasibility and applicability of such tools.[91] The adaptation of the bacterial immune defense machinery of class II clustered regularly interspaced short palindromic repeats (CRISPR) as a gene editing tool offered unprecedented precision to manipulate the genome.[92] Unlike previously employed genome editing tools such as TALEN and zinc finger transcription factor-based approaches[93] which relied on direct DNA/peptide interaction, CRISPR/Cas9 was programmable by a guide (g) RNA and therefore mediated DNA interactions via RNA/DNA hybridization.[94] CRISPR/Cas9 gRNAs consisted of a CRISPR RNA (crRNA) complementary to its target DNA strand and a trans-activating CRISPR RNA (tracrRNA) serving as a scaffold to form the functional Cas9/gRNA ribonucleoprotein (RNP) able to associate to its DNA target site and to introduce a double strand break.[95] Simplifying the methodology, tracrRNA and crRNA were combined to yield a single gRNA.[96] Enzymatically inactive Cas9 (dCas9) with a minimum of two mutations (D10A and H840A) in the RUVC-like and the HNH catalytic domains rendered Cas9 deficient for DNA cleavage without losing DNA binding capacity serving as a protein platform for DNA association.[97] Fused to transcriptional activators or inhibitors, dCas9 was engineered to regulate genes in bacteria, yeast, insect, and mammalian cells. Initially, dCas9 fusion to VP16 or multiple VP16 (i.e. VP64 to VP160) domains were used with modest gene activation potential.[98] The first *in vivo* study with a CRISPR-based gene activator was conducted to modulate wingless expression in *Drosophila melanogaster*, which was sufficient to recapitulate wing disk defects and demonstrating biological implications of endogenous gene activation.[99] More potent second generation Cas9-transcriptional activators were designed fusing scaffolds to the dCas9 platform to recruit multiple transactivation domains (SAM and SunTag). The SunTag method employs dCas9 fused to a peptide chain recruiting antibody-linked transcriptional activators.[100] SAM employs dCas9 fused to transcriptional activators in combination with modified gRNAs harboring a MS2-loop to recruit MS2-transcriptional activator fusion peptides.[101] Both approaches allowed the recruitment of multiple transactivation domains to a single genomic locus. Direct fusion to heteromeric activation domains such as VP64, the P65 transactivation domains, and the Epstein Barr Virus RTA (VPR) were developed to diversify the transcriptional activation modulation per gene locus.[102] SAM, Sun-Tag and VPR yielded up to five magnitudes fold higher transcript levels than first generation versions with VP16 fusions alone and were similar with respect to gene activation potency when compared to each other, which was also found to be consistent among species.[103] For instance, induced gene activity was achieved in neurons, skeletal muscle, kidney, and liver tissue *in vivo*.[104–106] Additionally, *ex-vivo* transcriptome editing of

tumor cells and subsequent implantation was used to dissect *Chek2* mediated decelerated tumor progression *in vivo*.[107] For transcriptional repression, the ZNF10 KRAB domain was fused to dCas9 for epigenetic silencing of target loci. This was applied in *in vitro* studies and *in vivo* applications for targeted gene repression as well as for unbiased screening purposes.[108,109] Next-generation CRISPRi systems, involved the identification of more potent transcriptional repressors such as ZIM3[110] and multimeric fusion repressor domains such as KRAB-MECP2.[111] Introduction figure 3 illustrates the different endogenous gene modulation approaches based on CRISPR/Cas9. However, despite applications in a variety of cell types and species, these tools were not readily available for gene activation and repression to modulate endogenous gene expression in cardiomyocytes at the onset of this work.

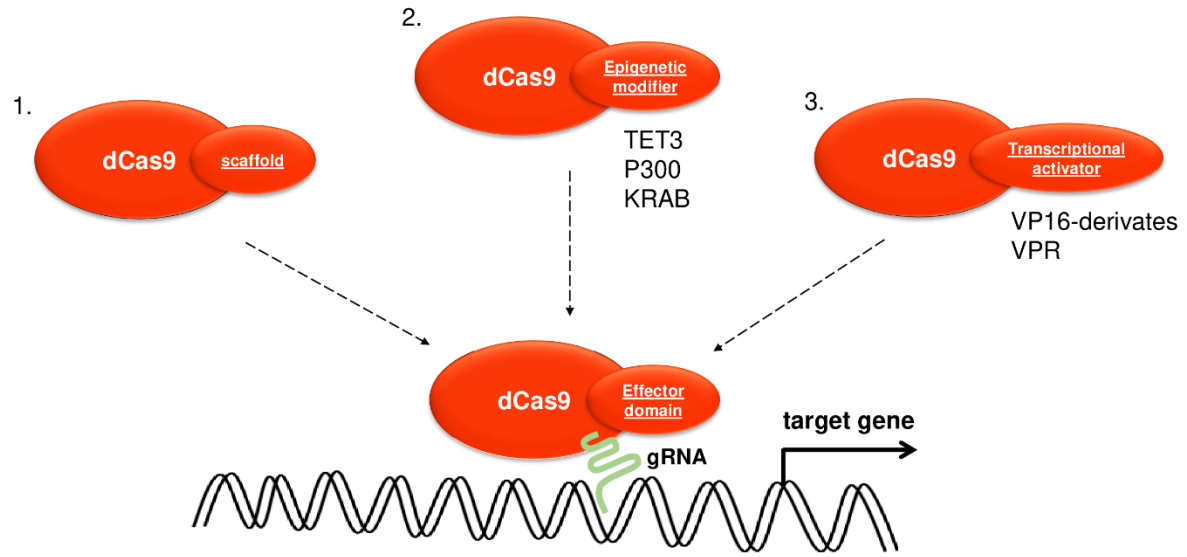

Introduction figure 3. Enzymatically dead Cas9 platforms for transcription modulation. Fusion dCas9 proteins are used carrying 1. a scaffold allowing the recruitment of exogenous transactivation domains, 2. an epigenetic modifier to locally remodel the chromatin architecture for transcriptional activation or inactivation or 3. a direct fusion to transcriptional activation domains (i.e. VPR) recruiting the basal transcriptional machinery. These dCas9 platforms are recruited to gene regulatory regions with a sequence homologous gRNA to act as a programmable, synthetic transcription factor.

In this work, I applied CRISPR-based gene expression modulation in cardiomyocytes with the aim to re-normalize *KLF15* expression in failing murine and human cardiomyocytes, to test its role as a member of the nuclear WNT/CTNNB1 complex, to repress WNT/CTNNB1 signaling upon myocardial stress, and to prevent maladaptive cardiac remodeling.

References (General Introduction)

1. Burbaum, L. *et al.* Molecular-scale visualization of sarcomere contraction within native cardiomyocytes. *Nat Commun* **12**, 4086 (2021).
2. Metra, M. & Teerlink, J. R. Heart failure. *The Lancet* **390**, 1981–1995 (2017).
3. Virani, S. S. *et al.* Heart Disease and Stroke Statistics—2020 Update: A Report From the American Heart Association. *Circulation* **141**, E139–E596 (2020).

4. Hartupee, J. & Mann, D. L. Neurohormonal activation in heart failure with reduced ejection fraction. *Nat Rev Cardiol* **14**, 30–38 (2017).

5. Floras, J. S. Sympathetic Nervous System Activation in Human Heart Failure. Clinical Implications of an Updated Model. *J Am Coll Cardiol* **54**, 375–385 (2009).

6. Bader, M. Tissue renin-angiotensin-aldosterone systems: Targets for pharmacological therapy. *Annu Rev Pharmacol Toxicol* **50**, 439–465 (2010).

7. Jessup, M. Neprilysin inhibition--a novel therapy for heart failure. *N Engl J Med* **371**, 1062-1064 (2014).

8. Bosch, J. *et al.* Long-term effects of Ramipril on cardiovascular events and on diabetes: Results of the HOPE study extension. *Circulation* **112**, 1339–1346 (2005).

9. White, M. *et al.* Effects of metoprolol CR in patients with ischemic and dilated cardiomyopathy: The randomized evaluation of strategies for left ventricular dysfunction pilot study. *Circulation* **101**, 378–384 (2000).

10. Arnold, J. M. O. *et al.* Prevention of heart failure in patients in the Heart Outcomes Prevention Evaluation (HOPE) study. *Circulation* **107**, 1284–1290 (2003).

11. Tepper, D. Effect of metoprolol CR/XL in chronic heart failure: Metoprolol CR/XL randomised intervention trial in congestive heart failure (MERIT-HF). *Congestive Heart Failure* **5**, 184–185 (1999).

12. Maron, B. J. *et al.* Contemporary definitions and classification of the cardiomyopathies: An American Heart Association Scientific Statement from the Council on Clinical Cardiology, Heart Failure and Transplantation Committee; Quality of Care and Outcomes Research and Functio. *Circulation* **113**, 1807–1816 (2006).

13. Frey, N. & Olson, E. N. Cardiac hypertrophy: the good, the bad, and the ugly. *Annu. Rev. Physiol.* **65**, 45–79 (2003).

14. van Empel, V. P. M. *et al.* Myocyte apoptosis in heart failure. *Cardiovasc Res* **67**, 21–29 (2005).

15. Neubauer, S. The Failing Heart — An Engine Out of Fuel. *New England Journal of Medicine* **356**, 1140–1151 (2007).

16. Tran, D. H. & Wang, Z. v. Glucose Metabolism in Cardiac Hypertrophy and Heart Failure. *J Am Heart Assoc* **8**, 1–18 (2019).

17. Cluntun, A. A. *et al.* The pyruvate-lactate axis modulates cardiac hypertrophy and heart failure. *Cell Metab* **33**, 629-648.e10 (2021).

18. Tan, F.-L. *et al.* The gene expression fingerprint of human heart failure. *Proceedings of the National Academy of Sciences* **99**, 11387–11392 (2002).

19. Liu, Y. *et al.* RNA-Seq identifies novel myocardial gene expression signatures of heart failure. *Genomics* **105**, 83–89 (2015).

20. Bergmann, O. *et al.* Dynamics of Cell Generation and Turnover in the Human Heart. *Cell* **161**, 1566–1575 (2015).

21. Molkentin, J. D. *et al.* A calcineurin-dependent transcriptional pathway for cardiac hypertrophy. *Cell* **93**, 215–228 (1998).

22. Antos, C. L. *et al.* Activated glycogen synthase-3β suppresses cardiac hypertrophy in vivo. *Proc Natl Acad Sci U S A* **99**, 907–912 (2002).

23. Dirkx, E., da Costa Martins, P. A. & de Windt, L. J. Regulation of fetal gene expression in heart failure. *Biochim Biophys Acta Mol Basis Dis* **1832**, 2414–2424 (2013).

24. Molkentin, J. D. Calcineurin and Beyond. *Circ Res* **87**, 731–738 (2000).

25. Pereira, A. H. M. *et al.* MEF2C silencing attenuates load-induced left ventricular hypertrophy by modulating mTOR/S6K pathway in mice. *PLoS One* **4**, (2009).

26. Nimura, K. & Kaneda, Y. Elucidating the mechanisms of transcription regulation during heart development by next-generation sequencing. *J Hum Genet* **61**, 5–12 (2015).

27. Vigil-Garcia, M. *et al.* Gene expression profiling of hypertrophic cardiomyocytes identifies new players in pathological remodelling. *Cardiovasc Res* **117**, 1532–1545 (2021).

28. Hashimoto, H., Olson, E. N. & Bassel-Duby, R. Therapeutic approaches for cardiac regeneration and repair. *Nat Rev Cardiol* **15**, 585–600 (2018).

29. Burridge, P. W. *et al.* A universal system for highly efficient cardiac differentiation of human induced pluripotent stem cells that eliminates interline variability. *PLoS One* **6**, (2011).

30. Zhao, M., Tang, Y., Zhou, Y. & Zhang, J. Deciphering Role of Wnt Signalling in Cardiac Mesoderm and Cardiomyocyte Differentiation from Human iPSCs: Four-dimensional control of Wnt pathway for hiPSC-CMs differentiation. *Sci Rep* **9**, 1–15 (2019).

31. Liu, Y. W. *et al.* Human embryonic stem cell-derived cardiomyocytes restore function in infarcted hearts of non-human primates. *Nat Biotechnol* **36**, 597–605 (2018).

32. Rojas, S. v. *et al.* Transplantation of purified iPSC-derived cardiomyocytes in myocardial infarction. *PLoS One* **12**, 1–14 (2017).

33. Vagnozzi, R. J., Sargent, M. A. & Molkentin, J. D. Cardiac Cell Therapy Rejuvenates the Infarcted Rodent Heart via Direct Injection but Not by Vascular Infusion. *Circulation* **141**, 1037–1039 (2020).

34. Zimmermann, W. H. Tissue engineered heart repair from preclinical models to first-in-patient studies. *Curr Opin Physiol* **14**, 70–77 (2020).

35. Tiburcy, M. *et al.* Defined engineered human myocardium with advanced maturation for applications in heart failure modeling and repair. *Circulation* **135**, 1832–1847 (2017).

36. Querdel, E. *et al.* Human Engineered Heart Tissue Patches Remuscularize the Injured Heart in a Dose-Dependent Manner. *Circulation* **143**, 1991–2006 (2021).

37. Ieda, M. *et al.* Direct reprogramming of fibroblasts into functional cardiomyocytes by defined factors. *Cell* **142**, 375–386 (2010).

38. Nam, Y.-J. *et al.* Reprogramming of human fibroblasts toward a cardiac fate. *Proc Natl Acad Sci U S A* **110**, 5588–93 (2013).

39. Fu, Y. *et al.* Direct reprogramming of mouse fibroblasts into cardiomyocytes with chemical cocktails. *Nature Publishing Group* **25**, 1013–1024 (2015).

40. Garry, G. A. *et al.* The histone reader PHF7 cooperates with the SWI/SNF complex at cardiac super enhancers to promote direct reprogramming. *Nat Cell Biol* **23**, 467–475 (2021).

41. Porrello, E. R. *et al.* of the Neonatal Mouse Heart. *Science* **331**, 2–4 (2011).

42. Lien, C. L., Harrison, M. R., Tuan, T. L. & Starnes, V. A. Heart repair and regeneration: Recent insights from zebrafish studies. *Wound Repair and Regeneration* **20**, 638–646 (2012).

43. Haubner, B. J. *et al.* Functional Recovery of a Human Neonatal Heart after Severe Myocardial Infarction. *Circ Res* **118**, 216–221 (2016).

44. Landim-Vieira, M., Schipper, J. M., Pinto, J. R. & Chase, P. B. Cardiomyocyte nuclearity and ploidy: when is double trouble? *J Muscle Res Cell Motil* **41**, 329–340 (2020).

45. Li, J. M. & Brooks, G. Cell cycle regulatory molecules (cyclins, cyclin-dependent kinases and cyclin-dependent kinase inhibitors) and the cardiovascular system. Potential targets for therapy? *Eur Heart J* **20**, 406–420 (1999).

46. Burton, P. B. J., Yacoub, M. H. & Barton, P. J. R. Cyclin-dependent kinase inhibitor expression in human heart failure. A comparison with fetal development. *Eur Heart J* **20**, 604–611 (1999).

47. Liu, Z., Yue, S., Chen, X., Kubin, T. & Braun, T. Regulation of cardiomyocyte polyploidy and multinucleation by cyclinG1. *Circ Res* **106**, 1498–1506 (2010).

48. Hauck, L. *et al.* Protein kinase CK2 links extracellular growth factor signaling with the control of p27Kip1 stability in the heart. *Nat Med* **14**, 315–324 (2008).

49. Toischer, K. *et al.* Cardiomyocyte proliferation prevents failure in pressure overload but not volume overload. *J Clin Invest* **127**, 1–12 (2017).

50. Zhu, W., Reuter, S. & Field, L. J. Targeted expression of cyclin D2 ameliorates late stage anthracycline cardiotoxicity. *Cardiovasc Res* **115**, 960–965 (2019).

51. Zhu, W., Zhao, M., Mattapally, S., Chen, S. & Zhang, J. CCND2 Overexpression Enhances the Regenerative Potency of Human Induced Pluripotent Stem Cell-Derived Cardiomyocytes: Remuscularization of Injured Ventricle. *Circ Res* **122**, 88–96 (2018).

52. Zhao, M. *et al.* Cyclin D2 Overexpression Enhances the Efficacy of Human Induced Pluripotent Stem Cell–Derived Cardiomyocytes for Myocardial Repair in a Swine Model of Myocardial Infarction. *Circulation* **144**, 210–228 (2021).

53. Heallen, T. *et al.* Hippo pathway inhibits wnt signaling to restrain cardiomyocyte proliferation and heart size. *Science* **332**, 458–461 (2011).

54. Leach, J. P. *et al.* Hippo pathway deficiency reverses systolic heart failure after infarction. *Nature* **550**, 260–264 (2017).

55. Buikema, J. W. *et al.* Wnt Activation and Reduced Cell-Cell Contact Synergistically Induce Massive Expansion of Functional Human iPSC-Derived Cardiomyocytes. *Cell Stem Cell* **27**, 50-63.e5 (2020).

56. Iyer, L. M. *et al.* A context-specific cardiac β-catenin and GATA4 interaction influences TCF7L2 occupancy and remodels chromatin driving disease progression in the adult heart. *Nucleic Acids Res* **46**, 2850–2867 (2018).

57. Marín-García, J. Signaling Cascades in Heart Failure: From Cardiomyocytes Growth and Survival to Mitochondrial Signaling Pathways. In *Heart Failure. Contemporary Cardiology* Humana Press, Totowa, NJ. https://doi.org/10.1007/978-1-60761-147-9_7

58. Fiedler, L. R., Maifoshie, E. & Schneider, M. D. Mouse Models of Heart Failure. in *Current Topics in Developmental Biology* **109** 171–247 (2014).

59. Clevers, H. Wnt/β-Catenin Signaling in Development and Disease. *Cell* **127**, 469–480 (2006).

60. Clevers, H. & Nusse, R. Wnt/β-catenin signaling and disease. *Cell* **149**, 1192–1205 (2012).

61. Chen, X. *et al.* The β-Catenin/T-Cell Factor/Lymphocyte Enhancer Factor Signaling Pathway Is Required for Normal and Stress-Induced Cardiac Hypertrophy. *Mol Cell Biol* **26**, 4462–4473 (2006).

62. Noack, C. *et al.* Krueppel-like factor 15 regulates Wnt/β-catenin transcription and controls cardiac progenitor cell fate in the postnatal heart. *EMBO Mol Med* **4**, 992–1007 (2012).

63. Noack, C., Haupt, L. P., Zimmermann, W. H., Streckfuss-Bömeke, K. & Zelarayán, L. C. Generation of a KLF15 homozygous knockout human embryonic stem cell line using paired CRISPR/Cas9n, and human cardiomyocytes derivation. *Stem Cell Res* **23**, 127–131 (2017).

64. Noack, C. *et al.* KLF15-Wnt–Dependent Cardiac Reprogramming Up-Regulates SHISA3 in the Mammalian Heart. *J Am Coll Cardiol* **74**, 1804–1819 (2019).

65. Haq, S. *et al.* Stabilization of beta-catenin by a Wnt-independent mechanism regulates cardiomyocyte growth. *Proc Natl Acad Sci U S A* **100**, 4610–5 (2003).

66. Zelarayán, L. C. *et al.* Beta-Catenin downregulation attenuates ischemic cardiac remodeling through enhanced resident precursor cell differentiation. *Proc Natl Acad Sci U S A* **105**, 19762–7 (2008).

67. Qu, J. *et al.* Cardiac-specific haploinsufficiency of β-catenin attenuates cardiac hypertrophy but enhances fetal gene expression in response to aortic constriction. *J Mol Cell Cardiol* **43**, 319–326 (2007).

68. Hou, N. *et al.* Transcription Factor 7-like 2 Mediates Canonical Wnt/β-Catenin Signaling and c-Myc Upregulation in Heart Failure. *Circ Heart Fail* **9**, 1–9 (2016).

69. Xiang, F.-L., Fang, M. & Yutzey, K. E. Loss of β-catenin in resident cardiac fibroblasts attenuates fibrosis induced by pressure overload in mice. *Nat Commun* **8**, 712 (2017).

70. Shields, J. M. & Yang, V. W. Identification of the DNA sequence that interacts with the gut-enriched Kruppel-like factor. *Nucleic Acids Res* **26**, 796–802 (1998).

71. Brown, J. L. et al. An Sp1/KLF binding site is important for the activity of a Polycomb group response element from the Drosophila engrailed gene. *Nucleic Acids Res* **33**, 5181–5189 (2005).

72. McConnell, B. B. & Yang, V. W. Mammalian Krüppel-Like Factors in Health and Diseases. *Physiol Rev* **90**, 1337–1381 (2010).

73. Pei, J. & Grishin, N. v. A New Family of Predicted Krüppel-Like Factor Genes and Pseudogenes in Placental Mammals. *PLoS One* **8**, e81109 (2013).

74. Takahashi, K. *et al.* Induction of Pluripotent Stem Cells from Adult Human Fibroblasts by Defined Factors. *Cell* **131**, 861–872 (2007).

75. Liao, X. *et al.* Kruppel-like factor 4 is critical for transcriptional control of cardiac mitochondrial homeostasis. *Journal of Clinical Investigation* **125**, 3461–3476 (2015).

76. Shindo, T. *et al.* Krüppel-like zinc-finger transcription factor KLF5/BTEB2 is a target for angiotensin II signaling and an essential regulator of cardiovascular remodeling. *Nat Med* **8**, 856–863 (2002).

77. Rajamannan, N. M. *et al.* TGFβ inducible early gene-1 (TIEG1) and cardiac hypertrophy: Discovery and characterization of a novel signaling pathway. *J Cell Biochem* **100**, 315–325 (2007).

78. Lavallée, G. *et al.* The Kruppel-like transcription factor KLF13 is a novel regulator of heart development. *EMBO J* **25**, 5201–5213 (2006).

79. Uchida, S. *et al.* Transcriptional Regulation of the CLC-K1 Promoter by myc-Associated Zinc Finger Protein and Kidney-Enriched Krüppel-Like Factor, a Novel Zinc Finger Repressor. *Mol Cell Biol* **20**, 7319–7331 (2000).

80. Lu, Y. *et al.* Kruppel-like Factor 15 Regulates Smooth Muscle Response to Vascular Injury—Brief Report. *Arterioscler Thromb Vasc Biol* **30**, 1550–1552 (2010).

81. Leenders, J. J. *et al.* Repression of Cardiac Hypertrophy by KLF15: Underlying Mechanisms and Therapeutic Implications. *PLoS One* **7**, e36754 (2012).

82. Horie, T. *et al.* MicroRNA-133 regulates the expression of GLUT4 by targeting KLF15 and is involved in metabolic control in cardiac myocytes. *Biochem Biophys Res Commun* **389**, 315–320 (2009).

83. Prosdocimo, D. A. *et al.* KLF15 and PPAR α Cooperate to Regulate Cardiomyocyte Lipid Gene Expression and Oxidation. *PPAR Res* **2015**, 1–10 (2015).

84. Gao, L., Guo, Y., Liu, X., Shang, D. & Du, Y. KLF15 protects against isoproterenol-induced cardiac hypertrophy via regulation of cell death and inhibition of Akt/mTOR signaling. *Biochem Biophys Res Commun* **487**, 22–27 (2017).

85. He, S. *et al.* Krüppel-Like Factor 15 Modulates CXCL1/CXCR2 Signaling-Mediated Inflammatory Response Contributing to Angiotensin II-Induced Cardiac Remodeling. *Front Cell Dev Biol* **9**, 1–11 (2021).

86. Hoa, N., Ge, L., Korach, K. S. & Levin, E. R. Estrogen receptor beta maintains expression of KLF15 to prevent cardiac myocyte hypertrophy in female rodents. *Mol Cell Endocrinol* **470**, 240–250 (2018).

87. Saunders, T. L. Inducible Transgenic Mouse Models. in *Methods in molecular biology (Clifton, N.J.)* vol. 693 103–115 (2011).

88. Metzger, D. & Chambon, P. Site- and Time-Specific Gene Targeting in the Mouse. *Methods* **24**, 71–80 (2001).

89. Davis, J., Maillet, M., Miano, J. M. & Molkentin, J. D. Lost in Transgenesis. *Circ Res* **111**, 761–777 (2012).

90. Wu, Z., Yang, H. & Colosi, P. Effect of Genome Size on AAV Vector Packaging. *Molecular Therapy* **18**, 80–86 (2010).

91. Gaj, T., Gersbach, C. A. & Barbas, C. F. ZFN, TALEN, and CRISPR/Cas-based methods for genome engineering. *Trends Biotechnol* **31**, 397–405 (2013).

92. Cong, L. *et al.* Multiplex Genome Engineering Using CRISPR/Cas Systems. *Science (1979)* **339**, 819–823 (2013).

93. Gao, X. *et al.* Comparison of TALE designer transcription factors and the CRISPR/dCas9 in regulation of gene expression by targeting enhancers. *Nucleic Acids Res* **42**, e155–e155 (2014).

94. Doudna, J. A. & Charpentier, E. The new frontier of genome engineering with CRISPR-Cas9. *Science* **346**, 1258096 (2014).

95. Ran, F. A. *et al.* Genome engineering using the CRISPR-Cas9 system. *Nat Protoc* **8**, 2281–2308 (2013).

96. Jinek, M. *et al.* A Programmable Dual-RNA-Guided DNA Endonuclease in Adaptive Bacterial Immunity. *Science* **337**, 816–821 (2012).

97. Bikard, D. *et al.* Programmable repression and activation of bacterial gene expression using an engineered CRISPR-Cas system. *Nucleic Acids Res* **41**, 7429–7437 (2013).

98. Maeder, M. L. *et al.* CRISPR RNA–guided activation of endogenous human genes. *Nat Methods* **10**, 977–979 (2013).

99. Lin, S., Ewen-Campen, B., Ni, X., Housden, B. E. & Perrimon, N. In Vivo Transcriptional Activation Using CRISPR/Cas9 in Drosophila. *Genetics* **201**, 433–442 (2015).

100. Tanenbaum, M. E., Gilbert, L. A., Qi, L. S., Weissman, J. S. & Vale, R. D. A Protein-Tagging System for Signal Amplification in Gene Expression and Fluorescence Imaging. *Cell* **159**, 635–646 (2014).

101. Konermann, S. *et al.* Genome-scale transcriptional activation by an engineered CRISPR-Cas9 complex. *Nature* **517**, 583–588 (2015).

102. Chavez, A. *et al.* Highly efficient Cas9-mediated transcriptional programming. *Nat Methods* **12**, 326–328 (2015).

103. Chavez, A. *et al.* Comparison of Cas9 activators in multiple species. *Nat Methods* **13**, 563–567 (2016).

104. Liao, H. K. *et al.* In Vivo Target Gene Activation via CRISPR/Cas9-Mediated Trans-epigenetic Modulation. *Cell* **171**, 1495-1507.e15 (2017).

105. Colasante, G. *et al.* In vivo CRISPRa decreases seizures and rescues cognitive deficits in a rodent model of epilepsy. *Brain* **143**, 891–905 (2020).

106. Zhou, H. *et al.* In vivo simultaneous transcriptional activation of multiple genes in the brain using CRISPR–dCas9-activator transgenic mice. *Nat Neurosci* **21**, 440–446 (2018).

107. Braun, C. J. *et al.* Versatile in vivo regulation of tumor phenotypes by dCas9-mediated transcriptional perturbation. *Proceedings of the National Academy of Sciences* **113**, E3892–E3900 (2016).

108. Li, R. *et al.* Generation and validation of versatile inducible CRISPRi embryonic stem cell and mouse model. *PLoS Biol* **18**, e3000749 (2020).

109. Zheng, Y. *et al.* CRISPR interference-based specific and efficient gene inactivation in the brain. *Nat Neurosci* **21**, 447–454 (2018).

110. Alerasool, N., Segal, D., Lee, H. & Taipale, M. An efficient KRAB domain for CRISPRi applications in human cells. *Nat Methods* **17**, 1093–1096 (2020).

111. Yeo, N. C. *et al.* An enhanced CRISPR repressor for targeted mammalian gene regulation. *Nat Methods* **15**, 611–616 (2018).

3. Summary of aims

Overall, this work aimed to investigate aspects concerning the fundamental biology of diseased cardiomyocytes with a focus on WNT/CTNNB1 signaling regulators and to develop proper tools to manipulate disease signaling cascades. This resulted in the application of CRISPR-based gene expression modulation in cardiomyocytes.

5. Chapter 1: Identification of BZW2 interaction interfaces with KLF15 and CTNNB1

The understanding of tissue-specific mechanisms that control gene expression regulation is essential to interfere with aberrant molecular signaling in disease conditions. For an in depth understanding of WNT/CTNNB1 activity in cardiomyocytes, I focused on a previously described WNT/CTNNB1 nuclear regulatory multiprotein complex comprised of *β-catenin* (*CTNNB1*) and *Krüppel-like factor 15* (*KLF15*) specifically controlling pathological gene networks in cardiomyocytes. The interaction sites of a novel CTNNB1 and KLF15 interaction partner, BZW2, was elucidated.

6. Chapter 2: Establishment of a mouse model for cardiomyocyte-specific gene activation

Controlling gene activity is a fundamental prerequisite to understand normal and disease gene programs. A mammalian model for *in vivo* endogenous gene activation, specifically for cardiomyocytes, was not available. Here, I established a mouse model for CRISPR/dCas9VPR-based transcriptional activation and tested the activation of *Mef2d* as a proof-of-concept to evaluate the efficiency of targeted gene activation as well as the molecular organ response. I also investigated the feasibility to induce *Klf15* expression in an epigenetically silenced condition in the neonatal heart.

7. Chapter 3: Human induced pluripotent stem cells for CRISPR based gene activation

In order to adapt the *in vivo* system to translate endogenous gene activation into human cardiomyocytes, I tested the integration of the previously established dCas9VPR expression cassette into the *AAVS1* locus in human induced pluripotent stem cells (hiPSC) with concomitant constitutive expression of dCas9VPR. As a proof-of-concept, I tested endogenous *KLF15* activation in these newly generated hiPSC lines.

8. Chapter 4: Enhanced gene activation in human induced pluripotent stem cells

Not only robust, but also titratable gene activation is necessary to elucidate gene dose specific effects in target cells. I hypothesized that enhanced dCas9VPR expression will potentiate endogenous gene activation in hiPSC and derived cell types. Human iPSC lines with enhanced dCas9VPR expression were generated, the levels of endogenous gene activation of *KLF15* were tested and compared to the previously established cell line.

9. Chapter 5: Human induced pluripotent stem cells for titratable gene inactivation

Expanding the toolkit for full control over endogenous gene activity levels, I aimed to generate a CRISPR transcriptional inhibition (CRISPRi) stem cell line by integration of the dCas9KRAB repression domain at the *AAVS1* locus in hiPSC. This was attempted under the intention to make use of the previously described CRISPRa constructs and cell lines for complementary studies. As a proof-of-concept, I inhibited the expression of *KLF15* to mimic transcriptional repression under disease conditions in hiPSC-cardiomyocytes.

10. Chapter 6: Titratability of gene activity by dCas9 expression levels and guide RNA selection

General rules for effective CRISPR based gene activity modulation are essential to use these novel tools for precise control over gene activity. However, empirical validation of gRNAs designed for endogenous gene activation with synthetic CRISPR/dCas9 transcription factors were scarce. I compiled in-house data sets from *in vitro* tested gRNAs (mouse and human target genes) to identify most potent candidates for downstream targeted gene activation purposes overall yielding an improved understanding of gRNA target site selection.

11. Chapter 7: Re-activation of *Krüppel-like factor 15* in diseased mouse and human cardiomyocytes

Decline of *Krüppel-like factor 15* (*KLF15*) expression was described in failing hearts before. Exogenous overexpression of *KLF15* alleviated cardiac dysfunction. However, restoration of *KLF15* expression to physiologically relevant levels were not investigated before. I hypothesized that *KLF15* normalization with CRISPR/dCas9VPR in diseased mouse and human cardiomyocytes is sufficient to restore a healthy cardiomyocyte gene expression signature with a specific focus on WNT/CTNNB1 signaling repression.

4. Author contributions

6. Chapter 2

Individual contribution(s) to published article

Applicant (Name): Eric Schoger (first author)

Individual contribution:

1. Figures and Supplementary Figures (actively performed experiments and/or analyzed data)

Main Figures: 1 A, B, C, D, E, F, G, H, I, J; 2 A, B, C, D, E, F; 3 A, B, C, D; 4 A, B, C, D, E, F; 5 A, C, E, F; 6 A, B, C, D, E, F, G, H; 7 A, B, C, D, 8 A, B.

Supplementary Figures: 1 A, B, C, D, E; 2; 3 C; 4; 5; 6 A, B, C, D; 7 A, B, C, D, E; 10 C, D; 13.

2. Written

Main Text: Abstract, experimental procedures, main figure legends, part of introduction, results, and discussion.

Supplementary Text: Supplementary experimental procedures and supplementary figure legends.

3. Intellectual contribution

a. Experimental design and cloning/modification of construct with selection of dCas9 construct and gRNA expression constructs. Design and validation strategy of guide RNAs targeted to the mouse genome for CRISPRa purposes. Delivery strategy of Adeno-associated viruses *in vivo* in close collaboration with Dr. Kelli J. Carroll and Dr. Leonela Amoasii.

b. Selection of proof-of-concept target (*Myocyte enhancer factor 2 D*).

c. Phenotypical characterization of *Mef2d* activated hearts.

d. Wrote significant parts of the manuscript.

e. Corrected and edited the manuscript.

Publication: Schoger E, Carroll KJ, Iyer LM, McAnally JR, Tan W, Liu N, Noack C, Shomroni O, Salinas G, Groß J, Herzog N, Doroudgar S, Bassel-Duby R, Zimmermann WH, Zelarayán LC. CRISPR-Mediated Activation of Endogenous Gene Expression in the Postnatal Heart. Circ Res. 2020 Jan 3;126(1):6-24. doi: 10.1161/CIRCRESAHA.118.314522. Epub 2019 Nov 15. PMID: 31730408.

……

Signature of the applicant

7. Chapter 3

Individual contribution(s) to published article

Applicant (Name): Eric Schoger (first author)

Individual contribution:

1. Figures and Supplementary Figures (actively performed experiments and/or analyzed data)

Main Figures: 1 A, B, C, E, G.

Supplementary Figures: 1 A, B, C, D.

2. Written

Main Text: Abstract, experimental procedures, main figure legends, part of introduction, results, and discussion.

Supplementary Text: Supplementary experimental procedures and supplementary figure legends.

3. Intellectual contribution

a. Experimental design and cloning/modification of constructs as well as electroporation and clonal expansion strategy of CRISPRa human induced pluripotent stem cell clones. Design and validation strategy for guide RNAs targeted to the human genome for CRISPRa purposes. Identification and testing of *AAVS1* guide RNA off-target sites.

b. Wrote significant parts of the manuscript.

c. Corrected and edited the manuscript.

Publication: Schoger E, Argyriou L, Zimmermann WH, Cyganek L, Zelarayán LC. Generation of homozygous CRISPRa human induced pluripotent stem cell (hiPSC) lines for sustained endogenous gene activation. Stem Cell Res. 2020 Oct;48:101944. doi: 10.1016/j.scr.2020.101944. Epub 2020 Aug 14. PMID: 33038615.

……
Signature of the applicant

8. Chapter 4

Individual contribution(s) to published article

Applicant (Name): Eric Schoger (first author)

Individual contribution:

1. Figures and Supplementary Figures (actively performed experiments and/or analyzed data)

Main Figures: 1 A, B, C, E, G, H.

Supplementary Figures: 1 A, B, C.

2. Written

Main Text: Abstract, experimental procedures, main figure legends, part of introduction, results, and discussion.

Supplementary Text: Supplementary experimental procedures and supplementary figure legends.

3. Intellectual contribution

a. Experimental design and cloning/modification of constructs as well as electroporation and clonal expansion strategy of CRISPRi and CRISPRi2 human induced pluripotent stem cell clones. Design and validation strategy for guide RNAs targeted to the human genome for CRISPRi purposes. Identification and testing of *AAVS1* guide RNA off-target sites.

b. Wrote significant parts of the manuscript.

c. Corrected and edited the manuscript.

Publication: Schoger E, Zimmermann WH, Cyganek L, Zelarayán LC. Establishment of two homozygous CRISPR interference (CRISPRi) knock-in human induced pluripotent stem cell (hiPSC) lines for titratable endogenous gene repression. Stem Cell Res. 2021 Aug;55:102473. doi: 10.1016/j.scr.2021.102473. Epub 2021 Jul 27. PMID: 34343828.

……
Signature of the applicant

9. Chapter 5

Individual contribution(s) to published article

Applicant (Name): Eric Schoger (first author)

Individual contribution:

1. Figures and Supplementary Figures (actively performed experiments and/or analyzed data)

Main Figures: 1 A, B, C, E, G.

Supplementary Figures: 1 A, B, C.

2. Written

Main Text: Abstract, experimental procedures, main figure legends, part of introduction, results, and discussion.

Supplementary Text: Supplementary experimental procedures and supplementary figure legends.

3. Intellectual contribution

a. Experimental design and modification of constructs as well as electroporation and clonal expansion strategy of CRISPRa2 human induced pluripotent stem cell clones. Design and validation strategy for guide RNAs targeted to the human genome for CRISPRa purposes. Identification and testing of *AAVS1* guide RNA off-target sites.

b. Wrote significant parts of the manuscript.

c. Corrected and edited the manuscript.

Publication: Schoger E, Zimmermann WH, Cyganek L, Zelarayán LC. Establishment of a second generation homozygous CRISPRa human induced pluripotent stem cell (hiPSC) line for enhanced levels of endogenous gene activation. Stem Cell Res. 2021 Aug 26;56:102518. doi: 10.1016/j.scr.2021.102518. Epub ahead of print. PMID: 34481190.

……
Signature of the applicant

5. Chapter 1:

Identification of BZW2 interaction interfaces with KLF15 and CTNNB1

Abstract

Quiescent WNT/CTNNB1 signaling is required for adult heart tissue homeostasis. The previous identification of a nuclear WNT/CTNNB1 protein complex in cardiomyocytes offers insight into tissue-specific regulatory mechanism in normal and diseased cardiomyocytes. The following chapter summarizes efforts to further elucidate the contribution of *Basic-leucine zipper and W2 domain containing protein 2* (BZW2) as an interaction partner of KLF15 and CTNNB1 in the context of a nuclear WNT/CTNNB1 complex in cardiomyocytes. Employing mutant versions of BZW2 lacking the leucine zipper domain or the W2-domain (located at the N- or C-terminus respectively and therefore termed ΔN and ΔC), subdomain interactions with previously identified protein interaction partners were investigated. Physical interactions between BZW2 and CTNNB1 as well as with KLF15 were confirmed. Additionally, protein-protein interactions between BZW2 and the closely related family member BZW1 was found, suggesting (hetero-) dimerization of BZW proteins. While CTNNB1 and KLF15 interaction sites were identified in the C-terminal W2 domain, BZW1 interacted with the basic leucine zipper domain at the N-terminus. These findings support a picture of a molecular interaction platform controlling WNT/CTNNB1 downstream transcriptional activity harboring a cardiomyocyte-specific regulatory function. Here, BZW2 may function as a scaffold protein in this multimeric complex. Additionally, a BZW2 knockout mouse model was characterized which revealed a mild cardiomyopathy phenotype in elderly mice, further indicating compensatory mechanisms of BZW2 in the heart.

Introduction

Nuclear multiprotein complexes control gene expression programs, often in a tissue specific manner. The evolutionary conserved WNT/CTNNB1 pathway regulates cell proliferation, growth, and motility[1] in a variety of organs and is involved in heart development and adult cardiac tissue homeostasis.[2,3] Aberrantly active WNT/CTNNB1 signaling in the adult heart is associated with cardiac remodeling and heart failure progression which is in part the result of transcriptional changes in cardiomyocytes.[4,5] CTNNB1 is a key mediator of WNT/CTNNB1 signaling which translocates upon WNT stimulation to the nucleus where it exhibits co-transcriptional activities by interacting with TCF/LEF transcription factor family members. In absence of WNT stimuli, CTNNB1 is phosphorylated and degraded in the cytosol.[6] Additionally, a nuclear repression of CTNNB1 and downstream transcriptional output via TCF/LEF family members is controlled by epigenetic remodeling mediated by Groucho/TLE factors and fine-tuned by PYGO/BCL9 overall highlighting the multilevel regulation of the pathway activity.[7] KLF15 was identified as a nuclear interaction partner of CTNNB1 with a cardiac-specific WNT downstream transcriptional repressive role.[8] With the aim to identify novel cardiac interaction partners of the nuclear WNT/CTNNB1 responsive protein complex, a yeast-two-hybrid screen with a fetal cardiac library revealed an intermolecular interaction of CTNNB1 and KLF15 with BZW2. This protein-protein interaction was confirmed by co-immunoprecipitation and mass-spectrometry analyses.[9] BZW2 is expressed in the developing mouse fetus in the heart, somites, brain, and limb buds, however expression in the adult organism is restricted to muscle-tissue including the heart.[10,11] In the heart, BZW2 is expressed primarily in cardiomyocytes.[12] BZW2 was described to play a role in protein translation[13] and in the regulation of Histone H4 expression. Notably, the authors highlighted that BZW2 alone was not sufficient to promote and likely required binding partners to exert gene activity controlling roles.[14]

BZW2 was found expressed in tumor entities where its expression was generally associated with increased proliferation and overall aggressivity. Mechanistically, this was connected to ERK/MAPK signaling in colorectal cancer as well as to MYC expression control in hepatocellular carcinoma.[15,16] Vice-versa, a correlation of MYC and BZW2 expression was found in human lymphomas.[17] In the present study, it was hypothesized that BZW2 fine-tunes WNT/CTNNB1 signaling activity in a tissue-specific manner. However, intramolecular association sites between the identified interactors were not known and its role in the heart remained largely unexplored.

Material and Methods

Cell culture

HEK293T (ATCC #CRL-1573) were cultured in DMEM +10% fetal bovine serum, 100 U/mL penicillin and 100 µg/mL streptomycin and passaged using DPBS and 0.25% Trypsin (all Gibco). $3 \cdot 10^5$ cells were seeded in 10 cm dishes and transfected 48 h later with 5 µg BZW2-Flag or mutant-Flag (pBZW2-Flag, pΔNBZW2-Flag, pΔCBZW2-Flag) plasmid DNA, 5 µg respective interaction partner plasmid DNA (pCTNNB1-myc, pBZW1-HA, pKLF15-HA) mixed in 1 ml MEM (Gibco) with 20 µl TurboFect (Thermo Fisher Scientific) per immunoprecipitation. Cells were harvested 48 h post-transfection.

Co-immunoprecipitation

Cells were rinsed with DPBS (Gibco) and proteins were crosslinked with 2 mmol/L Dithiobis(succinimidyl propionate), Lomant's reagent (DSP) (prepared from a 20 mmol/L stock in DMSO and diluted in DPBS, Thermo Fisher Scientific) for 30 min at room temperature. The reaction was stopped by addition of Tris-HCl (Carl Roth) to a final concentration of 20 mmol/L and incubation for 15 min at room temperature. Cells were lysed in IP-Lysis Buffer (150 mmol/L NaCl, 50 mmol/L HEPES, 1.5 mmol/L $MgCl_2$, 1 mmol/L EDTA, 1 v/v % Triton X-100, 10 v/v % glycerol) and centrifuged at 100 xg, 4 °C for 20 min. Protein lysates were collected and protein content was quantified with RotiQuant (Carl Roth) on a FlexStation 3 multi-mode microplate reader and Softmax Pro 5.4 (Molecular Devices). Protein G Sepharose 4 Fast Flow Beads (GE Healthcare) were washed in DPBS by centrifugation at 1700 xg, 4 °C, 1 min, three times. Washed Protein G Sepharose 4 Fast Flow Beads were added to 500 µg of protein lysate and incubated for 1 h, 4 °C under constant rotation. Beads were removed by centrifugation at 100 xg, 4 °C for 1 min. Pre-cleared lysates were incubated with 1 µg precipitation antibody or suitable IgG control antibody for 16 h at 4 °C under constant rotation. Washed Protein G Sepharose 4 Fast Flow Bead were added to protein-antibody mixes and incubated for 1.5 h at 4 °C under constant rotation. Precipitation complexes were washed five times in DPBS by centrifugation at 100 xg, 4 °C for 1 min before complete removal of supernatant and re-uptake in 1x Sample Buffer (25 mmol/L TRIS-HCl, $6.25 \cdot 10^{-3}$ v/v % bromophenol blue, 2 w/v % SDS, 2.5 v/v % glycerol, 2.5 v/v % β-mercaptoethanol). Samples were denatured at 95 °C for 5 min before proceeding to further analyses.

Mouse husbandry

Mice were fed ad libitum and kept in a 12 h day/night cycle. C57BL6N mice were bred with BZW2KI mice (UC DAVIS KOMP Repository) with a lacZ cassette integration upstream of BZW2's exon 4 resulting in a frame shift of the BZW2 open reading frame rendering the allele non-functional. These mice were crossed with Flp transgenic mice to remove the lacZ cassette and subsequently with E2a-Cre expressing mice for the removal of exon 4. Animal work was approved by Niedersächsisches Landesamt

für Verbraucherschutz und Lebensmittelsicherheit (Tierversuchsvorhaben AZ-G 15-1840 and AZ-G 33.9-42502-04-20/3434) Genotyping was performed with the REDExtract-N-Amp Tissue PCR Kit (Sigma Aldrich) and the following genotyping primers: BZW2 fwd: 5' TAACGTGGTTGACACCACAGTTGG 3', BZW2 rev: 5' TAGAAGAGTAGCCAGTGGTC 3', TTR rev: 5' TTATTCACAGTGGCACTTCTGCTGC 3'.

Echocardiography

Mice were anaesthetized with Isoflurane (Isofluran CP 1 ml/ml, CP-Pharma) 2,5-4 v/v % in O2. Echocardiography was performed with a VisualSonics Vevo 2100 Imaging System (Fujifilm) equipped with a 30 MHz MS-400 MicroScan transducer. Data was acquired by Marcel Zoremba and imaging analyses were performed by Beate Knocke, SFB1002 Service Unit. Experimenters were blinded for genotypes.

Heart weight (HW) was calculated with:

$HW = 1.05 \cdot 5/6 \cdot Epi\text{-}s \cdot (L\text{-}s + (AWTh\text{-}s \cdot PWTh\text{-}s)/2) - area\text{-}s \cdot L\text{-}s$

Fractional area shortening (FAS) was calculated with:

$FAS = (area\text{-}s - area\text{-}d)/area\text{-}d \cdot 100$

Epi-s: epicardial circumference in systole
L-s: left ventricular (long axis) length in systole
AWTh-s: left anterior wall thickness in systole
PWTh-s: left posterior wall thickness in systole
area-d: cross-sectional left ventricular myocardial area in diastole
area-s: cross-sectional left ventricular myocardial area in systole

Statistics

GraphPad Prism 9 (GraphPad Software, Inc.) was used to present echocardiography data and to test for statistical significance. One-way ANOVA and Tukey *post hoc* test was used for multiple group comparisons and unpaired student's t-test was performed for two-group comparisons.

Immunoblotting

Lysates (heart lysates or 10% of immunoprecipitation input = 50 µg) were separated on 10% discontinuous SDS polyacrylamide gels. Electrophoresis was performed for 2 h at 110 V in Electrophoresis Buffer (10x: 25 mmol/L TRIS ultrapure, 190 mmol/L Glycine, 0.1 w/v % SDS). Transfer was performed for 1.5 h at 100 V in Transfer Buffer (25 mmol/L TRIS ultrapure, 190 mmol/L Glycine, 20 v/v % methanol). Membranes were blocked with 5% non-fat dried milk powder (AppliChem) in TBST (20 mmol/L Tris ultrapure, 150 mmol/L NaCl, 0.1 v/v % Tween (Carl Roth), pH 7.6). Membranes were probed with primary antibodies (listed in table 1.1) for 16 h at 4 °C. Membranes were washed with TBST and incubated with secondary antibodies (listed in table 1.1) for 2 hours at room-temperature. Proteins were detected on a ChemiDoc MP Imaging System with Image Lab Version 5.1 (both BioRad) using the femtoLUCENT PLUS-HRP Kit (G-Biosciences).

Table 1.1. Primary and secondary antibodies chapter 1.

Antibody	Manufacturer	Catalogue Number	Host organism	Dilution
Anti-BZW2	Sigma Aldrich	HPA022813	rabbit	1:1 000
Anti-CTNNB1	BD Transduction	610153	mouse	1:2 000
Anti-Flag-HRP	Sigma Aldrich	A8592	mouse	1:5 000
Anti-HA	Sigma Aldrich	H3663	mouse	1:1 000
Anti-GAPDH	Proteintech	60004-1-Ig	mouse	1:50 000
Anti-mouse HRP	Dako	P0260	rabbit	1:10 000
Anti-rabbit HRP	Dako	P0448	goat	1: 5 000

Peptide-Spot-Array

Human BZW2 amino acid sequences were synthesized on nitrocellulose membranes with a AutoSpot Robot ASS222 (Intavis Bioanalytical Instruments). Each spot contained 50 nmol of peptide per spot, each with 25 amino acids with five amino acids overlap to the subsequent spot. Recombinant human GST-tagged CTNNB1 and KLF15 were expressed from IPTG-inducible pGEX-4T-3 vectors in competent E-coli (BL21 (DE3), Invitrogen) and purified by affinity chromatography.[18] Plasmids and experiments were provided and performed by Dr. Claudia Noack and peptide-spot-membranes as well as recombinant protein expression and purification were supported by Dr. Enno Klußmann's group, Max-Delbrück-Center Berlin.

Results

Protein-protein interactions of BZW2 with KLF15 and CTNNB1 *in vitro*

A protein-protein interaction of BZW2, CTNNB1, KLF15 and TCF7L2 was described in heart tissue previously.[8,9] However, protein subdomain interaction sites of BZW2 with identified interaction partners remained unclear. Using mutant variants of the BZW2 open-reading frame containing the basic leucine zipper domain (ΔN = amino acids (aa): 248 - 419) or the W2 protein domain (ΔC = aa: 1 - 247) (Figure 1.1 A), co-immunoprecipitations for the detection of CTNNB1 and KLF15 interaction sites of BZW2 were performed. This revealed a C-terminal interaction of the W2 domain of BZW2 with both interaction partners (Figure 1.1 B (i) and (ii)). A potential interaction with closely related Basic leucine zipper and W2 domain containing protein 1 (BZW1) was investigated likewise and revealed BZW2/BZW1 heterodimerization potential *in vitro* (Figure 1 B (iii)). This interaction was found to be specific for the N-terminal basic leucine zipper domain of BZW2. An empty vector was used to confirm specific peptide detection in pull-down experiments (Figure 1 B (iv)). A schematic overview of the BZW2 protein subdomains and interaction partners is depicted in Figure 1.1 C.

To further evaluate these results, a peptide-spot-array with overlapping peptide sequence of human BZW2 was exposed to GST-CTNNB1 or GST-KLF15 recombinant proteins. This revealed CTNNB1 association mainly with the C-terminally located W2 domain and a distinct interaction site of KLF15 with the W2 protein domain of BZW2 confirming the co-immunoprecipitation data (Figure 1.2 A and B).

Figure 1.1

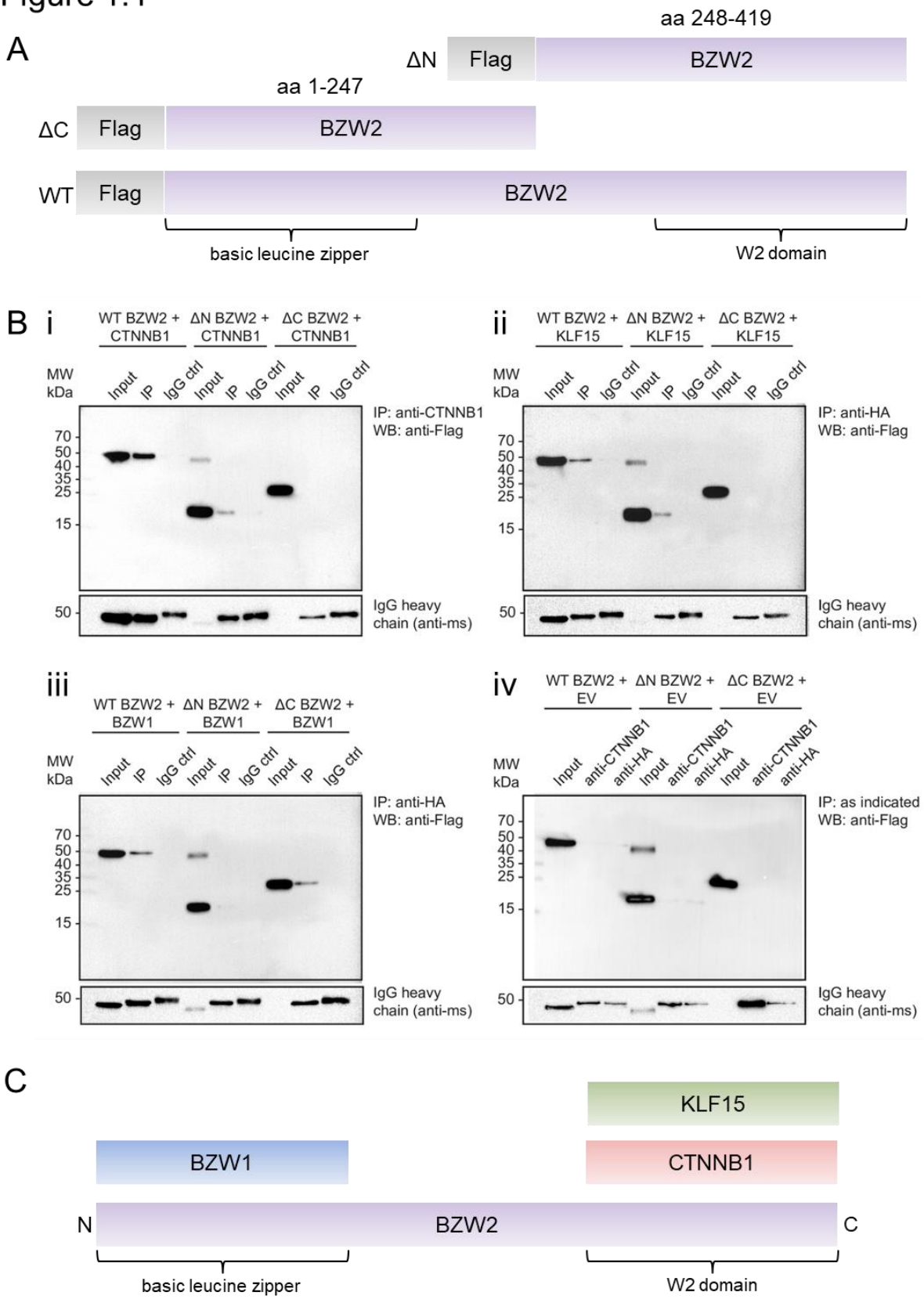

Figure 1.1. BZW2 interacts via the W2 protein domain with KLF15 and CTNNB1. A. Co-immunoprecipitation experiments with full-length BZW2 (WT BZW2), lacking the basic leucine zipper domain (ΔN BZW2 = amino acids (aa): 248 - 419) or lacking the W2 domain (ΔC BZW2 = aa: 1 - 247) were performed in HEK293T cells. **B.** BZW2 interaction was confirmed between CTNNB1 (**i**) and KLF15 (**ii**) with full length

BZW2 as well as with ΔN BZW2 while the lack of the W2 domain (ΔC BZW2) abolished this interaction. In contrast, BZW1 interacted with BZW2 via the basic leucine zipper domain (ΔC BZW2) and was not detectable with ΔN BZW2 (**iii**). Empty vector (pcDNA3.1) co-transfections with BZW2 constructs served as negative control (**iv**). IgG heavy chain detection indicated comparable pull-down antibody abundance in each experiment. **C.** Schematic overview of BZW2 interaction sites with KLF15 and CTNNB1 at the C-terminal W2 domain and with BZW1 at the N-terminal basic leucine zipper domain.

Figure 1.2

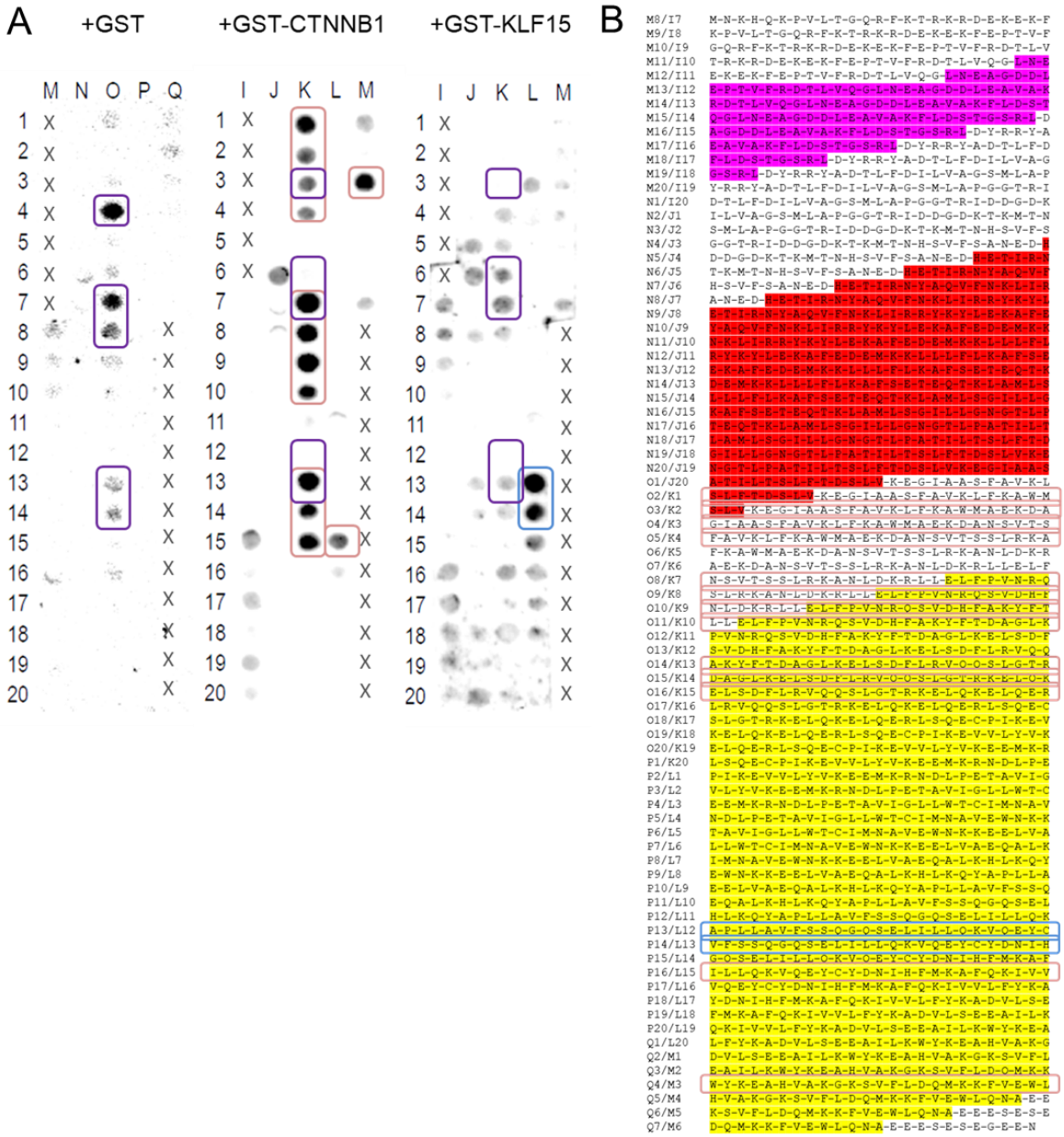

Figure 1.2. CTNNB1 and KLF15 bind to amino acid sequences within the W2 protein domain of BZW2. A. Peptide-spot-array was performed to map interaction domains of BZW2 with CTNNB1 and KLF15. Five amino acids overlapping human BZW2 peptide sequences were distributed in series on nitrocellulose membranes and probed with GST-tagged human CTNNB1 or human KLF15 peptides. GST-peptide was used as negative control. Purple boxes indicate unspecific binding to peptide sequences. Red boxes indicate peptide sequences associating with CTNNB1. Blue box indicates peptide sequences interacting with KLF15. Coordinates (letters and numbers)

indicate peptide position on the membrane. **B.** Human BZW2 peptide sequences corresponding to peptide-spot-arrays and interaction sites with CTNNB1 (red boxes) and KLF15 (blue boxes) in (A). BZW2 protein subdomains are indicated as follows: 1.) pink: leucine zipper domain, 2.) red: basic leucine zipper domain, 3.) yellow: W2-domain. These data further confirmed the W2 protein domain interaction with KLF15 and CTNNB1. Peptide-spot membranes were prepared in collaboration with Dr. Enno Klußmann, Max-Delbrück Center for Molecular Medicine in the Helmholtz Association, Berlin and experiments were performed by Dr. Claudia Noack, Institute of Pharmacology and Toxicology, University Medical Center Göttingen.

Loss of *BZW2* leads to a late onset cardiomyopathy

Additionally, a global BZW2 knockout mouse model was evaluated to investigate potential phenotypic consequences of a lack of BZW2 (Figure 1.3 A). The knockout strategy was confirmed by allele specific PCRs (Figure 1.3 B) and validated on protein level by immunoblotting, showing decreased BZW2 protein levels in heterozygous (BZW2 +/-) animals and a complete lack of BZW2 protein in homozygous (BZW2 -/-) mouse hearts compared to wild-type controls (BZW2 +/+). Overall, the lack of BZW2 did not affect protein levels of its interaction partner CTNNB1 (Figure 1.3 C). Echocardiography analyses revealed a modest decrease in anterior wall thickness in diastole (AWThd) of BZW2 -/- mice compared to BZW2 +/+ and +/- hearts at 20 weeks of age which was accompanied by increased heart weight (HW) to body weight (BW) ratio suggesting pathological cardiac remodeling. However, heart function as evaluated by fractional area shortening was not significantly changed at 16 weeks of age (Figure 1.3 D). BZW2 -/- mice were analyzed again at 16 months of age and showed a significantly decreased cardiac function assessed by fractional area shortening and accompanied by increased HW to BW ratios as well as increased left ventricular inner diameter in diastole (LVIDd) compared to BZW2 +/+ (Figure 1.3 E).

Figure 1.3

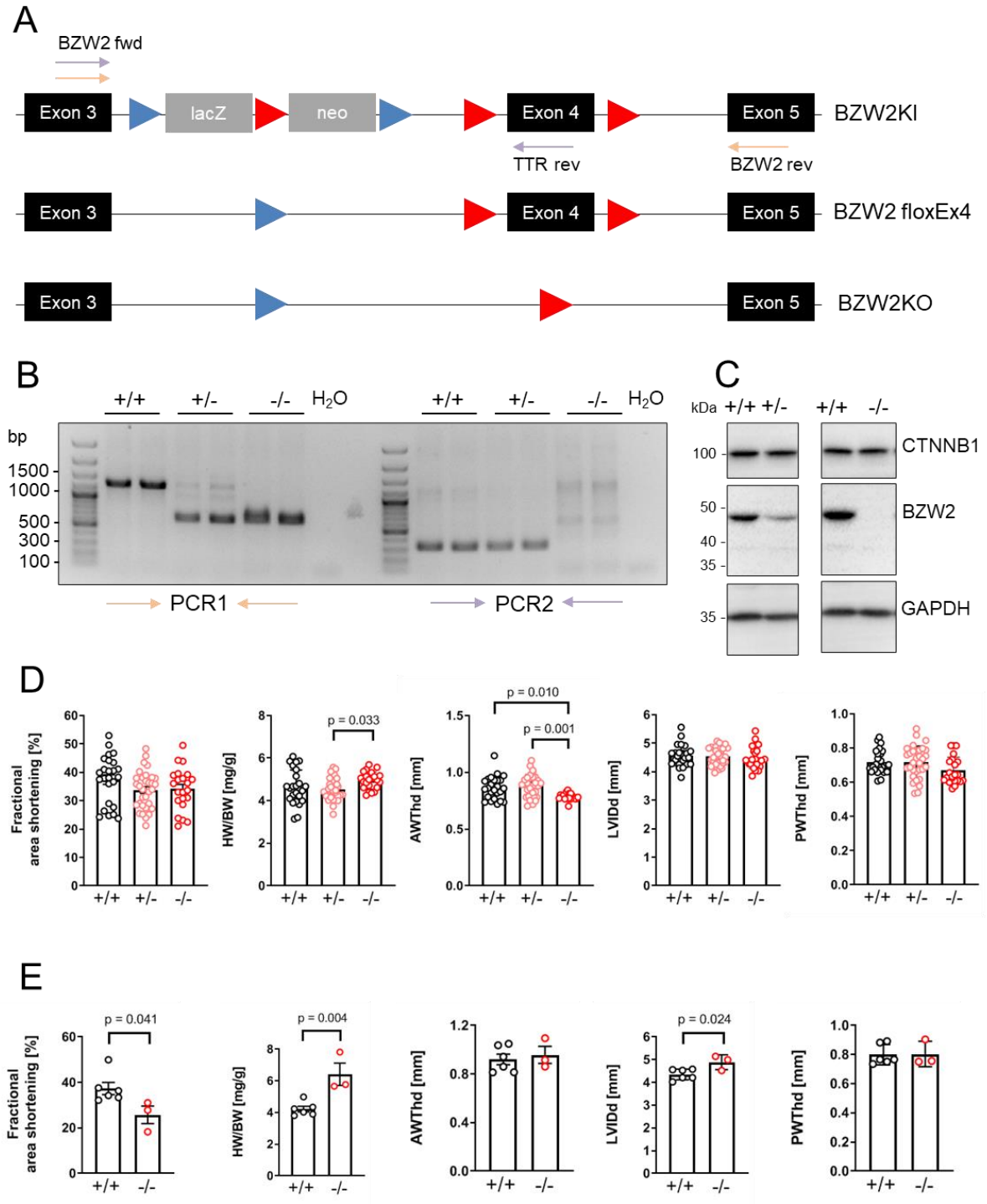

Figure 1.3. Lack of BZW2 results in modest late onset cardiomyopathy. A. Schematic exon/intron structure and genotyping strategy for BZW2 constitutive knock-out mice. Exon 4 was flanked with loxP sites and a lacZ/Neo expression cassette flanked by flp sites was integrated upstream of exon 4 (BZW2KI). First, the lacZ/Neo cassette was removed by breeding BZW2KI with flp transgenic mice (BZW2floxEx4). Next, exon 4 was removed by breeding BZW2floxEx4 with E2a-Cre transgenic mice (BZW2KO) inducing a frame shift in exon 5 and leaving a shortened allele. **B.** Deletion of exon 4 was checked by PCR confirming a shortened amplicon (PCR1: orange arrows) in heterozygous (+/-) and homozygous mice (-/-) and absence of amplicon (PCR2: purple arrows) in homozygous mice. **C.** BZW2 protein levels in ventricular tissue were reduced in heterozygous mice and was not detectable in homozygous animals confirming the knockout strategy. CTNNB1 steady-state protein levels were not affected upon BZW2 reduction. GAPDH was used as loading control. **D.** Fractional area shortening was

unchanged in 20-weeks heterozygous and homozygous mice compared to controls. Heart weight (HW) was significantly elevated in homozygous mice. Anterior wall thickness in diastole (AWThd) was decreased in homozygous mice compared to heterozygous and control animals while left ventricular inner diameter in diastole (LVIDd) and posterior wall thickness in diastole (PWThd) was similar between groups. **E.** 16-month-old BZW2-/- mice showed reduced fractional area shortening as well as significantly increased heart weight to body weight ratios and increased left ventricular diameter compared to BZW2+/+ controls indicating a late manifesting development of cardiomyopathy. Depicted is the mean ± SEM. One-way ANOVA was performed with Tukey correction for multiple group comparisons and student's t-test for two group comparisons.

Discussion

Tight control of WNT/CTNNB1 signaling in a variety of tissues including its low activity in healthy, adult cardiomyocytes is necessary to maintain homeostasis. This is achieved by several mechanisms including the sequestration of CTNNB1 by the CTNNB1-degradation complex in the cytosol. Furthermore, nuclear import control and compartmentalization within the cell are mechanisms by which CTNNB1 signaling, and co-transcriptional activity are tightly controlled.[19] However, these mechanisms are ubiquitously employed and therefore harbor little possibilities for tissue-specific interference and therapeutic targetability. Here, the interfaces of CTNNB1, KLF15 and BZW2 were identified. Since KLF15 was shown to exert a cardiac-specific WNT inhibitory role[20], and BZW2 was expressed with a remarkable muscle-specificity[10], a functional role for BZW2 to co-regulate WNT/CTNNB1 signaling in the heart was hypothesized. Tissue-specific regulation of the WNT/CTNNB1 pathway gained increasing attention.[21] Detailed analyses of the nuclear WNT/CTNNB1 complex as well as transcriptional target sites in the normal and diseased heart remain to be further investigated. This will allow for an in-depth understanding of the gene regulatory network under control of this multiprotein complex. Here, a protein-protein interaction between BZW2 and WNT downstream components essential for its activity, CTNNB1 and KLF15, was confirmed. Both interaction partners bound to the W2 domain of BZW2 in line with the known protein-protein interaction function of the W2 domain.[22,23] This data supported our understanding of a WNT activity controlling protein complex with striking cell specificity for cardiomyocytes.[9] A global lack of BZW2 in a murine knockout model revealed a mild, late-onset cardiomyopathy phenotype. A possible explanation may be found in compensatory replacement by its highly homologous family member BZW1. In fact, a potential protein-protein interaction between BZW2 and BZW1 via the basic leucine zipper domain was observed in this study. BZW1 and BZW2 share homology with other proteins pivotal for protein translation such as eIF5 all being involved in start codon selection, in part in an autoregulatory manner.[24] However, BZW1 expression is low in heart tissue and mainly expressed in the non-myocyte population (https://www.proteinatlas.org/ENSG00000082153-BZW1/celltype)[25] and the relevance of this heterodimerization deserves further elucidation particularly in a tissue and cell-type specific manner. Furthermore, it cannot be ruled out that the loss of BZW2 may play minor co-regulatory functions in otherwise non-challenged, homeostatic hearts at baseline. Further studies are required to clarify BZW2's role in cardiomyocytes, which may benefit from combinatorial genetic models untangling protein complex functions rather than single component contributions. Overall, these findings are necessary pre-requisites for targeted intervention strategies and for further detailed investigation of intermolecular interfaces with these and potentially additional interaction partners of the nuclear WNT complex in cardiomyocytes.

References (Chapter 1)

1. Clevers, H. Wnt/β-Catenin Signaling in Development and Disease. *Cell* **127**, 469–480 (2006).

2. Buikema, J., Zwetsloot, P.-P., Doevendans, P., Domian, I. & Sluijter, J. Wnt/β-Catenin Signaling during Cardiac Development and Repair. *J Cardiovasc Dev Dis* **1**, 98–110 (2014).

3. Brade, T., Männer, J. & Kühl, M. The role of Wnt signalling in cardiac development and tissue remodelling in the mature heart. **72**, 198–209 (2006).

4. Iyer, L. M. *et al.* A context-specific cardiac β-catenin and GATA4 interaction influences TCF7L2 occupancy and remodels chromatin driving disease progression in the adult heart. *Nucleic Acids Res* **46**, 2850–2867 (2018).

5. Hou, N. *et al.* Transcription Factor 7-like 2 Mediates Canonical Wnt/β-Catenin Signaling and c-Myc Upregulation in Heart Failure. *Circ Heart Fail* **9**, 1–9 (2016).

6. Hart, M. *et al.* The F-box protein β-TrCP associates with phosphorylated β-catenin and regulates its activity in the cell. *Current Biology* **9**, 207–211 (1999).

7. Fiedler, M. *et al.* An ancient Pygo-dependent Wnt enhanceosome integrated by chip/LDB-SSDP. *Elife* **4**, 1–22 (2015).

8. Noack, C. *et al.* Krueppel-like factor 15 regulates Wnt/β-catenin transcription and controls cardiac progenitor cell fate in the postnatal heart. *EMBO Mol Med* **4**, 992–1007 (2012).

9. Chebbok, E. Basic leucine zipper and W2 domain- containing protein 2 (BZW2) : A novel cardiac WNT component. *Georg-August-Universität Göttingen - Molekulare Medizin* (2015).

10. Nishinaka, N. *et al.* Identification of the novel developmentally regulated gene, Bdm2, which is highly expressed in fetal rat brain. *Brain Res Dev Brain Res* **120**, 57–64 (2000).

11. Tachikawa, K., Sasaki, S., Maeda, T. & Nakajima, K. Identification of molecules preferentially expressed beneath the marginal zone in the developing cerebral cortex. *Neurosci Res* **60**, 135–146 (2008).

12. Schoger, E. Characterization of Basic Leucine Zipper and W2 Domain-Containing Protein 2 (BZW2) Expression. *Georg-August-Universität Göttingen - Molekulare Medizin* (2015).

13. Singh, C. R. *et al.* Mechanisms of translational regulation by a human eIF5-mimic protein. *Nucleic Acids Res* **39**, 8314–8328 (2011).

14. Mitra, P., Vaughan, P. S., Stein, J. L., Stein, G. S. & van Wijnen, A. J. Purification and functional analysis of a novel leucine-zipper/nucleotide-fold protein, BZAP45, stimulating cell cycle regulated histone H4 gene transcription. *Biochemistry* **40**, 10693–10699 (2001).

15. Huang, L., Chen, S., Fan, H., Ai, F. & Sheng, W. BZW2 promotes the malignant progression of colorectal cancer via activating the ERK/MAPK pathway. *J Cell Physiol* **235**, 4834–4842 (2020).

16. Li, G. *et al.* BZW2/5MP1 acts as a promising target in hepatocellular carcinoma. *J Cancer* **12**, 5125–5135 (2021).

17. Wu, C. H. *et al.* Combined analysis of murine and human microarrays and ChIP analysis reveals genes associated with the ability of MYC to maintain tumorigenesis. *PLoS Genet* **4**, 21–26 (2008).

18. Hundsrucker, C. *et al.* Glycogen synthase kinase 3β interaction protein functions as an a-kinase anchoring protein. *Journal of Biological Chemistry* **285**, 5507–5521 (2010).

19. Haq, S. *et al.* Stabilization of beta-catenin by a Wnt-independent mechanism regulates cardiomyocyte growth. *Proc Natl Acad Sci U S A* **100**, 4610–5 (2003).

20. Noack, C. *et al.* KLF15-Wnt–Dependent Cardiac Reprogramming Up-Regulates SHISA3 in the Mammalian Heart. *J Am Coll Cardiol* **74**, 1804–1819 (2019).

21. Söderholm, S. & Cantù, C. The WNT/β-catenin dependent transcription: A tissue-specific business. *WIREs Mechanisms of Disease* **13**, 1–41 (2021).

22. Koonin, E. v. Multidomain organization of eukaryotic guanine nucleotide exchange translation initiation factor eIF-2B subunits revealed by analysis of conserved sequence motifs. *Protein Science* **4**, 1608–1617 (1995).

23. Yamamoto, Y. *et al.* The eukaryotic initiation factor (eIF) 5 HEAT domain mediates multifactor assembly and scanning with distinct to interacts to eIF1, eIF2, eIF3, and eIF4G. *Proc Natl Acad Sci U S A* **102**, 16164–16169 (2005).

24. Loughran, G., Firth, A. E., Atkins, J. F. & Ivanov, I. P. Translational autoregulation of BZW1 and BZW2 expression by modulating the stringency of start codon selection. *PLoS One* **13**, 1–13 (2018).

25. Thul, P. J. *et al.* A subcellular map of the human proteome. *Science* **356** (2017).

6. Chapter 2:

Establishment of a mouse model for cardiomyocyte-specific gene activation

"CRISPR-mediated activation of endogenous gene expression in the postnatal heart"

Short title: Cardiomyocyte-specific CRISPRa

Eric Schoger[1,2], Kelli J. Carroll[3], Lavanya M. Iyer[1,2], John R. McAnally[3], Wei Tan[3], Ning Liu[3], Claudia Noack[1,2], Orr Shomroni[4], Gabriela Salinas[4], Julia Groß[5,6], and Nicole Herzog[5,6], Shirin Doroudgar[5,6], Rhonda Bassel-Duby[3], Wolfram H. Zimmermann[1,2], Laura C. Zelarayán[1,2]

[1] Institute of Pharmacology and Toxicology, University Medical Center Goettingen, Georg-August University, Goettingen 37075, Germany.

[2] DZHK (German Center for Cardiovascular Research) Partner Site Goettingen, Germany.

[3] Department of Molecular Biology and the Hamon Center for Regenerative Science and Medicine, University of Texas Southwestern Medical Center, Dallas, TX 75390-9148.

[4] NGS-Integrative Genomics (NIG) Institute Human Genetics, University Medical Center Goettingen, Georg- August University, Goettingen 37075, Germany.

[5] Department of Internal Medicine III (Cardiology, Angiology, and Pneumology), Heidelberg University Hospital, Im Neuenheimer Feld 669, 69120 Heidelberg, Germany.

[6] DZHK (German Center for Cardiovascular Research), Partner Site Heidelberg/Mannheim, Germany.

Current Affiliations:

K.J.C Austin College, Sherman, TX 75090, United States of America

L.M.Y Computational and Systems Biology, Genome Institute of Singapore (GIS), Singapore

C.N Research & Development Pharmaceuticals, Bayer AG, Berlin, Germany

Address for correspondence: Laura C. Zelarayán, PhD, Institute of Pharmacology and Toxicology, University Medical Center, Goettingen & DZHK (German Center for Cardiovascular Research), partner site Goettingen, 37075 Germany. Telephone number: +49 551 39 20730; Fax: +49 551 39 5699; Email: laura.zelarayan@med.uni-goettingen.de.

Translational Studies, Genetically Altered and Transgenic Models, Endogenous Gene Regulation

Abstract

Rationale: Genome editing by CRISPR/Cas9 is evolving rapidly. Recently, second generation CRISPR/Cas9 activation systems based on nuclease inactive "dead" (d)Cas9 fused to transcriptional transactivation domains were developed for directing specific guide (g)RNAs to regulatory regions of any gene of interest, to enhance transcription. The application of dCas9 to activate cardiomyocyte transcription in targeted genomic loci *in vivo* has not been demonstrated so far.

Objective: We aimed to develop a mouse model for cardiomyocyte-specific, CRISPR-mediated transcriptional modulation, and to demonstrate its versatility by targeting *Mef2d* and *Klf15* loci (two well-characterized genes implicated in cardiac hypertrophy and homeostasis) for enhanced transcription.

Methods and Results: A mouse model expressing dCas9 with the VPR transcriptional transactivation domains under the control of the myosin heavy chain (*Myh*) 6 promotor was generated. These mice innocuously expressed dCas9 exclusively in cardiomyocytes. For initial proof-of-concept, we selected *Mef2d*, which when overexpressed, led to hypertrophy and heart failure, and *Klf15*, which is lowly expressed in the neonatal heart. The most effective gRNAs were first identified in fibroblast (C3H/10T1/2) and myoblast (C2C12) cell lines. Using an improved triple gRNA expression system (TRISPR), up to three different gRNAs were transduced simultaneously to identify optimal conditions for transcriptional activation. For *in vivo* delivery of the validated gRNA combinations, we employed systemic administration via adeno-associated virus serotype (AAV) 9. Upon gRNA delivery targeting *Mef2d* expression, we recapitulated the anticipated cardiac hypertrophy phenotype. Using gRNA targeting *Klf15*, we could enhance its transcription significantly, although *Klf15* is physiologically silenced at that time point. We further confirmed specific and robust dCas9VPR on-target effects.

Conclusions: The developed mouse model permits enhancement of gene expression by utilizing endogenous regulatory genomic elements. Proof-of-concept in two independent genomic loci suggests versatile applications in controlling transcription in cardiomyocytes of the postnatal heart.

Keywords: in vivo CRISPR/Cas9 system; endogenous gene activation; cardiomyocytes; gene regulation; genetic mouse model

Non-standard Abbreviations and Acronyms:

CRISPR clustered regularly interspaced short palindromic repeats
dCas9 endonuclease-dead Cas9
VPR VP64, p65, and RTA
AAV adeno-associated virus
Mef2d Myocyte enhancer factor 2 D
Klf15 Krueppel like factor 15
Myh6 Myosin heavy chain 6
ChIP chromatin immunoprecipitation
TSS transcriptional start site
CM cardiomyocytes
TG transgenic
WT wild type
CT control

Introduction

Dysregulation of gene expression, often called fetal gene re-programing, is a hallmark of heart failure and is conserved across species. Genetically modified mouse models have been widely used to study the phenotypic consequences associated with these transcriptional alterations in heart failure. Random integration transgenesis, constitutive and conditional knockout/knockin mouse models are most commonly employed for that purpose.[1] Conditional models employing the Cre/lox system have been helpful for studying cardiac-specific gene deletions using cell-type and temporally restricted Cre recombinase expression.[2] Gene knockdown can also be achieved by viral transduction or oligonucleotide-based knockdown technologies.[3] Induction of gene expression is limited to just a few approaches including transgenic mice, a rather laborious and time consuming approach.[4] In the heart, long-term episomal expression is most commonly achieved by adeno-associated (AAV) virus transduction with cardiomyocyte tropism and a low propensity for integration. AAV serotype 9 is considered most effective in mouse cardiomyocyte transduction *in vivo*.[5] However, AAV displays maximum effective packaging capacity of less than 5 kbp,[6] rendering it unsuitable for larger transcripts and often restricting it to a single transcript variant.

The class II clustered regularly interspaced short palindromic repeats (CRISPR) and CRISPR-associated protein (Cas) 9 system have been adapted from the bacterial adaptive immune system to defend against viral infections. Cas9 recognizes and cuts specific double-stranded DNA when directed by two RNA molecules, the CRISPR (cr)RNA and trans-activating (tracr)RNA.[7] Since its discovery the Cas9 protein has been mutated to lose its catalytic activity completely by mutating the enzyme within both the RUVC-like and HNH (minimal mutations: D10A and H840A) endonuclease domains. The endonuclease-dead (d)Cas9 protein can be fused to fluorescent reporters for gene mapping purposes or to transcriptional activators or repressors to modulate gene expression.[8] Artificial transactivation domains have been employed to induce endogenous gene expression by dCas9 fusion proteins. The first generation of CRISPR activation (CRISPRa) approaches fused four VP16 domains (VP64) to dCas9 resulting in moderate transcriptional activation.[9] The VP16 domain originates from *Herpes simplex* virus and recruits the host transcription factors OCT-1 and HCF-1 to induce transcription.[10] The second generation of CRISPRa systems are reported to be more efficient using heteromeric transactivation domains or peptide scaffolding approaches to recruit activators to the dCas9 protein.[11] The heterotrimeric VPR transactivator consists of VP64, p65, and RTA transactivation domain from Epstein-Barr virus transcription factor R. The p65 and RTA domains are employed due to their strong transactivation capability[12,13, 14] recruiting further transcriptional activators.[15] Alternative CRISPRa technologies include the synergistic activator mediator (SAM) system, which combines optimized dCas9-transactivation domain fusion and recruitment of heteromeric transactivation domains comprising VP64, p65, and HSF1 (SPH).[16] The dCas9SunTag system is based on a fusion of dCas9 with a single chain antibody scaffold recruiting multiple VP64 domains.[17] Comparison of these different gene activation systems revealed that dCas9VPR, dCas9SAM, and dCas9SunTag are robust approaches to activate endogenous gene expression.

CRISPR-based endogenous gene activation systems have been extensively applied *in vitro*. Just recently, promising *in vivo* approaches in mouse models have been presented, with a

demonstration of transcription regulation in the brain and liver using CRISPRa[18, 19] or epigenetic modulation for the treatment of diabetes, muscular dystrophy, and acute kidney disease.[20]

We hypothesized that for our purposes, the dCas9VPR system would render a better control of gene expression activation in cardiomyocytes *in vivo* and tested it in the postnatal heart. In this study, we aimed to generate a mouse model for dCas9-enhanced endogenous gene activation in cardiomyocytes, with the ultimate goal of normalizing expression of genes, which are reduced upon cardiac remodeling and are essential to maintain homeostasis. We first validated dCas9VPR transcriptional enhancement by targeting the *Mef2d* locus, as a read-out for the described cardiac hypertrophy induced by *Mef2d* overexpression.[21] We also targeted the *Klf15* locus in neonatal life to test the ability of the system for activating genes that are physiologically not expressed.

Methods

dCas9VPR transgenic mouse generation

Animal work described in this manuscript has been approved and conducted under the oversight of the UT Southwestern Institutional Animal Care and Use Committee and the Lower Saxony Animal Review Board (LAVES, AZ-G15-1840) (a checklist is provided in Table I, Online Data Supplement). The human codon optimized dCas9VPR coding region was PCR-amplified from a SP-dCas9VPR plasmid (Addgene plasmid #63798; kindly provided by George Church) and cloned into NheI and BshTI restriction sites in the Myh6-Cas9-2A-tdTomato backbone vector[22] by HD Infusion cloning (TAKARA) using the primers listed in Online Table II. Vector sequence is available in the Online Data Supplement Section I. The stop codon of dCas9VPR was exchanged for a glycine codon using a QuickChange site-directed mutagenesis (Agilent) approach using the primers listed in Online Table II. The linearized Myh6-dCas9VPR-2A-tdTomato construct was injected into the pronucleus of mouse zygotes from B6C3F1 or C57/BL6N mice (both Charles River), which were implanted into pseudo-pregnant ICR mice (Envigo). Offspring was considered as independent mouse lines and founders. Mice were crossed to C57/BL6N wild-type mice in the subsequent generations. DNA for genotyping was isolated from tail tip biopsies. Genotyping PCR was conducted using the primers listed in Online Table II. For *in vivo* CRISPRa, $n \geq 7$ (8 weeks *Mef2d* activation), $n \geq 2$ (neonatal *Klf15* activation) mice per group were injected intraperitoneally at postnatal day 4 (P4) with 1.1×10^{11} viral genomes (vg)/g if not otherwise stated. Saline was used for control injections. Cardiac function was assessed by a VisualSonics Vevo 2100 system with a 35-MHz transducer. The observer was unaware of the genotypes and treatments. Hearts were analysed for transgene expression by stereomicroscopy (Axio Zoom.V16, Zeiss).

Statistical analyses

G-Power3.1 was used to determine the sample size for animal studies (description in Online Data). Statistical analyses were performed using GraphPad PRISM 7. Two-tailed unpaired student's t-tests were conducted on two group comparisons. One-way ANOVA and *post hoc* Bonferroni correction comparing all groups with each other was performed on group

comparisons. Pearson's correlation was performed for correlation plots. Statistical significance was assumed when $p < 0.05$ (*). The ROUT outlier test with Q = 1% was performed when indicated.

An expanded Methods section is available in the Online Supplemental Material.

Results

Generation of cardiomyocyte-specific CRISPRa mice

We established a cardiomyocyte-restricted CRISPRa transgenic mouse model employing a transactivation domain, VPR, fused to the nuclease-inactive dCas9 protein,[11] in *Myh6*-expressing cells. In this model, dCas9VPR has the potential to bind DNA sequences by providing specific gRNAs (Figure 1A). To track transgene expression, a tdTomato reporter was included, separated from the dCas9VPR coding sequence by a post-translationally self-cleaving T2A peptide encoding sequence (Figure 1B). After pronucleus injection of the *Myh6*-dCas9VPR-2A-tdTomato construct, identified positive transgenics were bred to wild-type C57/BL6N mice (Online Figure IA). Three mouse lines with homogenous tdTomato signal were identified, possessing distinct transgene expression levels as assessed by RT-qPCR for dCas9VPR (line 1 (high), Figure 1C and D and line 1-3 (high, medium and low) Online Figure IB-D). The tdTomato reporter signal was not detectable by fluorescence stereomicroscopy in brain, liver, kidney, lung, spleen, and quadriceps examined in all identified mouse lines (Online Figure IE). dCas9VPR mRNA was exclusively detected in ventricles and in atria of transgenic mice, but expression was less prominent in atria (Figure 1E). Mice of all identified lines were born in Mendelian ratios and did not exhibit any overt pathological phenotype. *Myh6*-dCas9VPR-expressing mice did not show any cardiac phenotype up to 8 months of life (Figure 1F and Online Figure II). Three mouse lines with low, medium, and high dCas9VPR expression (lines 1 (high), 2 (medium), and 3 (low), respectively) were selected for further downstream validation.

Validation of gRNAs for dCas9VPR-mediated transcriptional activation

We next designed and validated gRNAs binding to the 5´ upstream region of the transcriptional start site (TSS) of two transcription factors: one implicated in cardiomyocyte hypertrophy and another in metabolic homeostasis, i.e., Myocyte enhancer factor 2 D (*Mef2d*) and Krueppel like factor 15 (*Klf15*). Variation in expression of these genes offers an ideal phenotypic readout. We tested several gRNAs covering the 5´ upstream regions of the respective TSS, since no algorithm is defined for the design of gRNAs targeting promoter regions of genes. Two different mouse cell lines, C3H/10T1/2 fibroblasts and C2C12 myoblasts, were used for this test. Cells were transiently transfected with a plasmid encoding (SP-CMV)-dCas9VPR and combinations of pX333 (p) plasmids expression containing 2xgRNA-GFP. The p-2xgRNA construct expressed two gRNAs. We tested a total of eight gRNAs for *Mef2d* (A_i-H_i) and four for *Klf15* (A-D) (Online Table III, Figure 1G and H), either as single gRNA or in combination, using the p-2xgRNA vector. Untransfected cells, Sp-dCas9VPR single-transfected cells, and cells transfected with Sp-dCas9VPR along with an empty p-2xgRNA construct served as controls. Results were normalized to baseline expression of *Mef2d* and *Klf15*.

Single gRNA targeting the *Mef2d* locus induced at best 1.2- and 1.3-fold transcriptional activation (F_i) in C3H/10T1/2 and C2C12 cells, respectively. When used in combination, induction of *Mef2d* transcription in both cell lines increased to more than 2-fold (Figure 1I). Enhancement of endogenous *Klf15* was more efficient as compared with this technique. Single gRNAs A and B were able to induce *Klf15* expression up to 2.5-fold in C3H/10T1/2 cells and up to 10-fold each in C2C12 cells, but did not reach statistical significance. In contrast, gRNAs C and D failed to induce significant *Klf15* expression in both cell lines. When expressed from the same construct, gRNAs A and B induced *Klf15* expression (p-2xgRNA *Klf15* A+B) up to 7.5 fold in C3H/10T1/2 cells and up to 32.5-fold in C2C12 cells. Similarly, gRNAs C and D were more efficient when simultaneously expressed (p-2xgRNA *Klf15* C+D) but less substantially than gRNAs A and B (Figure 1J).

Increased expression of MEF2D was observed at the protein level in both C3H/10T1/2 and C2C12 cell lines (Figure 2A). Immunocytochemistry in C3H/10T1/2 cells transfected with Sp-dCas9VPR and variations of p-2xgRNA constructs targeting *Mef2d* confirmed activation by single and multiplexed gRNAs. GFP reporter in p-2xgRNA, indicative of gRNA plasmid expression, as well as MEF2D expression, showed increased level of nuclear MEF2D. When compared to standard *Mef2d* overexpression strategies, MEF2D was abundantly ectopically detected in the cytosol, which was never observed by immunofluorescence in dCas9VPR-mediated activation (Figure 2B and Online Figure IIIA). Western blot analysis of the different cell compartments showed that by using multiple gRNAs increasing levels of MEF2D induction resulted in low detection of MEF2D protein in the cytosol, while standard *Mef2d* overexpression showed robust expression in this compartment *in vitro* (Figure 2C). To be sure that differences in MEF2D expression were caused by the applied gRNAs (*Mef2d* or controls) and not by non-homogenous transfection efficiency, we next checked the percentage of double-transfected cells (as detected by dCas9-tdTomato and GFP) expressing MEF2D by flow cytometry. This analysis showed that double tdTomato/GFP positive cells were constant around 30% in different transfection conditions, and that in this population, MEF2D-activated cells were around 3% and 22% in control and *Mef2d* (F_i+E_i) gRNA-transfected cells, respectively. MEF2D-activated cells were also significantly higher in the GFP positive population, but with a lower difference between the transfected gRNA (1% vs 7.5%) since not all cells were positive for dCas9 (n=3, Online Figure IIIB and C). Furthermore, confocal microscopy analysis showed that 32.16 ± 5.6 % and 36.39 ± 2.9 % were GFP-positive in empty p-2xgRNA- and gRNA *Mef2d* (F_i+E_i)-transfected cells, respectively. GFP-positive *Mef2d* (F_i+E_i)-transfected cells showed a greater MEF2D expression, confirming expression induction (Online Figure IIID). Altogether, these data indicate that the system has a consistent transfection efficiency of all components, which allows for using these cells for rapidly validating suitable gRNAs to target mouse genomic regions. Although several antibodies were tested, KLF15 activation at the protein level could not be detected due to the absence of suitable antibodies.

We further explored the ability to titrate the system by modulating the expression of either dCas9VPR or gRNA and selected two gRNA for *Mef2d* (F_i+E_i) in Neuro2a cells. At stable dCas9VPR concentration and increasing amount of gRNA (0.01, 0.03, 0.1, 0.3, 1, 3, 10, 30, and 100 ng), transfected cells showed increasing MEF2D activation, reaching a maximum activation of approximately 5-fold over control at 10 ng or higher. Conversely, cells transfected with increasing dCas9VPR concentrations (1, 3, 10, 30, 100, 300, and 1000 ng) but the same

amount of gRNAs, showed increasing levels of MEF2D, maximizing at 100 ng transfected dCas9VPR construct (Figure 2D and Online Figure IV and V). This data suggests that the system strongly depends on both gRNA, but more importantly, dCas9VPR abundance.
Next, we validated the identified gRNA combinations in *Myh6*-dCas9VPR-2A-tdTomato cardiomyocytes (line 1) *in vitro* with a plasmid-free established protocol (Online Figure VIA-B). As we aimed for traceable transcriptional activation efficiency for this proof-of-concept study, the most potent combination of gRNAs, C_i, F_i, and G_i for *Mef2d*, and A, B, and C for *Klf15* were co-transfected in isolated adult cardiomyocytes of *Myh6*-dCas9VPR-2A-tdTomato animals along with control gRNAs. A 30-fold enrichment in *Mef2d* and a 15-fold increase in *Klf15* mRNA levels was observed compared to control gRNA transfected or untransfected transgenic cardiomyocytes (Figure 2E). Furthermore, increased MEF2D protein level could be confirmed in these cardiomyocytes (Figure 2F). These results indicate that endogenous activation of both targets is efficiently achievable in cardiomyocytes of *Myh6*-dCas9VPR-2A-tdTomato transgenic mice.

Validation of CRISPRa with multiple gRNAs *in vitro*

Taking advantage of the multiplexing ability of the system, we used the TRISPR plasmid to express three gRNAs under three independent RNA polymerase class III promoters (U6, H1, 7SK), from a single construct.[23] The TRISPR construct also contained a GFP reporter under the control of the murine muscle creatine kinase (CK) 8 promoter.[24] Based on the validation findings, gRNAs C_i, F_i, and G_i, and gRNAs A, B, and C were selected to enhance *Mef2d* and *Klf15*, respectively. The TRISPR constructs were first tested *in vitro* in C3H/10T1/2 and C2C12 lines stably expressing dCas9VPR. Consistent with our previous results, *Mef2d* transcriptional activation appears to be less efficient than *Klf15* activation. TRISPR-*Mef2d*-gRNAs induce transcriptional enhancement up to 1.5-fold in C3H/10T1/2 fibroblasts and 1.2-fold in C2C12 myoblasts compared to cells transfected with a TRISPR control. TRISPR-*Klf15*-gRNAs showed an activation of up to 3-fold in C3H/10T1/2 fibroblasts and up to 14-fold in C2C12 myoblasts compared to cells transfected with a construct expressing non-targeted gRNA (TRISPR control) (Figure 3A). These resulted in increased MEF2D protein expression in C3H/10T1/2 and C2C12, stably expressing dCas9VPR under CAG promoter, transfected with TRISPR-*Mef2d*-gRNAs as well as N2A glioblastoma cells that were transiently transfected with both CRISPRa components (Figure 3B). Despite low transfection efficiencies, significantly elevated levels of both targets can be observed confirming the efficiency of the chosen CRISPRa/TRISPR approach in endogenous activation of *Mef2d* and *Klf15*.

Next, we used adeno-associated virus serotype (AAV) 9 for systemic delivery of TRISPR constructs in the generated *Myh6*-dCas9VPR-2A-tdTomato mouse model. Immunofluorescence images confirmed GFP positive cells as well as tdTomato expression in murine cardiomyocytes, which were systemically provided with the AAV9-expressing TRISPR-*Mef2d* gRNA (Figure 3C). These cardiomyocytes showed significantly increased expression of *Mef2d* in comparison to respective controls (saline and TRISPR-*Mef2d* injected wild-type as well as saline injected dCas9VPR) (Figure 3D).

CRISPRa-mediated endogenous activation of *Mef2d* and *Klf15 in vivo*

We next injected 1.1×10^{11} AAV9 TRISPR-*Mef2d*-gRNA vg/g containing the C_i, F_i, and G_i *Mef2d* gRNA combination intraperitoneally in 4-day-old *Myh6*-dCas9VPR-2A-tdTomato mice. Eight weeks after AAV9 injection, *Mef2d* AAV9 injected transgenic mouse hearts were enlarged compared to control littermate hearts (Figure 4A). We checked expression of the different reporters of the system and observed in 91 % counted viable cardiomyocytes: 84.9 % cardiomyocytes displaying tdTomato signal (indicative of dCas9VPR expression), 71% GFP-positive (indicative of TRISPR transduction), and 57.9 % labelled by both tdTomato and GFP in all *Myh6*-dCas9VPR-2A-tdTomato/AAV9 TRISPR transduced mouse hearts, indicating uniform expression of the transgene and the gRNAs (Figure 4B). Moreover, increased cardiomyocyte area correlated with high MEF2D expression as observed in whole heart by immunofluorescence (Figure 4C-D and Online Figure VIC). *Mef2d* steady-state mRNA and protein levels were measured as the primary read-out for CRISPRa efficiency and revealed increased *Mef2d* mRNA level of up to 3-fold, which translated to a similar increase in protein level (Figure 4E and F and Online Figure VID). *Mef2d* isoform α1 (ubiquitous) and α2 (muscle-specific)[25] were similarly increased, but *Mef2a* was unaffected (Figure 4G), indicating specificity of the CRISPRa approach.

Four and eight weeks post-AAV9 injection, cardiac function was assessed by echocardiography. Ejection fraction and fractional shortening were significantly reduced at both time points as compared to saline-injected *Myh6*-dCas9VPR-2A-tdTomato, AAV9-injected, as well as saline-injected wild-type littermates (Figure 5A and B and Online Figure VIIA). Eight weeks post-AAV9 injection, hearts were analyzed. TRISPR *Mef2d* AAV9-injected transgenic mouse heart sections showed fibrotic and hypertrophic phenotypes as compared to respective control wild-type littermate hearts. Natriuretic peptides *a* and *b* (*Nppa* and *Nppb*), as well as the fibrosis marker, connective tissue growth factor (*Ctgf*), normally upregulated in pathological heart remodeling, were significantly elevated in TRISPR *Mef2d* AAV9-injected *Myh6*-dCas9VPR-2A-tdTomato transgenic mouse hearts compared to controls (Figure 5C-E and Online Figure VIIB). A negative correlation between *Mef2d* expression and fractional shortening, as well as a positive correlation with *Nppa*, *Nppb* and *Ctgf* expression was validated. Moreover, a positive correlation of *GFP* and *Mef2d* expression further supported the transduction efficiency ($p<0.0001$, Figure 5F and Online Figure VIIC). These observations are in line with the cardiomyopathy phenotype described in transgenic mice overexpressing *Mef2d*,[21] indicating that CRISPRa-mediated activation of *Mef2d* is sufficient to drive downstream pathways activation. However, *Mef2d* AAV9-injected transgenic mouse of the line 3 (low expression of dCas9VPR) did not result in a significant phenotype (Online Figure VIID and E).

To further characterize our mouse model, we performed RNA sequencing of heart ventricular tissue from TRISPR *Mef2d* AAV9-injected dCas9VPR (line 1) and respective control mice (n=3/group). Principal component analysis (PCA) showed that dCas9VPR-TRISPR *Mef2d* injected mouse hearts were clearly separated from all the controls (wild-type-saline and TRISPR-*Mef2d* controls, as well as from dCas9VPR-saline) (Figure 5G). The sample-to-sample distance plot shows distinct grouping of dCas9VPR-TRISPR *Mef2d* hearts as compared to all the controls, which were indistinguishable from each other (Online Figure VIIIA).

Heatmap of differentially expressed genes (DEGs) showed a clear difference of up- and down-regulated genes between dCas9VPR-TRISPR *Mef2d* and all respective controls (Online Figure VIIIB and Table V). Gene ontology (GO) analysis showed that DEGs in dCas9VPR-TRISPR *Mef2d* clustered to processes and pathways regulating hypertrophic remodeling and cardiomyopathy when compared to all controls and *versus* dCas9VPR-saline alone. The comparison of dCas9VPR-saline *versus* wild-type saline showed few DEGs that classified to GABAergic and glutamatergic processes (Figure 5H and Online Figure VIIC). Next, to infer possible off-target effects of dCas9VPR activity, we searched for predicted off-target binding of the *Mef2d* gRNA included in the injected TRISPR AAV9 (C_i, G_i, and F_i). This resulted in a list of 35 (C_i), 104 (F_i), and 15 (G_i), as well as 408 (C_i), 949 (F_i), and 187 (G_i) genomic regions when up to 5 or 4 mismatches were allowed, respectively. Using those regions, we searched for the nearest gene located ±500bp distances and identified 71 (C_i), 110 (F_i), and 21 (G_i), as well as 10 (C_i), 12 (F_i), and 1 (G_i) genes for 4 or 5 mismatches, respectively. Only few (five) predicted off targets overlapped with regulated genes in TRISPR *Mef2d* hearts (Online Figure IX and Table VI).

We further tested the potential of the system to activate genes that are normally silenced. We focused on *Klf15*, with a significant role in controlling metabolic gene expression and heart homeostasis and silenced in the heart in early postnatal life. In line with low enrichment of histone 3 lysine 27 acetylation, H3K27ac (an established chromatin mark for active enhancers and transcriptionally active regions[26]), at the *Klf15* locus in P6 hearts, but a markedly increased enrichment in the adult heart, cardiac *Klf15* mRNA expression is low in the early postnatal life until postnatal day 10 (P10), with a subsequent increase of expression in the adult heart (Online Figure XA and B).[27] To activate the expression of *Klf15* in early postnatal cardiomyocytes, we injected *Myh6*-dCas9VPR-2A-tdTomato mice with 1.1×10^{11} AAV9 TRISPR-*Klf15*-gRNA vg/g containing the more efficient gRNAs A, B, and C combination in P4 mice and analyzed the tissue at P10. GFP and tdTomato reporter activity was uniformly detected in three different *Myh6*-dCas9VPR-2A-tdTomato mouse lines (representative images in Figure 6A). Induction of *Klf15* expression in heart tissue showed similar 6- to 10-fold inductions in the different lines in comparison to non-injected *Myh6*-dCas9VPR-2A-tdTomato, injected, as well as non-injected wild-type littermates (Figure 6B and Online Figure XC). dCas9VPR-mediated *Klf15* increase was able to enhance expression of validated *Klf15* metabolic target genes, including aldehyde dehydrogenase 2 family member (*Aldh2*) and alcohol dehydrogenase iron containing 1 (*Adhfe1*) (Figure 6C). Taking advantage of the dynamicity of *Klf15* expression (very low till P10), we performed a temporal analysis of dCas9-dependent induction. *Myh6*-dCas9VPR-2A-tdTomato mice were injected with 1.1×10^{11} AAV9 TRISPR-*Klf15*-gRNA vg/g at P4 and analyzed 4 (P8), 8 (P12), and 10 (P14) days later. This analysis showed that the potency of gene induction decreased over time as endogenous *Klf15* expression arose. Expression of gRNA as indicated by GFP expression was consistently similar throughout all the stages (Figure 6D-F). This indicates that the system allows gene expression induction according to endogenous levels and does not exceed endogenous locus activity to a high degree. Next, we tested the ability to titrate the system by varying the AAV9 doses. We injected dCas9VPR mice with different AAV9 doses (low: 1.1×10^{10}, middle: 1.8×10^{10}, high: 3.3×10^{10} and, full: 1.1×10^{11} vg/g) and observed increasing induction of *Klf15* expression from 1.6- to 6-fold. AAV dose was positively correlated to the myocardial area containing GFP positive cardiomyocytes. Interestingly, low

AAV9 doses, exhibiting very scattered GFP positive cells along the myocardium, were still able to significantly induce *Klf15* activation (Figure 6G-H).

Specificity of the CRISPRa-mediated gene activation *in vivo*

To confidently validate our model, we further investigated recruitment of dCas9VPR to *Mef2d* and *Klf15* 5´ upstream TSS regions (as guided by the designed gRNA) by chromatin immunoprecipitation (ChIP) of Cas9VPR and RT-qPCR in mice injected with *Mef2d* and *Klf15* gRNAs, respectively. Induced expression of both *Mef2d* and *Klf15* was confirmed in the respective groups (Figure 7A and B). We performed ChIP sequencing of dCas9VPR mouse hearts injected with *Mef2d* and *Klf15* at P14 (n=3/condition including non-enriched chromatin DNA (input)). On-target effect was validated by ChIP-qPCR, which demonstrated significant enrichment of both *Mef2d* and *Klf15* on the 5´ upstream regions of the TSS, at the place where gRNAs were designed to bind. Overall, dCas9VPR was highly significantly enriched at the corresponding on-target sites in TRISPR *Mef2d*- and *Klf15*-injected dCas9VPR mice (Figure 7C, validation in Online Figure XD). We next tested enrichment of predicted off-targets for *Mef2d* C_i, F_i, and G_i gRNAs (*Kcnj4, Enpp1, Itpka, and Fam20c*) in *Mef2d*-injected dCas9VPR mice. This showed no significant enrichment of dCas9 to their respective TSS 5´ regions upstream as indicated by ChIP-qPCR and integrative genomics viewer (IGV) occupancy profiles of sequencing data (Figure 7D). Similarly, predicted off-target of *Kfl15* gRNAs A, B, and C (*Bmp3, Shh, Hmcn1)* showed no significant enrichment and only background noise was detected (Online Figure XE).
Genome-wide binding sites were identified using the MACS2 peak caller using input DNA as background. The numbers of ChIP-bound regions are summarized in Online Figure XIA. These data showed a high number of peaks independent of the condition (saline-, *Mef2d*-, *Klf15*-injected), which mapped for 8945, 8954, 7578 genes, respectively, in line with previous Cas9 ChIP data[28] (Online Figure XIA). Intersection of ChIP-seq (P14) with the DEGs data from *Mef2d*-injected (8-weeks) dCas9VPR mice demonstrated 209 genes, from which only five were predicted to be off-targets (*Fam20c, Lix1l, Pigz, Ptpn13, Pde1c*). Out of these five genes, only one gene, *Pigz*, was observed significantly enriched in *Mef2d*-injected mice and not in the other conditions (saline, TRISPR *Klf15*-injected). Interestingly, the remaining four genes showed low peaks in all conditions, indicating that they are not specific for *Mef2d* targeting (Online Figure XIB-D). Importantly, although these genes showed similar peaks in all conditions, they were only regulated in the *Mef2d*-injected mice and not in saline- and/or *Klf15*-injected mice (heatmap in Online Figure XIB) indicating that this regulation is not dependent on dCas9. Intersected genes, which were not predicted *Mef2d* gRNA off-targets (203 genes), peaks not intersected with DEGs (8348) in *Mef2d*-injected mice, as well as regions at the intersection of peaks in *Klf15*-injected mice with predicted off-targets for *Klf15* showed no significant enrichment (Online Figure XIE and XIIA). Moreover, neighbor *Mef2d* genes (5´upstream: *Iqgap3, Ttc24* and 3´downstream: *Rhbg, Mir3093*) were either not or very low expressed and not significantly regulated in TRISPR *Mef2d*-injected mice (Figure 7E). These observations indicate a high-specificity of the CRISPRa system for a given target. Next, we tested the ability of the CRISPRa system for multiplexed activation. We injected P4 dCas9VPR mice with 5.5 ×

10^{10} vg/g of TRISPR *Mef2d* and TRISPR *Klf15* and observed simultaneous activation of *Mef2d* and *Klf15* comparable to the single activation (Figure 8A and B).
In order to analyze the extent of transcript upregulation in transduced cardiomyocytes at single cell resolution we performed single cell (sc) RNA-seq of dCas9VPR mouse P14 hearts injected with AAV9 TRISPR *Mef2d* as well as saline-treated dCas9VPR and wild-type mice with AAV9 TRISPR *Klf15* as controls. Based on image-based quality control using the ICELL8 platform, artifacts perturbing scRNA-seq analysis were eradicated and therefore expression data for every cell can be confidently analyzed.[29] We analyzed a total of 213, 242 and 272 cells in AAV9 TRISPR *Mef2d*, dCas9VPR saline and wild-type AAV9 TRISPR *Klf15* control, respectively (Figure 8C). Quality control criteria included primarily the percentage of reads at different stages of the analysis, including those with sample barcodes, uniquely mapped to genome, associated with exons/introns and mitochondrial/ribosomal-associated reads, as well as presence of cardiomyocyte markers within the analysed cells. Cells in all conditions similarly expressed the cardiomyocyte marker *Tnnt2* (average 260.71 reads) and did not result in cell clustering in t-SNE plots as well as it was not detected in the negative control cells. This indicated a homogenous cardiomyocyte population across samples (Online Figure XIIB-E). In AAV9 TRISPR *Mef2d* mouse heart we identified 54.9% GFP positive cells (indicative of AAV9 transduction). The total *Mef2d* expression in this condition was 10.9 reads (12.26 in the GFP positive cells and 9.9 in the GFP negative population). In dCas9VPR saline mouse heart (with no GFP detectable as expected) *Mef2d* reads average was 2.8 and in wild-type AAV TRISPR *Klf15*, the average was 4.9 in the total population. In line with AAV9 preferentially transducing cardiomyocytes, the *Tnnt2* reads average was consistently lower in the GFP negative fraction (Online Figure XIIB). Accordingly, t-SNE plots showing average transcript expressions of *Mef2d* and GFP demonstrated an increased number of *Mef2d* reads per cell in the AAV TRISPR *Mef2d* injected hearts (Figure 8D). The *Mef2d* fold activation per cell was 4.27 (compared to saline) and 2.44 (compared to AAV TRISPR *Klf15*) in AAV TRISPR *Mef2d* in line with our mRNA bulk analysis. Moreover, this data precisely dissected regulation of the targeted gene only detected in AAV9 (GFP) transduced cells. Altogether, our data showed the feasibility of CRISPRa system to specifically and efficiently activate gRNA-targeted locus *in vivo*.

Discussion

In this study, we developed a CRISPR/Cas9-based *in vivo* model for endogenous gene activation in the mammalian heart. This approach represents a robust, specific, and tractably valuable tool for cardiovascular research, as a straightforward and rapid strategy for modulating transcriptional programs of interest in cardiomyocytes.
To improve the efficiency of CRISPR/Cas9-mediated transcriptional activation, multiple domains have been fused to the dCas9/gRNA complex including VPR, SAM, or Suntag.[17, 30, 31] Recent studies reported the ability of CRISPR/Cas9-mediated transcriptional activation *in vivo*. One study used the SAM module and an engineered hairpin aptamer containing two MS2 domains that can recruit the MS2:P65:HSF1 (MPH) activation complex to the target locus, which significantly enhances the efficiency of transcriptional activation for dCas9-VP64.[20] SunTag-based systems were established including the SunTag-p65-HSF1 system, allowing higher activation induction compared to SAM, SunTag, or VPR.[32] Another system consisting of a combination of an integrated dCas9 fused to the SunTag domain, with the remaining

components (gRNAs, SunTag transactivator domain, and a specific Cre recombinase) provided with an AAV system, which depends on both the AAV transduction and the Cre recombination efficiency.[18] Those systems were improved for very high gene activation.
The primary purpose of our study was to generate a tool to normalize expression of genes which are reduced during heart remodeling. Thus, we decided to use the VPR system due to its consistent and efficient fold increase in transcriptional activation, but rather moderate compared to the currently described *in vivo* systems.[13-15, 19, 20]

To allow for the high efficiency of the system, we generated cardiomyocyte-specific dCas9VPR- expressing mouse lines. We have confirmed that constitutive expression of cardiomyocyte- specific dCas9VPR does not result in transcriptomic and phenotypic variation. Only upon gRNA delivery, successfully activated target gene expression and increased protein levels at moderate levels were shown *in vivo*. This was accompanied by physiological nuclear localization as demonstrated for *Mef2d* activation. *In vitro,* we could observe that ectopic MEF2D protein cytosolic localization could be avoided by single gRNA application. This is an advantage over ectopic expression of exogenous transgenes usually introducing uncontrolled multiple copies of genes, which can be easily titrated with the CRISPRa system. *Mef2d* induction was sufficient to trigger transcriptomic changes leading to cardiomyopathy phenotype, in line with previous reports showing that excess MEF2D induces cardiac remodeling and cardiomyopathy. We also confirmed a correlation of MEF2D high expression with increased cardiomyocytes area at the cellular level *in vivo*. Of note, MEF2D overexpression resulted in a more severe cardiomyopathy with atrial enlargement, probably due to secondary effects, which was less pronounced upon dCas9VPR-mediated *Mef2d* increased expression.[21] Expression levels of MEF2D positively correlated with the expression of the AAV9 reporter, GFP, and with the induction of its target genes and loss of cardiac function, indicating that the phenotype entirely depends on the gRNA-mediated induction of the gene of interest. Unfortunately, no suitable antibody was identified and therefore, KLF15 expression could not be tested at the protein level. However, we also confirmed activation of *Klf15* expression and its target metabolic genes in dCas9VPR expressing mice.

We also have demonstrated the specific binding of the dCas9VPR-gRNA complex to the designated promoter region with a consequent transcriptional activation. Although several off-targets were predicted, in our analysis we have identified only one gRNA-specific off target in *Mef2d* injected mice and none in *Klf15* injected mice, indicating a robust model. Our analysis suggests that stable interactions are specific between dCas9 and designed gRNA for the desired target site as reflected by high enrichments of the on-target site, which was distinguishable from all off-targets, similar to O'Geen findings.[28] Off-target binding do not form such stable interactions, as demonstrated by much lower ChIP enrichments and the lack of corresponding gene regulation in all conditions tested in our study. Moreover, the presence of false positive peaks in ChIP-seq data has to be carefully analyzed as they are easily introduced by a particular type of error in the reference genome, multicopy sequences which have been incorrectly assembled and collapsed into a single copy, which were not considered in our analysis.[33] Our observations indicate that systematic off-target identification together with ChIP-qPCR analysis will be sufficient to infer the specificity of a given target.

Thus, our data confirm that dCas9VPR enhances endogenous gene expression safely by using an endogenous mechanism of action and preserving molecular function,[32] therefore, providing an advantage for enhancing expression of genes reduced upon defined conditions but also for investigating genes with an unknown role. Since generation of transgenic mice requires careful validation and is time consuming, CRISPR/Cas9-based mouse models to activate gene expression represent a feasible and rapid alternative to overexpress genes, as well as lncRNAs and miRNAs.[34] One of the big advantages of the system is the possibility of multiplexed activation allowing for more complex studies of transcriptional network activation, which was validated in our study for *Mef2d* and *Klf15 in vivo*.

Most CRISPRa related systems used gRNAs targeting regions in a range between -1000 to +650 bp relative to the TSS.[35, 36] In this study, we adhered to recommendations of *in vivo* approaches suggesting to target gRNAs up to -400 bp upstream of the TSS. The elementary properties of gRNAs such as GC-content seem to play subordinate relevance regarding transcriptional activation capacity.[37] For the selected target genes, *Klf15* and *Mef2d*, we found the highest activation potential when gRNAs were targeted in a region of -120 to -200 bp upstream of TSS by comparing single gRNAs *in vitro*. Consistent with previous reports, we found a synergistic increase of efficiency when multiple gRNAs are targeted to the same but non-overlapping regulatory region of the given gene of interest.[35]
We also observed that a gene with high cardiac expression, such as *Mef2d*, showed less dCas9VPR-mediated induction in comparison to *Klf15*, which shows very low basal expression at the time of induction. Moreover, induction of *Klf15* expression by dCas9VPR was negatively correlated with the physiological expression of the gene at different postnatal time points. These findings are consistent with previous reports of lower transcriptional activation efficiency of already highly expressed genes [38] and indicate that the system prevents aberrant regulation. Thus, different extents of gene activation are a result of their basal expression levels, epigenetic status, or tight cellular regulatory mechanisms, preventing severe overexpression in order to ensure a physiological range of expression level.[39, 40] We further determined the role of the different components and observed that concentrations of dCas9VPR are more critical than gRNA amounts to induce long-term gene activation. Similar to studies by Pu and colleagues,[41] we demonstrated the ability of the CRISPRa system to be titrated by AAV dosage, which offers advantages to perform mosaic gene activation for direct, cell-autonomous roles of a gene of interest.

With the emergence of CRISPR/Cas9 strategies to tackle so far untreatable diseases by genome editing, it has become possible to correct genetic mutations with high efficiency and specificity. Therefore, related techniques such as CRISPRa have a therapeutic potential and hold promise for clinical applications.[11] The mouse model presented in this study offers a suitable, rapid tool for proof-of-concept studies in an *in vivo* system independent of the size of genetic material.

In summary, we have developed and extensively characterized a rapid and powerful technical platform for gene activation in postnatal cardiomyocytes (single or multiplex) consisting of only two components, the dCas9VPR constitutively-expressed gene, and the AAV9-mediated gRNA construct, with high specificity and efficiency. We also established the protocols for gRNA validation and defined the temporal consequences of dCas9VPR-mediated gene

activation. We believe that our tool will be of great use for the cardiovascular research community.

Acknowledgements

The authors thank George Church (Harvard University) for providing the SP-dCas9-VPR plasmid (Addgene plasmid # 63798),[30] Andrea Ventura (Sloan Kettering Institute) for providing the pX333 plasmid (Addgene plasmid # 64073),[42] Dirk Grimm (Heidelberg University), Leonela Amoasii (UT Southwestern Medical Center) for providing the TRISPR constructs and Boris Greber (RheinCell Therapeutics GmbH) for providing PiggyBac/Transposase constructs. We thank Joshua Heinrich and Alex Mireault (both UT Southwestern Medical Center) as well as Jutta Schroeder (Central animal facility, UMG), Daniela Liebig-Wolter and Silvia Bierkamp (Institute of Pharmacology and Toxicology) for superb technical support, and Fabian Ludewig (NGS-Integrative Genomics (NIG), UMG) for sequencing support. We specially thank Eric Olson for advice, reviewing, and editing the manuscript, as well as all members of his laboratory for discussions and assistance. This work was part of the doctoral thesis of Eric Schoger within the Georg August University School of Sciences (GAUSS) and the Göttingen Graduate School for Neurosciences, Biophysics, and Molecular Biosciences (GGNB) - Molecular Medicine program at the University Medical Center Göttingen.

Disclosure

The authors declare no conflict of interest. WHZ is co-founder and scientific advisor of Repairon GmbH and Myriamed GmbH.

Source of Funding

This work was supported by a Deutsche Forschungsgemeinschaft (DFG) grant (ZE900-3 to LCZ), the Collaborative Research Center (CRC/SFB) 1002 (Project C07 to LCZ and C04, S01 to WHZ), German Heart Research Foundation, German Center for Cardiovascular Research (DZHK), DZHK Excellence Program (to SD), and Foundation Leducq (14CVD04; E.O., W.H.Z.). Funding for open access charge was provided by internal institutional funding (UMG).

References

1. Moon A. Mouse models of congenital cardiovascular disease. *Current topics in developmental biology*. 2008;84:171-248
2. Doetschman T, Azhar M. Cardiac-specific inducible and conditional gene targeting in mice. *Circulation research*. 2012;110:1498-1512
3. Boon RA, Iekushi K, Lechner S, Seeger T, Fischer A, Heydt S, Kaluza D, Treguer K, Carmona G, Bonauer A, Horrevoets AJ, Didier N, Girmatsion Z, Biliczki P, Ehrlich JR, Katus HA, Muller OJ, Potente M, Zeiher AM, Hermeking H, Dimmeler S. Microrna-34a regulates cardiac ageing and function. *Nature*. 2013;495:107-110

4. Davis J, Maillet M, Miano JM, Molkentin JD. Lost in transgenesis: A user's guide for genetically manipulating the mouse in cardiac research. *Circulation research*. 2012;111:761-777
5. Zincarelli C, Soltys S, Rengo G, Rabinowitz JE. Analysis of aav serotypes 1-9 mediated gene expression and tropism in mice after systemic injection. *Molecular therapy : the journal of the American Society of Gene Therapy*. 2008;16:1073-1080
6. Wu Z, Yang H, Colosi P. Effect of genome size on aav vector packaging. *Molecular therapy : the journal of the American Society of Gene Therapy*. 2010;18:80-86
7. Doudna JA, Charpentier E. Genome editing. The new frontier of genome engineering with crispr-cas9. *Science*. 2014;346:1258096
8. La Russa MF, Qi LS. The new state of the art: Cas9 for gene activation and repression. *Molecular and cellular biology*. 2015;35:3800-3809
9. Gimenez CA, Ielpi M, Mutto A, Grosembacher L, Argibay P, Pereyra-Bonnet F. Crispr-on system for the activation of the endogenous human ins gene. *Gene therapy*. 2016;23:543-547
10. Wysocka J, Herr W. The herpes simplex virus vp16-induced complex: The makings of a regulatory switch. *Trends in biochemical sciences*. 2003;28:294-304
11. Vora S, Tuttle M, Cheng J, Church G. Next stop for the crispr revolution: Rna-guided epigenetic regulators. *The FEBS journal*. 2016;283:3181-3193
12. Schmitz ML, Baeuerle PA. The p65 subunit is responsible for the strong transcription activating potential of nf-kappa b. *The EMBO journal*. 1991;10:3805-3817
13. Chang LK, Chung JY, Hong YR, Ichimura T, Nakao M, Liu ST. Activation of sp1-mediated transcription by rta of epstein-barr virus via an interaction with mcaf1. *Nucleic acids research*. 2017;45:5009
14. Hung CC, Kuo CW, Wang WH, Chang TH, Chang PJ, Chang LK, Liu ST. Transcriptional activation of epstein-barr virus brlf1 by usf1 and rta. *The Journal of general virology*. 2015;96:2855-2866
15. Thakore PI, Black JB, Hilton IB, Gersbach CA. Editing the epigenome: Technologies for programmable transcription and epigenetic modulation. *Nature methods*. 2016;13:127-137
16. Konermann S, Brigham MD, Trevino AE, Joung J, Abudayyeh OO, Barcena C, Hsu PD, Habib N, Gootenberg JS, Nishimasu H, Nureki O, Zhang F. Genome-scale transcriptional activation by an engineered crispr-cas9 complex. *Nature*. 2015;517:583-588
17. Tanenbaum ME, Gilbert LA, Qi LS, Weissman JS, Vale RD. A protein-tagging system for signal amplification in gene expression and fluorescence imaging. *Cell*. 2014;159:635-646
18. Wangensteen KJ, Wang YJ, Dou Z, Wang AW, Mosleh-Shirazi E, Horlbeck MA, Gilbert LA, Weissman JS, Berger SL, Kaestner KH. Combinatorial genetics in liver repopulation and carcinogenesis with a in vivo crispr activation platform. *Hepatology*. 2018;68:663-676
19. Zhou H, Liu J, Zhou C, Gao N, Rao Z, Li H, Hu X, Li C, Yao X, Shen X, Sun Y, Wei Y, Liu F, Ying W, Zhang J, Tang C, Zhang X, Xu H, Shi L, Cheng L, Huang P, Yang H. In vivo simultaneous transcriptional activation of multiple genes in the brain using crispr-dcas9-activator transgenic mice. *Nature neuroscience*. 2018;21:440-446

20. Liao HK, Hatanaka F, Araoka T, Reddy P, Wu MZ, Sui Y, Yamauchi T, Sakurai M, O'Keefe DD, Nunez-Delicado E, Guillen P, Campistol JM, Wu CJ, Lu LF, Esteban CR, Izpisua Belmonte JC. In vivo target gene activation via crispr/cas9-mediated trans-epigenetic modulation. *Cell*. 2017;171:1495-1507 e1415
21. Kim Y, Phan D, van Rooij E, Wang DZ, McAnally J, Qi X, Richardson JA, Hill JA, Bassel-Duby R, Olson EN. The mef2d transcription factor mediates stress-dependent cardiac remodeling in mice. *J Clin Invest*. 2008;118:124-132
22. Kelli J. Carroll CAM, John McAnally, Douglas M. Anderson, Lorena Zentilin, Ning Liu, Mauro Giacca, Rhonda Bassel-Duby, and Eric N. Olson. A mouse model for adult cardiac-specific gene deletion with crispr/cas9. *Proceedings of the National Academy of Sciences of the United States of America*. 2015;113:338–343
23. Amoasii L, Hildyard JCW, Li H, Sanchez-Ortiz E, Mireault A, Caballero D, Harron R, Stathopoulou T-R, Massey C, Shelton JM, Bassel-Duby R, Piercy RJ, Olson EN. Gene editing restores dystrophin expression in a canine model of duchenne muscular dystrophy. *Science*. 2018
24. Martari M, Sagazio A, Mohamadi A, Nguyen Q, Hauschka SD, Kim E, Salvatori R. Partial rescue of growth failure in growth hormone (gh)-deficient mice by a single injection of a double-stranded adeno-associated viral vector expressing the gh gene driven by a muscle-specific regulatory cassette. *Hum Gene Ther*. 2009;20:759-766
25. Sebastian S, Faralli H, Yao Z, Rakopoulos P, Palii C, Cao Y, Singh K, Liu QC, Chu A, Aziz A, Brand M, Tapscott SJ, Dilworth FJ. Tissue-specific splicing of a ubiquitously expressed transcription factor is essential for muscle differentiation. *Genes Dev*. 2013;27:1247-1259
26. Creyghton MP, Cheng AW, Welstead GG, Kooistra T, Carey BW, Steine EJ, Hanna J, Lodato MA, Frampton GM, Sharp PA, Boyer LA, Young RA, Jaenisch R. Histone h3k27ac separates active from poised enhancers and predicts developmental state. *Proc Natl Acad Sci U S A*. 2010;107:21931-21936
27. Noack C, Iyer LM, Liaw NY, Schoger E, Khadjeh S, Wagner E, Woelfer M, Zafiriou MP, Milting H, Sossalla S, Streckfuss-Boemeke K, Hasenfuss G, Zimmermann WH, Zelarayan LC. Klf15-wnt-dependent cardiac reprogramming up-regulates shisa3 in the mammalian heart. *J Am Coll Cardiol*. 2019;74:1804-1819
28. O'Geen H, Henry IM, Bhakta MS, Meckler JF, Segal DJ. A genome-wide analysis of cas9 binding specificity using chip-seq and targeted sequence capture. *Nucleic Acids Res*. 2015;43:3389-3404
29. Yekelchyk M, Guenther S, Preussner J, Braun T. Mono- and multi-nucleated ventricular cardiomyocytes constitute a transcriptionally homogenous cell population. *Basic Res Cardiol*. 2019;114:36
30. Chavez A, Scheiman J, Vora S, Pruitt BW, Tuttle M, E PRI, Lin S, Kiani S, Guzman CD, Wiegand DJ, Ter-Ovanesyan D, Braff JL, Davidsohn N, Housden BE, Perrimon N, Weiss R, Aach J, Collins JJ, Church GM. Highly efficient cas9-mediated transcriptional programming. *Nature methods*. 2015;12:326-328
31. Kearns NA, Genga RM, Enuameh MS, Garber M, Wolfe SA, Maehr R. Cas9 effector-mediated regulation of transcription and differentiation in human pluripotent stem cells. *Development*. 2014;141:219-223

32. Braun CJ, Bruno PM, Horlbeck MA, Gilbert LA, Weissman JS, Hemann MT. Versatile in vivo regulation of tumor phenotypes by dcas9-mediated transcriptional perturbation. *Proceedings of the National Academy of Sciences of the United States of America*. 2016;113:E3892-3900
33. Pickrell JK, Gaffney DJ, Gilad Y, Pritchard JK. False positive peaks in chip-seq and other sequencing-based functional assays caused by unannotated high copy number regions. *Bioinformatics*. 2011;27:2144-2146
34. Goyal A, Myacheva K, Gross M, Klingenberg M, Duran Arque B, Diederichs S. Challenges of crispr/cas9 applications for long non-coding rna genes. *Nucleic acids research*. 2017;45:e12
35. Maeder ML, Linder SJ, Cascio VM, Fu Y, Ho QH, Joung JK. Crispr rna-guided activation of endogenous human genes. *Nature methods*. 2013;10:977-979
36. Cheng AW, Wang H, Yang H, Shi L, Katz Y, Theunissen TW, Rangarajan S, Shivalila CS, Dadon DB, Jaenisch R. Multiplexed activation of endogenous genes by crispr-on, an rna-guided transcriptional activator system. *Cell research*. 2013;23:1163-1171
37. Lin S, Ewen-Campen B, Ni X, Housden BE, Perrimon N. In vivo transcriptional activation using crispr/cas9 in drosophila. *Genetics*. 2015;201:433-442
38. Chavez A, Tuttle M, Pruitt BW, Ewen-Campen B, Chari R, Ter-Ovanesyan D, Haque SJ, Cecchi RJ, Kowal EJK, Buchthal J, Housden BE, Perrimon N, Collins JJ, Church G. Comparison of cas9 activators in multiple species. *Nature methods*. 2016;13:563-567
39. Parsi KM, Hennessy E, Kearns N, Maehr R. Using an inducible crispr-dcas9-krab effector system to dissect transcriptional regulation in human embryonic stem cells. *Methods in molecular biology*. 2017;1507:221-233
40. Hilton IB, D'Ippolito AM, Vockley CM, Thakore PI, Crawford GE, Reddy TE, Gersbach CA. Epigenome editing by a crispr-cas9-based acetyltransferase activates genes from promoters and enhancers. *Nature biotechnology*. 2015;33:510-517
41. Guo Y, VanDusen NJ, Zhang L, Gu W, Sethi I, Guatimosim S, Ma Q, Jardin BD, Ai Y, Zhang D, Chen B, Guo A, Yuan GC, Song LS, Pu WT. Analysis of cardiac myocyte maturation using casaav, a platform for rapid dissection of cardiac myocyte gene function in vivo. *Circ Res*. 2017;120:1874-1888
42. Maddalo D, Manchado E, Concepcion CP, Bonetti C, Vidigal JA, Han YC, Ogrodowski P, Crippa A, Rekhtman N, de Stanchina E, Lowe SW, Ventura A. Corrigendum: In vivo engineering of oncogenic chromosomal rearrangements with the crispr/cas9 system. *Nature*. 2015;524:502

Figure 1

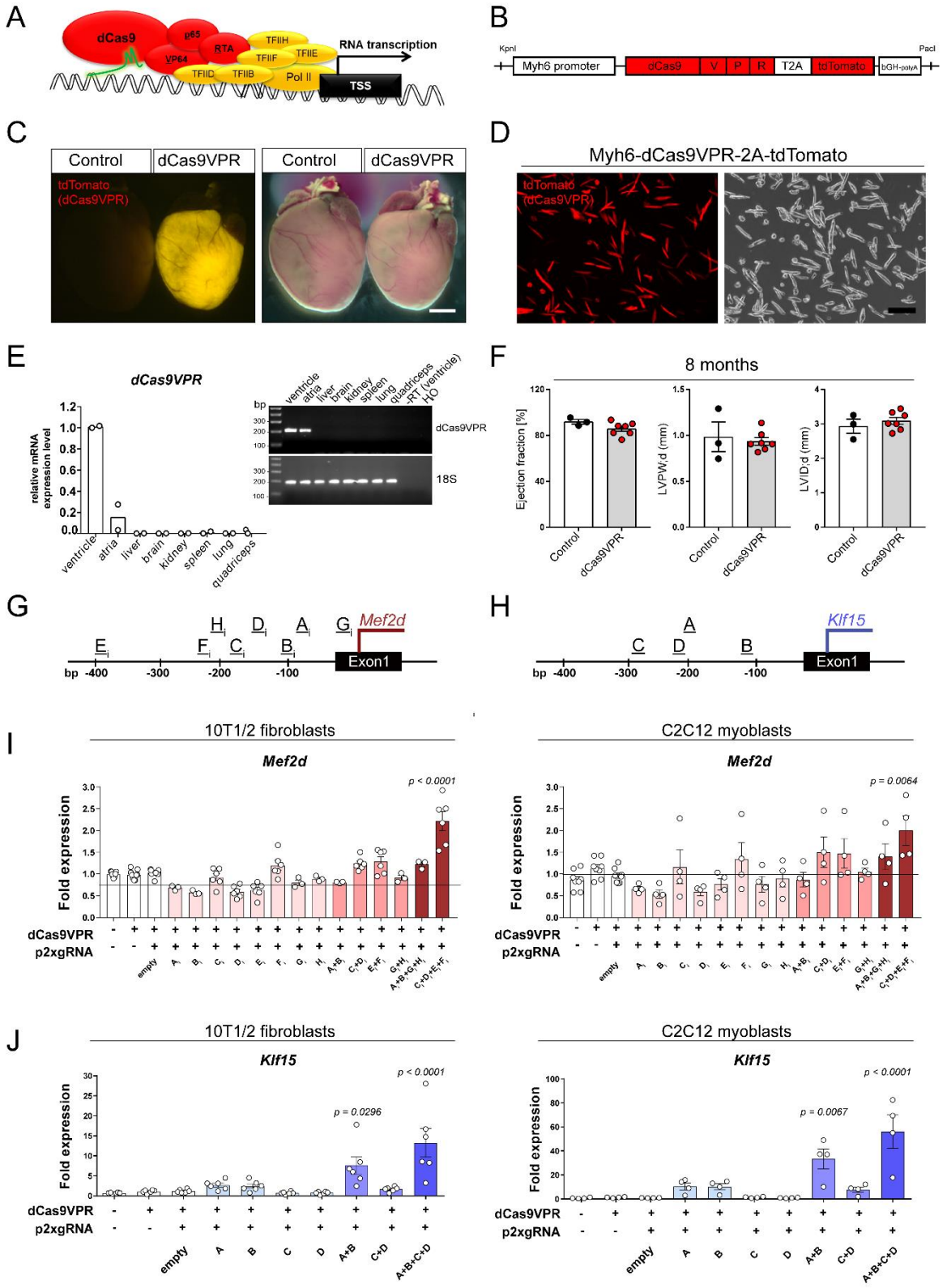

Figure 1: Cardiomyocyte-specific expression of dCas9VPR-2A-tdTomato and validation of gRNAs for efficient transcriptional activation induction of *Klf15* and *Mef2d in vitro*. A. Schematic representation of dCas9VPR in *Myh6*-expressing cells, targeting the 5' upstream region of the TSS, guided by specific gRNAs for recruitment of the transcriptional machinery

and **B** the construct used for dCas9VPR integration. **C.** Representative images of *Myh6*-dCas9VPR adult transgenic heart (line 1, high) showed homogenous and robust expression of the transgene as demonstrated by tdTomato reporter compared to a wild-type age- and sex-matched heart (2 months-old). **D.** Cardiomyocytes from *Myh6*-dCas9VPR mice were isolated showing transgene expression in >80% of cardiomyocytes (4 weeks-old, line 1, high). **E.** RT qPCR confirmed dCas9VPR transcript expression exclusively in the ventricular and, to a lesser extent, in atrial tissue of *Myh6*-dCas9VPR transgenic mice (line 1, high). **F.** Echocardiography of 8 months old transgenic mice (line 1, high) exhibit no phenotype with constitutive dCas9VPR expression (n≥3 per group). **G-H.** Indicated gRNAs targeting *Mef2d* 5' (G) and *Klf15* (H) 5' upstream TSS region were selected for *in vitro* testing in C3H/10T/1/2 and C2C12 cells transfected with CMV-dCas9VPR construct. **I-J.** Co-transfection of single and combined gRNAs with p-2xgRNA constructs induced *Mef2d* and *Klf15* transcription at different levels (n≥3). *18S* was used as a control and all data are normalized to control groups. Statistics: error bars depict mean ± SEM, one-way ANOVA with Bonferroni's post-hoc multiple comparison test. Scale bar = (C) 2 mm; (D) 200 µm.

Figure 2

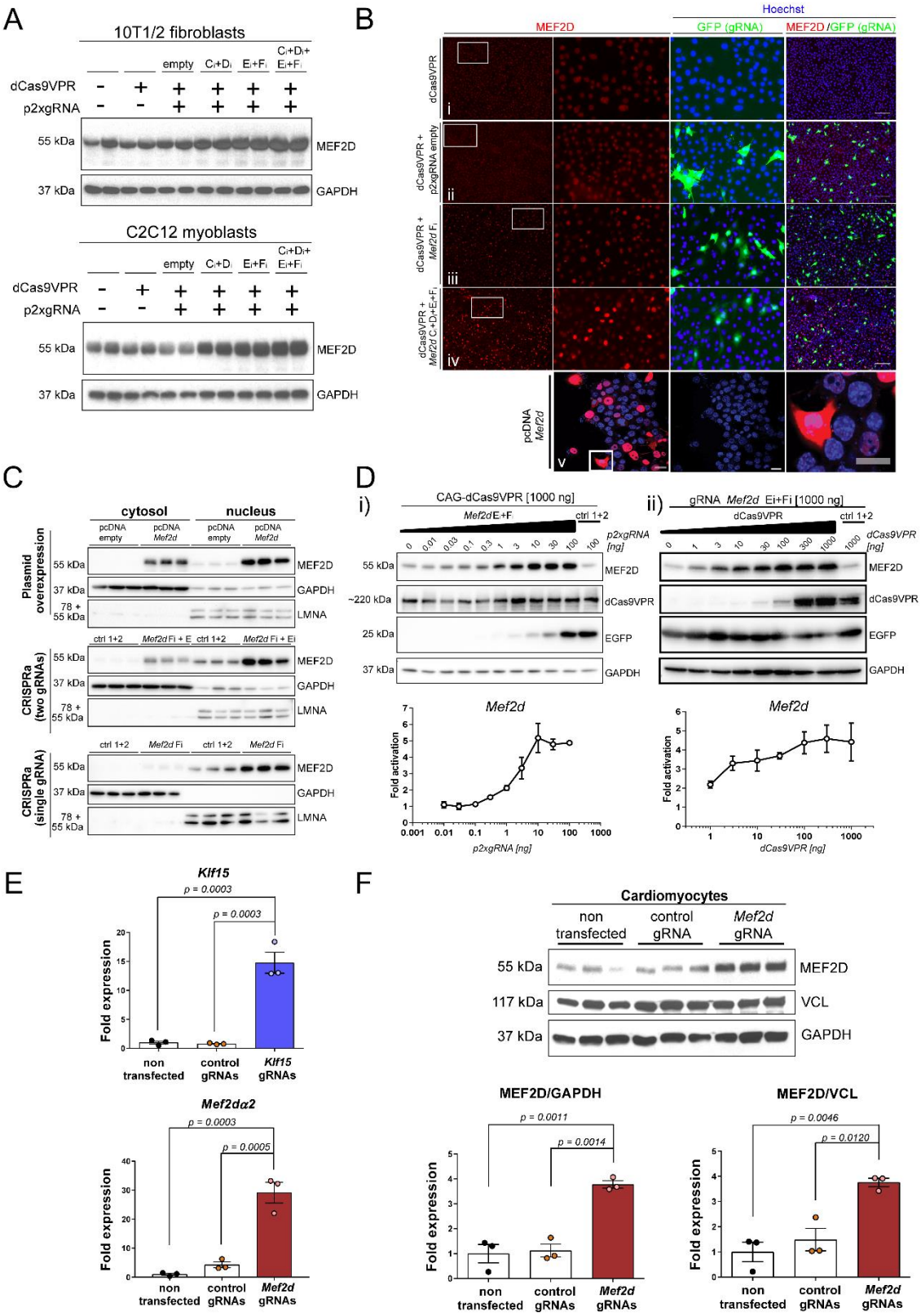

Figure 2: Endogenous activation of *Klf15* and *Mef2d* by selected gRNAs *in vitro*. A. C3H/10T/1/2 and C2C12 cells were transfected with CMV-dCas9VPR and p-2xgRNA containing 2xgRNA constructs. Activation of *Mef2d* was confirmed on protein level by immunoblots using combinations of gRNAs as indicated. **B.** Immunofluorescence (overview

and magnification images) of C3H/10T/1/2 showing increased MEF2D in gRNA *Mef2d* transfected cells. Panel showing transfected cells with (i) CMV-dCas9VPR; (ii) CMV-dCas9VPR and empty p-2xgRNA; (iii) CMV-dCas9VPR and single gRNA (F_i) and (iv) CMV-dCas9VPR and combinations of 4 gRNAs, which showed more efficient MEF2D induced expression in GFP-positive cells. (v) Conventional *Mef2d*-cDNA-overexpression in Neuro2a cells shows MEF2D abundance in the nucleus and cytosol. **C.** Subcellular fractionation and immunoblotting showing cytosolic MEF2D abundantly detectable in conventional plasmid overexpression and reduced cytosolic abundance when two gRNAs were used for CRISPRa-mediated *Mef2d* activation. Single gRNA use prevented cytosolic presence of MEF2D. Increased MEF2D protein levels in the nucleus were detectable in all cases. **D.** Titration of CRISPRa components revealed a stronger dependency of *Mef2d* activation (ii) on dCas9VPR presence than (i) on gRNA expression, while remaining components were co-transfected at constant level. MEF2D fold protein level was normalized to either only dCas9VPR or p-2xgRNA control 1+2 construct transfected cells. Transfections were performed in Neuro2a cells, n=3 technical replicates and see Online Figure IV and V for additional information. Each concentration depicts mean ± SEM. **E.** *In vitro* transcribed and transfected gRNAs (A, B, C for *Klf15* and C_i, F_i, G_i for *Mef2d*) showing 30- and 15-fold increase for *Mef2d* and *Klf15*, respectively in Myh6-dCas9VPR-2A-tdTomato-cardiomyocytes *in vitro*. **F.** Immunoblot and densiometric analyses of these cardiomyocytes confirming elevated MEF2D protein levels in CRISPRa-*Mef2d* cardiomyocytes. For immunoblots, (A, C, D, F) GAPDH, (C) Lamin A (LMNA) and (D) Vinculin (VCL) were used as loading controls. (E) *18S* expression served as control and groups are normalized to non-transfected cardiomyocytes group. Statistics in E and F: n≥3 technical replicates, error bars depict mean ± SEM, one-way ANOVA with Bonferroni's post-hoc multiple comparison test. Scale bar = (B i-iv) 200 µm; (v) 10 µm.

Figure 3

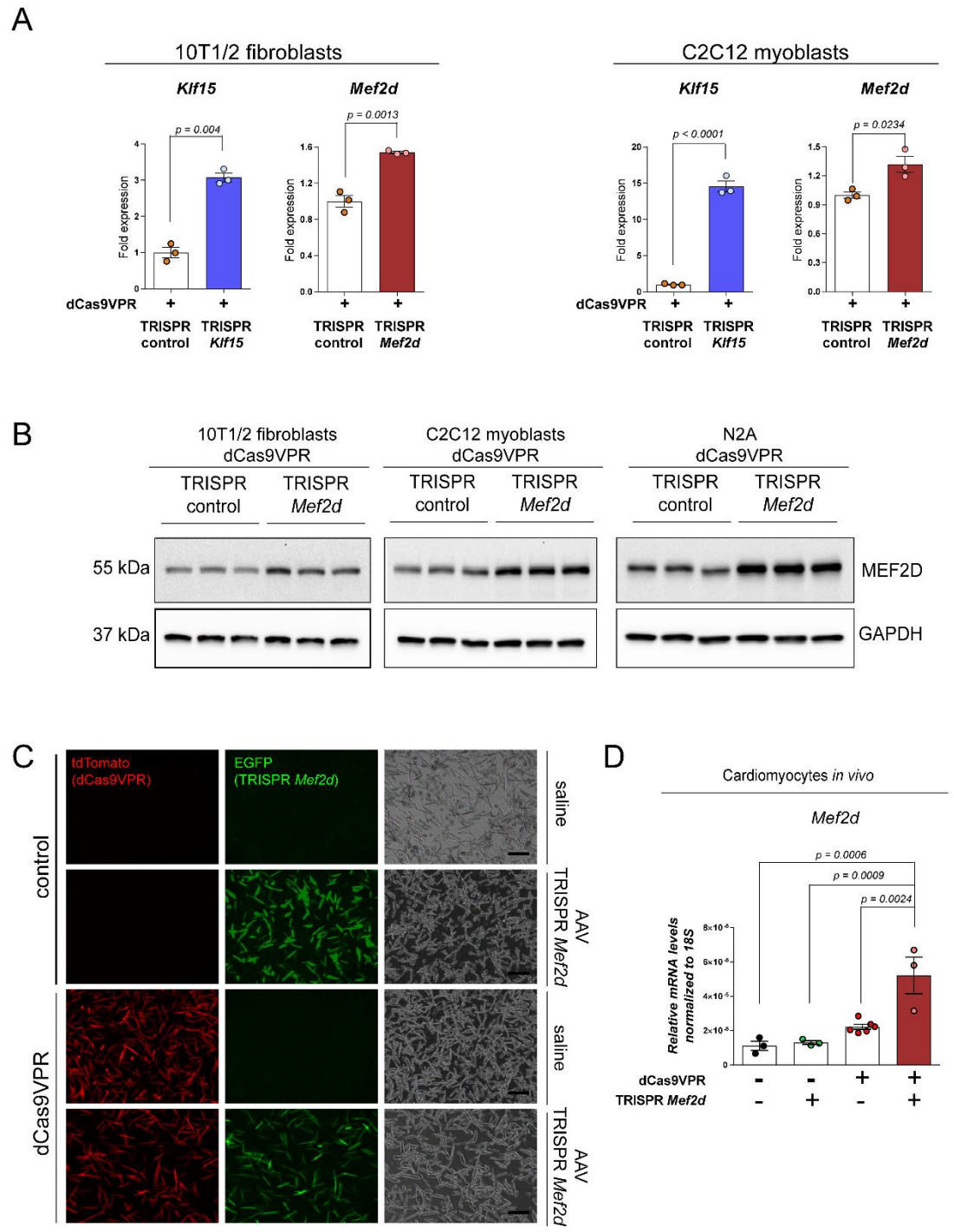

Figure 3: The CRISPRa (dCas9VPR/TRISPR) system induces endogenous gene activation in cardiomyocytes *in vitro*. A. Significant *Mef2d* and *Klf15* activation in C3H/10T/1/2 and C2C12 cells transfected with CMV-dCas9VPR and corresponding TRISPR constructs (gRNAs A, B, C for *Klf15* and C_i, F_i, G_i for *Mef2d*) (n=3, technical replicates). *18S* served as loading control and transcript levels are normalized to TRISPR control group. **B.** TRISPR construct induced MEF2D protein increase in C3H/10T/1/2 and C2C12 constitutively expressing dCas9VPR as well as in Neuro2a cells that were transiently transfected with both components. TRISPR construct encoding for three non-targeted gRNAs served as control. GAPDH was used as loading control. **C.** CRISPRa components expression was additionally

confirmed in cardiomyocytes by immunofluorescence of 4 weeks old Myh6-dCas9VPR animals (line 1, high) injected with AAV9 TRISPR *Mef2d* at P4**. D.** Elevated *Mef2d* transcript levels compared to controls were confirmed in these cardiomyocytes by qPCR. *18S* was used to normalize transcript levels. n=3 per group. Statistics: error bars depict mean ± SEM, in (A) student's t-test, in (D) one-way ANOVA with Bonferroni's post-hoc multiple comparison test. Scale bar = (C) 200 µm

Figure 4

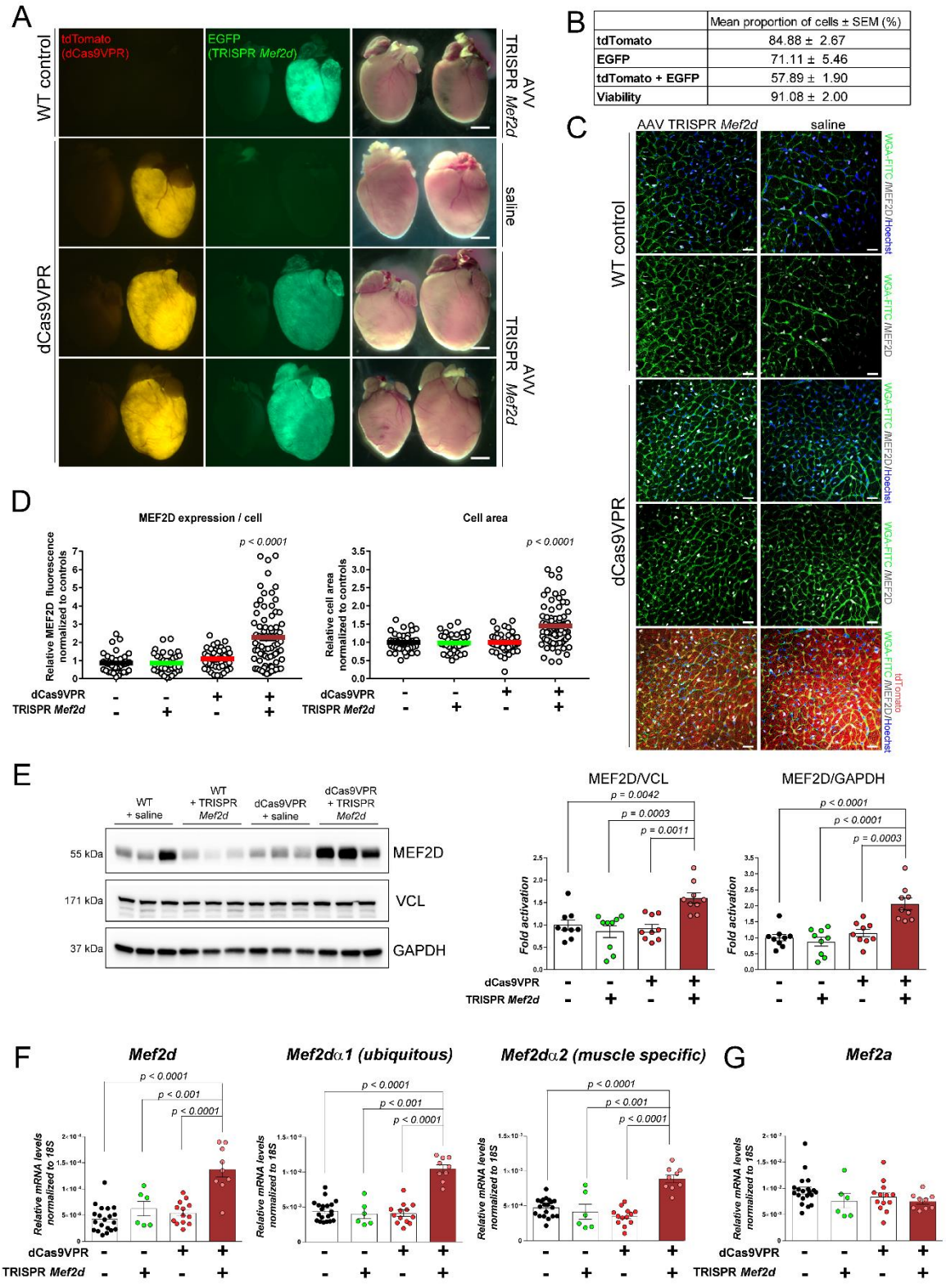

Figure 4: CRISPRa-mediated endogenous activation of *Mef2d* in the postnatal heart. A. Representative hearts of controls (wild-type littermates injected with saline or TRISPR-*Mef2d* and CRISPRa transgenic mice injected with saline) and CRISPRa mice injected with AAV9-TRISPR-*Mef2d*. CRISPRa-*Mef2d* resulted in enlarged ventricles compared to controls. **B.** Quantification of tdTomato transgene and GFP expression from transduced cardiomyocytes

(n=3 mice, ≥200 cardiomyocytes/mouse). Mean proportion of fluorescent cells are depicted as percentage ± SEM. **C.** Immunostaining and confocal images of dCas9VPR and AAV9-TRISPR-*Mef2d* hearts show increased MEF2D protein level (white) in cardiomyocyte nuclei (blue) compared to controls. **D.** MEF2D expression and cardiomyocyte cross-sectional area (WGA-FITC staining, green) were quantified confirming increased MEF2D abundance and cardiomyocyte size. Statistics (D) n≥36 cells per condition in ≥3 imaged areas. **E.** Immunoblotting and densiometric analyses showing increased MEF2D expression in CRISPRa-*Mef2d* hearts compared to controls. MEF2D protein level was normalized to VCL and GAPDH. **F.** Total *Mef2d* transcripts as well as *Mef2d* splice variants mRNA levels were elevated compared to controls. **G.** *Mef2* gene family member *Mef2a* was unchanged. *18S* was used to normalize transcript levels. Statistics: (E) n≥6 per group and 3 independent immunoblots, (F-G) n≥6 per group, error bars depict mean ± SEM, one-way ANOVA with Bonferroni's post-hoc multiple comparison test. Scale bar in (A) = 2 mm, in (C) = 25 µm.

Figure 5

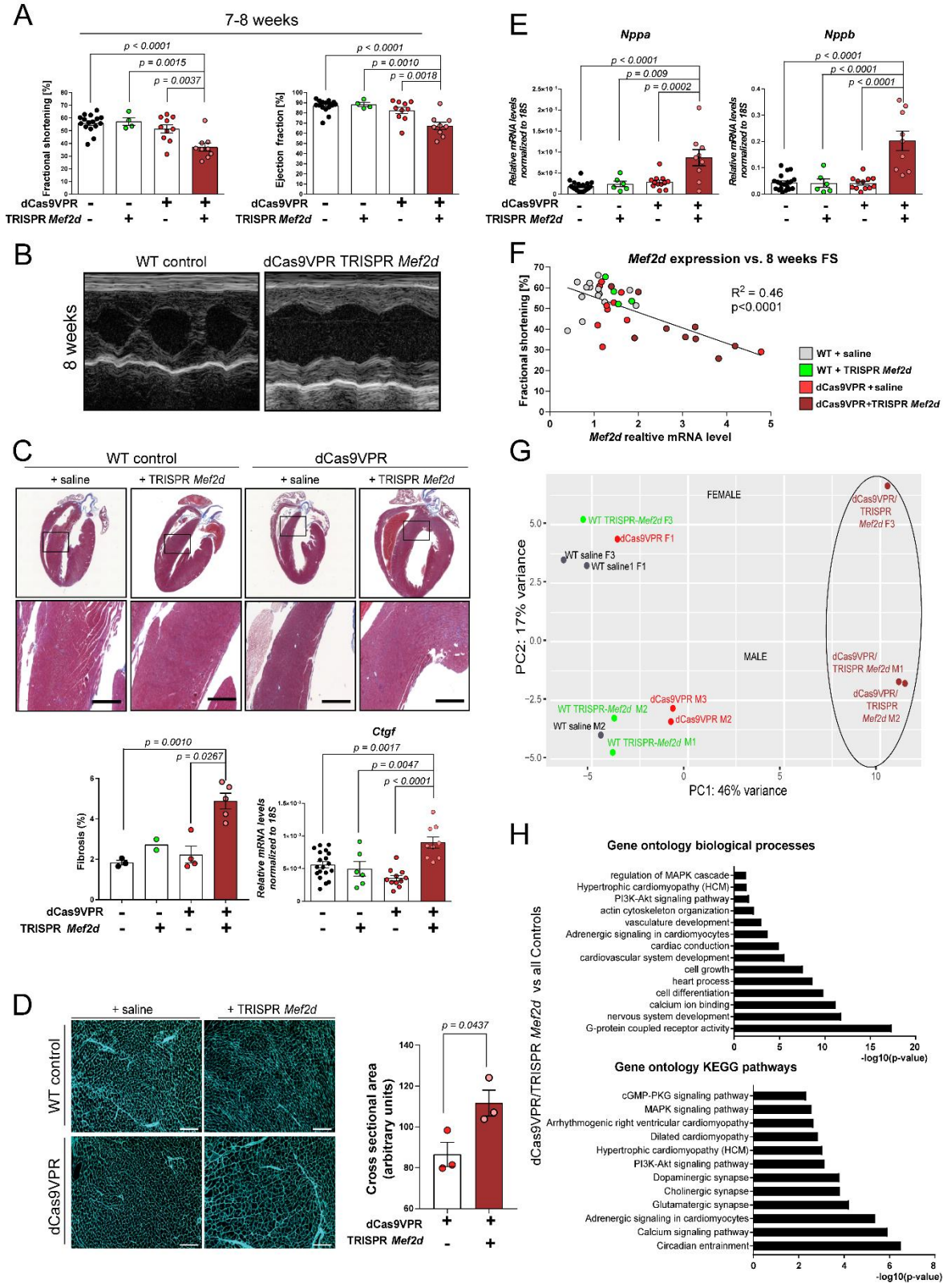

Figure 5: CRISPRa-mediated endogenous activation of *Mef2d* exhibits a cardiac hypertrophic phenotype. A. *Mef2d* activated hearts exhibit decreased fractional shortening and ejection fraction at 7-8 weeks post-injection compared to control groups. Statistics: n≥4 per group and time point, error bars depict ± SEM, one-way ANOVA with Bonferroni's post-hoc

multiple comparison test. **B.** Representative M-Mode images from echocardiography analyses revealed dilation of the left ventricular chamber compared to controls. **C.** Trichrome staining and magnifications of indicated areas, collagen deposition quantification ($n \geq 2$ hearts per group, mean ± SEM, one-way ANOVA with Bonferroni's post-hoc multiple comparison test.) and elevated transcript level of fibrosis marker *Ctgf* ($n \geq 6$ hearts per group, mean ± SEM, one-way ANOVA with Bonferroni's post-hoc multiple comparison test.) suggest increased collagen deposition in *Mef2d* activated hearts compared to controls. **D.** Quantification of cardiomyocyte cross-sectional area and representative WGA-FITC staining. Statistics: n=3 areas per group, student's t-test. Scale bar (Trichrome) = 200 µm; (WGA-FITC) = 50 µm. **E.** Elevated cardiac remodeling markers (*Nppa* and *Nppb*) in *Mef2d* activated hearts compared to controls. *18S* was used for normalization. Statistics: $n \geq 6$ per group, error bars depict ± SEM, one-way ANOVA with Bonferroni's post-hoc multiple comparison test, outlier test excluded 3 data points for *Nppa* analysis. **F.** Correlation plot of fractional shortening versus *Mef2d* transcript levels indicating decreasing heart function with increasing *Mef2d* expression. **G.** RNA-sequencing of dCas9VPR TRISPR *Mef2d* hearts showed distinct separation from all control groups in principle component analysis. **H.** GO and KEGG pathway analysis of DEGs ($log2FC \geq 0.5$ $P \leq 0.05$) revealed cardiomyopathy related processes and pathways in *Mef2d* activated hearts compared to controls.

Figure 6

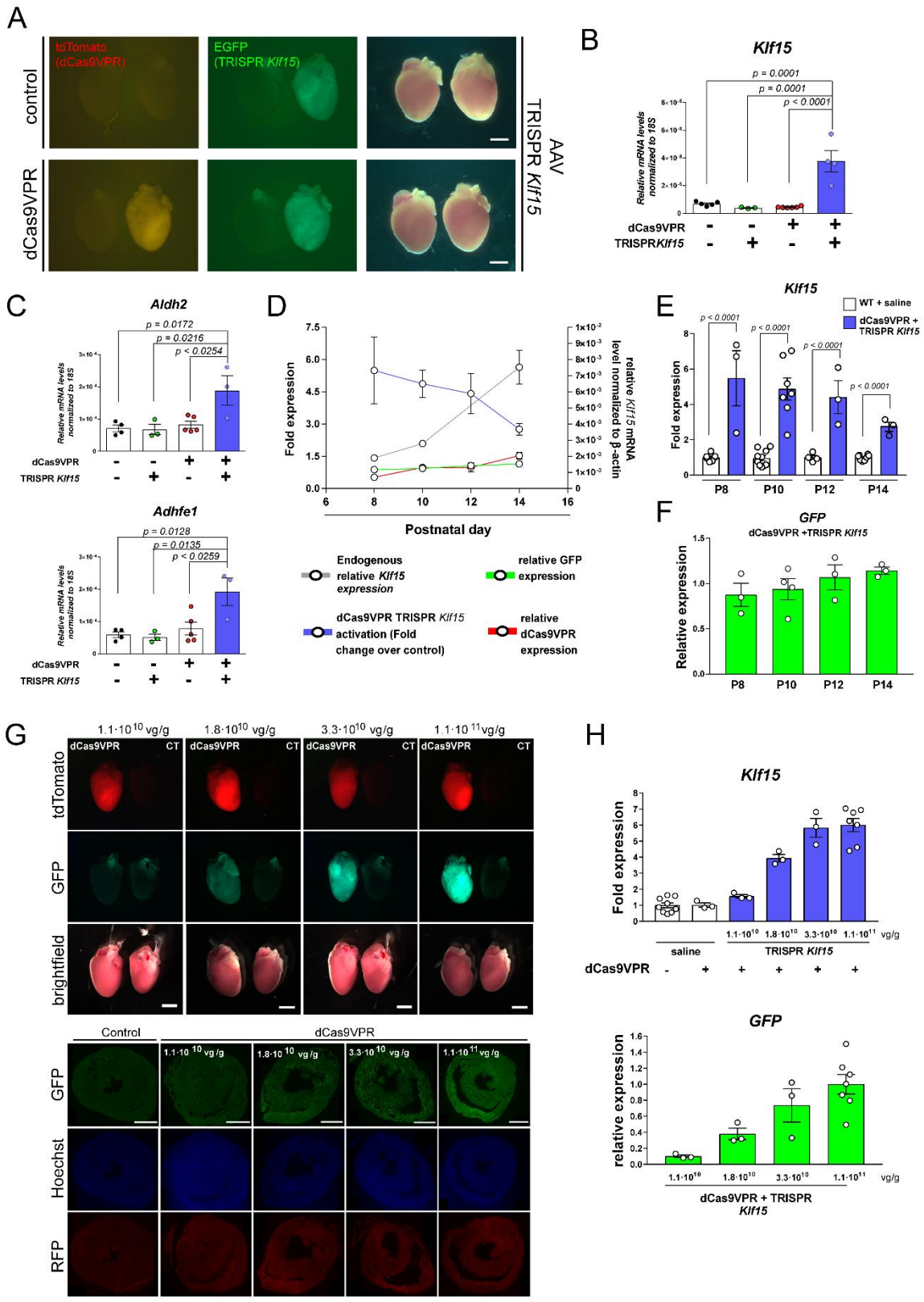

Figure 6: Endogenous activation of *Klf15* in the neonatal heart. A. Representative P10 transgenic hearts showing dCas9VPR-2A-tdTomato expression and successful TRISPR *Klf15* delivery based on tdTomato and GFP reporter signals (Line 1, high). **B.** Significant increase in *Klf15* transcript levels (line 1, high) and **(C)** its target genes *Aldh2* and *Adhfe1* at postnatal day

10 compared to control groups was observed (wild-type littermates injected with saline or TRISPR *Klf15* and dCas9VPR transgenic mice injected with saline). Transcript levels were normalized to *18S*. **D.** *Klf15* activation over a time period between P8 and P14 decreases (blue line) was compared to physiological *Klf15* induction over the same period (grey line). **E.** *Klf15* activation normalized to control littermates used for activation potential depiction in D. *Tbp* or *β-actin* was used to normalize transcript levels. **F.** GFP (indirect marker for gRNA expression) remained unchanged over this time period. GFP transcript levels were normalized to *Tbp*. **G.** Titration of AAV delivered TRISPR *Klf15* showed increasing GFP positive cardiomyocytes with increasing viral titer, indicative of gRNA expression (upper panel whole heart images; lower panel cryosections of the hearts with respective immunofluorescence detecting GFP and tdTomato (RFP). **H.** More importantly, increasing *Klf15* transcript levels accompanied by increasing GFP expression was detectable indicating titratability of the *in vivo* CRISPRa system. Statistics: n (B and C) ≥3 per groups, n (D, E and F) ≥3 per time point, n (G, H) ≥3 per condition, error bars depict mean ± SEM, (B-C) one-way ANOVA with Bonferroni's post-hoc multiple comparison test, (E) student's t-test. Scale bar (A and G) = 2 mm.

Figure 7

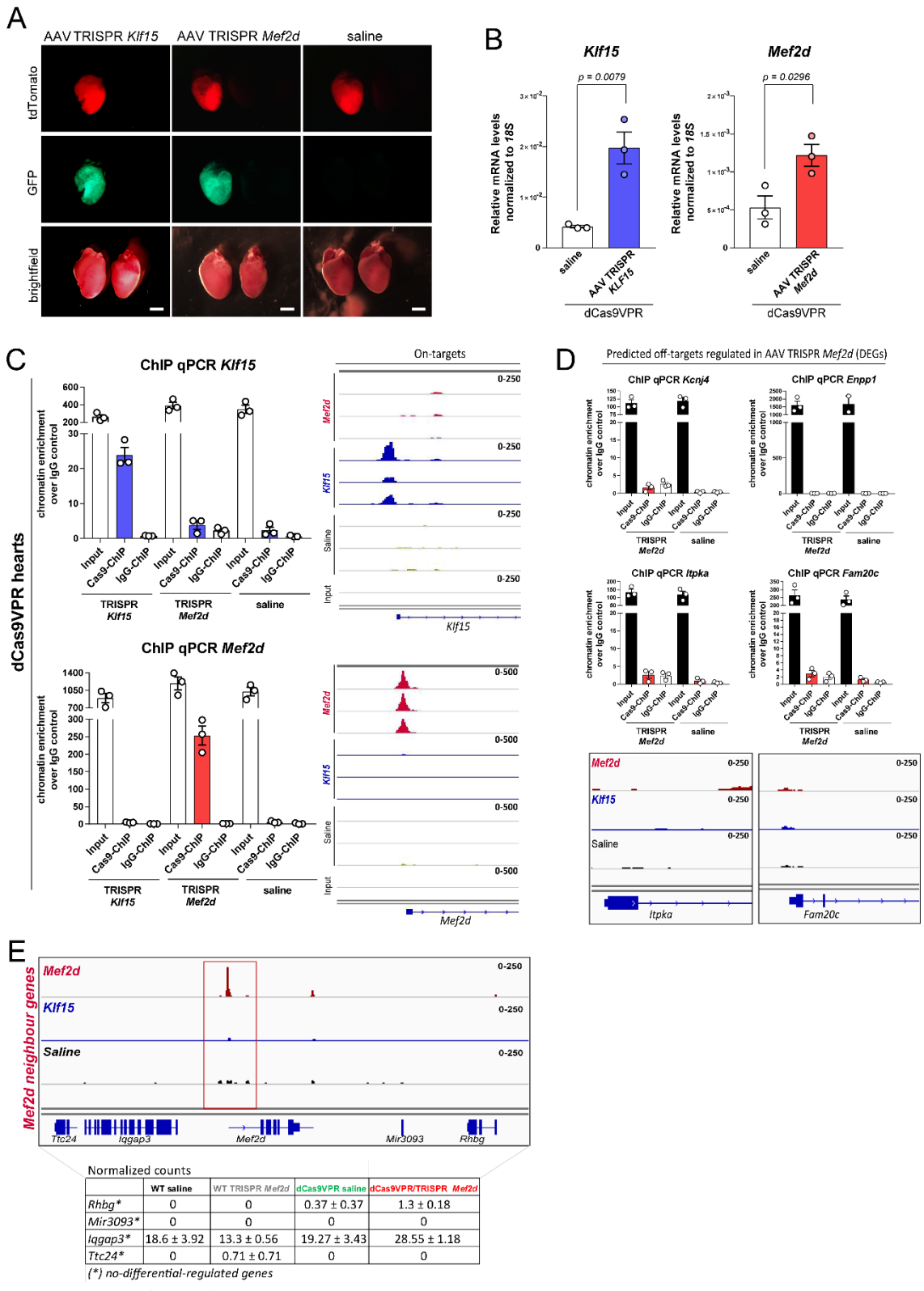

Figure 7: Assessment of on- and off-target activity by chromatin immunoprecipitation (ChIP) of dCas9VPR *in vivo*. A. Representative P14 hearts of dCas9VPR mice (line 1, high) injected with indicated AAV TRISPR *Mef2d* and *Klf15* or saline at P4 and subjected to ChIP. **B.** Gene activation of the respective target was confirmed in these hearts by qPCR. *18S* was

used for normalization. **C.** ChIP qPCR and ChIP-seq results for gRNA targeting sites confirmed dCas9VPR association to its on-targets (*Mef2d* and *Klf15) in vivo*, while (**D)** no chromatin association to *Mef2d* predicted off target sites was detectable by ChIP qPCR and ChIP-seq. **E.** Overview of dCas9VPR occupancy profiles showing dCas9VPR enrichment on on-target *Mef2d* site and indication of neighboring genes, which were not significantly regulated at transcript levels in AAV TRISPR *Mef2d* mice. Statistics: n=3 hearts per group, error bars depict mean ± SEM, (B) student's t-test. Scale bar (A) = 2 mm.

Figure 8

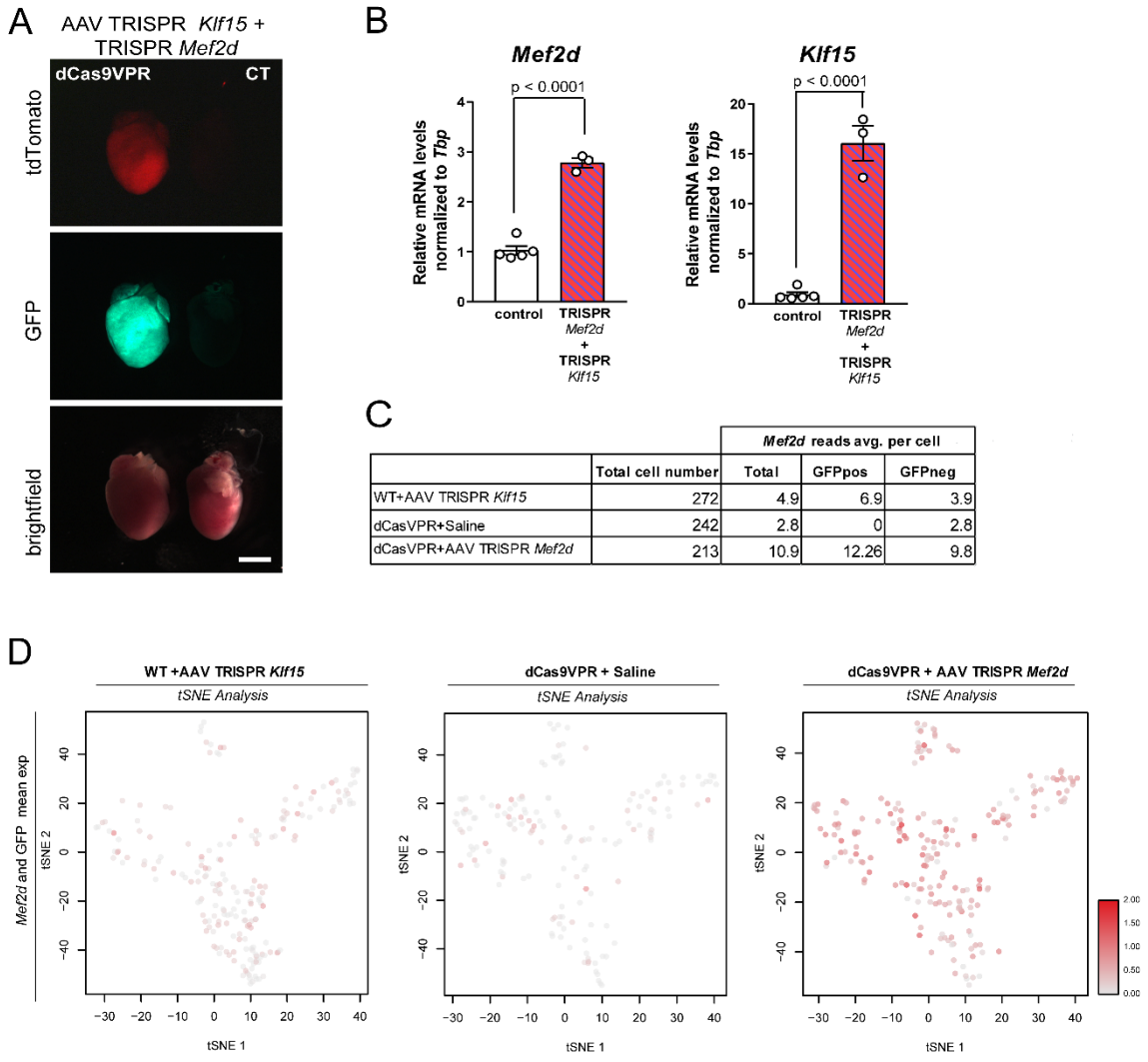

Figure 8: Double activation of *Mef2d* and *Klf15* in the neonatal heart and *Mef2d* activation at single cell resolution. A. P4 dCas9VPR mice (Line 1, high) were injected with 5.5 x 10^{10} vg/g of TRISPR *Mef2d* and TRISPR *Klf15*. **B.** *Mef2d* and *Klf15* mRNA was evaluated at P10 showing significantly increased transcript levels for both targets when compared to control hearts. Transcript levels were normalized to *Tbp*. Statistics: n≥3 hearts per group, error bars depict mean ± SEM, student's t-test. Scale bar (A) = 2 mm. **C.** Table summarizing the single cell sequencing experimental overview and data on percentage of cells and average (avg.) mean reads per cell for the three conditions: AAV TRISPR *Mef2d*-, saline-treated dCas9VPR and wild-type mice with AAV9 TRISPR *Klf15* as controls. **D.** t-SNE-based cell clustering showing the expression gradient of *Mef2d* and GFP transcripts in the different samples and

demonstrating transcriptional differences among cells and a consistently higher *Mef2d* gradient in AAV9 TRISPR *Mef2d* hearts.

Supplemental Material

Section I

Detailed Methods

dCas9VPR transgenic mouse generation

Animal experiments were approved by the IACUC of the University of Texas Southwestern Medical Center and the Lower Saxony Animal Review Board (LAVES, AZ-G15-1840). The human codon optimized dCas9VPR coding region was amplified from SP-dCas9-VPR plasmid (a kind gift from George Church's lab, Addgene plasmid #63798) and cloned into Myh6-Cas9-2A-tdTomato backbone by HD Infusion cloning (TAKARA),[1] where the Cas9 coding region was removed by NheI (Thermo Fisher Scientific) and BshTI (Thermo Fisher Scientific) digestion, using the following primers: infusion fwd: 5' TTGAGTCGACACCGGATGGGCGGTAGGCGTGTAC 3' and infusion rev: 5' CTCTGCCCTCGCTAGTCAAAACAGAGATGTGTCGAAGATGGAC 3'. The stop codon of dCas9VPR was exchanged for a glycine codon using a QuickChange site-directed mutagenesis (Agilent) approach using the following primers: mutagenesis fwd: 5' CACATCTCTGTTTGGAGCTAGCGAGGGCAGAGGAAGTC 3' and mutagenesis rev: 5' GACTTCCTCTGCCCTCGCTAGCTCCAAACAGAGATGTG 3'. The KpnI/PacI (NEB) linearized Myh6-dCas9VPR-2A-tdTomato construct was injected into the pronucleus of mouse zygotes from B6C3F1 or C57/BL6N mice (Charles River), which were implanted into pseudo-pregnant ICR mice (Envigo). Offspring was considered as independent mouse lines and founders. Mice were crossed to C57/BL6N wild-type mice in the subsequent generations. DNA for genotyping was isolated from tails by incubation in 100 µl Lysis Buffer (25 mM NaOH, 0.2 mM EDTA, pH 12) for 20 min at 95 °C and subsequent neutralization with 40 mM TRIS-HCl, pH 5. Genotyping PCR was conducted using the following primers: dCas9VPRgeno fwd: 5' TGGCCAAATGGACCTTTCCCATC 3' and dCas9VPRgeno rev: 5' GTTCATGGAGCCCTCCATGC 3' followed by gel electrophoresis of PCR products. Hearts were analyzed for transgene expression by stereomicroscopy (Axio Zoom.V16, Zeiss). For *in vivo* CRISPRa, mice were injected intraperitoneally at postnatal day 4 (P4) with 1.1E11 vg/g if not otherwise stated in a total volume of AAV2/9 diluted in saline of 80 µl. Saline was used for control injections. For *Mef2d* activation, cardiac function was checked 4-5 weeks and 7-8 weeks post-injection using a Visual SonicsVevo 2100 system with a 35-MHz transducer. Fractional Shortening (FS) and Ejection Fraction (EF) were determined by Left Ventricle Internal Dimension at Diastole (LVIDd) and Left Ventricle Internal Dimension at Systole (LVIDs) using the following formulas: $FS(\%)=[(LVIDd - LVIDs)/LVIDd] \times 100$ and $EF(\%)=[[(LVIDd^2 - LVIDs^2)/LVIDd^2]+[1-(LVIDd^2 - LVIDs^2)/LVIDd^2]] \times 0.15$. The investigator was unaware of the genotypes and treatments.

gRNAs constructs

For gRNA design, Ensembl genome browser derived sequences for the 5' TSS upstream region of *Klf15* and *Mef2d* were used and gRNAs where designed using e-crispr.org (German Cancer Research Center). Control gRNAs do not bind with less than three mismatches in the mouse genome as determined using rgenome.net/cas-offinder (Center for Genome Engineering at IBS, Korea) and cm.jefferson.edu/Off-Spotter/ (Computational Medicine Center, University Thomas Jefferson University, United States of America) (a list of gRNA is provided in Online Table III). For *in vitro* experiments, the dual gRNA expression construct pX333 (a kind gift from Andrea Ventura, Addgene plasmid #64073) was modified by removing the Cas9 coding sequence by BshTI (Thermo Fisher Scientific), Eco32I (Thermo Fisher Scientific) and NotI (Thermo Fisher Scientific) digestion followed by EGFP reporter integration that was derived from pEGFP-N1 (Clontech) extracted by NsiI (Thermo Fisher Scientific) and NotI (Thermo Fisher Scientific) digestion (=p-2xgRNA). Oligonucleotides encoding for gRNAs targeted to the promoter region of *Mef2d* or *Klf15* were cloned into p-2xgRNA using the BbsI (NEB) or BsaI (NEB) restriction sites. For the TRISPR plasmid (a kind gift from Dirk Grimm, modified by Stephen Hauschka and Leonela Amoasii,[2-4] selected gRNAs were cloned into donor plasmids and assembled via two consecutive Golden Gate Assembly reactions. Briefly, for each gRNA, 40 fmol of donor backbone (U6 Golden Gate Donor plasmid/H1 Golden Gate Donor plasmid/7SK Golden Gate Donor plasmid were combined with 1 µl of 5 µM PNK (NEB) phosphorylated annealed oligonucleotides, 0.75 µl Esp3I (Thermo Fisher Scientific), 1 µl Buffer Tango (Thermo Fisher Scientific), 1 µl T4 DNA Ligase (NEB) and a final concentration of 1 mM ATP and 1 mM of DTT brought to a total volume of 10 µl, respectively. Reaction was conducted for 90 min at 37 °C followed by 5 min at 20 °C and enzyme inactivation at 80 °C for 20 min. Products were transformed into One-Shot Stabl3 Chemically Competent E.coli (Thermo Fisher Scientific) and grown for 16 h on LB-chloramphenicol agar plates (25 µg/ml) at 37 °C. Donor plasmids were assembled with AAV acceptor plasmid by combining 20 fmol of each donor plasmid and AAV9 acceptor plasmid, 0.75 µl BpiI (Thermo Fisher Scientific), 2 µl Buffer G (Thermo Fisher Scientific), 0.5 µl T4 DNA Ligase (NEB) and a final concentration of 1 mM ATP and 1 mM of DTT brought to a total volume of 20 µl. Reaction was conducted for 90 min at 37 °C followed by 5 min at 20 °C and enzyme inactivation at 80 °C for 20 min. Products were transformed into One-Shot Stabl3 Chemically Competent E.coli (Thermo Fisher Scientific) and grown for 16 h on LB-Ampicillin agar plates (100 µg/ml) at 37 °C. ITR integrity was checked by XmaI and KpnI (NEB) digestion and subsequent gel electrophoresis. AAV2/9 particles were synthesized by the Boston Children's Hospital Virus Core Facility or at the Department of Cardiology, Heidelberg University Hospital, Heidelberg, Germany as previously published.[5] Briefly, AAV9 vectors were generated by co-transfection of the helper plasmid, pDG-9 (a gift from Dr. Roger Hajjar), with each TRISPR construct in HEK293T cells. To prepare the recombinant AAV9, HEK293T cells (TAKARA, catalogue #632273) were plated at a density of 1.5×10^6 per 150 mm culture dish and maintained in DMEM (Sigma, catalogue #5796) containing 10% FBS and penicillin/streptomycin at 37 °C and 5% CO_2. For each virus preparation, 48 flasks were used. Seventy-two hours after plating, cultures were transfected using Polyethylenimine "Max" (MW 40,000, Polysciences, catalogue # 24765) with 15µg of helper plasmid and 5 µg of TRISPR plasmid, which were mixed with 1 ml of DMEM (no antibiotics) and 160 µl of polyethylenimine (0.517 mg/ml), vortexed for 30 seconds, and

incubated for 15 min at room temperature. This was then mixed with 18 ml DMEM containing 10% FBS and penicillin/streptomycin for replacing the culture media. The cultures were then rocked intermittently for 15 min before incubation. Three days after transfection, the cells collected from six 150 mm plates were centrifuged at 500 × g for 10 min and resuspended in 10 ml of lysis buffer (150 mM NaCl, 50 mM Tris-HCL; pH 8.5). The resuspended cells were then subjected to three rounds of freeze-thaw, followed by treatment with benzonase (1500 U benzonase; Novagen) and 1 mM $MgCl_2$ at 37 °C for 30 min. The cell debris was collected by centrifugation at 3,400 × g for 20 min. The supernatant obtained from six 150 mm plates containing the AAV9 was then purified on an iodixanol gradient comprised of the following four phases: 7.3 ml of 15%, 4.9 ml of 25%, 4 ml of 40%, and 4 ml of 60% iodixanol (Optiprep; Sigma-Aldrich) overlayed with 8 ml of cell supernatant. The gradients were centrifuged in a 50.2Ti rotor (Beckman Coulter) at 50,000 rpm for 2h using OptiSeal Polyallomer Tubes (Beckman Coulter). Virus was collected by inserting a needle 2 mm below the 40%-60% interface and collecting 4 or 5 fractions (~6 ml) of this interface and most of the 40% layer. The fractions were analyzed for viral content and purity by examining 10 µl of each fraction on a 12% SDS-PAGE gel (BioRad), followed by staining with InstantBlue (Expedeon) to visualize the viral capsid proteins, VP1, VP2, and VP3. The virus was then collected from the fractions of several gradients and the buffer was exchanged with lactated Ringer's solution using an ultrafiltration device, Vivaspin 20 (100 kDa MWCO, GE Healthcare). The final viral preparation was then fractionated on a 12% SDS-PAGE gel, stained with InstantBlue, and then compared with a similarly stained gel of a virus of a known titer.

Isolation and gRNA transfection of adult cardiomyocytes

Cardiomyocytes were isolated based on a modified Langendorff protocol. Briefly, hearts of 4-week old mice were retrogradially perfused with Tyrode's Buffer (10 mM Glucose, 5 mM HEPES, 5.4 mM KCl, 1.2 mM $MgCl_2$, 150 mM NaCl, 2 mM sodium pyruvate, 10 mM taurine, 10 mM 2,3-Butanedione monoxime, pH 7.35) and digested with Digestion Buffer (0.2 mg/ml Liberase DH (Roche), 25 µM $CaCl_2$, in Tyrode's Buffer). Digested tissue was minced and resuspended. Cardiomyocytes (CM) were washed in a series of buffer exchanges that contained Tyrode's Buffer, 0.5 % BSA and increasing concentrations of $CaCl_2$ (25 µM – 250 µM). CM were kept in culture plated on 20 µg/ml laminin (Invitrogen) coated plates and in Adult CM Medium (MEM + 2 mM L-GlutaMax + 100 U/ml Penicillin / 100 µg/ml Streptomycin + 10 mM 2,3-Butanedione monoxime). 3 nmol of pooled gRNAs, that were *in vitro* transcribed using MEGAshortscript T7 Transcription Kit (Thermo Fisher Scientific) and subsequent purification with NucAway Spin Columns (Thermo Fisher Scientific), were transfected into 10E4 cells 16 h post-plating using Lipofectamin RNAiMax Transfection Reagent (Thermo Fisher Scientific). Transfection was repeated after additional 8 h with 1.5 nmol pooled gRNAs. CMs were harvested for RNA and protein analysis 48 h post-plating.

Cell culture and Immunofluorescence

C3H/10T1/2 mouse fibroblasts (ATCC CRL-3216) or C2C12 mouse myoblasts (ATCC CRL-1772) were transiently transfected with SP-dCas9-VPR and p-2xgRNA constructs or TRISPR constructs, respectively, using Lipofectamine 3000 (Thermo Fisher Scientific) according to manufacturer's instructions. For plasmid transfections, a total of 1.25 µg of p-2xgRNA or TRISPR constructs and 1.25 µg dCas9VPR plasmid was used in 12 well plate formats. For the

generation of stable dCas9VPR expressing C3H/10T1/2 and C2C12 cell lines, CAG-dCas9VPR-2A-tdTomato was cloned into a PiggyBac backbone with Neomycin resistance encoding sequence (a kind gift from Boris Greber) using NotI and XhoI (both Thermo Fisher scientific) restriction sites to insert FseI (NEB) and SmiI (Thermo Fisher Scientific) sites for subsequent HD Infusion cloning (pPB-CAG-dCas9VPR-2A-tdTomato) and co-transfection with SuperPiggyBac Transposase. Neuro-2A cells (ATCC CCL-131) were transfected with 1 µg of pPB-dCas9VPR-2A-tdTomato and 1 µg TRISPR constructs using Fugene HD (Promega) or Turbofect (Thermo Fisher Scientific) according to manufacturer's instructions. All transfections were performed in a 12-multiwell format. Cells were harvested for further analyses 48 h post-transfection. For immunofluorescence staining, cells were fixed in 4% PFA/PBS for 15 min, permeabilized with 0.1% v/v Triton X-100/PBS for 10 min and blocked in 1% w/v BSA/PBS for 1 h. Cells were incubated with mouse anti-MEF2D (BD Transduction, catalogue #610774) 1:200 diluted in 1% w/v BSA/PBS for 16 h at 4 °C. No primary antibody was used as control. Cells were stained with Anti-Mouse IgG (H+L) Cross-Adsorbed Secondary Antibody, Alexa Fluor 555 (Thermo Fisher Scientific, catalogue #A-21424) 1:400 and Hoechst 33342 Trihydrochloride, Trihydrate (Life Technologies) in a final concentration of 1 µg/ml for 1 h at 37 °C. Fluorescence images were acquired with a BZ-X710 - All-in-One Fluorescence Microscope (Keyence) or LSM710 confocal microscope and ZEN software (ZEISS). Images were analysed using ImageJ software.

Reverse-transcriptase quantitative PCR

Whole RNA was isolated using TRIzol (Thermo Fisher Scientific) / Chloroform extraction. RNA was subjected to cDNA synthesis using iScript, gDNA clear iScript (Bio-Rad) or M-MLV Reverse Transcriptase (Promega). Reverse-Transcriptase Quantitative PCR was performed on a StepOnePlus Real-Time PCR System (Thermo Fisher Scientific) or on a 7900HT fast Real-Time PCR System (Applied Biosystems) and using KAPA SYBR Fast qPCR Master Mix (KAPA Biosystems) or Takyon ROX SYBR 2X Master Mix dTTP blue (Eurogentec), respectively. Results were analysed using standard curve comparison and normalized to *18S* RNA (Applied Biosystems), *Tbp* or *β-actin* as indicated. See Online Data Supplement Section II – Table III for qPCR primer list.

Cytosol and nuclear protein fractionation

Cells were washed with PBS and Hypotonic Buffer was added (10 mM KCl, 10 mM HEPES, 2 mM $MgCl_2$, 0.1 mM EDTA, 1 mM dithiothreitol, cOmplete Mini protease inhibitor cocktail (Sigma Aldrich), PhosSTOP (Sigma Aldrich)) followed by incubation for 15 min on ice. A final concentration of 1% v/v IGEPAL CA-630 (Sigma Aldrich) was supplemented and samples were incubated for 5 min on ice. Samples were centrifuged for 5 min at 1,500 xg, 4 °C and supernatants were collected and considered as cytosolic fraction. Hypertonic Buffer (300 mM NaCl, 50 mM KCl, 50 mM HEPES, 0.1 mM EDTA, 1 mM dithiothreitol, 10% v/v glycerol, cOmplete Mini protease inhibitor cocktail (Sigma Aldrich), PhosSTOP (Sigma Aldrich)) was added to the pellet, resuspended and incubated on ice for 25 min. IGEPAL CA-630 (Sigma Aldrich) was added to a final concentration of 1% v/v and incubated for 10 min on ice. Samples were centrifuged for 5 min at 16,000 xg, 4 °C. Supernatants were collected and considered as nuclear fraction.

Immunoblotting

Protein was isolated using RIPA buffer (Sigma Aldrich) or Cell Lysis Buffer (20 mM HEPES, 350 mM NaCl, 1 mM $MgCl_2$, 0.5 mM EDTA, 0.1 M EGTA, 20% v/v glycerol, 1% v/v IGEPAL CA-630) including cOmplete Mini protease inhibitor cocktail (Sigma Aldrich) and PhosSTOP (Sigma Aldrich) and mechanical disruption of tissue and cells. Protein concentration was determined using Pierce BSA Protein Assay Kit (Thermo Fisher) or by RotiQuant (Carl Roth) Bradford Assay and measured on CLARIOstar Microplate Reader (BMG LABTECH). Protein was loaded on Any kD Mini-PROTEAN TGX Precast Protein Gels (Bio-Rad) and run for 90 min at 120 V in Electrophoresis Buffer (25 mM TRIS Base, 192 mM Glycine, 0.1% w/v sodium dodecyl sulfate). Proteins were transferred on Immobilon P membranes (Millipore) for 60 min at 100 V in Transfer Buffer (25 mM TRIS Base, Glycine 192 mM, 20% Methanol). Membranes were blocked in 5% Non-Fat Dried milk in TBST (50 mM TRIS Base, 150 mM NaCl, 0.1% v/v Tween, pH 7.6) for 1 h at room temperature and incubated for 16 h at 4 °C in primary antibody (mouse anti-MEF2D (BD Transduction, catalogue #610774) 1:1,000, mouse anti-Vinculin (Sigma Aldrich, catalogue #V9131) 1:2,000, mouse anti-GAPDH (Proteintech, catalog #60004-1-Ig) and (EMD Millipore, catalogue #MAB374) 1:10,000, rabbit anti-Cas9 (Diagenode, catalogue #C15200203-100) 1:2,000, rabbit anti-GFP (Thermo Fisher Scientific, catalogue #CAB4211) 1:5,000), goat anti-Lamin A/C (Santa Cruz, catalogue #sc-6215)). Membranes were incubated in secondary antibody for 2 h at room temperature (anti-mouse IgG (H+L) HRP conjugate (Bio-Rad, catalogue # 172-1011) 1:10,000, Polyclonal rabbit anti-mouse HRP (Dako, catalogue #P0260), Polyclonal goat anti-rabbit HRP, (Dako, catalogue #P0448) 1:5,000 and Polyclonal rabbit anti-goat HRP (Dako, P0449) 1:5,000). Membranes were developed and imaged using radiofilm, ChemiDoc Touch Imaging System or ChemiDoc MP Imaging System (both Bio-Rad). Full unedited gels images for all representative cropped gels in the manuscript are presented in Online figure XIII.

Fluorescence-activated cell sorting

Cells were detached with 0.25% Trypsin (1x) (Gibco) and resuspended in 5% v/v FCS/PBS. Cells were centrifuged for 10 min at 100 xg, 4°C and fixed in 2 % Histofix (Carl Roth) for 15 min at room temperature. Cells were washed twice in PBS, resuspended in Blocking Buffer (5% v/v FCS, 1% w/v BSA, 0.5% v/v Triton X-100, in PBS) and incubated for 10 min on ice. Cells were strained through a 70 µm cell strainer and centrifuged for 5 min at 300 xg, 4 °C. Primary antibodies were added in Blocking Buffer (mouse anti-MEF2D (BD Transduction, catalogue #610774) 1:200; rabbit anti-RFP (Rockland Immunochemicals, catalogue #600-401-379) 1:200, normal mouse IgG (Santa Cruz, catalogue #sc-2025) or normal rabbit IgG (Millipore, catalogue #12-370) 1:200 and incubated for 45 min at room temperature. Secondary antibodies were added prepared in Blocking Buffer (Anti-Mouse IgG (H+L) Cross-Adsorbed Secondary Antibody, Alexa Fluor 633 (Thermo Fisher Scientific, catalogue #A-21052) 1:1000, Anti-Rabbit IgG (H+L) Cross-Adsorbed Secondary Antibody, Alexa Fluor 546 (Thermo Fisher Scientific, catalogue #A-11010) 1:1000) containing a final concentration of 1 µg/ml Hoechst 33342 Trihydrochloride, Trihydrate (Life Technologies) and incubated for 30 min at room temperature. Cells were washed twice with PBS. Cells were sorted with a LSRII SORP Cytometer (BD Biosciences) and recorded with BD FACSDiva Software (BD Biosciences).

Analyses were performed with Flowing Software (Cell Imaging Core, Turku Centre for Biotechnology).

Histological analyses and immunofluorescence staining

Heart tissue was rinsed in ice-cold PBS and fixed in 10% formalin at 4 °C for 48 h and subsequently kept in 70% ethanol. Tissue was paraffin embedded, cut in 4 µm slices and Trichrome stained according to standard protocols. For cryosections, tissue was embedded in TFM Tissue Freezing Medium (GeneralData) and cooled in 2-methylbutane surrounded by liquid nitrogen. Tissue was cut on a CM3050 S Research Cryostat (Leica) at -20 °C in 10 µm slices and mounted on Superfrost Plus Microscope Slides (Thermo Fisher Scientific). For staining, sections were deparaffinized in RotiHistol (twice, 5 min each) and re-hydrated in a decreasing ethanol concentration row (100% twice, 90%, 80%, 70%, 50% v/v, 3 min each). Sections were washed in ddH_2O for 5 min and in PBS for 5 min. Antigens were unmasked by incubation in Citrate Buffer (10 mM sodium citrate, 0.05% v/v Tween, pH 6.0) at 95 °C for 35 min. Sections were rinsed in PBS and blocked in 5% w/v BSA, 0.1% v/v Triton X-100 in PBS for 30 min at room temperature. Sections were incubated with primary antibody (mouse anti-MEF2D (BD Transduction, catalogue #610774) 1:200), rabbit anti-RFP (Rockland Immunochemicals, catalogue #600-401-379) 1:50, rabbit anti-GFP (Thermo Fisher Scientific, catalogue #CAB4211) 1:200 and WGA-FITC (10 µg/ml final concentration) (Sigma Aldrich) in 2% w/v BSA, 0.1% v/v Triton X-100 in PBS for 4 h at room temperature. No primary antibody was used as control. Sections were washed in PBS thrice for 5 min each and incubated with secondary antibody (Anti-Mouse IgG (H+L) Cross-Adsorbed Secondary Antibody, Alexa Fluor 633 (Thermo Fisher Scientific, catalogue #A-21052) 1:200, Anti-Rabbit IgG (H+L) Cross-Adsorbed Secondary Antibody, Alexa Fluor 546 (Thermo Fisher Scientific, catalogue #A-11010) 1:200, Anti-Rabbit IgG (H+L) Cross-Adsorbed Secondary Antibody, Alexa Fluor 488 (Thermo Fisher Scientific, catalogue #A-11008) 1:200) in 2% w/v BSA, 0.1% v/v Triton X-100 in PBS for 2 h at room temperature. Sections were washed thrice in PBS and incubated in Hoechst 33342 Trihydrochloride, Trihydrate (Life Technologies) in a final concentration of 1 µg/ml. Sections were washed in PBS and twice in ddH_2O for 5 min each and covered with Mowiol 4-88 (Carl Roth). Fluorescence images were acquired with a BZ-X710 - All-in-One Fluorescence Microscope (Keyence) or LSM710 confocal microscope and ZEN software (ZEISS). Images were analysed using ImageJ following fluorescence measurements protocols (https://theolb.readthedocs.io/en/latest/imaging/measuring-cell-fluorescence-using-imagej.html) and images of cross sectioned hearts were combined with the ImageJ Stitching Tool. [6]

RNA sequencing (RNA-seq) and data analyses

Total RNA-seq was performed at the Transcriptome and Genome Analysis Laboratory (TAL), University Medical Center Goettingen, in biological triplicates. RNA was extracted, quality and integrity was assessed by using the Fragment Analyzer (Advanced Analytical). An mRNA Seq approach was performed starting with 0.5 µg of total RNA using the TruSeq RNA Library Preparation Kit v2 (Illumina, Cat no RS-122-2001). For accurate quantitation of cDNA libraries a fluorometric based system, the QuantiFluor™ dsDNA System from Promega was used. The size of final cDNA libraries was determined by using the Fragment Analyzer from Advanced Bioanalytical (320 bp in average). Sequencing was performed by using the HT mode of the

HiSeq2500 (SR; 1x50 bp; 30 Mio reads/sample). Sequence reads were aligned to the mouse reference assembly (UCSC version mm9) using Bowtie 2.0. For each gene, the number of mapped reads was counted and DESeq2 was used to analyze the differential expression. A cut-off of log2FC > 0.5 (upregulated genes), log2FC < -0.5 (downregulated genes) and P-adj < 0.05 was used to determine significantly differentially expressed genes. Gene ontology (GO) analyses were performed on DEGs using default parameters and stringency in 'ClueGO': a Cytoscape plug-in. The significant 'GO Biological Processes' were shown with $P \leq 0.05$, with multiple testing corrected with Bonferroni method. For heatmap generation, log2-transformation of the normalized gene counts from DESeq2 was utilized within the 'ClustVis' visualization tool (version 1). The investigator was unaware of the genotypes and treatments. Sequencing data files have been deposited in NCBI GEO (https://www.ncbi.nlm.nih.gov/geo/query/acc.cgi?acc=GSE137148) under the accession GSE137148).

Chromatin Immunoprecipitation and sequencing

P14 ventricles were isolated and minced. Tissue or $2.4 * 10^6$ cells were fixed with 2% PFA/PBS for 25 min at room temperature. Tissue and cells were washed twice with PBS and centrifuged for 2 min at 12,000 xg, 4 °C. Nuclei isolation was performed using 1 ml Nuclei Preparation Buffer (0.15 M NaCl, 0.02 M NaF, 0.02 M EDTA, 0.05 M TRIS-HCl, 0.5 % v/v IGEPAL CA-630, 1 % v/v Triton X-100, cOmplete Mini protease inhibitor cocktail (Sigma Aldrich), PhosSTOP (Sigma Aldrich)) and mechanical disruption. Nuclei were pelleted and washed again in 500 µl Nuclei Preparation Buffer. Sonication Buffer I (0.01 M EDTA, 0.05 M TRIS-HCl, 1% w/v sodium dodecyl sulfate, cOmplete Mini protease inhibitor cocktail (Sigma Aldrich), PhosSTOP (Sigma Aldrich)) was added to the nuclei and incubated for 10 min on ice. Sonication Buffer II (0.15 M NaCl, 0.02 M NaF, 0.02 M EDTA, 0.05 M TRIS-HCl, 1 % v/v IGEPAL CA-630, cOmplete Mini protease inhibitor cocktail (Sigma Aldrich), PhosSTOP (Sigma Aldrich)) was added to samples and sonicated in 1.5 ml Bioruptor Plus TPX microtubes (Diagenode) in a Bioruptor Plus sonication device (Diagenode) for 30 cycles (30 s On/Off per cycle). Samples were centrifuged for 2 min at 12,000 xg, 4 °C and supernatants were collected. The pellet was resuspended in Sonication Buffer I and incubated on ice for 10 min. After addition of Sonication Buffer II, samples were sonicated for 20 cycles (30 s On/Off per cycle). Samples were centrifuged for 2 min at 12,000 xg, 4 °C and supernatants were combined. Supernatant were pre-cleared by incubation with Sepharose 4B beads (GE Healthcare) for 45 min at 4 °C. Beads were pelleted by centrifugation for 5 min at 2000 xg, 4 °C and 10% of each sample was kept as input. The remaining sample was divided and either incubated with 4 µl rabbit anti-Cas9 (Diagenode, catalogue ##C15200203-100) or 2 µg normal rabbit IgG (Millipore, catalogue #12-370) and supplemented with 500 µl Immunoprecipitation Buffer (0.15 M NaCl, 0.02 M NaF, 0.02 M EDTA, 0.05 M TRIS-HCl, 1% v/v IGEPAL CA-630, 0.5% w/v sodium deoxycholate, 0.1% w/v sodium dodecyl sulfate, cOmplete Mini protease inhibitor cocktail (Sigma Aldrich), PhosSTOP (Sigma Aldrich)) for 16 h at 4 °C. Protein A Sepharose CL-4B beads (GE Healthcare) were added to samples and incubated for 16 h at 4 °C. Samples were centrifuged for 2 min at 12,000 xg, 4 °C and supernatant was removed. Bead-antibody-chromatin complexes were washed with Immunoprecipitation Buffer twice (without cOmplete Mini protease inhibitor cocktail (Sigma Aldrich) and PhosSTOP (Sigma Aldrich)), with IP

Wash Buffer (0.5 M LiCl, 0.02 M NaF, 0.02 M EDTA, 0.1 M TRIS-HCl, 1% v/v IGEPAL CA-630, 1% w/v sodium deoxycholate) twice, again with Immunoprecipitation Buffer four times (without cOmplete Mini protease inhibitor cocktail (Sigma Aldrich) and PhosSTOP (Sigma Aldrich)) and with TE Buffer (0.01 M TRIS-HCl, 0.001 M EDTA). To Bead-antibody-chromatin complexes pellet, 400 µl of Elution Buffer (50 mM NaCl, 50 mM TRIS-HCl, 5 mM EDTA, 1% w/v sodium dodecyl sulfate, pH 7.5) was added and incubated at 65 °C for 90 min. Beads were pelleted for 2 min at 6,000 xg and supernatants were collected. Inputs were supplemented with 400 µl Elution Buffer. To all samples 24 µl of 5 M NaCl and 8 µl of 20 mg/ml Proteinase K (Macherey Nagel) was added and incubated for 16 h at 62 °C. DNA was purified using NucleoSpin Gel and PCR clean-up (Buffer NTB Protocol) according to manufacturer's instructions (Macherey Nagel). Immunoprecipitation was validated by ChIP qPCR and analysed by ΔCt method comparing input and Cas9 immunoprecipitation to IgG control samples. See Online Data Supplement Section II – Table III for qPCR primer list.

For sequencing ChIP-seq library preparation was performed using NEBNext Ultra DNA library prep kit for Illumina (E7370) as per manual's instructions. Quantitation of DNA libraries was done on an Invitrogen Qubit 2.0 Fluorometer and the size range of DNA libraries was performed on an Agilent Bioanalyzer 2100 (High Sensitivity DNA Assay). DNA libraries were amplified and sequenced by using the cBot and HiSeq2500 from Illumina (20-25 million reads per sample). The investigator was unaware of the genotypes and treatments.

ChIP-seq data analyses

Sequence reads were aligned to the mouse reference assembly (UCSC version mm9) using Bowtie2. Peak calling was performed with Model Based Analysis of ChIP-seq (MACS2) version 2.1.1.20160309.6, which is the updated version of MACS.[3] All the BED (peak) files were subtracted with a mm9 genome blacklist UCSC BED file (using subtractBED tool), thereby eliminating all background peaks usually detected in the mm9 genome. Genes proximal to the bound chromatin regions were identified by GREAT using 'Basal plus extension' method where each genomic region is overlapped with genes, which are 5kb upstream and 1 kb downstream (proximal), plus up to 1000 kb (distal). To identify differentially bound regions, 'DiffBind' tool in Galaxy was used, with default settings. This identifies all regions that are not only differentially occupied, but also for regions with same occupancy but different binding intensities.

Off-targets prediction

Off-targets were predicted using cm.jefferson.edu/Off-Spotter/ (Computational Medicine Center, University Thomas Jefferson University, United States of America) using up to 5 mismatches for all employed gRNA sequences targeting *Mef2d* and *Klf15*. A BED files containing the genomic predicted regions were used to map genes proximal to TSS regions (0.5 kb distances) using GREAT (Online Table VI and VII). Identified genes were overlapped with the DEGs from RNA-seq (Online Table V) and the peaks from ChIP-seq data using GeneVenn (http://genevenn.sourceforge.net). Their 5´upstream genomic regions were visualized using intergenomic view (IGV) with the ChIP-seq data.

Single Cell preparation for RNA sequencing

For single cell preparation from P10 hearts, ventricles were minced and digested in Collagenase I solution (2 mg/ml Collagenase I (Sigma Aldrich), 20 v/v % FBS (Gibco) in DPBS (Gibco)) for 40 min at 37 °C. Collagenase I solution was exchanged with Accutase mix (97 v/v % StemPro Accutase Cell Dissociation Reagent (Millipore), 0.025 v/v % Trypsin (Gibco), 20 µg/ml DNase I (CalbioChem)) and incubated for 20 min at room temperature. Cells were dissociated by pipetting and strained with a 100 µm cell strainer. Cells were pelleted by 300 xg centrifugation for 3 min at 4 °C and resuspended in DPBS (Gibco). Cell suspensions were used for dispensing.

Library preparation, sequencing and data analysis

The protocol used was a high-throughput full-length analysis of single cells, the SMART-Seq ICELL8[7] cx application (CatN° 640188, 640189, 640222, 640223). Cells were diluted for a final concentration of 1.4 cells/50 nl in a total volume of 1 ml in 1xPBS. After staining with WGA- FITC and DAPI cells were dispensed from a 384-well source plate to a 5184 well plate (Takara) using the ICELL8 system. Imaging and analysis of the nanowell ICELL8 cx were done using the CellSelect Software. A Full-Length cDNA Synthesis by RT-PCR were done according to the SMART-Seq ICELL8 cx application protocol (Takara) by dispensing the reagents directly into the 5184 well plate. Forward indexing primers were dispensed. The Nextera XT DNA library preparation kit (Illumina, USA, cat. FC-131-1024) were used for library preparation. Purification of the extracted library, library amplification and purification of the sequencing-ready library were performed using AMPUure XP Beads according to the standard protocol. Library validation and quantification were done using the Fragment Analyzer by using the dsDNA 905 Reagent Kit (Advanced Bioanalytical) and the QuantiFluor™dsDNA System from Promega. Single cell libraries were sequenced on the HiSeq4000 (SE 51/8/8), 0.5 Mio reads/cell. For data analysis following steps were taken: (I) bcl2fastq was used to retrieve fastq files with dual-indexed barcodes in their read headers; (II) using the mappa_demuxer.py script from Takara, the resulting fastq files were used to associate reads with individual cells based on their barcodes, as well as quantify how many reads are in each cell. (III) Using the mappa_analysed.py script from Takara, the demultiplexed fastq file was run through the analysis pipeline as follows: a) the demultiplexed reads were trimmed for adapters using cutadapt version 2.5; b) the reads kept after trimming were aligned to a custom mouse genome (mm10 version 96) using STAR version 2.7.2b; c) the uniquely mapped reads were counted for exons, genes (exons+introns) and mitochondrial chromosome using featureCoutns version 1.6.4. TSNE analysis were used for clustering analysis.

Statistical analyses

G-Power3.1 was used to determine the sample size for animal studies. A priori: Compute required sample size analysis and T tests – Means (difference between two independent means groups) was used. Input: tail(s) = One; effect size d = 2; α err prob = 0.2; power (1-β err prob) = 0.93; allocation ratio N2/N1=1; sample size group 1 = 3; sample size group 2 = 3; total sample size = 6; actual power =0.9315897.

Vector sequence

Myh6-dCas9VPR-2A-tdTomato (16,375 bp):

gagggcctatttcccatgattccttcatatttgcatatacgatacaaggctgttagagagataattggaattaatttgac
tgtaaacacaaagatattagtacaaaatacgtgacgtagaaagtaataatttcttgggtagtttgcagttttaaaattat
gttttaaaatggactatcatatgcttaccgtaacttgaaagtatttcgatttcttggctttatatatcttGTGGAAAGGA
CGAAACACCggGTCTTCgaGAAGACctgttttagagctaGAAAtagcaagttaaaataaggctagtccgttatcaacttg
aaaaagtggcaccgagtcggtgcTTTTTgttttagagctagaaatagcaagttaaaataaggctagtccgtTTTTagcg
cgtgcgccaattctgcagacaaatggctctagaGGATCGTTGACAGGTACCTCACTGAGATCCTGCAAGGTCACACAAGG
GTCTCCACCCACCAGGTGCCCTAGTCTCAATTTCAGTTTCCATGCCTTGTTCTCACAATGCTGGCCTCCCCAGAGCTAAT
TTGGACTTTGTTTTTATTTCAAAAGGGCCTGAATGAGGAGTAGATCTTGTGCTACCCAGCTCTAAGGGTGCCCGTGAAGC
CCTCAGACCTGGAGCCTTTGCAACAGCCCTTTAGGTGGAAGCAGAATAAAGCAATTTTCCTTAAAGCCAAAATCCTGCCT
CTAGACTCTTCTTCTCTGACCTCGGTCCCTGGGCTCTAGGGTGGGGAGGTGGGGCTTGGAAGAAGAAGGTGGGGAAGTGG
CAAAAGCCGATCCCTAGGGCCCTGTGAAGTTCGGAGCCTTCCCTGTACAGCACTGGCTCATAGATCCTCCTCCAGCCAAA
CATAGCAAGAAGTGATACCTCCTTTGTGACTTCCCCAGGCCCAGTACCTGTCAGGTTGAAACAGGATTTAGAGAAGCCTC
TGAACTCACCTGAACTCTGAAGCTCATCCACCAAGCAAGCACCTAGGTGCCACTGCTAGTTAGTATCCTACGCTGATAAT
ATGCAGAGCTGGGCCACAGAAGTCCTGGGGTGTAGGAACTGACCAGTGACTTTTCAGTCGGCAAAGGTATGACCCCCTCA
GCAGATGTAGTAATGTCCCCTTAGATCCCATCCCAGGCAGGTCTCTAAGAGGACATGGGATGAGAGATGTAGTCATGTGG
CATTCCAAACACAGCTATCCACAGTGTCCCTTGCCCCTTCCACTTAGCCAGGAGGACAGTAACCTTAGCCTATCTTTCTT
CCTCCCCATCCTCCCAGGACACACCCCCTGGTCTGCAGTATTCATTTCTTCCTTCACGTCCCCTCTGTGACTTCCATTTG
CAAGGCTTTTGACCTCTGCAGCTGCTGGAAGATAGAGTTTGGCCCTAGGTGTGGCAAGCCATCTCAAGAGAAAGCAGACA
ACAGGGGGACCAGATTTTGGAAGGATCAGGAACTAAATCACTGGCGGGCCTGGGGGTAGAAAAAAGAGTGAGTGAGTCCG
CTCCAGCTAAGCCAAGCTAGTCCCCGAGATACTCTGCCACAGCTGGGCTGCTCGGGGTAGCTTTAGGAATGTGGGTCTGA
AAGACAATGGGATTGGAAGACATCTCTTTGAGTCTCCCCTCAACCCCACCTACAGACACACTCGTGTGTGGCCAGACTCC
TGTTCAACAGCCCTCTGTGTTCTGACCACTGAGCTAGGCAACCAGAGCATGGGCCCTGTGCTGAGGATGAAGAGTTGGTT
ACCAATAGCAAAAACAGCAGGGGAGGGAGAACAGAGAACGAAATAAGGAAGGAAGAAGGAAAGGCCAGTCAATCAGATGC
AGTCAGAAGAGATGGGAAGCCAACACACAGCTTGAGCAGAGGAAACAGAAAAGGGAGAGATTCTGGGCATAAGGAGGCCA
CAGAAAGAAGAGCCCAGGCCCCCCAAGTCTCCTCTTTATACCCTCATCCCGTCTCCCAATTAAGCCCACTCTTCTTCCTA
GATCAGACCTGAGCTGCAGCGAAGAGACCCGTAGGGAGGATCACACTGGATGAAGGAGATGTGTGGAGAAGTCCAGGGCA
ACCTAAGAGCCAGAGCCTAAAAGAGCAAGAGATAAAGGTGCTTCAAAGGTGGCCAGGCTGTGCACACAGAGGGTCGAGGA
CTGGTGGTAGAGCCTCAAGATAAGGATGATGCTCAGAATGGGCGGGGGGGGGGGATTCTGGGGGGGGGAGAGAGAAGGTGA
GAAGGAGCCTGGAACAGAGAATCTGGAAGCGCTGGAAACGATACCATAAAGGGAAGAACCCAGGCTACCTTTAGATGTAA
ATCATGAAAGACAGGGAGAAGGGAAGCTGGAGAGAGTAGAAGGACCCCGGGGCAAGACATGGAAGCAAGGACAAGCCAGG
TTGAGCGCTCCGTGAAATCAGCCTGCTGAAGGCAGAGCCCTGGTATGAGCACCAGAACAGCAGAGGCTAGGGTTAATGTC
GAGACAGGGAACAGAAGGTAGACACAGGAACAGACAGAGACGGGGGAGCCAGGTAACAAAGGAATGGTCCTTCTCACCTG
TGGCCAGAGCGTCCATCTGTGTCCACATACTCTAGAATGTTCATCAGACTGCAGGGCTGGCTTGGGAGGCAGCTGGAAAG
AGTATGTGAGAGCCAGGGGAGACAAGGGGGCCTAGGAAAGGAAGAAGAGGGCAAACCAGGCCACACAAGAGGGCAGAGCC
CAGAACTGAGTTAACTCCTTCCTTGTTGCATCTTCCATAGGAGGCAGTGGGAACTCTGTGACCACCATCCCCCATGAGCC
CCCACTACCCATACCAAGTTTGGCCTGAGTGGCATTCTAGGTTCCCTGAGGACAGAGCCTGGCCTTTGTCTCTTGGACCT
GACCCAAGCTGACCCAATGTTCTCAGTACCTTATCATGCCCTCAAGAGCTTGAGAACCAGGCAGTGACATATTAGGCCAT
GGGCTAACCCTGGAGCTTGCACACAGGAGCCTCAAGTGACCTCCAGGGACACAGCTGCAGACAGGTGGCCTTTATCCCCA
AAGAGCAACCATTTGGCATAGGTGGCTGCAAATGGGAATGCAAGGTTGAATCAGGTCCCTTCAAGAATACTGCATGCAAG
ACCTAAGACCCCTGGAGAGAGGGGTATGCTCCTGCCCCCACCCACCATAAGGGGAGTGAACTATCCTAGGGGGCTGGCGA
CCTTGGGGAGACACCACATTACTGAGAGTGCTGAGCCCAGAAAAACTGACCGCCCTGTGTCCTGCCCACCTCCACACTCT
AGAGCTATATTGAGAGGTGACAGTAGATAGGGTGGGAGCTGGTAGCAGGGAGAGTGTTCCTGGGTGTGAGGGTGTAGGGG
AAAGCCAGAGCAGGGGAGTCTGGCTTTGTCTCCTGAACACAATGTCTACTTAGTTATAACAGGCATGACCTGCTAAAGAC
CCAACATCTACGACCTCTGAAAAGACAGCAGCCCTGGAGGACAGGGGTTGTCTCTGAGCCTTGGGTGCTTGATGGTGCCA
CAAAGGAGGGCATGAGTGTGAGTATAAGGCCCCAGGAGCGTTAGAGAAGGGCACTTGGGAAGGGGTCAGTCTGCAGAGCC
CCTATCCATGGAATCTGGAGCCTGGGGCCAACTGGTGTAAATCTCTGGGCCTGCCAGGCATTCAAAGCAGCACCTGCATC
CTCTGGCAGCCTGGGGAGGCGGAAGGGAGCAACCCCCCACTTATACCCTTTCTCCCTCAGCCCCAGGATTAACACCTCTG
GCCTTCCCCCTTCCCACCTCCCATCAGGAGTGGAGGGTTGCAGAGGGAGGGTAAAAACCTACATGTCCAAACATCATGGT
GCACGATATATGGATCAGTATGTGTAGAGGCAAGAAAGGAAATCTGCAGGCTTAACTGGGTTAATGTGTAAAGTCTGTGT
GCATGTGTGTGTGTCTGACTGAAAACGGGCATGGCTGTGCAGCTGTTCAGTTCTGTGCGTGAGGTTACCAGACTGCAGGT
TTGTGTGTAAATTGCCCAAGGCAAAGTGGGTGAATCCCTTCCATGGTTTAAAGAGATTGGATGATGGCCTGCATCTCAAG
GACCATGGAAAATAGAATGGACACTCTATATGTGTCTCTAAGCTAAGGTAGCAAGGTCTTTGGAGGACACCTGTCTAGAG
ATGTGGGCAACAGAGACTACAGACAGTATCTGTACAGAGTAAGGAGAGAGAGGAGGGGGTGTAGAATTCTCTTACTATCA
AAGGGAAACTGAGTCGTGCACCTGCAAAGTGGATGCTCTCCCTAGACATCATGACTTTGTCTCTGGGGAGCCAGCACTGT
GGAACTTCAGGTCTGAGAGAGTAGGAGGCTCCCCTCAGCCTGAAGCTATGCAGATAGCCAGGGTTGAAAGGGGGAAGGGA
GAGCCTGGGATGGGAGCTTGTGTGTTGGAGGCAGGGGACAGATATTAAGCCTGGAAGAGAAGGTGACCCTTACCCAGTTG

TTCAACTCACCCTTCAGATTAAAAATAACTGAGGTAAGGGCCTGGGTAGGGGAGGTGGTGTGAGACGCTCCTGTCTCTCC
TCTATCTGCCCATCGGCCCTTTGGGGAGGAGGAATGTGCCCAAGGACTAAAAAAAGGCCATGGAGCCAGAGGGGCGAGGG
CAACAGACCTTTCATGGGCAAACCTTGGGGCCCTGCTGTCCTCCTGTCACCTCCAGAGCCAAGGGATCAAAGGAGGAGGA
GCCAGGACAGGAGGGAAGTGGGAGGGAGGGTCCCAGCAGAGGACTCCAAATTTAGGCAGCAGGCATATGGGATGGGATAT
AAAGGGGCTGGAGCACTGAGAGCTGTCAGAGATTTCTCCAACCCAGGTAAGAGGGAGTTTCGGGTGGGGGCTCTTCACCC
ACACCAGACCTCTCCCCACCTAGAAGGAAACTGCCTTTCCTGGAAGTGGGGTTCAGGCCGGTCAGAGATCTGACAGGGTG
GCCTTCCACCAGCCTGGGAAGTTCTCAGTGGCAGGAGGTTTCCACAAGAAACACTGGATGCCCCTTCCCTTACGCTGTCT
TCTCCATCTTCCTCCTGGGGATGCTCCTCCCCGTCTTGGTTTATCTTGGCTCTTCGTCTTCAGCAAGATTTGCCCTGTGC
TGTCCACTCCATCTTTCTCTACTGTCTCCGTGCCTTGCCTTGCCTTCTTGCGTGTCCTTCCTTTCCACCCATTTCTCACT
TCACCTTTTCTCCCCTTCTCATTTGTATTCATCCTTCCTTCCTTCCTTCCTTCCTTCCTTCCTTCCTTCCTTCCTT
TCTCCCTTCCTTCCTTCCTTCCTTCCTTCCTTCCTTCCTTCCTTCCTGTGTCAGAGTGCTGAGAATCACACCTGGGGTTC
CCACCCTTATGTAAACAATCTTCCAGTGAGCCACAGCTTCAGTGCTGCTGGGTGCTCTCTTACCTTCCTCACCCCCTGGC
TTGTCCTGTTCCATCCTGGTCAGGATCTCTAGATTGGTCTCCCAGCCTCTGCTACTCCTCTTCCTGCCTGTTCCTCTCTC
TGTCCAGCTGCGCCACTGTGGTGCCTCGTTCCAGCTGTGGTCCACATTCTTCAGGATTCTCTGAAAAGTTAACCAGGTGA
GAATGTTTCCCCTGTAGACAGCAGATCACGATTCTCCCGGAAGTCAGGCTTCCAGCCCTCTCTTTCTCTGCCCAGCTGCC
CGGCACTCTTAGCAAACCTCAGGCACCCTTACCCCACATAGACCTCTGACAGAGAAGCAGGCACTTTACATGGAGTCCTG
GTGGGAGAGCCATAGGCTACGGTGTAAAAGAGGCAGGGAAGTGGTGGTGTAGGAAAGTCAGGACTTCACATAGAAGCCTA
GCCCACACCAGAAATGACAGACAGATCCCTCCTATCTCCCCCATAAGAGTTTGAGTCGACaccggatgggcggtaggcgt
gtacggtgggaggtctatataagcagagctcgtttagtgaaccgtcagatcgcctggagacgccatccacgctgttttga
cctccatagaagacaccgggaccgatccagcctccggactctagaggatcgaaccctt**GCCACC**ATGGACAAGAAGTACT
CCATTGGGCTCGCTATCGGCACAAACAGCGTCGGCTGGGCCGTCATTACGGACGAGTACAAGGTGCCGAGCAAAAAATTC
AAAGTTCTGGGCAATACCGATCGCCACAGCATAAAGAAGAACCTCATTGGCGCCCTCCTGTTCGACTCCGGGGAGACGGC
CGAAGCCACGCGGCTCAAAAGAACAGCACGGCGCAGATATACCCGCAGAAAGAATCGGATCTGCTACCTGCAGGAGATCT
TTAGTAATGAGATGGCTAAGGTGGATGACTCTTTCTTCCATAGGCTGGAGGAGTCCTTTTTGGTGGAGGAGGATAAAAAG
CACGAGCGCCACCCAATCTTTGGCAATATCGTGGACGAGGTGGCGTACCATGAAAAGTACCCAACCATATATCATCTGAG
GAAGAAGCTTGTAGACAGTACTGATAAGGCTGACTTGCGGTTGATCTATCTCGCGCTGGCGCATATGATCAAATTTCGGG
GACACTTCCTCATCGAGGGGGACCTGAACCCAGACAACAGCGATGTCGACAAACTCTTTATCCAACTGGTTCAGACTTAC
AATCAGCTTTTCGAAGAGAACCCGATCAACGCATCCGGAGTTGACGCCAAAGCAATCCTGAGCGCTAGGCTGTCCAAATC
CCGGCGGCTCGAAAACCTCATCGCACAGCTCCCTGGGGAGAAGAAGAACGGCCTGTTTGGTAATCTTATCGCCCTGTCAC
TCGGGCTGACCCCCAACTTTAAATCTAACTTCGACCTGGCCGAAGATGCCAAGCTTCAACTGAGCAAAGACACCTACGAT
GATGATCTCGACAATCTGCTGGCCCAGATCGGCGACCAGTACGCAGACCTTTTTTTGGCGGCAAAGAACCTGTCAGACGC
CATTCTGCTGAGTGATATTCTGCGAGTGAACACGGAGATCACCAAAGCTCCGCTGAGCGCTAGTATGATCAAGCGCTATG
ATGAGCACCACCAAGACTTGACTTTGCTGAAGGCCCTTGTCAGACAGCAACTGCCTGAGAAGTACAAGGAAATTTTCTTC
GATCAGTCTAAAAATGGCTACGCCGGATACATTGACGGCGGAGCAAGCCAGGAGGAATTTTACAAATTTATTAAGCCCAT
CTTGGAAAAAATGGACGGCACCGAGGAGCTGCTGGTAAAGCTTAACAGAGAAGATCTGTTGCGCAAACAGCGCACTTTCG
ACAATGGAAGCATCCCCCACCAGATTCACCTGGGCGAACTGCACGCTATCCTCAGGCGGCAAGAGGATTTCTACCCCTTT
TTGAAAGATAACAGGGAAAAGATTGAGAAAATCCTCACATTTCGGATACCCTACTATGTAGGCCCCCTCGCCCGGGGAAA
TTCCAGATTCGCGTGGATGACTCGCAAATCAGAAGAGACCATCACTCCCTGGAACTTCGAGGAAGTCGTGGATAAGGGGG
CCTCTGCCCAGTCCTTCATCGAAAGGATGACTAACTTTGATAAAAATCTGCCTAACGAAAAGGTGCTTCCTAAACACTCT
CTGCTGTACGAGTACTTCACAGTTTATAACGAGCTCACCAAGGTCAAATACGTCACAGAAGGGATGAGAAAGCCAGCATT
CCTGTCTGGAGAGCAGAAGAAAGCTATCGTGGACCTCCTCTTCAAGACGAACCGGAAAGTTACCGTGAAACAGCTCAAAG
AAGACTATTTCAAAAAGATTGAATGTTTCGACTCTGTTGAAATCAGCGGAGTGGAGGATCGCTTCAACGCATCCCTGGGA
ACGTATCACGATCTCCTGAAAATCATTAAAGACAAGGACTTCCTGGACAATGAGGAGAACGAGGACATTCTTGAGGACAT
TGTCCTCACCCTTACGTTGTTTGAAGATAGGGAGATGATTGAAGAACGCTTGAAAACTTACGCTCATCTCTTCGACGACA
AAGTCATGAAACAGCTCAAGAGGCGCCGATATACAGGATGGGGGCGGCTGTCAAGAAAACTGATCAATGGGATCCGAGAC
AAGCAGAGTGGAAAGACAATCCTGGATTTTCTTAAGTCCGATGGATTTGCCAACCGGAACTTCATGCAGTTGATCCATGA
TGACTCTCTCACCTTTAAGGAGGACATCCAGAAAGCACAAGTTTCTGGCCAGGGGGACAGTCTTCACGAGCACATCGCTA
ATCTTGCAGGTAGCCCAGCTATCAAAAAGGGAATACTGCAGACCGTTAAGGTCGTGGATGAACTCGTCAAAGTAATGGGA
AGGCATAAGCCCGAGAATATCGTTATCGAGATGGCCCGAGAGAACCAAACTACCCAGAAGGGACAGAAGAACAGTAGGGA
AAGGATGAAGAGGATTGAAGAGGGTATAAAAGAACTGGGGTCCCAAATCCTTAAGGAACACCCAGTTGAAAACACCCAGC
TTCAGAATGAGAAGCTCTACCTGTACTACCTGCAGAACGGCAGGGACATGTACGTGGATCAGGAACTGGACATCAATCGG
CTCTCCGACTACGACGTGGCTGCTATCGTGCCCCAGTCTTTTCTCAAAGATGATTCTATTGATAATAAAGTGTTGACAAG
ATCCGATAAAgcTAGAGGGAAGAGTGATAACGTCCCCTCAGAAGAAGTTGTCAAGAAAATGAAAAATTATTGGCGGCAGC
TGCTGAACGCCAAACTGATCACACAACGGAAGTTCGATAATCTGACTAAGGCTGAACGAGGTGGCCTGTCTGAGTTGGAT
AAAGCCGGCTTCATCAAAAGGCAGCTTGTTGAGACACGCCAGATCACCAAGCACGTGGCCCAAATTCTCGATTCACGCAT
GAACACCAAGTACGATGAAAATGACAAACTGATTCGAGAGGTGAAAGTTATTACTCTGAAGTCTAAGCTGGTCTCAGATT
TCAGAAAGGACTTTCAGTTTTATAAGGTGAGAGAGATCAACAATTACCACCATGCGCATGATGCCTACCTGAATGCAGTG
GTAGGCACTGCACTTATCAAAAAATATCCCAAGCTTGAATCTGAATTTGTTTACGGAGACTATAAAGTGTACGATGTTAG
GAAAATGATCGCAAAGTCTGAGCAGGAAATAGGCAAGGCCACCGCTAAGTACTTCTTTTACAGCAATATTATGAATTTTT
TCAAGACCGAGATTACACTGGCCAATGGAGAGATTCGGAAGCGACCACTTATCGAAACAAACGGAGAAACAGGAGAAATC
GTGTGGGACAAGGGTAGGGATTTCGCGACAGTCCGGAAGGTCCTGTCCATGCCGCAGGTGAACATCGTTAAAAAGACCGA

AGTACAGACCGGAGGCTTCTCCAAGGAAAGTATCCTCCCGAAAAGGAACAGCGACAAGCTGATCGCACGCAAAAAAGATT
GGGACCCCAAGAAATACGGCGGATTCGATTCTCCTACAGTCGCTTACAGTGTACTGGTTGTGGCCAAAGTGGAGAAAGGG
AAGTCTAAAAAACTCAAAAGCGTCAAGGAACTGCTGGGCATCACAATCATGGAGCGATCAAGCTTCGAAAAAAACCCCAT
CGACTTTCTCGAGGCGAAAGGATATAAAGAGGTCAAAAAAGACCTCATCATTAAGCTTCCCAAGTACTCTCTCTTTGAGC
TTGAAAACGGCCGGAAACGAATGCTCGCTAGTGCGGGCGAGCTGCAGAAAGGTAACGAGCTGGCACTGCCCTCTAAATAC
GTTAATTTCTTGTATCTGGCCAGCCACTATGAAAAGCTCAAAGGGTCTCCCGAAGATAATGAGCAGAAGCAGCTGTTCGT
GGAACAACACAAACACTACCTTGATGAGATCATCGAGCAAATAAGCGAATTCTCCAAAAGAGTGATCCTCGCCGACGCTA
ACCTCGATAAGGTGCTTTCTGCTTACAATAAGCACAGGGATAAGCCCATCAGGGAGCAGGCAGAAAACATTATCCACTTG
TTTACTCTGACCAACTTGGGCGCGCCTGCAGCCTTCAAGTACTTCGACACCACCATAGACAGAAAGCGGTACACCTCTAC
AAAGGAGGTCCTGGACGCCACACTGATTCATCAGTCAATTACGGGGCTCTATGAAACAAGAATCGACCTCTCTCAGCTCG
GTGGAGACAGCAGGGCTGACCCCAAGAAGAAGAGGAAGGTGTCGCCAGGGATCCGTCGACTTGACGCGTTGATATCAACA
AGTTTGTACAAAAAAGCAGGCTACAAAGAGGCCAGCGGTTCCGGACGGGCTGACGCATTGGACGATTTTGATCTGGATAT
GCTGGGAAGTGACGCCCTCGATGATTTTGACCTTGACATGCTTGGTTCGGATGCCCTTGATGACTTTGACCTCGACATGC
TCGGCAGTGACGCCCTTGATGATTTCGACCTGGACATGCTGATTAACTCTAGAAGTTCCGGATCTCCGAAAAAGAAACGC
AAAGTTGGTAGCCAGTACCTGCCCGACACCGACGACCGGCACCGGATCGAGGAAAAGCGGAAGCGGACCTACGAGACATT
CAAGAGCATCATGAAGAAGTCCCCCTTCAGCGGCCCCACCGACCCTAGACCTCCACCTAGAAGAATCGCCGTGCCCAGCA
GATCCAGCGCCAGCGTGCCAAAACCTGCCCCCCAGCCTTACCCCTTCACCAGCAGCCTGAGCACCATCAACTACGACGAG
TTCCCTACCATGGTGTTCCCCAGCGGCCAGATCTCTCAGGCCTCTGCTCTGGCTCCAGCCCCTCCTCAGGTGCTGCCTCA
GGCTCCTGCTCCTGCACCAGCTCCAGCCATGGTGTCTGCACTGGCTCAGGCACCAGCACCCGTGCCTGTGCTGGCTCCTG
GACCTCCACAGGCTGTGGCTCCACCAGCCCCTAAACCTACACAGGCCGGCGAGGGCACACTGTCTGAAGCTCTGCTGCAG
CTGCAGTTCGACGACGAGGATCTGGGAGCCCTGCTGGGAAACAGCACCGATCCTGCCGTGTTCACCGACCTGGCCAGCGT
GGACAACAGCGAGTTCCAGCAGCTGCTGAACCAGGGCATCCCTGTGGCCCCTCACACCACCGAGCCCATGCTGATGGAAT
ACCCCGAGGCCATCACCCGGCTCGTGACAGGCGCTCAGAGGCCTCCTGATCCAGCTCCTGCCCCTCTGGGAGCACCAGGC
CTGCCTAATGGACTGCTGTCTGGCGACGAGGACTTCAGCTCTATCGCCGATATGGATTTCTCAGCCTTGCTGGGCTCTGG
CAGCGGCAGCCGGGATTCCAGGGAAGGGATGTTTTTGCCGAAGCCTGAGGCCGGCTCCGCTATTAGTGACGTGTTTGAGG
GCCGCGAGGTGTGCCAGCCAAAACGAATCCGGCCATTTCATCCTCCAGGAAGTCCATGGGCCAACCGCCCACTCCCCGCC
AGCCTCGCACCAACACCAACCGGTCCAGTACATGAGCCAGTCGGGTCACTGACCCCGGCACCAGTCCCTCAGCCACTGGA
TCCAGCGCCCGCAGTGACTCCCGAGGCCAGTCACCTGTTGGAGGATCCCGATGAAGAGACGAGCCAGGCTGTCAAAGCCC
TTCGGGAGATGGCCGATACTGTGATTCCCCAGAAGGAAGAGGCTGCAATCTGTGGCCAAATGGACCTTTCCCATCCGCCC
CCAAGGGGCCATCTGGATGAGCTGACAACCACACTTGAGTCCATGACCGAGGATCTGAACCTGGACTCACCCCTGACCCC
GGAATTGAACGAGATTCTGGATACCTTCCTGAACGACGAGTGCCTCTTGCATGCCATGCATATCAGCACAGGACTGTCCA
TCTTCGACACATCTCTGTTTGGAGCTAGCGAGGGCAGAGGAAGTCTTCTAACATGCGGTGACGTGGAGGAGAATCCCGGC
CCTACTAGTATGGTGAGCAAGGGCGAGGAGGTCATCAAAGAGTTCATGCGCTTCAAGGTGCGCATGGAGGGCTCCATGAA
CGGCCACGAGTTCGAGATCGAGGGCGAGGGCGAGGGCCGCCCCTACGAGGGCACCCAGACCGCCAAGCTGAAGGTGACCA
AGGGCGGCCCCCTGCCCTTCGCCTGGGACATCCTGTCCCCCCAGTTCATGTACGGCTCCAAGGCGTACGTGAAGCACCCC
GCCGACATCCCCGATTACAAGAAGCTGTCCTTCCCCGAGGGCTTCAAGTGGGAGCGCGTGATGAACTTCGAGGACGGCGG
TCTGGTGACCGTGACCCAGGACTCCTCCCTGCAGGACGGCACGCTGATCTACAAGGTGAAGATGCGCGGCACCAACTTCC
CCCCCGACGGCCCCGTAATGCAGAAGAAGACCATGGGCTGGGAGGCCTCCACCGAGCGCCTGTACCCCCGCGACGGCGTG
CTGAAGGGCGAGATCCACCAGGCCCTGAAGCTGAAGGACGGCGGCCACTACCTGGTGGAGTTCAAGACCATCTACATGGC
CAAGAAGCCCGTGCAACTGCCCGGCTACTACTACGTGGACACCAAGCTGGACATCACCTCCCACAACGAGGACTACACCA
TCGTGGAACAGTACGAGCGCTCCGAGGGCCGCCACCACCTGTTCCTGGGGCATGGCACCGGCAGCACCGGCAGCGGCAGC
TCCGGCACCGCCTCCTCCGAGGACAACAACATGGCCGTCATCAAAGAGTTCATGCGCTTCAAGGTGCGCATGGAGGGCTC
CATGAACGGCCACGAGTTCGAGATCGAGGGCGAGGGCGAGGGCCGCCCCTACGAGGGCACCCAGACCGCCAAGCTGAAGG
TGACCAAGGGCGGCCCCCTGCCCTTCGCCTGGGACATCCTGTCCCCCCAGTTCATGTACGGCTCCAAGGCGTACGTGAAG
CACCCCGCCGACATCCCCGATTACAAGAAGCTGTCCTTCCCCGAGGGCTTCAAGTGGGAGCGCGTGATGAACTTCGAGGA
CGGCGGTCTGGTGACCGTGACCCAGGACTCCTCCCTGCAGGACGGCACGCTGATCTACAAGGTGAAGATGCGCGGCACCA
ACTTCCCCCCCGACGGCCCCGTAATGCAGAAGAAGACCATGGGCTGGGAGGCCTCCACCGAGCGCCTGTACCCCCGCGAC
GGCGTGCTGAAGGGCGAGATCCACCAGGCCCTGAAGCTGAAGGACGGCGGCCGCTACCTGGTGGAGTTCAAGACCATCTA
CATGGCCAAGAAGCCCGTGCAACTGCCCGGCTACTACTACGTGGACACCAAGCTGGACATCACCTCCCACAACGAGGACT
ACACCATCGTGGAACAGTACGAGCGCTCCGAGGGCCGCCACCACCTGTTCCTGTACGGCATGGACGAGCTGTACAAGTAA
ATCGATgaattctaaCTAGAGCTCGCTGATCAGCCTCGACTGTGCCTTCTAGTTGCCAGCCATCTGTTGTTTGCCCCTCC
CCCGTGCCTTCCTTGACCCTGGAAGGTGCCACTCCCACTGTCCTTTCCTAATAAAATGAGGAAATTGCATCGCATTGTCT
GAGTAGGTGTCATTCTATTCTGGGGGGTGGGGTGGGGCAGGACAGCAAGGGGGAGGATTGGGAAGAgAATAGCAGGCATG
CTGGGGAgcggccgcaggaaccctagtgatggagttggccactccctctctgcgcgctcgctcgctcactgaggccggg
cgaccaaaggtcgcccgacgcccgggctttgcccgggcggcctcagtgagcgagcgagcgcgcagctgcctgcaggggCG
AGGCCGTTAATTAACCCTGCcgcctgatgcggtattttctccttacgcatctgtgcggtatttcacaccgcatacgtcaa
agcaaccatagtacgcgccctgtagcggcgcattaagcgcggcgggtgtggtggttacgcgcagcgtgaccgctacactt
gccagcgccctagcgcccgctcctttcgctttcttcccttcctttctcgccacgttcgccggctttccccgtcaagctct
aaatcgggggctccctttagggttccgatttagtgctttacggcacctcgaccccaaaaaacttgatttgggtgatggtt
cacgtagtgggccatcgccctgatagacggtttttcgccctttgacgttggagtccacgttctttaatagtggactcttg
ttccaaactggaacaacactcaaccctatctcgggctattcttttgatttataagggattttgccgatttcggcctattg

gttaaaaaatgagctgatttaacaaaaatttaacgcgaattttaacaaaatattaacgtttacaattttatggtgcactc
tcagtacaatctgctctgatgccgcatagttaagccagccccgacacccgccaacacccgctgacgcgccctgacgggct
tgtctgctcccggcatccgcttacagacaagctgtgaccgtctccgggagctgcatgtgtcagaggttttcaccgtcatc
accgaaacgcgcgagacgaaagggcctcgtgatacgcctatttttataggttaatgtcatgataataatggtttcttaga
cgtcaggtggcacttttcggggaaatgtgcgcggaacccctatttgtttatttttctaaatacattcaaatatgtatccg
ctcatgagacaataaccctgataaatgcttcaataatattgaaaaaggaagagtatgagtattcaacatttccgtgtcgc
ccttattcccttttttgcggcattttgccttcctgtttttgctcacccagaaacgctggtgaaagtaaaagatgctgaag
atcagttgggtgcacgagtgggttacatcgaactggatctcaacagcggtaagatccttgagagttttcgccccgaagaa
cgttttccaatgatgagcacttttaaagttctgctatgtggcgcggtattatcccgtattgacgccgggcaagagcaact
cggtcgccgcatacactattctcagaatgacttggttgagtactcaccagtcacagaaaagcatcttacggatggcatga
cagtaagagaattatgcagtgctgccataaccatgagtgataacactgcggccaacttacttctgacaacgatcggagga
ccgaaggagctaaccgcttttttgcacaacatgggggatcatgtaactcgccttgatcgttgggaaccggagctgaatga
agccataccaaacgacgagcgtgacaccacgatgcctgtagcaatggcaacaacgttgcgcaaactattaactggcgaac
tacttactctagcttcccggcaacaattaatagactggatggaggcggataaagttgcaggaccacttctgcgctcggcc
cttccggctggctggtttattgctgataaatctggagccggtgagcgtggaagccgcggtatcattgcagcactggggcc
agatggtaagccctcccgtatcgtagttatctacacgacggggagtcaggcaactatggatgaacgaaatagacagatcg
ctgagataggtgcctcactgattaagcattggtaactgtcagaccaagtttactcatatatactttagattgatttaaaa
cttcatttttaatttaaaaggatctaggtgaagatccttttgataatctcatgaccaaaatcccttaacgtgagttttc
gttccactgagcgtcagaccccgtagaaaagatcaaaggatcttcttgagatcctttttttctgcgcgtaatctgctgct
tgcaaacaaaaaaaccaccgctaccagcggtggtttgtttgccggatcaagagctaccaactctttttccgaaggtaact
ggcttcagcagagcgcagataccaaatactgtccttctagtgtagccgtagttaggccaccacttcaagaactctgtagc
accgcctacatacctcgctctgctaatcctgttaccagtggctgctgccagtggcgataagtcgtgtcttaccgggttgg
actcaagacgatagttaccggataaggcgcagcggtcgggctgaacgggggttcgtgcacacagcccagcttggagcga
acgacctacaccgaactgagatacctacagcgtgagctatgagaaagcgccacgcttcccgaagggagaaaggcggacag
gtatccggtaagcggcagggtcggaacaggagagcgcacgagggagcttccagggggaaacgcctggtatctttatagtc
ctgtcgggtttcgccacctctgacttgagcgtcgatttttgtgatgctcgtcaggggggcggagcctatggaaaaacgcc
agcaacgcggccttttacggttcctggccttttgctggccttttgctcacatgt

Myh6 promoter
Kozak
dCas9VPR
T2A
tdTomato
KpnI site
PacI site

Section II

Table I. Checklist animal studies

Preclinical testing	No
Animals	Species, age, sex, strains, and sources of animals are described: yes
Randomization	Randomization and allocation concealment were performed: no
Blinding	Blinding was performed: yes
Inclusions and exclusions	Specific criteria for inclusions and exclusions are specified: yes
	Criteria for inclusions and exclusions were set before the study: no
Statistical methods o	Statistical methods are described: yes

Table II. Primers

Primers used for		**Sequence 5'→3'**
Infusion	fwd	TTGAGTCGACACCGGATGGGCGGTAGGCGTGTAC
Infusion	rev	CTCTGCCCTCGCTAGTCAAAACAGAGATGTGTCGAAGATGGAC
Site-directed mutagenesis	fwd	CACATCTCTGTTTGGAGCTAGCGAGGGCAGAGGAAGTC
Site-directed mutagenesis	rev	GACTTCCTCTGCCCTCGCTAGCTCCAAACAGAGATGTG
Genotyping PCR	fwd	TGGCCAAATGGACCTTTCCCATC
Genotyping PCR	rev	GTTCATGGAGCCCTCCATGC
PB-CAG-dCas9VPR Infusion	fwd	CAAAGAATTCCTCGACTCTAGAGGATCGAACCCTTG
PB-CAG-dCas9VPR Infusion	rev	GCTTATCGAGCGGCCCGATTTACTTGTACAGCTCGTC
T7 gRNA Klf15 A	fwd	ggatcctaatacgactcactataggGGGACTCTGCGGGCTTTCAG
T7 gRNA Klf15 B	fwd	ggatcctaatacgactcactataggGTGCAGATCCACGAAGAGAC
T7 gRNA Klf15 C	fwd	ggatcctaatacgactcactataggGACACGGTCCCTACTAGATC
T7 gRNA Mef2d C_i	fwd	ggatcctaatacgactcactataggGATCTGGGCTCCACGCGCCG
T7 gRNA Mef2d F_i	fwd	ggatcctaatacgactcactataggGCAGCCTCGCTCTGTCCCGC
T7 gRNA Mef2d G_i	fwd	ggatcctaatacgactcactataggGCCTACGTCGGCCTCGAGTC
T7 gRNA ctrl1	fwd	ggatcctaatacgactcactataggGTCCAGCGGATAGAATGGCG
T7 gRNA ctrl2	fwd	ggatcctaatacgactcactataggGGAGCGGTTTTGGATATTAG
T7 gRNA ctrl3	fwd	ggatcctaatacgactcactataggGTATGAGCGCGATGAAGGTG
T7 gRNA rev	rev	AAAAGCACCGACTCGGTGCC

Table III. gRNAs

ID	Sequence 5' → 3'	5' upstream of TSS
Klf15 A	GGGACTCTGCGGGCTTTCAG	-188 bp
Klf15 B	GTGCAGATCCACGAAGAGAC	-127 bp
Klf15 C	GACACGGTCCCTACTAGATC	-280 bp
Klf15 D	GTCCCACGTGGTCTGCACTT	-209 bp
Mef2d A_i	GCCCTGCGGGGCCCTCCCAT	-57 bp
Mef2d B_i	GCGTCCCAGGCCTCCCTGCC	-91 bp
Mef2d C_i	GATCTGGGCTCCACGCGCCG	-164 bp
Mef2d D_i	GCCCCAAAGGGGTGGGGCGC	-135 bp
Mef2d E_i	GTCACAGGTAGAGGGAGCAG	-373 bp
Mef2d F_i	GCAGCCTCGCTCTGTCCCGC	-193
Mef2d G_i	GCCTACGTCGGCCTCGAGTC	+8 bp
Mef2d H_i	GTCCCGCAGGCGGAGGGATC	-180 bp
control gRNA 1	GTCCAGCGGATAGAATGGCG	
control gRNA 2	GGAGCGGTTTTGGATATTAG	
control gRNA 3	GTATGAGCGCGATGAAGGTG	

Table IV. qPCR primers

Target		**Sequence 5' → 3'**
dCas9VPR	fwd	GCCTCGCACCAACACCAAC
	rev	GCCTCTTCCTTCTGGGGAATCAC
Klf15	fwd	CAACTCATCTGAGCGGGAA
	rev	CAAGAGCAGCCACCTCAAG
Total *Mef2d*	fwd	CTTCGCGTAACCGAGGATT
	rev	TGTGCTCATGAATGTCTGGG
Mef2daI	fwd	GAGCCGCACCAATGCTGAC
	rev	GATGATGCAGAGTTATAGACTGG
Mef2daII	fwd	GCTGGAGGACAAGTACCGG
	rev	GATGATGCAGAGTTATAGACTGG
Nppa	fwd	CATCACCCTGGGCTTCTTCCT
	rev	TGGGCTCCAATCCTGTCAATC
Nppb	fwd	AAGTCCTAGCCAGTCTCCAGAGC
	rev	CTTCAGTGCGTTACAGCCCAAAC
Ctgf	fwd	CCGCCAACCGCAAGATCGGA
	rev	CGCAGCATTTCCCAGGCAGC
Mef2a	fwd	ACCTTCTAGTCCAGGGCTGC
	rev	GTAGCGGAGACTCGGAATTG
Myh7	fwd	ATGTGCCGGACCTTGGAA
	rev	CCTCGGGTTAGCTGAGAGATCA
Aldh2	fwd	ACGGCAAGCCTTATGTCATC
	rev	ACCTTCATCACCACCACGTT
AdhfeI	fwd	CAGCCCTCACTCTGAGTTCC
	rev	AGAGTGTGCAGGGGATCAAC
ChIP qPCR *Mef2d*	fwd	GCTTGTCCATCACTCTCGTC
	rev	GACTCGAGGCCGACGTAG
ChIP qPCR *Klf15* I	fwd	GATCGGGCCTTGTTAGGAAT
	rev	CTCTTCGTGGATCTGCACTG
ChIP qPCR *Klf15* II	fwd	TAGATCGGGCCTTGTTAGGA
	rev	CTTCGTGGATCTGCACTGG
ChIP qPCR *Kcnj4*	fwd	GACAGAGAGAGGCTGCCAAC
	rev	CTGTACCCAAACCCAACACC
ChIP qPCR *Enpp1*	fwd	TATTTTGCAACCCCAGTTCC
	rev	GCCAGGCTGGGTTTAAAGAT
ChIP qPCR *Itpka*	fwd	CTGTCTTAGCCAGGCTCCAC
	rev	CAGCCAGCTCTTCATGTCCT
ChIP qPCR *Fam20c*	fwd	CAACGTCGTCTCTTCGTCCT
	rev	GAGTGGAGGCCAGAAAACAG
GFP	fwd	GGTGAACTTCAAGATCCGCC
	rev	CTTGTACAGCTCGTCCATGC
Tbp	fwd	CCAGAACAACAGCCTTCCACC
	rev	CAACGGTGCAGTGGTCAGAGT
β-Actin	fwd	CACACCCGCCACCAGTTC
	rev	CCCATTCCCACCATCACACC

The following supplementary information is accessible online for reasons of conciseness (https://www.ahajournals.org/doi/suppl/10.1161/CIRCRESAHA.118.314522):

Table V. Differentially expressed genes (DEGs, bulk RNAseq, 8 weeks *Mef2d* activation)

Table VI. Off-target prediction for *Mef2d* gRNAs

Table VII. Off-target prediction for *Klf15* gRNAs

References (Supplemental Material)

1. Kelli J. Carroll CAM, John McAnally, Douglas M. Anderson, Lorena Zentilin, Ning Liu, Mauro Giacca, Rhonda Bassel-Duby, and Eric N. Olson. A mouse model for adult cardiac-specific gene deletion with crispr/cas9. *Proceedings of the National Academy of Sciences of the United States of America*. 2015;113:338–343
2. Amoasii L, Hildyard JCW, Li H, Sanchez-Ortiz E, Mireault A, Caballero D, Harron R, Stathopoulou T-R, Massey C, Shelton JM, Bassel-Duby R, Piercy RJ, Olson EN. Gene editing restores dystrophin expression in a canine model of duchenne muscular dystrophy. *Science*. 2018
3. Bengtsson NE, Hall JK, Odom GL, Phelps MP, Andrus CR, Hawkins RD, Hauschka SD, Chamberlain JR, Chamberlain JS. Muscle-specific crispr/cas9 dystrophin gene editing ameliorates pathophysiology in a mouse model for duchenne muscular dystrophy. *Nat Commun*. 2017;8:14454
4. Martari M, Sagazio A, Mohamadi A, Nguyen Q, Hauschka SD, Kim E, Salvatori R. Partial rescue of growth failure in growth hormone (gh)-deficient mice by a single injection of a double-stranded adeno-associated viral vector expressing the gh gene driven by a muscle-specific regulatory cassette. *Hum Gene Ther*. 2009;20:759-766
5. Jin JK, Blackwood EA, Azizi K, Thuerauf DJ, Fahem AG, Hofmann C, Kaufman RJ, Doroudgar S, Glembotski CC. Atf6 decreases myocardial ischemia/reperfusion damage and links er stress and oxidative stress signaling pathways in the heart. *Circ Res*. 2017;120:862-875
6. Preibisch S, Saalfeld S, Tomancak P. Globally optimal stitching of tiled 3d microscopic image acquisitions. *Bioinformatics*. 2009;25:1463-1465
7. Yekelchyk M, Guenther S, Preussner J, Braun T. Mono- and multi-nucleated ventricular cardiomyocytes constitute a transcriptionally homogenous cell population. *Basic Res Cardiol*. 2019;114:36

Section III

Supplemental Figures and Figure Legends

Online figure I

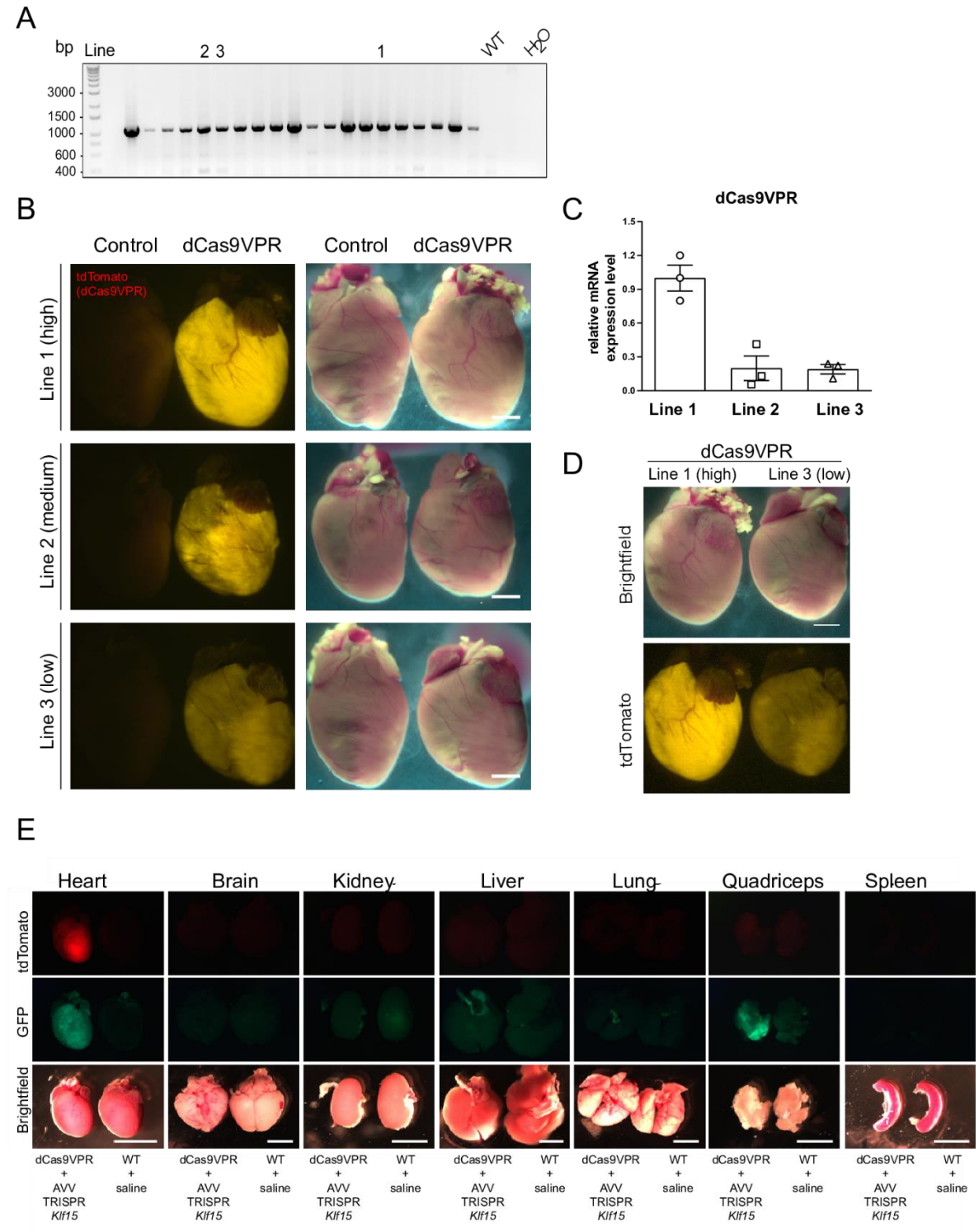

Online figure I: Identified Myh6-dCas9VPR mouse lines. A. Genotyping PCR for 20 identified dCas9VPR mouse lines. These mice were considered as independent founder mice and bred to the F1 generation for further screening. **B.** Representative adult hearts of *Myh6*-dCas9VPR-2A-tdTomato transgenic mice (age: 6 months) show distinct transgene expression

levels in the independent mouse lines based on tdTomato signal **(C)** which was confirmed on mRNA level by qPCRs for dCas9VPR (n=3 per mouse line). Error bars depict mean ± SEM; n = 3 mice per mouse line. **D.** Adult hearts from line 1 (high, left) and line 3 (low, right) in direct comparison highlighting transgene expression differences in identified mouse lines. **E.** Indicated organs were dissected from P12 mice which were injected with AAV TRISPR *Klf15* at P4. Transgenic organs (left) next to wild-type saline injected littermate organs (right) showing tdTomato signal exclusively in the heart. GFP expression from TRISPR *Klf15* is muscle specific (heart & quadriceps). Note, that GFP is expressed under muscle-specific CK8 promoter control. Scale bar (E) = 5 mm.

Online figure II

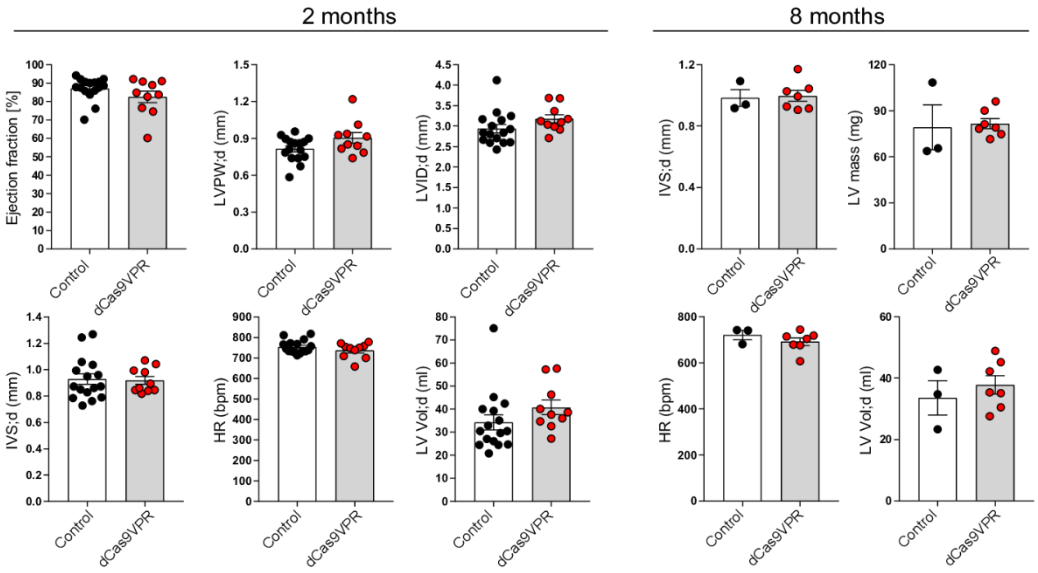

Online figure II: Heart function in dCas9VPR expressing mice. Echocardiography parameters comparing *Myh6*-dCas9VPR transgenic mice *versus* control littermates at 2 months and 8 months of age. No significant difference was observed in ejection fraction, left ventricular posterior wall (LVPW;d), left ventricular inner diamerter (LVID;d), intraventricular septum (IVS;d); left ventricle volume (LV Vol;d) in diastole and left ventricular (LV) mass and heart rate at both time points. Statistics: n≥3 per time point, error bars depict mean ± SEM, student's t-test.

Online figure III

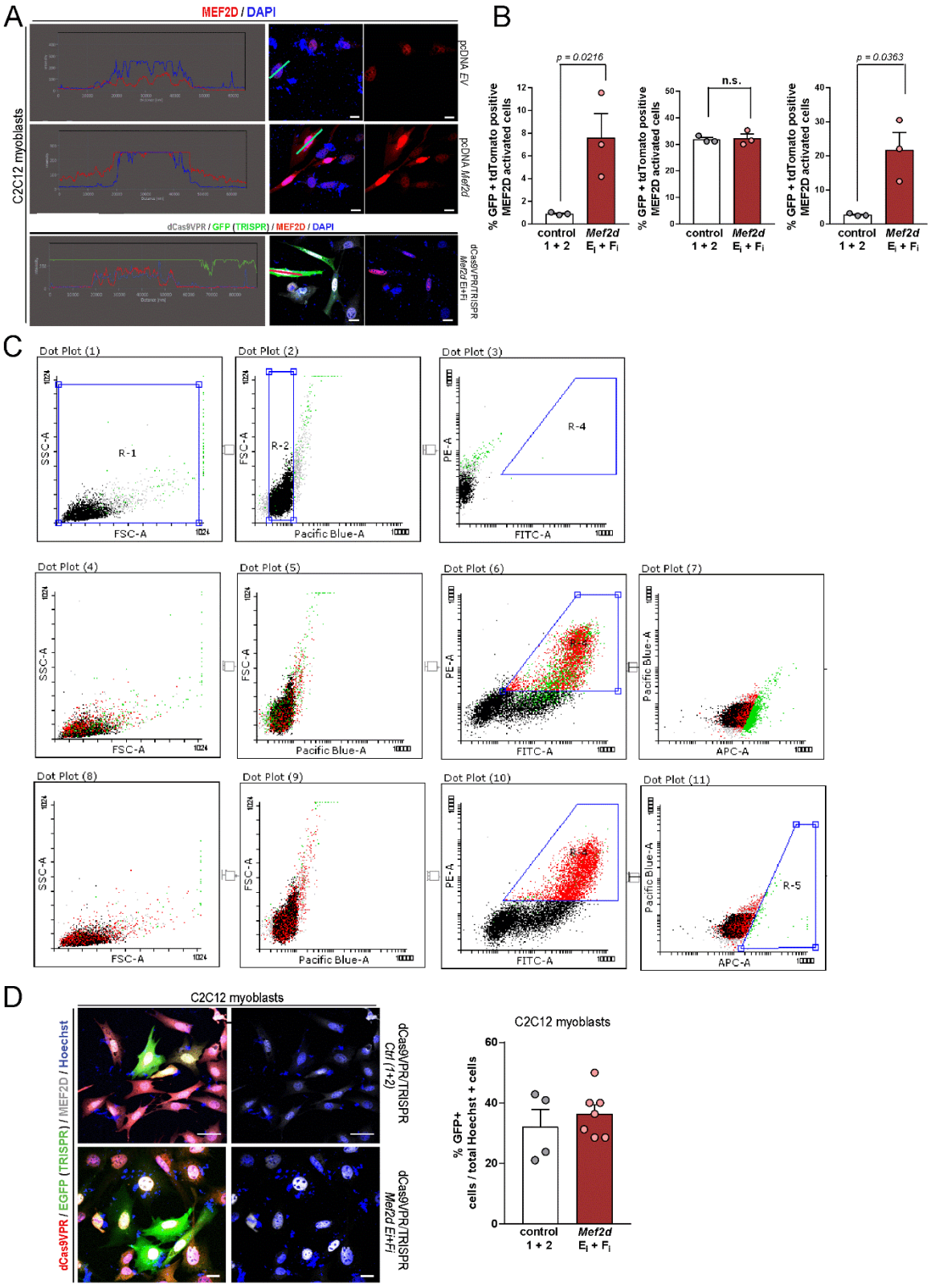

Online figure III: Evaluation of single cell CRISPRa potential *in vitro*. A. C2C12 myoblasts were transfected with pcDNA, pcDNA *Mef2d* and SP-dCas9VPR + TRISPR *Mef2d*. Subcellular intensity validation revealed nuclei specific abundance in pcDNA transfected and CRISPRa *Mef2d* activated cells but cytosolic *Mef2d* localization by pcDNA *Mef2d*

overexpression. **B.** Quantification of FACS analyses of transfected N2A cells reveals ~30% of tdTomato and GFP positive cells out of which ~20% show increased MEF2D expression. Statistics: n=3 technical replicates, error bars depict mean ± SEM, student's t-test. **C.** Gating for FACS measurements: From the whole cell population (R-1) single living cells were selected (R-2) and background fluorescence was assumed in pcDNA transfected cells for channels FITC-A and PE-A (R-4). Double positive cells (GFP and tdTomato = FITC-A and PE-A positive cells) were selected in PB-dCas9VPR-2A-tdTomato and p-2xgRNA control 1 + 2 (lower panel) or p-2xgRNA *Mef2d* E_i + F_i (middle panel) transfected cells (R-4, red population). High MEF2D expressing cells were selected for quantification in B (R-5, green population). **D.** Evaluation of C2C12 myoblasts, stably expressing dCas9VPR, transfection was evaluated by immunofluorescence and revealed 30-40% transfection efficiency (n≥4 imaged areas, error bars depict mean ± SEM). Presence of *Mef2d* gRNAs were sufficient to increase MEF2D levels on single cell level. Scale bar (A, D) = 20 mm.

Online figure IV

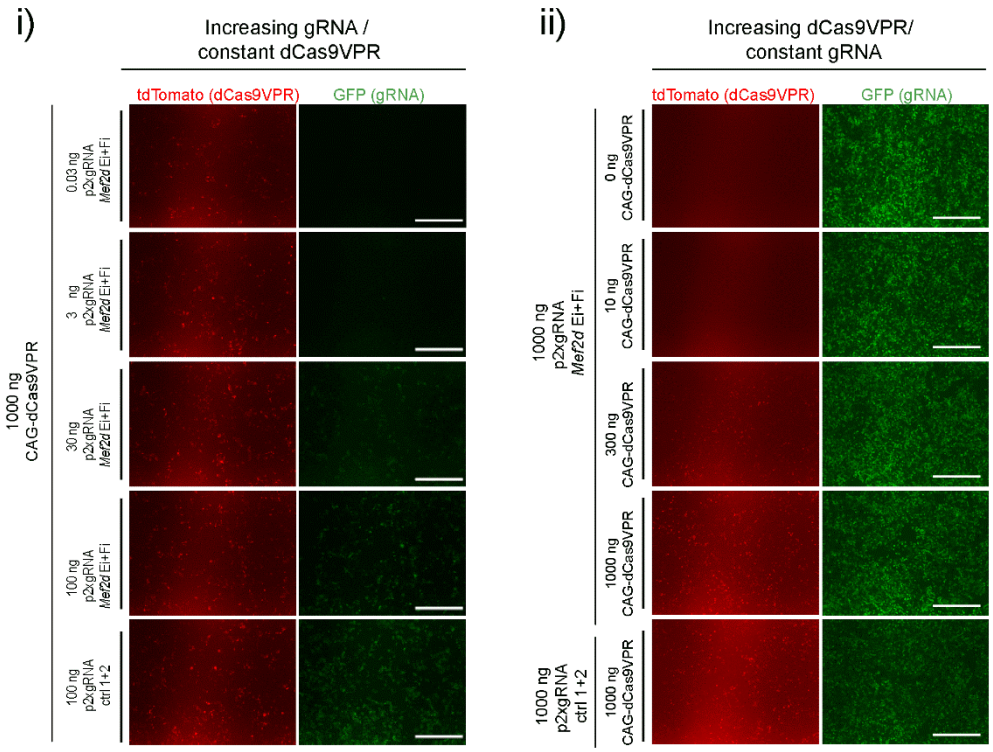

Online figure IV: Titration of CRISPRa components *in vitro*. A. Complementing data for figure 2D: Representative Neuro2a live-cell fluorescence images of indicated conditions (i) constant dCas9VPR and variable p-2xgRNA or (ii) constant p-2xgRNA and variable dCas9VPR. Scale bar = 50 µm.

Online figure V

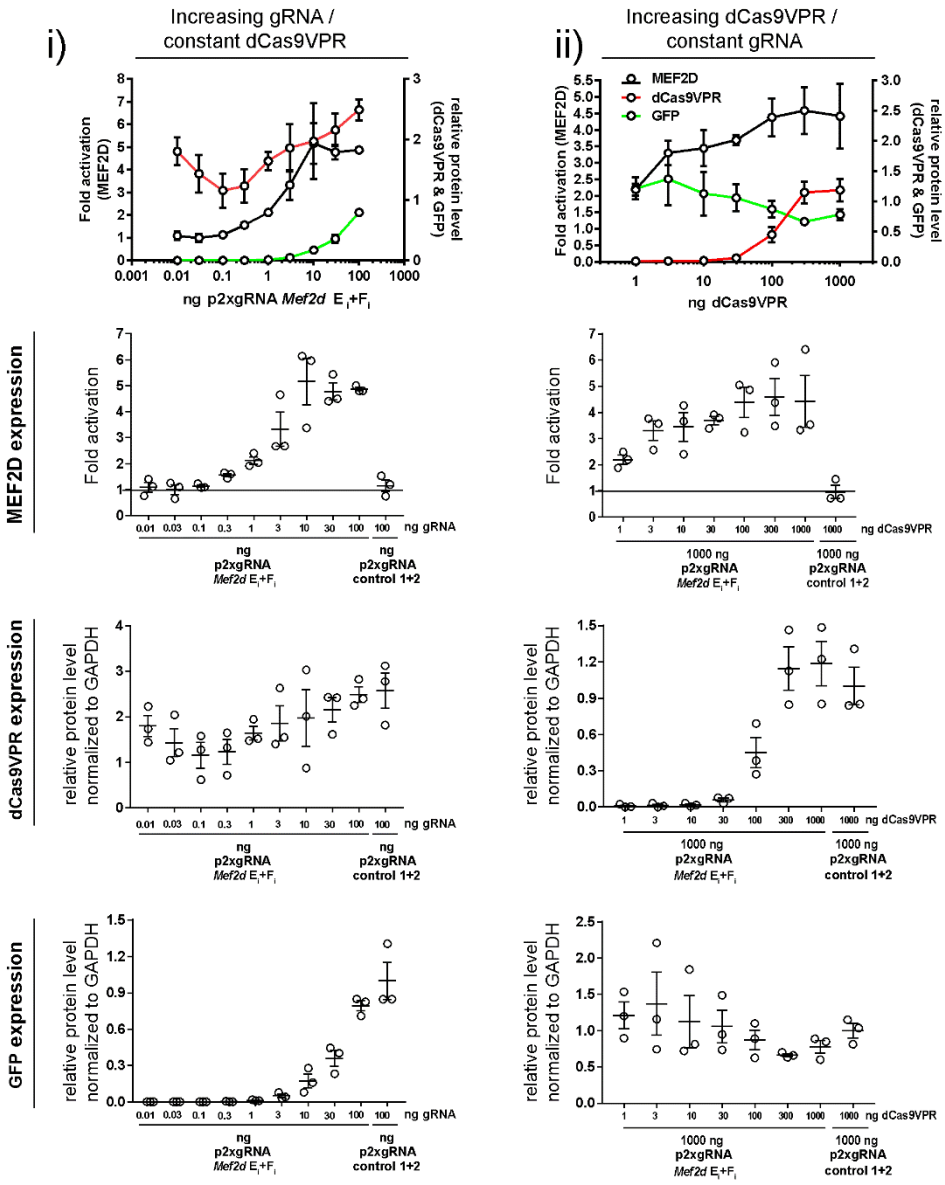

Online figure V: Quantification of *in vitro* titration of CRISPRa components. A. Densiometric analyses of immunoblots in figure 2D demonstrated gradual increase and CRISPRa component dependency of *Mef2d* activation in N2A cells. Maximum MEF2D activation on protein levels was achieved with 100 ng transfected dCas9VPR and with 10 ng gRNA expression construct. n=3 per condition, error bars depict mean ± SEM.

Online figure VI

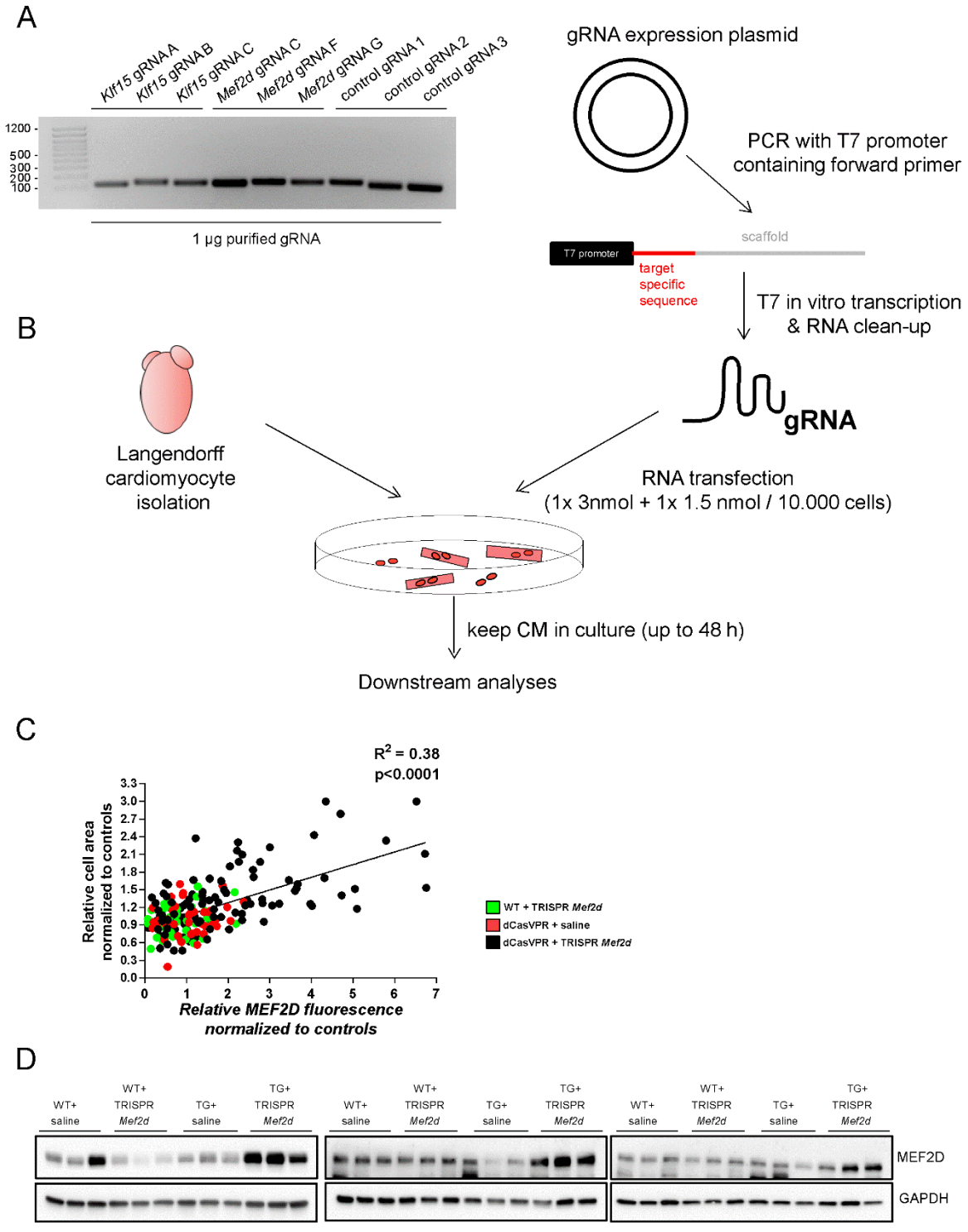

Online figure VI: Transfection of isolated postnatal cardiomyocytes with *in vitro* transcribed gRNAs and phenotypic consequences of *Mef2d* activation in the postnatal heart. A. Transcribed gRNAs for figure 2E and F run on agarose gel to check gRNA *in vitro* transcription. **B.** Schematic representation of gRNA template generation, *in vitro* gRNA transcription and transfection into isolated cardiomyocytes. A gRNA expression construct encoding for the desired gRNA was used to amplify the gRNA encoding region with primers flanking the gRNA scaffold and adding a T7 promoter sequence. PCR product was purified and subjected to T7 *in vitro* transcription. Transcribed gRNAs were purified and 3 nmol were

transfected into isolated postnatal cardiomyocytes (per ~10,000 cells) plated on Laminin coated plates. The transfection was repeated after 12 h with 1.5 nmol gRNAs. **C.** Complementing data for Figure 4C and D: Correlation plot comparing cardiomyocyte cross-sectional area and relative MEF2D immunofluorescence in paraffin embedded slices of 8 weeks old *Mef2d* activated hearts indicating positive dependency of cardiomyocyte size and *Mef2d* expression level (black dots). Control groups are depicted in: Green dots (wild-type + TRISPR *Mef2d*) and red dots (Myh6-dCas9VPR + saline). **D.** Immunoblots of *Mef2d* activated 8 weeks old mouse hearts (biological and technical replicates) used for densiometric analyses in Figure 4E ($n \geq 6$ per group and three independent immunoblots).

Online figure VII

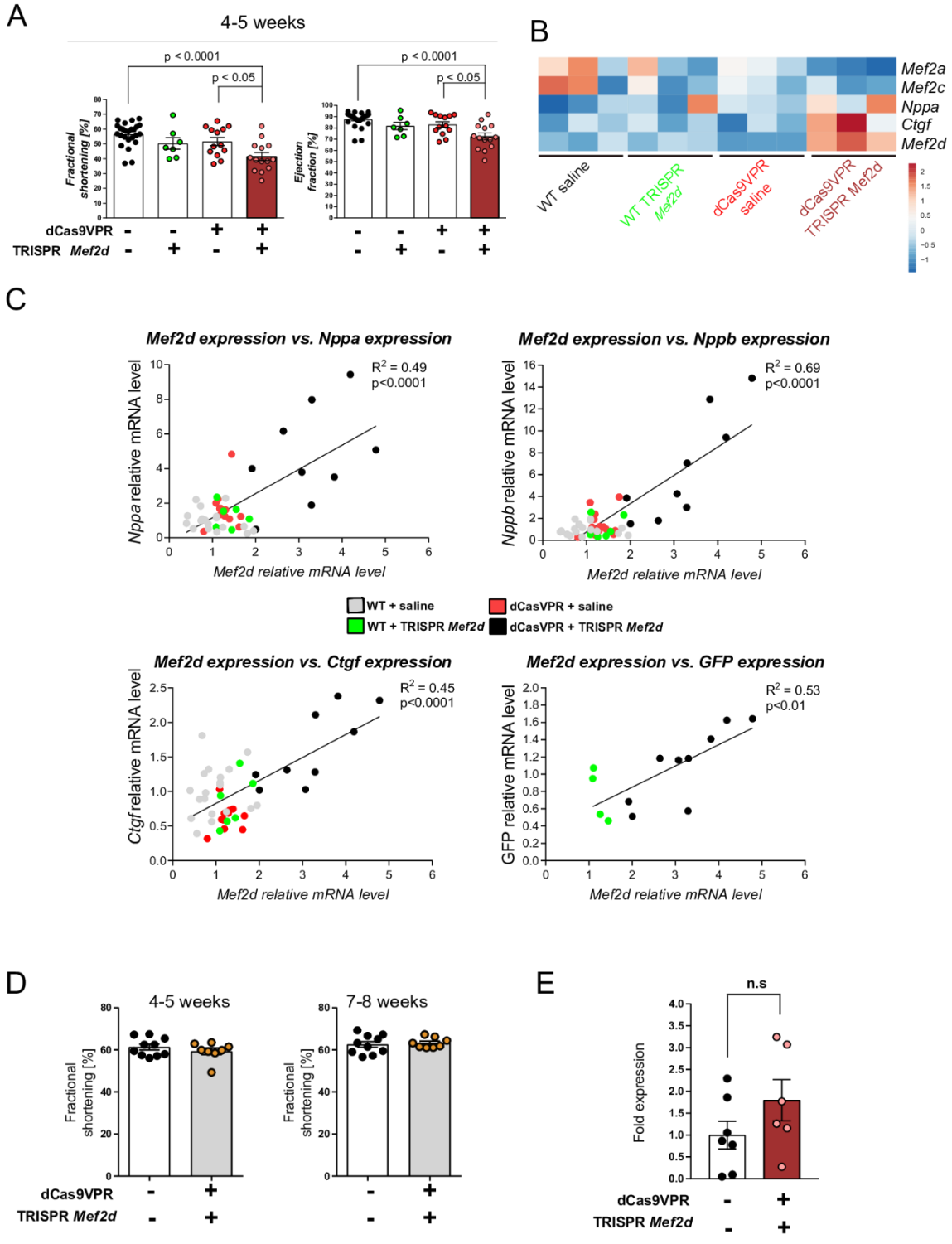

Online figure VII: *Mef2d* activation and consequences for heart failure parameters expression A. Echocardiography of 4-5 weeks old *Mef2d* activated mice showing decline in cardiac function when compared to control groups. Statistics: n≥7 per group, error bars depict mean ± SEM, one-way ANOVA with Bonferroni's post-hoc multiple comparison test. **B.** Heatmaps derived from RNA-seq experiment of 8 weeks old *Mef2d* activated mice showing elevated *Mef2d* and *Ctgf* transcript levels compared to all control groups including dCas9VPR transgenic mice injected with saline indicating that *Ctgf* expression is dependent on *Mef2d*

activation. **C.** Complementing data for figure 5F: Correlation plots between natriuretic peptide expression (*Nppa* and *Nppb*) versus *Mef2d* transcript level and *Ctgf* expression *versus Mef2d* transcript level indicate positive relation. Importantly, *Mef2d* activation level associates with GFP expression indicative for gRNA availability. **D.** Functional assessment of heart function in dCas9VPR mice expressing low levels of dCas9VPR (line 3, low) injected with 5.5 x 10^{10} AAV TRISPR *Mef2d* (1/2 of full dose AAV) at P4 showing no functional impairment compared to wild-type saline injected litter mates at 4-5 weeks and 7-8 weeks as well as no significant difference in **E.** *Nppb* expression level. Statistics (D, E) n≥6, error bars depict mean ± SEM, student's t-test, n.s. = not significant.

Online figure VIII

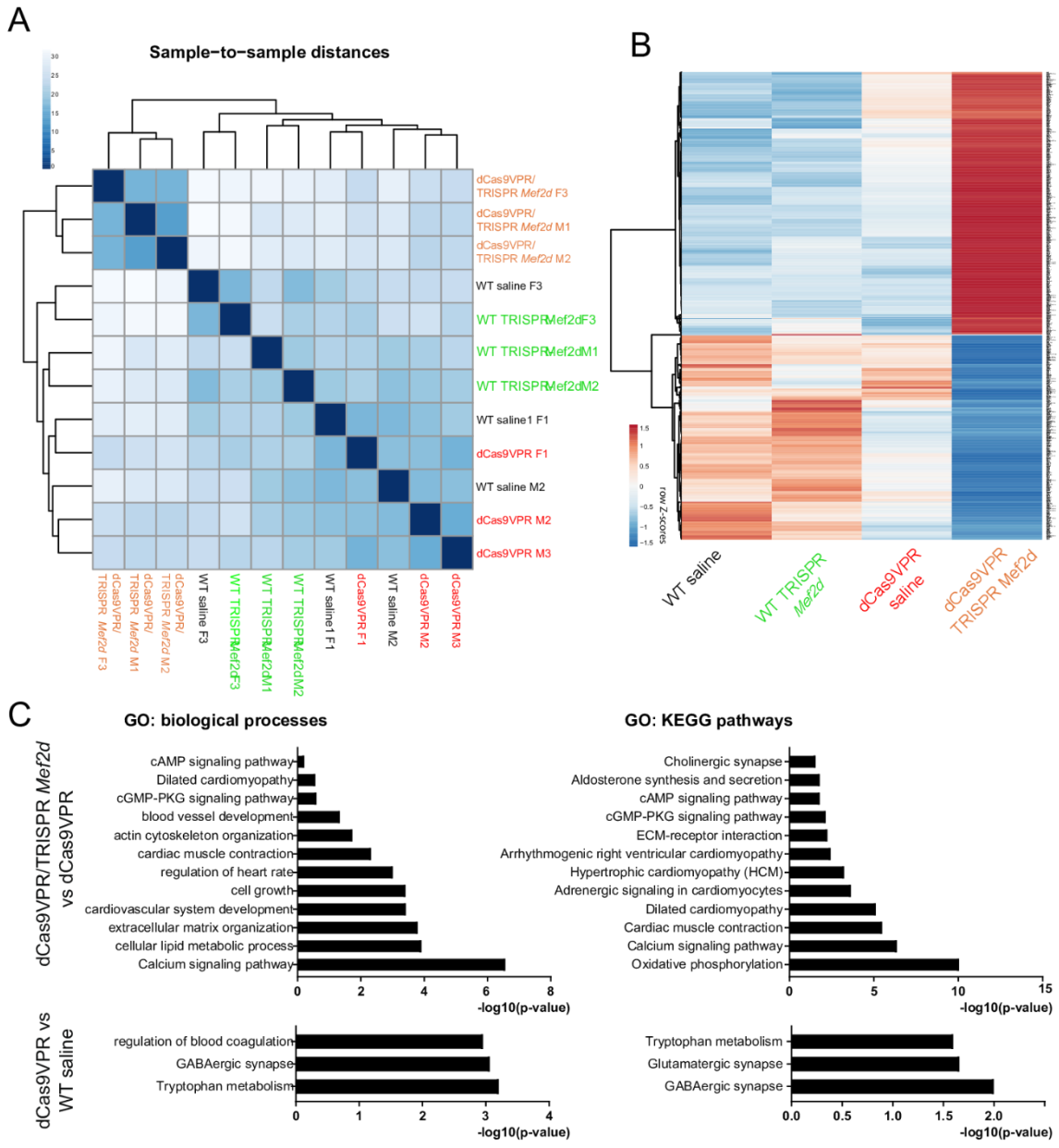

Online figure VIII: RNA sequencing of Myh6-dCas9VPR hearts and CRISPRa mediated *Mef2d* activated hearts. A. Sample-to-sample distant plots showing clustering of *Mef2d* activated heart samples and separation from all control groups. **B.** Heatmap of differentially expressed genes (DEGs) indicating pronounced transcriptional changes in *Mef2d* activated

hearts over controls. **C.** GO and KEGG term analyses of CRISPRa *Mef2d* activated hearts and transgenic saline injected litter mates confirm differential gene expression associated with cardiomyopathy terms while analyses between wild-type and transgenic saline injected hearts revealed few terms including GABA- and Glutamatergic processes.

Online figure IX

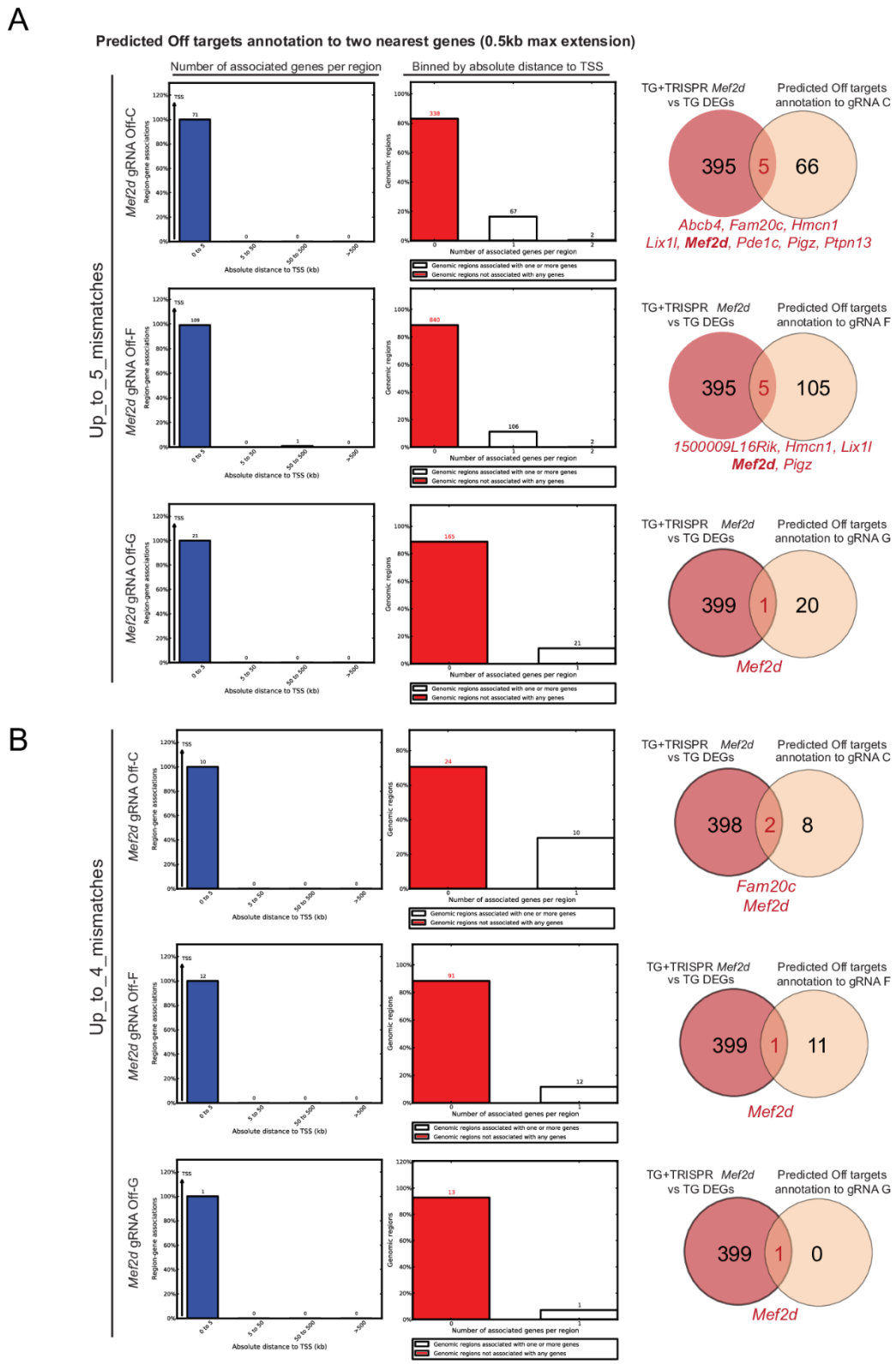

Online figure IX: *Mef2d* activation *in vivo* and dCas9VPR off-target prediction analyses. **A.** 5-mismatch off-target (up to 5 mismatches in gRNA to potential off-target site) and **B.** 4-mismatch off-target prediction for *Mef2d* gRNAs used in TRISPR construct synthesis and corresponding RNA-seq derived differentially expressed genes intersection, which were used

to identify potential dCas9VPR binding sites revealed limited number of genes which were chosen for further dCas9VPR-DNA association and expression studies.

Online figure X

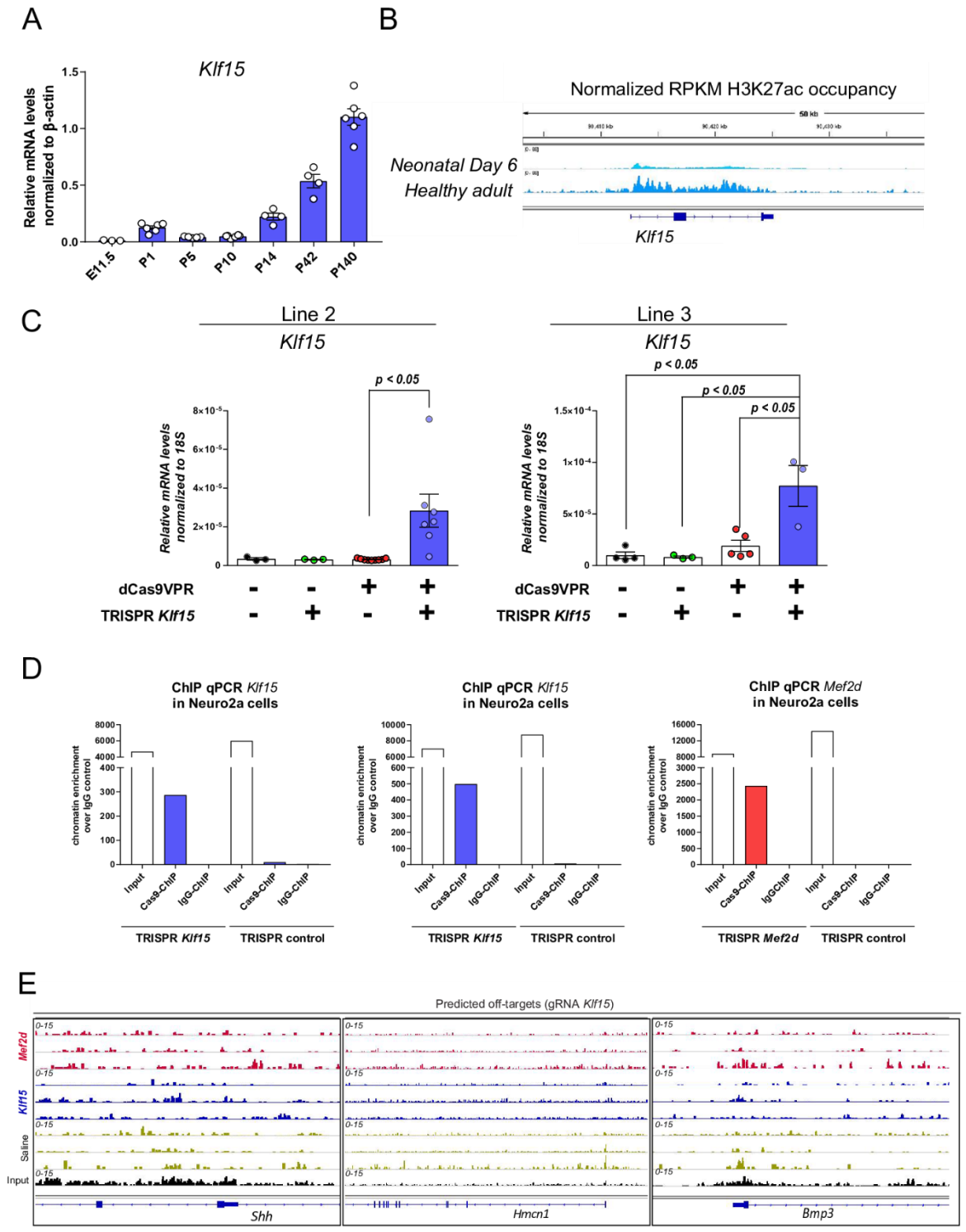

Online figure X: Endogenous *Klf15* expression, *Klf15* promoter region H3K27ac status and ChIP qPCR validation *in vitro*. A. Endogenous *Klf15* expression between Embryonic stage (E)13.5 and adulthood (P140) revealed progressively increasing *Klf15* expression between P10 and P14 up to adulthood. *Klf15* transcript level were normalized to β-actin (n≥3

per time point). **B.** The *Klf15* promoter region in neonatal hearts is characterized by low H3K27ac occupancy in contrast to adult hearts suggesting low endogenous *Klf15* transcriptional activity in neonatal hearts. **C.** Neonatal gene activation by CRISPRa was confirmed in all three identified mouse lines at P10 when injected at P4 with 1.1 x 10^{11} vg/g AAV TRISPR *Klf15* (Line 1, high in Figure 6B, here: line 2, medium, line 3, low). Transcripts were normalized to *18S*. Statistics: n≥3 per line and condition, one-way ANOVA with Bonferroni's post-hoc multiple comparison test. **D.** ChIPs were performed in Neuro2a cells transfected with CAG-dCas9VRP-2A-tdTomato and respective TRISPR constructs to validate anti-Cas9 ChIP grade antibody (Diagenode) and ChIP qPCR primers: (left) *Klf15* ChIP primer pair 1, (middle) *Klf15* ChIP primer pair II, (right) *Mef2d* ChIP primer. The respective dCas9VPR targets showed enrichment over IgG control ChIP and TRISPR control transfected cells. **E.** ChIP sequencing revealed no significant dCas9VPR off-target binding at predicted *Klf15* gRNA off-target sites.

Online figure XI

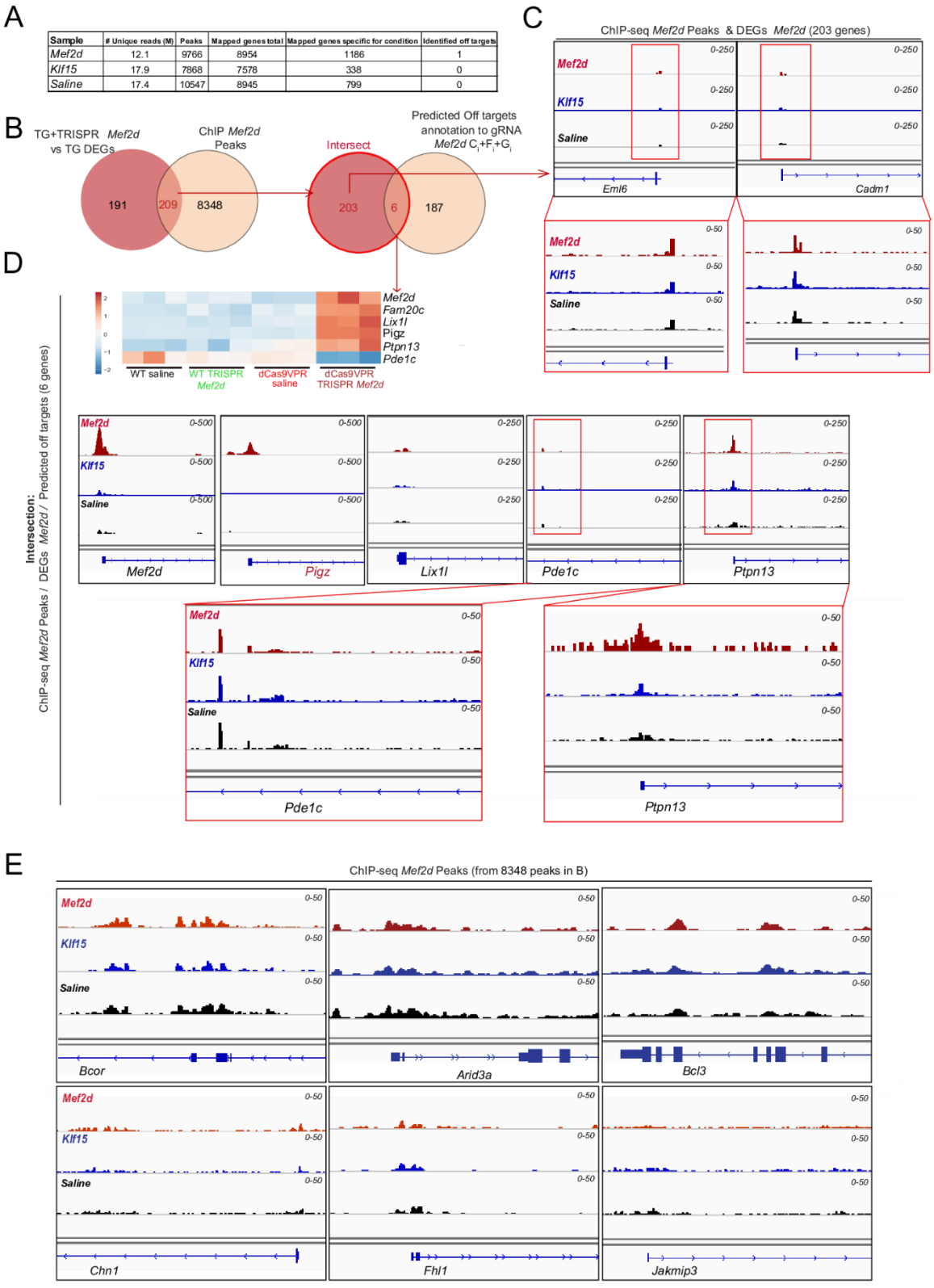

Sample	# Unique reads (M)	Peaks	Mapped genes total	Mapped genes specific for condition	Identified off targets
Mef2d	12.1	9766	8954	1186	1
Klf15	17.9	7868	7578	338	0
Saline	17.4	10547	8945	799	0

Online figure XI: Specificity of *Mef2d* activation A. Summary of identified peaks in the mouse genome associated with dCas9VPR in TRISPR *Mef2d*, *Klf15* or saline injected transgenic mice respectively. **B.** Intersect of identified potential off-target sites and differentially expressed genes from RNA-seq experiment as well as predicted *Mef2d gRNA* off-

target sites revealed 6 differentially expressed genes with dCas9VPR genomic association. **C.** ChIP-seq and RNA-seq intersect identified off-targets revealed peaks that were independent of gRNA presence. **D.** ChIP-seq, RNA-seq and *Mef2d* gRNA off-target prediction intersection revealed only 1 out of 6 genes (*Pigz*) showing a peak exclusively in the TRISPR *Mef2d* injected group indicative for a true gRNA dependent off-target site. The remaining 5 sites showed a peak in ChIP-seq in all conditions but no differential gene expression in the transgenic + saline injected group indicating no dCas9VPR mediated gene activation for these genes. Note, that off-target site dCas9VPR chromatin enrichment is in all cases lower than at the on-target site. **E.** Quality of dCas9VPR off-target peaks revealed low dCas9VPR-chromatin association in all conditions analyzed.

Online figure XII

A

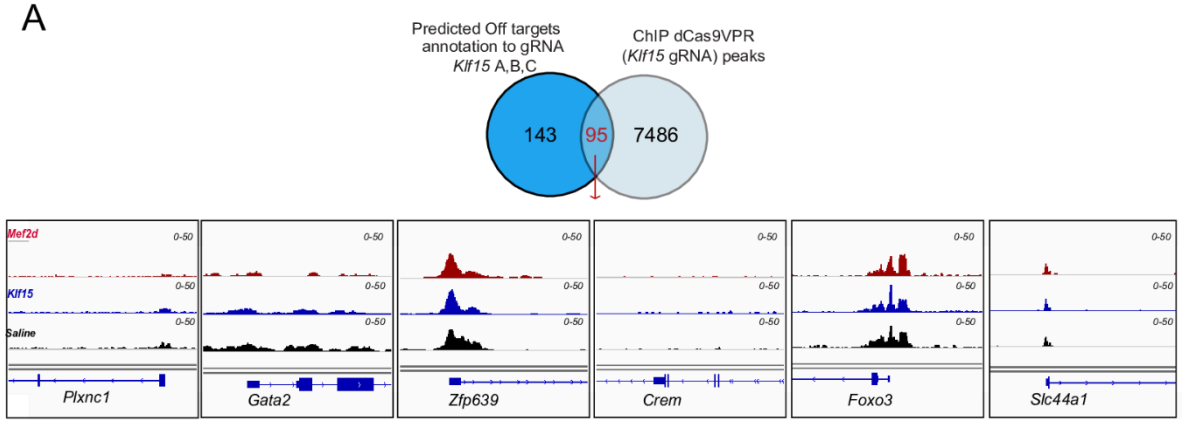

B

			Tnnt2 read avg. per cell	
	Total cell number	**% of cells GFP pos**	**GFPpos**	**GFPneg**
WT+AAV TRISPR *Klf15*	272	37.13	345.37	170.40
dCasVPR+Saline	242	0.00	0.00	223.02
dCasVPR+AAV TRISPR *Mef2d*	213	54.93	347.02	135.09

C

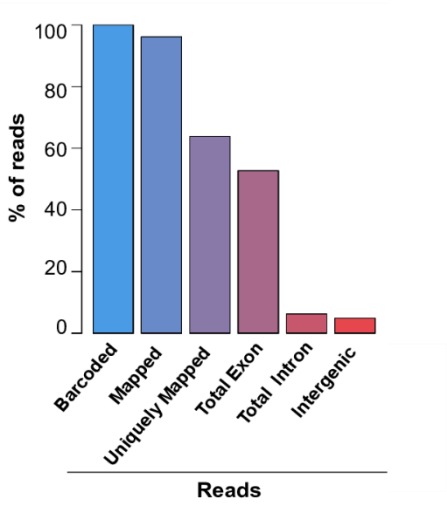

D

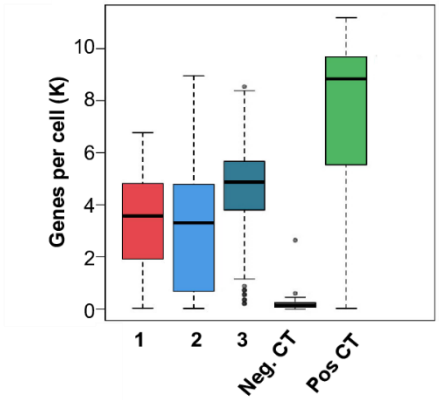

E

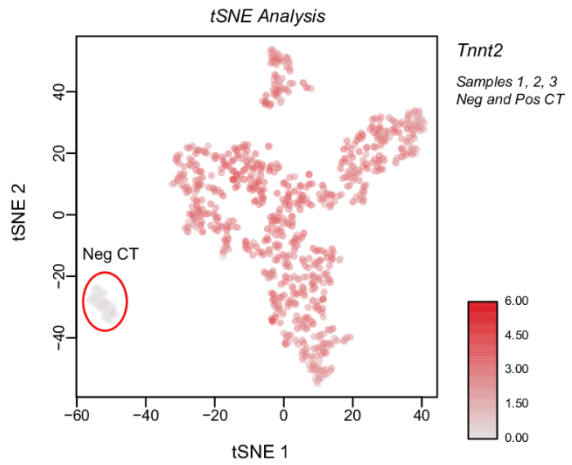

Online figure XII: Specificity of *Klf15* activation and *Mef2d* activation at single cell resolution. A. Identified off-target ChIP peaks and *Klf15* gRNA off-target prediction intersect revealed no gRNA-specific dCas9VPR DNA association. **B.** Table summarizing the single cell sequencing (SCseq) experimental overview including proportion of sequenced GFP positive cells and *Tnnt2* positive cells. Positive and negative controls were run. **C.** Read statistics and

quality control for SCseq experiment. **D.** Reads and genes by sample type. The gene expression analyses were performed post-QC. Samples that failed QC were dropped from the analysis. **E.** t-SNE plot summarizing similar distribution of *Tnnt2* positive cells in all conditions and separation from negative control.

Online figure XIII

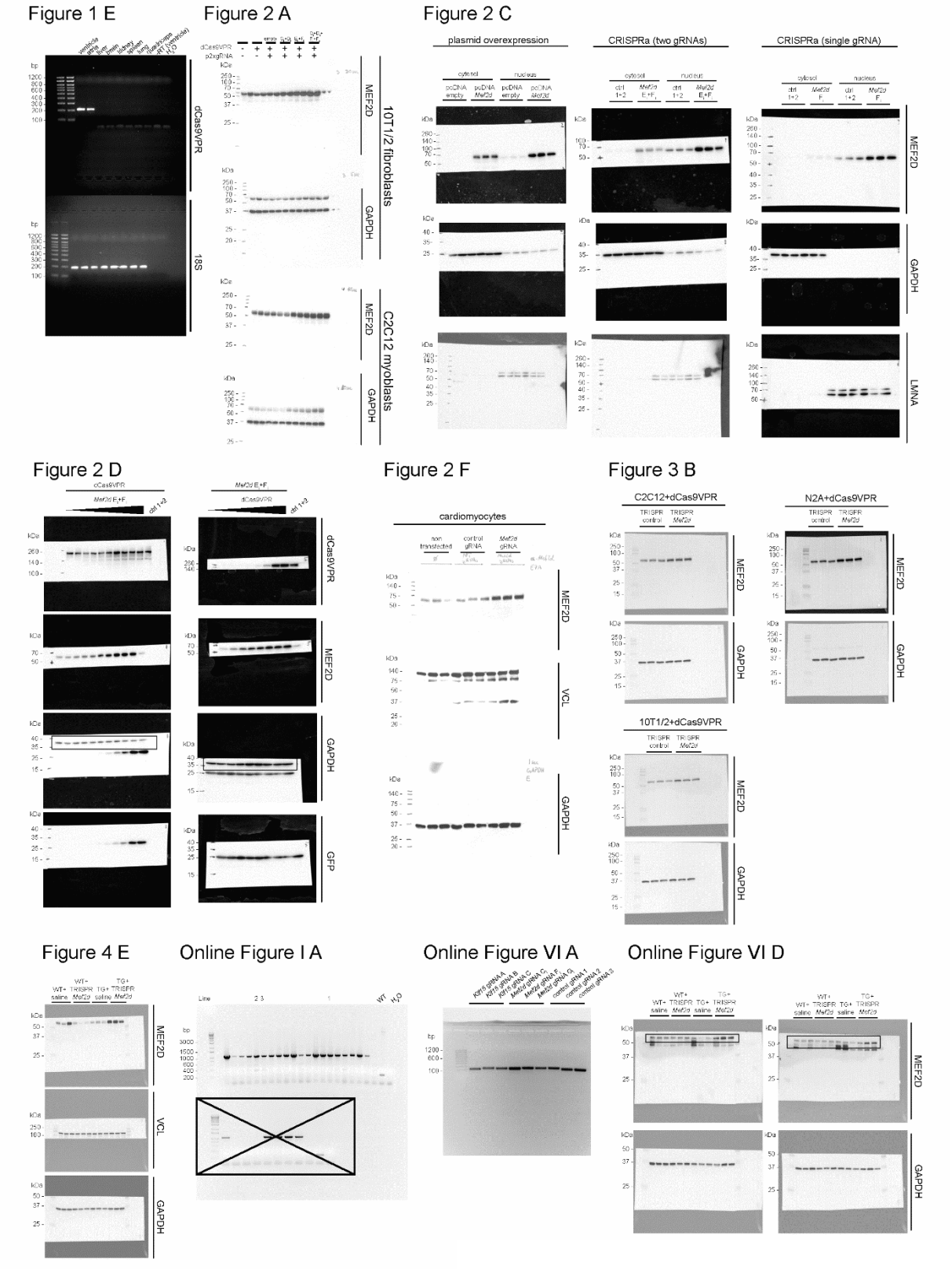

Online figure XIII: Full unedited gels and Immunoblots. Full unedited gel for Figure 1E; 2A; 2C; 2D; 2F; 3B; 4B and for Online Figure IA; VIA and VID. Lanes corresponding to those shown in the cropped images within the manuscript are indicated with squares.

7. Chapter 3:

Human induced pluripotent stem cells for CRISPR based gene activation

"Generation of homozygous CRISPRa human induced pluripotent stem cell (hiPSC) lines for sustained endogenous gene activation"

Eric Schoger[1,4], Loukas Argyriou[2,4], Lukas Cyganek[3,4] and Laura Cecilia Zelarayán[1,4]

Affiliations:

[1] Institute of Pharmacology and Toxicology, University Medical Center Goettingen (UMG), Göttingen, Germany;

[2] Institute of Human Genetics, University Medical Center Goettingen (UMG), Göttingen, Germany;

[3] Clinic for Cardiology and Pneumology, University Medical Center Goettingen (UMG), Göttingen, Germany;

[4] DZHK (German Center for Cardiovascular Research), partner site Goettingen, Germany

Abstract:
CRISPR/Cas9 technology is a powerful tool, owing to its robust on-target activity and high fidelity. Mutated Cas9 without nuclease activity (dCas9) fused to transcriptional modulators, can function as transcriptional inhibitors or activators (CRISPRa). We generated homozygous human induced pluripotent stem cell (hiPSC) lines with an inserted CRISPRa cassette into the *AAVS1* locus whilst maintaining pluripotency and genomic integrity, the ability to differentiate into all three germ layers, generate functional cardiomyocytes, and validated Cas9-mediated induction of endogenous gene expression. Our generated hiPSC-CRISPRa offers a valuable tool for studying endogenous transcriptional modulation with single and multiplexed possibilities in all human cell types.

Resource Table:

Unique stem cell line identifier	RUCDRi002-A-5
Alternative name of stem cell line	TC-1133-CRISPRa
Institution	Institute of Pharmacology and Toxicology, University Medical Center Goettingen, Germany
Contact information of distributor	Laura C. Zelarayán, laura.zelarayan@med.uni-goettingen.de
Type of cell line	Human induced pluripotent stem cell (hiPSC)
Origin	Human induced pluripotent stem cell (hiPSC) (LhiPSC-GR1.1), Accession: CVCL_RL65 (https://commonfund.nih.gov/stemcells/lines)
Additional origin info	Age: N/A Sex: male Ethnicity if known: N/A
Cell Source	Umbilical Cord Blood Cell (CD34+)
Method of reprogramming	Non-integrating, episomal
Associated disease	No disease was diagnosed
Gene/locus	CRISPR/dCas9VPR/tdTomato, 19q13.3
Method of modification	CRISPR/Cas9
Gene correction	No
Name of transgene or resistance	CRISPR/dCas9VPR/tdTomato
Inducible/constitutive system	*not applicable*
Date archived/stock date	Jan 2020
Cell line repository/bank	*not applicable*
Link to related literature	https://hpscreg.eu/cell-line/RUCDRi002-A-5 https://hpscreg.eu/cell-line/RUCDRi002-A DOI: 10.1016/j.stemcr.2015.08.015
Ethical approval	Reference number: 10/9/15

Resource utility

Transcriptional regulation by a nuclease-deficient CRISPR/Cas9 system is a valuable tool offering robust, titratable and reversible modulation as well as on-target specificity whilst providing the possibility to multiplex gene activation [1, 2]. The generated hiPSC-CRISPRa line allows gene regulation for basic and translational studies.

Resource Details

The bacterial CRISPR/Cas9 system, widely used for gene editing and modulation of expression, is rapidly advancing in the medical world with the development of therapies for Duchenne muscular dystrophy, cystic fibrosis and cancer [3-5]. CRISPR-based systems, which can reversibly modulate gene expression without affecting DNA structure, are especially attractive from the therapeutic perspective. We generated hiPSC transgenic lines with a second generation CRISPRa system carrying a nuclease-deficient dCas9 fused to heterotrimeric VPR transactivator consisting of VP64, p65, and RTA domains. This system can be exploited to decipher endogenous mechanisms of regulation in any desired cell type. Using the CRISPR/Cas9-based genome editing approach we targeted the *AAVS1* human genomic locus for introducing the previously described dCas9VPR-tdTomato [2] and puromycin cassettes under the control of the *CAG* and *EF1a* promoters, respectively (Fig. 1A). An optimized nucleofection protocol was employed to transfect LhiPSC-GR1.1 cells. After transfection, cells with tdTomato expression were selected and genotyped by PCR (Fig. 1B, primer binding shown in Fig. 1A, **black** primers amplified only the wild-type (WT) fragment; **green** primers amplified the inserted construct). Subsequently, two positive clones (#2 and #3) were expanded, analyzed and cryopreserved. DNA sequencing data corroborated both, corrected and homozygous knock-in transgene integration in the *AAVS1* locus in CRISPRa (Fig. 1C, shown for clone #2). The PCR results revealed that of the 15 clones screened, 11 clones contained a homozygous insertion (named as **CRISPRa** cells), one clone was heterozygous and three clones contained no insertion but instead a WT intact locus (used as **control** cells) (data not shown). Off-target analysis was performed by analyzing the top five predicted off-targets by PCR and sequencing; no editing event was identified in any of these sites. Control electroporated and non-electroporated (reference) lines were used for comparison (Fig. 1D). All lines tested negative for mycoplasma. Cell growth and morphology were normal compared to nucleofected (Fig. 1F*i*) and non-nucleofected controls. Transgene expression was corroborated by dCas9 and tdTomato expression in CRISPRa compared to control hiPSCs as demonstrated by western blot (Fig. 1E, shown for clones #2 and #3) and confocal microscopy (Fig. 1F*ii*, shown for clone #2, n=3 different passages). Pluripotency was assessed by immunofluorescence to analyze the expression of stemness marker OCT4 (Fig. 1F*iii*) and by flow cytometry analysis which showed 94.2% OCT4 and 99.9% TRA1-60 positive cells (Fig. 1F*iv*) (shown for clone #2). Genomic integrity of CRISPRa clones #2 and #3 as well as of control cells was demonstrated by SNP-based karyotyping and standard G-banding. No evidence for numeric or structural abnormalities was detected (Fig. 1G). Spontaneous differentiation capacity into all three germ layers was tested by formation of embryoid bodies (EBs) and directed differentiation in the CRISPRa and control lines. Analysis of transcript levels showed expression of Paired Box 3 (*PAX3*) and Microtubule-Associated Protein 2 (*MAP2*) indicating ectodermal differentiation; T-box transcription factor T (*TBXT*) indicating mesodermal fate and α-Feto-Protein (*AFP*) indicative of endodermal differentiation. Immunofluorescence analysis confirmed expression of AFP, β-III-Tubulin and α-Smooth Muscle Actin (ACTA2), further supporting endodermal, ectodermal and mesodermal fate, respectively (Fig. 1H, shown for clones #2 and #3). We investigated the suitability of the CRISPRa lines for studying cardiomyocytes generated by directed 2D differentiation which resulted in spontaneously beating cells (videos provided as Supplementary Material) with robust α-Actinin 2 (ACTN2) and cardiac Troponin T (TNNT2) cardiac marker expression (Fig. 1I, shown for clone #2). Finally, we tested the functionality of the CRISPRa line by ascertaining the induction of *KLF15* expression, implicated in

cardiac hypertrophy and metabolic homeostasis. We showed that a single guide-RNA, which was designed to bind a 44 bp 5´-upstream sequence of the *KLF15* transcriptional starting site (TSS), was able to significantly enhance transcription of *KLF15* in CRISPRa lines (clones #2 and #3) compared to their respective parental lines transfected with a non-targeting gRNA. Control cells did not show activation independent of the transfected gRNA (Fig. 1J).

In summary, using a fully characterized hiPSC line, we generated a human CRISPRa line with a homozygous targeted insertion, normal karyotype and pluripotency as well as showed its potential to activate endogenous gene expression. This represents an invaluable tool for *in vitro* translational studies and disease modelling.

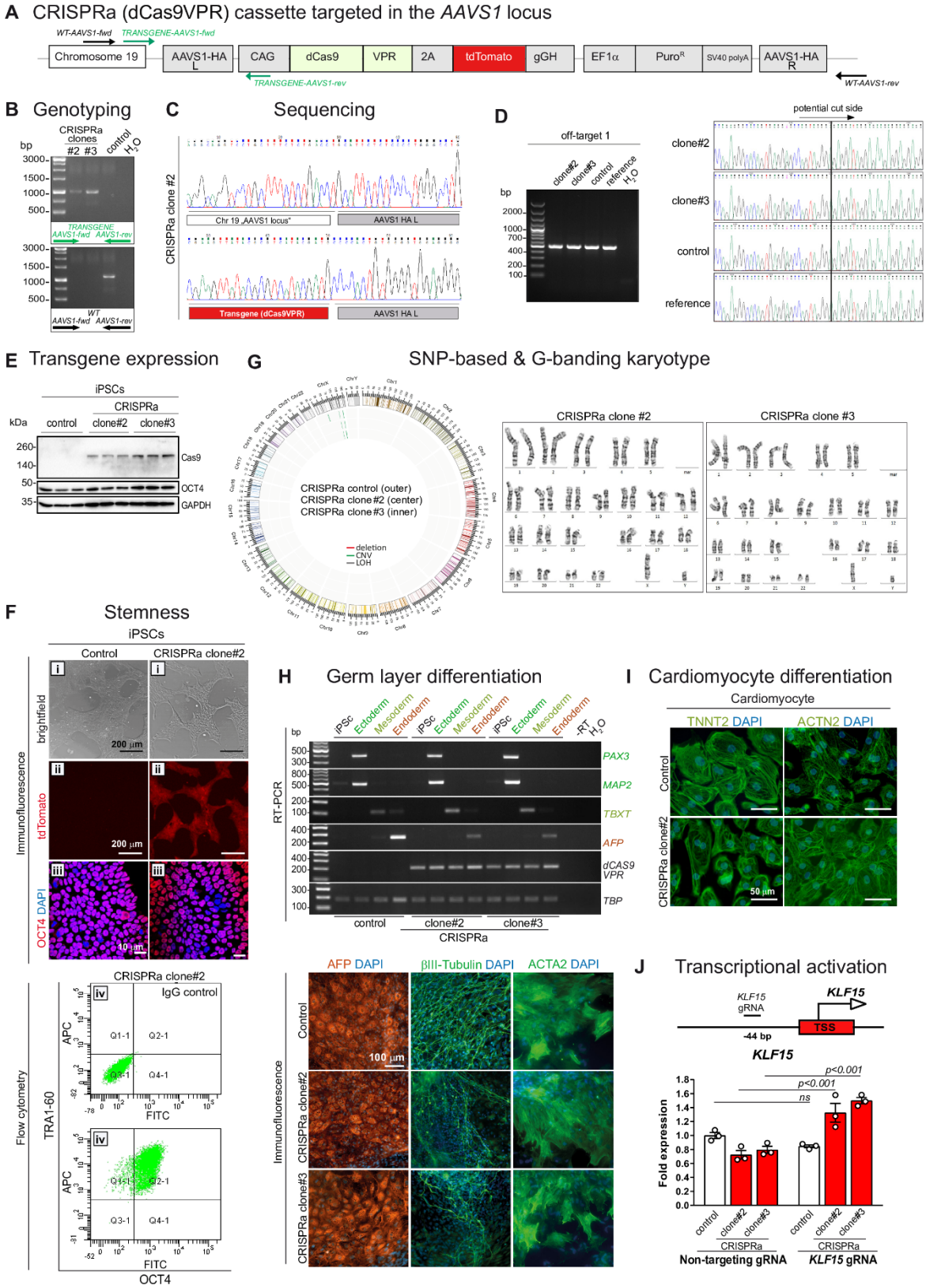
A CRISPRa (dCas9VPR) cassette targeted in the AAVS1 locus
WT-AAVS1-fwd
TRANSGENE-AAVS1-fwd
Chromosome 19
AAVS1-HA L
CAG
dCas9
VPR
2A
tdTomato
gGH
EF1α
Puro^R
SV40 polyA
AAVS1-HA R
TRANSGENE-AAVS1-rev
WT-AAVS1-rev
B Genotyping
CRISPRa clones #2 #3
control
H2O
bp
3000
1500
1000
500
TRANSGENE
AAVS1-fwd AAVS1-rev
WT
AAVS1-fwd AAVS1-rev
C Sequencing
CRISPRa clone #2
Chr 19 „AAVS1 locus"
AAVS1 HA L
Transgene (dCas9VPR)
AAVS1 HA L
D
off-target 1
clone#2
clone#3
control
reference
H2O
bp
2000
1000
700
400
200
100
potential cut side
clone#2
clone#3
control
reference
E Transgene expression
iPSCs
CRISPRa
kDa
control
clone#2
clone#3
260
140
50
35
Cas9
OCT4
GAPDH
G SNP-based & G-banding karyotype
CRISPRa control (outer)
CRISPRa clone#2 (center)
CRISPRa clone#3 (inner)
deletion
CNV
LOH
CRISPRa clone #2
CRISPRa clone #3
F Stemness
iPSCs
Control
CRISPRa clone#2
Immunofluorescence
brightfield
tdTomato
OCT4 DAPI
200 µm
10 µm
Flow cytometry
CRISPRa clone#2
IgG control
APC
FITC
TRA1-60
OCT4
Q1-1
Q2-1
Q3-1
Q4-1
H Germ layer differentiation
iPSc
Ectoderm
Mesoderm
Endoderm
-RT
H2O
RT-PCR
PAX3
MAP2
TBXT
AFP
dCAS9 VPR
TBP
control
clone#2
clone#3
CRISPRa
AFP DAPI
βIII-Tubulin DAPI
ACTA2 DAPI
Immunofluorescence
Control
CRISPRa clone#2
CRISPRa clone#3
100 µm
I Cardiomyocyte differentiation
Cardiomyocyte
TNNT2 DAPI
ACTN2 DAPI
Control
CRISPRa clone#2
50 µm
J Transcriptional activation
KLF15 gRNA
KLF15
TSS
-44 bp
KLF15
p<0.001
p<0.001
ns
Fold expression
control
clone#2
clone#3
CRISPRa
Non-targeting gRNA
KLF15 gRNA

Materials and Methods

Cell lines and culture

The LiPSC-GR1.1 cell line (Lonza, Walkersville, USA) was cultured on pre-coated Matrigel flasks under standard conditions (37 °C, 5% CO_2; BD Biosciences). Cells were passaged using Versene 1:5000 (Gibco) and StemMACS iPS-Brew XF (Milteny Biotec) with 5 µmol/L ROCK inhibitor Y27632 (Stemgent).

Molecular cloning of donor plasmid

The dCas9VPR-T2A-tdTomato sequence described in [2] was cloned into a modified pAAVS1 integration vector (System Biosciences, catalogue #GE602A-1). PGK was replaced by a CAG promoter and the GFP removed using the In-Fusion HD Cloning Kit (TAKARA) by inserted FseI and SmiI restriction sites. LoxP sites flanking the transgene were inserted using Bsp14I and MluI restriction sites. Primers are listed in Table 2.

Gene targeting and clonal selection

Alt-R S.p. HiFi Cas9, tracrRNA and crRNA targeted to the AAVS1 safe harbor locus (5' GGGGCCACUAGGGACAGGAUGUUUUAGAGCUAU 3') (IDT Integrated DNA Technologies) together with pAAVS1-CAG-dCas9VPR-2A-tdTomato-EF1alpha-Puro were electroporated into hLiPSC-GR1.1 using the Amaxa 4D Nucleofector and P3 Primary Cell 4D-Nucleofector X Kit L (Lonza).

Genotyping and sequence analysis

Genomic DNA was isolated and genotyping was performed using RedExtract-N-Amp Tissue PCR Kit (Sigma Aldrich). PCR sequenced at Seqlab Goettingen. Primers are listed in Table 2.

RNA isolation and qPCR analysis

Total RNA was isolated with TRIzol reagent (Thermo Fisher Scientific) according to manufacturer's instructions. Reverse transcription was performed using Oligo(dT)20 primers (Eurofins), dNTPs and M-MLV reverse transcriptase (Promega). RT-PCR and quantitative PCR were performed using Takyon ROX SYBR 2x Master Mix dTTP Blue (Eurogentec) with 1/5 diluted cDNA input on a 7900 HT Real Time Cycler (Applied Biosystems). Transcripts were calculated based on standard curves and normalized to *TBP*. Primers are listed in Table 2. RT-PCRs were performed with 30 cycles for PAX3, MAP2, TBXT, AFP and dCas9VPR and with 32 cycles for TBP.

Karyotyping

GTG-Banding (Gibco® Trypsin 1:250, Thermo Fisher Scientific) of 5 metaphase spreads/line were analysed using MetaClient 2.0.1-software (MetaSystems) on an Axio Imager Z2 microscope (Zeiss). SNP-based human microarray was performed with genomic DNA (QIAamp DNA Mini kit (Qiagen)) using the Infinium Global Screening Array-24 v3.0 BeadChip and the iScan array scanner (Illumina). Digital karyotypes were analyzed in GenomeStudio v2.0 software (Illumina) using the CNVpartition 3.2.0 algorithm with default settings. Copy number events were reported if larger than 3.5×10^5 bps and 1×10^6 bps for loss of heterozygosity.

Cell authentication/ STR analysis

Sample identification analysis was done by PCR-single-locus-technology. 16 independent PCR-systems D8S1179, D21S11, D7S820, CSF1PO, D3S1358, TH01, D13S317, D16S539, D2S1338, AMEL, D5S818, FGA, D19S433, vWA, TPOX and D18S51 were investigated with AmpFLSTR Identifiler Plus PCR Amplification Kit.

Directed germ layer, embryoid body (EB) and cardiomyocytes differentiation

Ectoderm and endoderm differentiations were performed with STEMdiff Trilineage Differentiation Kit (StemCell Technologies) according to manufacturer's instructions. Mesoderm was induced by culturing iPSCs in basal medium (RPMI 1640 + GlutaMAX, 2% B27, 200 µmol/L L-ascorbic acid, 1 mmol/L Na-pyruvate, 100 U/mL penicillin, 100 µg/mL streptomycin) and 9 ng/mL Activin A (Bio-Techne), 1 µmol/L CHIR99021 (Merck Chemicals GmbH), 5 ng/ml BMP4 (Bio-Techne) and 5 ng/mL FGF (Peprotech) for 3 days followed by cardiac differentiation in basal medium supplemented with 5 µmol/L IWP4 (ReproCELL Europe Ltd.) for 9 days. Cells underwent metabolic selection for 5 days (RPMI 1640, no glucose, 2.2 mmol/L Na-lactate, 100 µmol/L β-mercaptoethanol, 100 U/mL penicillin, 100 µg/mL streptomycin). For EB formation, 5×10^4 iPSCs were plated with 2.5×10^4 mouse embryonic fibroblasts on a 96-well plate in hES medium (DMEM-F12, 15% KnockOut Serum Replacement, 1× MEM Non-Essential Amino Acids (Thermo Fisher Scientific), 50 µmol/L β-mercaptoethanol (Serva Electrophoresis) and 2 µM Thiazovivin (Merck Millipore)). Plates were centrifuged for 5 min at 250 x g and co-cultures were grown in suspension. At day 2, medium was changed to differentiation medium (IMDM with Glutamax, 20% Fetal Bovine Serum (Thermo Fisher Scientific), 1× MEM Non-Essential Amino Acids Solution and 450 µmol/L 1-Thioglycerol (Sigma-Aldrich)) for further 6 days. Medium was changed every other day. At day 8, EBs were plated onto 0.1% gelatin-coated coverslips and cultured for up to one month in differentiation medium with medium changes every other day.

Immunoblotting

Proteins were isolated and quantified with ROTI Quant (Carl Roth). Lysates were run on SDS-PAGE, transferred to ROTI PVDF membranes (Carl Roth), blocked in 5% milk and incubated with primary and secondary antibodies (Table 2). Membranes were analyzed with a ChemiDoc MP Imaging System (BioRad).

Immunocytochemistry

Cells were fixed with ROTI Histofix 4% (Carl Roth), permeabilized (PBS with 0.2% BSA, 0.3% Triton X-100), blocked (PBS with 5% BSA, 0.1% Triton X-100) and incubated with corresponding antibodies (Table 2). Secondary antibodies alone served as controls. Nuclei were stained with 1 µg/ml Hoechst. Images were acquired with an Axio Imager M2 and ZEN software (Zeiss).

Flow cytometry

Cells were fixed with ice-cold 70% ethanol, blocked, permeabilized (PBS with 5% FCS, 1% BSA and 0.5% Triton X-100) and incubated with primary or suitable IgG antibodies and, if applicable, secondary antibodies (Table 2). Nuclei were stained with 1 µg/ml Hoechst. Cells were analyzed with a LSRII Flow Cytometer and FACSDiva software (BD Biosciences).

CRISPRa activation

Oligonucleotides for *KLF15* 5' TSS targeting gRNA or non-targeted gRNA (NT) (both sequences listed in Table 2) were cloned into pX333EGFP as described before [2]. iPSCs were transfected with gRNA

expression plasmid using Lipofectamine Stem Transfection Reagent (Thermo Fisher Scientific) according to manufacturer's instructions. Cells were harvested for transcript analyses after 48 h. Experiments were performed in triplicates and gene activation was indicated as fold activation compared to control CRISPRa cells transfected with non-targeting (NT) gRNAs.

Off-target analysis

Mismatch based off-target prediction was performed in the human genome (hg38/GRCh38) using "Off-Spotter" (Pliatsika, V, and Rigoutsos, I (2015) "Off-Spotter: very fast and exhaustive enumeration of genomic lookalikes for designing CRISPR/Cas guide RNAs" Biol. Direct 10(1):4). No off-target was detect that perfect matches the employed gRNAs, only one off-target with one mismatch was predicted (Top 1) and additional off-targets with more than 2 mismatches were identified. The top 5 loci were selected and flanking primers were designed for PCR amplification and Sanger sequencing. Off-target primers are listed in Table 2.

Statistics

GraphPad Prism 8 was used for statistical analyses. Normal distribution was checked with Shapiro-Wilk test and one-way ANOVA with Bonferroni correction was applied for multiple group comparisons. Statistically significant results were assumed if $p < 0.05$.

Acknowledgements
Generation of the GMP line LhiPSC-GR1.1 was supported by the NIH Common Fund Regenerative Medicine Program, and reported in Stem Cell Reports. The NIH Common Fund and the National Center for Advancing Translational Sciences (NCATS) are joint stewards of the LhiPSC-GR1.1 resource. We thank Ilona Eggert (Institute for Human Genetics, UMG) and Yvonne Hintz (Clinic for Cardiology and Pneumology, UMG) for superb technical support. This work was supported by the DFG grant SFB1002 C07 to LCZ and the DZHK (German Center for Cardiovascular Research).

References

[1] D.U. Kemaladewi, P.S. Bassi, S. Erwood, D. Al-Basha, K.I. Gawlik, K. Lindsay, E. Hyatt, R. Kember, K.M. Place, R.M. Marks, M. Durbeej, S.A. Prescott, E.A. Ivakine, R.D. Cohn, A mutation-independent approach for muscular dystrophy via upregulation of a modifier gene, Nature, 572 (2019) 125-130.
[2] E. Schoger, K.J. Carroll, L.M. Iyer, J. McAnally, W. Tan, N. Liu, C. Noack, O. Shomroni, G. Salinas, J. Gross, N. Herzog, S. Doroudgar, R. Bassel-Duby, W.H. Zimmermann, L.C. Zelarayan, CRISPR-Mediated Activation of Endogenous Gene Expression in the Postnatal Heart, Circ Res, (2019).
[3] Y.L. Min, R. Bassel-Duby, E.N. Olson, CRISPR Correction of Duchenne Muscular Dystrophy, Annual review of medicine, 70 (2019) 239-255.
[4] T. Zhan, N. Rindtorff, J. Betge, M.P. Ebert, M. Boutros, CRISPR/Cas9 for cancer research and therapy, Seminars in cancer biology, 55 (2019) 106-119.
[5] C.A. Hodges, R.A. Conlon, Delivering on the promise of gene editing for cystic fibrosis, Genes & diseases, 6 (2019) 97-108.

Table 1

Classification	Test	Result	Data
Morphology	Photography	Normal	Figure 1 panel F
Phenotype	Immunocytochemistry	Assess staining of pluripotency markers OCT4	Figure 1 panel F
	Flow cytometry	Assess antigen levels & cell surface markers OCT4 = 94.2% TRA1-60 = 99.9%	Figure 1 panel F
Genotype	Karyotype (G-banding)	46,XY Resolution 400	Figure 1 panel G and data available with authors
Identity	Microsatellite PCR (mPCR)	not performed	
	STR analysis	16 loci were tested with AmpFLSTR Identifiler Plus PCR Amplification Kit; 100% matched	Submitted in archive with journal
Mutation analysis (IF APPLICABLE)	Sequencing	Homozygous, insertion	Figure 1 panel B and C (Heterozygous insertion, data available with the authors)
	Southern Blot OR WGS	not performed	
Microbiology and virology	Mycoplasma	MycoALERT PLUS Mycoplasma Detection Kit (Lonza) Ratios <1 were considered mycoplasma free. Tested by bioluminescence Result: negative	not shown, but available with author
Differentiation potential	Embryoid body formation OR Teratoma formation OR Scorecard OR Directed differentiation	Embryoid body formation, expression of AFP, α-SMA and βIII-Tubulin Tri-lineage directed differentiation, expression of PAX3, MAP2, TBXT, AFP	Figure 1 panel H

Donor screening (OPTIONAL)	HIV 1 + 2 Hepatitis B, Hepatitis C	N/A	
Genotype additional info (OPTIONAL)	Blood group genotyping	N/A	
	HLA tissue typing	N/A	

Table 2

Antibodies used for immunocytochemistry/flow-cytometry/immunoblotting			
	Antibody	**Dilution**	**Company Cat # and RRID**
Pluripotency Markers	Rabbit anti-OCT4	1:50	Abcam, Cat# 19857, RRID: AB_445175
	Mouse anti-TRA1-60-DyLight 650	1:50	Thermo Fisher Scientific, Cat# MA1-023-D650, RRID: AB_2536702
Differentiation Markers	Mouse anti-ACTA2	1:3,000	Sigma-Aldrich, Cat# A2547, RRID: AB_476701
	Rabbit anti-AFP	1:100	Agilent, Cat# A0008, RRID: AB_2650473
	Mouse anti-β-III-Tubulin	1:2,000	Covance, Cat# MMS-435P, RRID: AB_2313773
	Mouse anti-ACTN2	1:1000	Sigma-Aldrich, Cat# A7811, RRID: AB_476766
	Rabbit anti-TNNT2	1:200	Abcam, Cat# ab45932, RRID: AB_956386
Secondary antibodies	Goat anti-rabbit IgG-Alexa Fluor®488	1:250	Thermo Fisher Scientific, Cat# A11008, RRID: AB_143165
	Goat anti-mouse IgG-Alexa Fluor®488	1:250	Thermo Fisher Scientific, Cat# A11029, RRID: AB_138404
Primary antibodies for immunoblots	Rabbit anti-Cas9	1:2,000	Diagenode, Cat# C15310258, RRID: AB_2715516
	Mouse anti-GAPDH	1:10,000	Proteintech, Cat# 60004-1-Ig, RRID: AB_2107436
Secondary antibodies for immunoblots	Rabbit anti-mouse-HRP	1:10,000	Dako, Cat# P0260, RRID: AB_2636929
	Goat anti-rabbit-HRP	1:5,000	Dako, Cat# P0448, RRID: RRID: AB_2617138
	Donkey anti-rabbit IgG Alexa Fluor 555	1:200	Thermo Fisher Scientific Cat# A-31572, RRID: AB_162543

	Donkey anti-mouse IgG Alexa Fluor 488	1:200	Thermo Fisher Scientific Cat# A-21202, RRID: AB_141607
Control antibodies	Normal rabbit IgG	1:50	EMD Millipore, Cat# 12-370, RRID: AB_145841
	Normal mouse IgG	1:20	Santa Cruz, Cat# sc-2025, RRID: AB_737182
	Rabbit anti-mouse IgG-Alexa Fluor®633	1:250	Thermo Fisher Scientific, Cat# A-21052, RRID: AB_2535719
Primers			
	Target	**Forward/Reverse primer (5‘-3‘)**	
Differentiation marker	*PAX3-fwd*	AGAAGCCGAACCACCTTCAC	
	PAX3-rev	GGGTTGGAAGGAATCGTGCT	
	MAP2-fwd	CCACCTAGAATTAAGGATCA	
	MAP2-rev	GGCTTACTTTGCTTCTCTGA	
	TBXT-fwd	AATTGGTCCAGCCTTGGAAT	
	TBXT-rev	CGTTGCTCACAGACCACA	
	AFP-fwd	ACTCCAGTAAACCCTGGTGTTG	
	AFP-rev	GAAATCTGCAATGACAGCCTCA	
Normalizing gene	*TBP-fwd*	GCACAGGAGCCAAGAGTGAA	
	TBP-rev	TTGTTGGTGGGTGAGCACAA	
RT qPCR	*dCas9VPR-fwd*	GCCTCGCACCAACACCAAC	
	dCas9VPR-rev	GCCTCTTCCTTCTGGGGAATCAC	
	KLF15-fwd	TGCGCCAAGTTCAGCCGC	
	KLF15-rev	GCGTGGCCTGGGACAATAGG	
DNA genotyping & sequencing	*WT-AAVS1-fwd*	CGGAACTCTGCCCTCTAACG	
	WT-AAVS1-rev	ATCCTCTCTGGCTCCATCGT	
	TRANSGENE-AAVS1-fwd	CCGGACCACTTTGAGCTCTA	
	TRANSGENE-AAVS1-rev	GGCTATGAACTAATGACCCCG	

Cloning primers	*AAVS1-dCas9VPR-fwd*	GACCGGTTCTATTGGCTCTAGAGGATCGAA
	AAVS1-dCas9VPR-fwd	CCGGTCCAGCCATTTCGATTTACTTGTACA
	AAVS1-FseI-SmiI-MCS-fwd	CCGGTTCTATTGGCCGGCCTAAGCTGCTTAATTTAAATGGCTGGA
	AAVS1-FseI-SmiI-MCS-rev	CCGGTCCAGCCATTTAAATTAAGCAGCTTAGGCCGGCCAATAGAA
	AAVS1-InFusion-fwd	GACCGGTTCTATTGGCTCTAGAGGATCGAA
	AAVS1-InFusion-rev	CCGGTCCAGCCATTTCGATTTACTTGTACA
	AAVS1-loxP-5'-fwd	CGCGTATAACTTCGTATAATGTATGCTATACGAAGTTAT
	AAVS1-loxP-5'-rev	GCGTAATAACTTCGTATAGCATACATTATACGAAGTTAT
	AAVS1-loxP-3'-fwd	GTATAAATAACTTCGTATAATGTATGCTATACGAAGTTAT
	AAVS1-loxP-3'-rev	GTACAAATAACTTCGTATAGCATACATTATACGAAGTTAT
gRNA oligonucleotides	*KLF15-A-fwd*	CACCGCGCCGCGAAGGCTCGCAGG
	KLF15-A-rev	AAACCCTGCGAGCCTTCGCGGCGC
	CT-fwd	CACCGTCCAGCGGATAGAATGGCG
	CT-rev	AAACCGCCATTCTATCCGCTGGAC
Off-target analysis	*Off-target-1-fwd*	TGAAGAAACAACCCGTTTCC
	Off-target-1-rev	TTCCCAGGAAACGATGAGAC
	Off-target-2-fwd	CCCTTGCTGAAGATCACACA
	Off-target-2-rev	CGTATGTTGCCCCCTACACT
	Off-target-3-fwd	GGCACAGAAGCATGAAGTGA
	Off-target-3-rev	CCTCCAGGTGCTGCTTACTC

	Off-target-4-fwd	TTTTCCCAGGAAACGATGAG
	Off-target-4-rev	GCTCCCAGCTCTCCCTAAGT
	Off-target-5-fwd	ATCAGCAGGGCCACTAGAGA
	Off-target-5-rev	AGCAAAGCTCCTCAAACCAA

Additional Files:

STR analysis

Supplementary Figure 1

Certificate Cell Line Authentication Test

Locus	Samples	
	hiPSCs	
	CRISPRa clone#2	**Control**
D8S1179	13,14	13,14
D21S11	31.2,33.2	31.2,33.2
D7S820	10,11	10,11
CSF1PO	12,12	12,12
D3S1358	15,15	15,15
TH01	6,9.3	6,9.3
D13S317	9,11	9,11
D16S539	11,13	11,13
D19S433	13,16	13,16
vWA	16,16	16,16
TPOX	8,8	8,8
D18S51	14,14*	14,14*
AMEL	X,Y	X,Y
D5S818	11,11	11,11
FGA	18,25*	18,25*
Database Name	LiPSC-GR1.1	LiPSC-GR1.1

STR analysis: The table shows the result of the cell line analysis for human induced pluripotent stem cells (hiPSC) **control** and **CRISPRa clone#2** and the comparison with the online database for cell line LiPSC-GR1.1 of the DSMZ (http://www.dsmz.de/de/service/services-human-and-animal-cell) and the Cellosaurus database (https://web.expasy.org/cellosaurus) showing a 100% matching.

Supplementary Figure 1

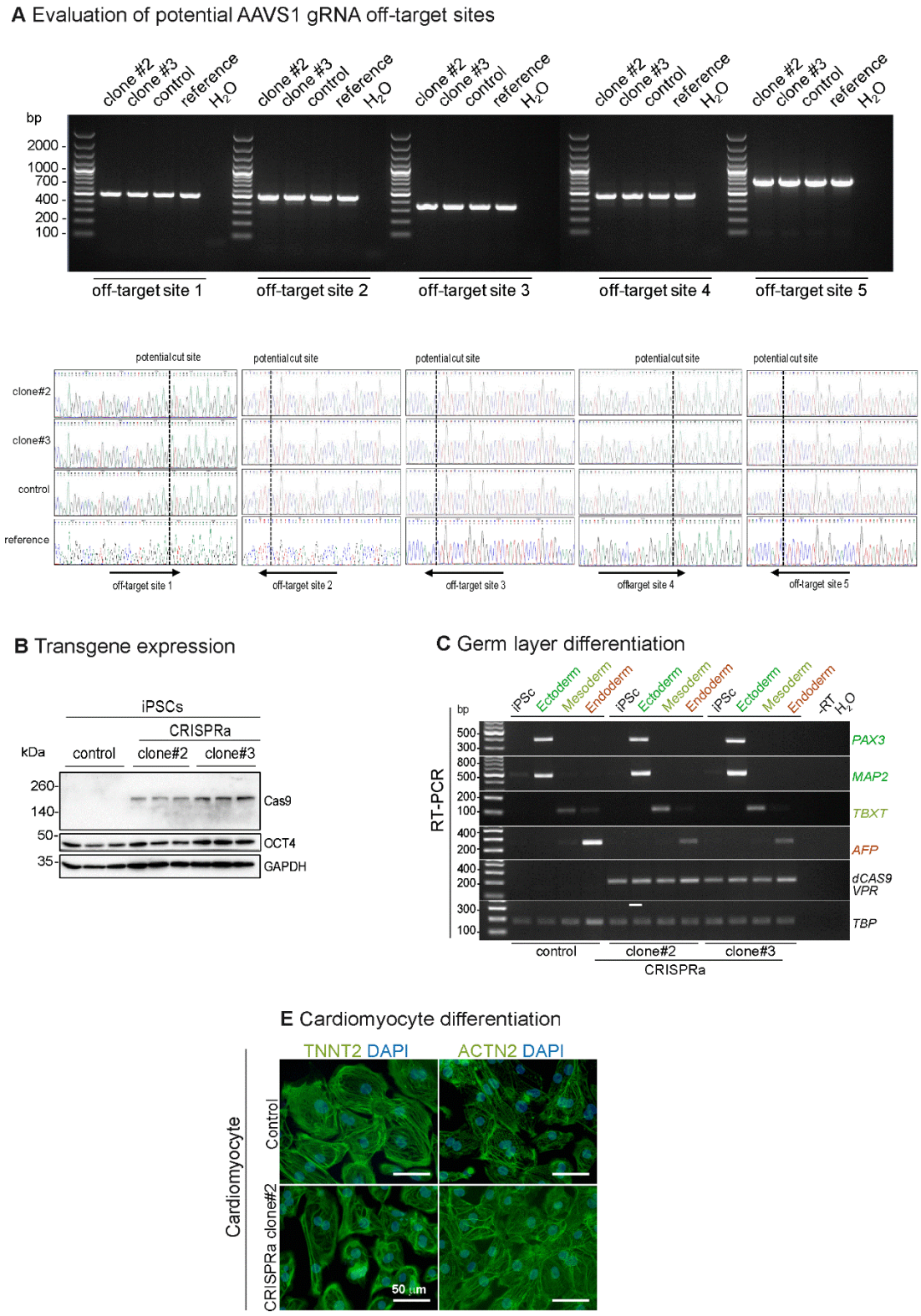

8. Chapter 4:

Human induced pluripotent stem cells for CRISPR based gene repression

"Establishment of two homozygous CRISPR interference (CRISPRi) knock-in human induced pluripotent stem cell (hiPSC) lines for titratable endogenous gene repression"

Eric Schoger[1,2*], Wolfram-Hubertus Zimmermann[1,2,3], Lukas Cyganek[2,4] and Laura Cecilia Zelarayán[1,2*]

*corresponding authors

Affiliations:

[1] Institute of Pharmacology and Toxicology, University Medical Center Goettingen (UMG), Göttingen, Germany;

[2] DZHK (German Center for Cardiovascular Research), partner site Goettingen, Germany

[3]Cluster of Excellence "Multiscale Bioimaging: from Molecular Machines to Networks of Excitable Cells" (MBExC), University of Göttingen, Germany

[4] Clinic for Cardiology and Pneumology, University Medical Center Goettingen (UMG), Göttingen, Germany

Abstract:

Using nuclease-deficient dead (d)Cas9 without enzymatic activity fused to transcriptional inhibitors (CRISPRi) allows for transcriptional interference and results in a powerful tool for the elucidation of developmental, homeostatic and disease mechanisms. We inserted dCas9KRAB (CRISPRi) cassette into the *AAVS1* locus of hiPSC lines, which resulted in homozygous knock-in with an otherwise unaltered genome. Expression of dCas9KRAB protein, pluripotency and the ability to differentiate into all three embryonic germ layers were validated. Furthermore, functional cardiomyocyte generation was tested. The hiPSC-CRISPRi cell lines offer a valuable tool for studying endogenous transcriptional repression with single and multiplexed possibilities in all human cell types.

Resource Table:

Unique stem cell line identifier	RUCDRi002-A-16 (CRISPRi) , RUCDRi002-A-17 (CRISPRi2) https://hpscreg.eu/cell-line/RUCDRi002-A-16 https://hpscreg.eu/cell-line/RUCDRi002-A-17
Alternative name of stem cell line	TC-1133-CRISPRi, TC-1133-CRISPRi2
Institution	Institute of Pharmacology and Toxicology, University Medical Center Goettingen, Germany
Contact information of distributor	Laura C. Zelarayán, laura.zelarayan@med.uni-goettingen.de
Type of cell line	Human induced pluripotent stem cell (hiPSC)
Origin	Human induced pluripotent stem cell (hiPSC) (LhiPSC-GR1.1), Accession: CVCL_RL65 (https://commonfund.nih.gov/stemcells/lines)
Additional origin info	Age: N/A Sex: male Ethnicity if known: N/A
Cell Source	Umbilical Cord Blood Cell (CD34+)
Method of reprogramming	Non-integrating, episomal
Associated disease	No disease was diagnosed
Type of Genetic Modification	Transgene generation *(overall structure, resistance, reported),*
Associated disease	*N.A*
Gene/locus	Targeted transgenesis in AAVS1. Integration: CRISPR/dCas9KRAB/tdTomato, 19q13.3
Method of modification/site-specific nuclease used	Site-specific nuclease (SSN) CRISPR/Cas9
Site-specific nuclease (SSN) delivery method	RNP
All genetic material introduced into the cells	HDR donor vectors: 1.) *pAAVS1-CAG-dCas9KRAB-T2A-tdTomato-EF1alpha-puro* and 2.) *pAAVS1-CAG-dCas9KRAB-T2A-tdTomato-WPRE*
Analysis of the nuclease-targeted allele status	Sequencing of the targeted allele and PCR for the untargeted allele
Method of the off-target nuclease activity surveillance	Targeted PCR/sequencing
Name of transgene	CRISPR/dCas9KRAB/tdTomato(/WPRE)
Eukaryotic selective agent resistance (including inducible/gene expressing cell-specific)	EF1alpha-Puromycin (CRISPRi line)
Date archived/stock date	30th September 2020
Cell line repository/bank	https://sfb1002.med.uni-goettingen.de/production/cellmodel/cell-line/view?tab=gen_mod&line=479 (RUCDRi002-A-16 (CRISPRi)) https://sfb1002.med.uni-goettingen.de/production/cellmodel/cell-line/view?tab=gen_mod&line=480 (RUCDRi002-A-17 (CRISPRi2))
Ethical/GMO work approvals	Reference number: 10/9/15

Addgene/public access repository recombinant DNA sources' disclaimers (if applicable)	Lenti-dCas9-KRAB-blast was a kind gift from Gary Hon's Lab (Addgene #89567).

Resource utility

Transcriptional interference by CRISPR/dCas9 system presents several advantages over genome editing strategy for loss-of-function studies including: dynamic, reversible and titratable transcriptional repression, along with reduced off-target effects [1]. The generated hiPSC-CRISPRi lines are suitable for titrating targeted single and multiple gene repression along with cell tracing for basic and translational studies in iPSCs and differentiated cell types.

Resource Details

Mammalian cell transcription can be modified by dCas9KRAB with high levels of precision without genetically altering the target sequence [2, 3]. We previously generated a CRISPR/dCas9-hiPSC-based system for enhancing endogenous gene expression [4]. Here we expanded the toolbox by generating hiPSC lines with a CRISPR-based system for titrating transcriptional repression. The CRISPR/Cas9-based genome editing approach was used to target the *AAVS1* human genomic locus of LhiPSC-GR1.1 (TC-1133) cells. A cassette containing dCas9KRAB fused to Krueppel-associated box (KRAB) repression domain along with either a previously described tdTomato (CRISPRi line) followed by a puromycin resistance under the control of the *EF1a* promoter or a tdTomato including the posttranscriptional regulatory element of the woodchuck hepatitis virus (WPRE) to boost the efficiency of transgene expression [5] (CRISPRi2) under the control of the *CAG* promoter was inserted (Fig. 1A).

Cells were selected by tdTomato expression and genotyped by PCR (Fig. 1B and Supplementary Fig. 1A, primer binding shown in Fig. 1A, **black** primers amplified only the wild-type (WT) allele; **green** primers amplified the inserted construct). Subsequently, two positive clones per line (CRISPRi #1 and #9; CRISPRi2 #5 and #7) were expanded, analysed and cryopreserved. DNA sequencing data corroborated both, correct and homozygous knock-in transgene integration in the *AAVS1* locus in all lines (Fig. 1C). Clones that were positive for an intact WT locus were used as electroporated control cells. The top five predicted genome-wide off-targetsites were analyzed by PCR and sequenced. Control electroporated and non-electroporated (reference) lines were used for comparison. The analyzed sequences showed no editing event (Supplementary Fig. 1A). All lines tested negative for mycoplasma. SNP-based karyotyping demonstrated genomic integrity of CRISPRi/i2 as well as of control cells as compared to the reference line [4] (Fig. 1D). Cell growth and morphology were comparable to controls (Fig. 1E*i*). Western blot and confocal microscopy corroborated expression of dCas9KRAB and tdTomato in CRISPRi/i2, respectively, as compared to control cells. Enhanced dCas9KRAB expression was confirmed in the CRISPRi2 line (Fig. 1E*ii* and E*iv*, n=2 different passages). Pluripotency was assessed by immunofluorescence and Western blot to analyse the expression of stemness markers OCT4 and TRA1-60 (Fig. 1E*iii* and *iv*), and by flow cytometry analysis which showed 97.46% OCT4 (CRISPRi) or 96.22% (CRISPRi2) and 92.14% TRA1-60 (CRISPRi) or 84.37% (CRISPRi2) positive cells (Fig. 1E*v*). Spontaneous differentiation capacity into all three germ layers was tested by formation of embryoid bodies (EBs) and directed differentiation in the CRISPRi/i2 and control lines. Immunofluorescence analysis confirmed expression of α-1-Feto-protein (AFP), β-III-Tubulin and α-Smooth Muscle Actin (ACTA2), supporting endodermal, ectodermal and mesodermal fate, respectively (Fig. 1F). Analysis of transcript levels showed expression of Paired Box 3 (*PAX3*) and Microtubule-Associated Protein 2 (*MAP2*) indicating ectodermal differentiation; T-box transcription factor T (*TBXT*)

indicating mesodermal fate and α-Feto-Protein (*AFP*) indicative of endodermal differentiation (Supplementary Fig. 1B). Furthermore, we investigated the suitability of the CRISPRi/i2 lines for generating cardiomyocytes by directed 2D differentiation which resulted in spontaneously beating cells (data not shown, available by the authors) with robust cardiac Troponin T (TNNT2) cardiomyocyte marker expression (Supplementary Fig. 1C). Finally, we validated the functionality of the CRISPRi/i2 lines by ascertaining the repression of *KLF15* expression. A combination of three (g)RNAs, which were designed to hybridize to the 5´-upstream sequence of the *KLF15* transcriptional start site (TSS), was able to significantly repress transcription of *KLF15* in CRISPRi and stronger in CRISPRi2 line compared to their respective parental lines transduced with non-targeting (NT) gRNAs. Control cells did not show transcriptional repression independent of the transfected gRNA (Fig. 1G).

In summary, homozygous hiPSC-CRISPRi/i2 lines are pluripotent and can differentiate into all germ cell derivates as well as showed its potential for interference with endogenous gene transcription according to the dCas9KRAB expression levels. This represents an invaluable tool for *in vitro* human development studies and disease modelling.

Figure 1

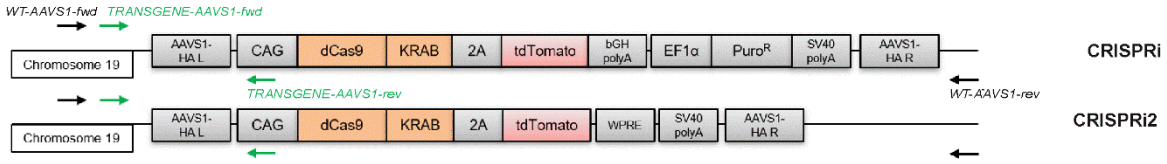
A CRISPRi (dCasKRAB) cassette targeted in the AAVS1 locus
WT-AAVS1-fwd
TRANSGENE-AAVS1-fwd
Chromosome 19
AAVS1-HA L
CAG
dCas9
KRAB
2A
tdTomato
bGH polyA
EF1α
Puro^R
SV40 polyA
AAVS1-HA R
CRISPRi
TRANSGENE-AAVS1-rev
WT-AAVS1-rev
WPRE
CRISPRi2

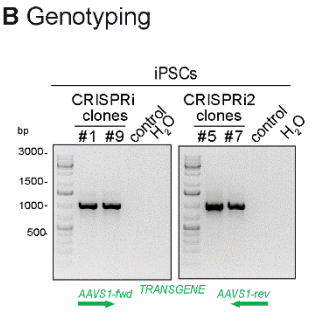
B Genotyping
iPSCs
CRISPRi clones
CRISPRi2 clones
control
H2O
#1 #9
#5 #7
bp
3000-
1500-
1000-
500-
AAVS1-fwd
TRANSGENE
AAVS1-rev

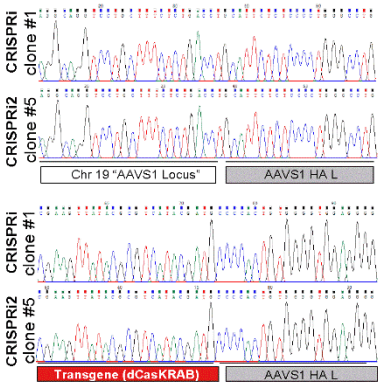
C Sequencing
CRISPRi clone #1
CRISPRi2 clone #5
Chr 19 "AAVS1 Locus"
AAVS1 HA L
Transgene (dCasKRAB)

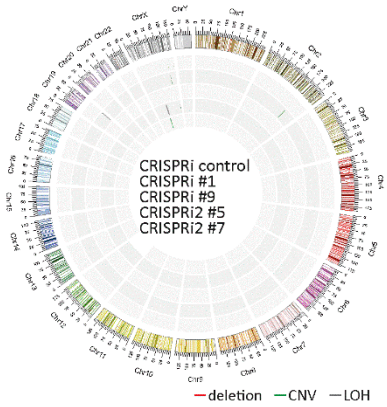
D SNP-based karyotype
CRISPRi control
CRISPRi #1
CRISPRi #9
CRISPRi2 #5
CRISPRi2 #7
deletion
CNV
LOH

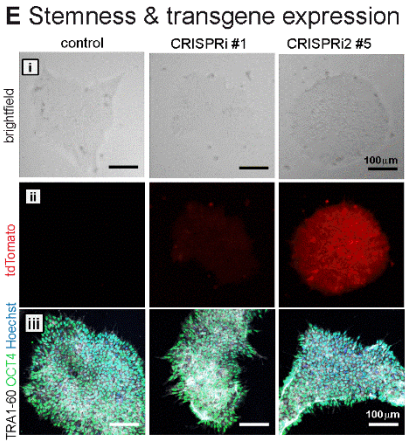
E Stemness & transgene expression
control
CRISPRi #1
CRISPRi2 #5
brightfield
tdTomato
TRA1-60 OCT4 Hoechst
100 µm

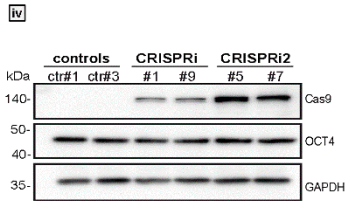
controls
CRISPRi
CRISPRi2
kDa
ctr#1 ctr#3
#1 #9
#5 #7
140-
50-
40-
35-
Cas9
OCT4
GAPDH

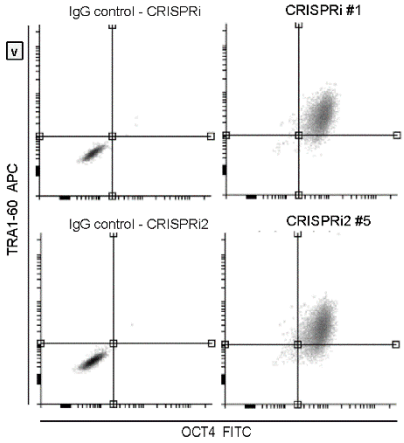
IgG control - CRISPRi
CRISPRi #1
IgG control - CRISPRi2
CRISPRi2 #5
TRA1-60 APC
OCT4 FITC

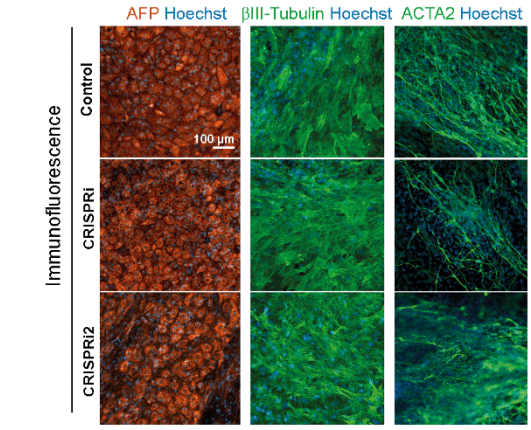
F Germ layer differentiation
AFP Hoechst
βIII-Tubulin Hoechst
ACTA2 Hoechst
Immunofluorescence
Control
CRISPRi
CRISPRi2
100 µm

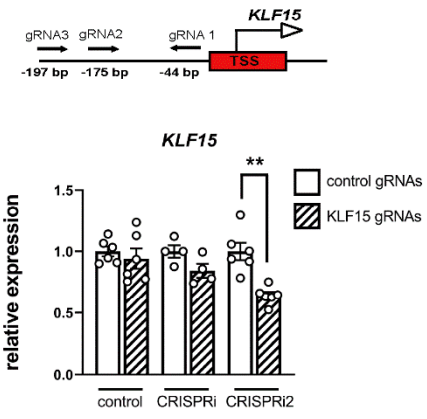
G Transcriptional repression
KLF15
gRNA3
gRNA2
gRNA 1
TSS
-197 bp
-175 bp
-44 bp
KLF15
**
control gRNAs
KLF15 gRNAs
relative expression
1.5
1.0
0.5
0.0
control
CRISPRi
CRISPRi2

Materials and Methods

Cell lines and culture

The LiPSC-GR1.1 cell line and derivates (Lonza, Walkersville, USA) were cultured in Matrigel (Corning) coated flasks under standard conditions (37 °C, 5% CO_2; BD Biosciences) and daily media changes with StemMACS iPS-Brew XF (Milteny Biotec). Cells were passaged with Versene 1:5000 (Gibco) and resuspended in StemMACS iPS-Brew XF (Milteny Biotec) supplemented with 5 µmol/L ROCK inhibitor Y27632 (Stemgent).

Molecular cloning of donor plasmid

From a previously published dCas9VPR construct [4], the VPR transactivator domain was exchanged with the KRAB domain (ZNF10 KRAB domain) from Lenti-dCas9-KRAB-blast (a gift from Gary Hon's Lab) by InFusion HD cloning (TAKARA) using NheI and MluI (both Thermo Fisher Scientific) sites. The dCas9KRAB-2A-tdTomato construct was cloned into a previously described AAVS1-donor construct [4] using FseI (NEB) and SmiI (Thermo Fisher Scientific) sites via InFusion HD cloning. For CRISPRi2, the bGH-polyA-EF1a-Puro cassette was removed by PacI and KspAI (both Thermo Fisher Scientific) and the WPRE site was amplified from a pGIPZ construct (Horizon Discovery) and integrated. Primers are listed in Table 2.

Gene targeting and clonal selection

Alt-R S.p. HiFi Cas9, tracrRNA and crRNA for targeting the AAVS1 locus (5' GGGGCCACUAGGGACAGGAUGUUUUAGAGCUAUGCU 3') (IDT Integrated DNA Technologies) together with pAAVS1-CAG-dCas9KRAB-2A-tdTomato-EF1alpha-Puro or pAAVS1-CAG-dCas9KRAB-2A-tdTomato-WPRE template constructs were electroporated into hLiPSC-GR1.1 with Neon Transfection System (Thermo Fisher Scientific) according to manufacturer's protocol with 2 pulses à 1000V for 30 ms.

Karyotyping

SNP-based human microarray was performed with genomic DNA (QIAamp DNA Mini kit (Qiagen)) using the Infinium Global Screening Array-24 v3.0 BeadChip and the iScan array scanner (Illumina). Digital karyotypes were analyzed in GenomeStudio v2.0 software (Illumina) using the CNVpartition 3.2.0 algorithm with default settings. Copy number events were reported if larger than 3.5×10^5 bps and 1×10^6 bps for loss of heterozygosity.

Genotyping and sequence analysis

Genomic DNA was isolated and genotyping was performed with RedExtract-N-Amp Tissue PCR Kit (Sigma Aldrich). PCR products were sequenced at Seqlab Goettingen. Primers are listed in Table 2.

RNA isolation and qPCR analysis

RNA was isolated extracted with TRIzol (Thermo Fisher Scientific) following manufacturer's protocol. Reverse transcription was performed with Random Hexamers dNTPs and M-MLV reverse transcriptase (all Promega). RT-PCR and quantitative PCR were performed using Takyon ROX SYBR 2x Master Mix dTTP Blue (Eurogentec) with 1/5 diluted cDNA input on a 7900 HT Real Time Cycler (Applied Biosystems). Gene expression levels were determined based on standard curve comparison and normalization to *TBP* expression. Primers are listed in Table 2. RT-PCRs were performed with 30 cycles for PAX3, MAP2, TBXT and dCas9KRAB and with 32 cycles for AFP and TATA-binding protein (TBP).

Cell authentication/ STR analysis

Sample identification analysis was performed by PCR-single-locus-technology. 16 independent PCR-systems D8S1179, D21S11, D7S820, CSF1PO, D3S1358, TH01, D13S317, D16S539, D2S1338, AMEL, D5S818, FGA, D19S433, vWA, TPOX and D18S51 were investigated with AmpFLSTR Identifiler Plus PCR Amplification Kit.

Directed germ layer, embryoid body (EB) and cardiomyocytes differentiation

Ectoderm and endoderm commitment was tested with STEMdiff Trilineage Differentiation Kit (StemCell Technologies) according to supplyer's protocol for 7 days. Mesoderm differentiation was performed in basal medium (RPMI 1640 + GlutaMAX, 2% B27, 200 µmol/L L-ascorbic acid, 1 mmol/L Na-pyruvate, 100 U/mL penicillin, 100 µg/mL streptomycin) and 9 ng/mL Activin A (Bio-Techne), 1 µmol/L CHIR99021 (Merck Chemicals GmbH), 5 ng/ml BMP4 (Bio-Techne) and 5 ng/mL FGF (Peprotech) for 3 days followed by cardiac differentiation in basal medium supplemented with 5 µmol/L IWP4 (ReproCELL Europe Ltd.) for 9 days. Cardiomyocytes were metabolically selected for 5 days (RPMI 1640, no glucose, 2.2 mmol/L Na-lactate, 100 µmol/L β-mercaptoethanol, 100 U/mL penicillin, 100 µg/mL streptomycin). For EB formation, 5×10^4 iPSCs were combined with 2.5×10^4 mouse embryonic fibroblasts on a 96-well plate in hES medium (DMEM-F12, 15% KnockOut Serum Replacement, 1× MEM Non-Essential Amino Acids (Thermo Fisher Scientific), 50 µmol/L β-mercaptoethanol (Serva Electrophoresis) and 2 µM Thiazovivin (Merck Millipore)). Plates were centrifuged for 5 min at 250 x g and co-cultures were grown in suspension. At day 2, medium was changed to differentiation medium (IMDM with Glutamax, 20% Fetal Bovine Serum (Thermo Fisher Scientific), 1× MEM Non-Essential Amino Acids Solution and 450 µmol/L 1-Thioglycerol (Sigma-Aldrich)) for further 6 days. Medium was changed every other day. At day 8, EBs were plated onto 0.1% gelatin-coated coverslips and cultured for up to one month in differentiation medium with medium changes every other day.

Immunoblotting

Proteins were extracted and quantified using ROTI Quant (Carl Roth). Proteins were separated on SDS-PAGE, transferred to ROTI PVDF membranes (Carl Roth), blocked in 5% milk and incubated with primary and secondary antibodies (Table 2). Membranes were analyzed using a ChemiDoc MP Imaging System (BioRad).

Immunocytochemistry

Cells were fixed with ROTI Histofix 4% (Carl Roth), permeabilized (PBS with 0.2% BSA, 0.3% Triton X-100), blocked (PBS with 5% BSA, 0.1% Triton X-100) and incubated with primary and secondary antibodies (PBS with 2% BSA, 0.1% Triton X-100) (Table 2). Secondary antibodies alone served as signal controls. Nuclei were counterstained with 10 µg/ml Hoechst. Images were acquired with a Zeiss LSM710 confocal microscope and ZEN software (Zeiss).

Flow cytometry

Cells were fixed with ice-cold 70% ethanol, blocked, permeabilized and incubated with primary or suitable IgG antibodies (all in PBS with 5% FCS, 1% BSA and 0.5% Triton X-100) and, if applicable, secondary antibodies (Table 2). Nuclei were counterstained with 10 µg/ml Hoechst. Cells were counted with a LSRII Flow Cytometer and FACSDiva software (BD Biosciences).

CRISPRi-mediated repression

Oligonucleotides for *KLF15* 5' TSS targeting gRNAs or non-targeted gRNA (NT) (both sequences listed in Table 2) were cloned into a triple gRNA expression construct (TRISPR) as described before [Schoger et al. 2019 Circ Res]. The lentiviral transfer vector pGIPZ (Horizon Discovery) was modified by integration of a multiple cloning site (see table 2) using NotI and XhoI (both Thermo Fisher Scientific) sites. The gRNA expression cassette was cloned into the modified pGIPZ vector using KpnI and XhoI (both Thermo Fisher Scientific) sites. For lentiviral gRNA delivery, pGIPZ transfer vectors, pMD2.G and psPAX2 (a gift from Didier Trono's lab) were transfected with Turbofect (Thermo Fisher Scientific) into HEK293T (TAKARA) cells. Media (DMEM, 5% FCS and 100 U/mL penicillin, 100 µg/mL streptomycin (all Gibco)) was exchanged daily and lentiviral particles were harvested 48-96 h post-transfection. $5x10^5$ iPSC-CM were transduced with 1 mL lentiviral particle supernatant and cultured for 5 days. Quantitative PCRs were performed in replicates (n=3-6) and gene repression was indicated as fold reduction compared to cells transfected with non-targeting (NT) gRNAs.

Off-target analysis

Genome-wide (hg38/GRCh38) mismatch based off-target prediction was performed using "Off-Spotter" (Pliatsika, V, and Rigoutsos, I (2015) "Off-Spotter: very fast and exhaustive enumeration of genomic lookalikes for designing CRISPR/Cas guide RNAs" Biol. Direct 10(1):4). For *AAVS1* gRNA, no off-target site was retrieved perfectly matching the employed gRNAs, only one off-target with two mismatches was predicted (Top 1) and additional off-targets with 3 or more mismatches were identified. The top 5 loci were selected, and flanking primers were designed for PCR amplification and Sanger sequencing. Off-target primers are listed in Table 2.

Statistics

Statistical analyses were performed with GraphPad Prism 8. Shapiro-Wilk test was employed to check for normal distribution and one-way ANOVA with Bonferroni correction was used for multiple group comparisons. Statistical significance was assumed if $p < 0.05$.

Acknowledgements

Generation of the GMP line LhiPSC-GR1.1 (TC1133 or RUCDRi002-A) was supported by the NIH Common Fund Regenerative Medicine Program and reported in Stem Cell Reports (Baghbaderani et al. 2015). The NIH Common Fund and the National Center for Advancing Translational Sciences (NCATS) are joint stewards of the LhiPSC-GR1.1 resource. The TC1133 line (Master Cell Bank Lot#: 50-001-21) was acquired by Repairon GmbH from the National Institute of Neurological Disorders and Stroke (NINDS) Human Cell and Data Repository (NHCDR) and processed to a GMP working cell bank (WCB). Post production cells from the WBC were kindly provided from Repairon to UMG for research use. We thank Yvonne Hintz and Kerstin Wenzel (Clinic for Cardiology and Pneumology, UMG), as well as Christina Weber (Institute of Pharmacology & Toxicology, UMG) for superb technical support. We acknowledge support by the Open Access Publication Funds of the Göttingen University. This work was supported by the DFG grant SFB1002 C07 and INF to LCZ; C04 to WHZ, S01 to LC/WHZ, the DZHK (German Center for Cardiovascular Research) and the Foundation Leducq.

References

[1] L.A. Gilbert, M.A. Horlbeck, B. Adamson, J.E. Villalta, Y. Chen, E.H. Whitehead, C. Guimaraes, B. Panning, H.L. Ploegh, M.C. Bassik, L.S. Qi, M. Kampmann, J.S. Weissman, Genome-Scale CRISPR-Mediated Control of Gene Repression and Activation, Cell, 159 (2014) 647-661.
[2] M.A. Mandegar, N. Huebsch, E.B. Frolov, E. Shin, A. Truong, M.P. Olvera, A.H. Chan, Y. Miyaoka, K. Holmes, C.I. Spencer, L.M. Judge, D.E. Gordon, T.V. Eskildsen, J.E. Villalta, M.A. Horlbeck, L.A. Gilbert, N.J. Krogan, S.P. Sheikh, J.S. Weissman, L.S. Qi, P.L. So, B.R. Conklin, CRISPR Interference Efficiently Induces Specific and Reversible Gene Silencing in Human iPSCs, Cell Stem Cell, 18 (2016) 541-553.
[3] L.S. Qi, M.H. Larson, L.A. Gilbert, J.A. Doudna, J.S. Weissman, A.P. Arkin, W.A. Lim, Repurposing CRISPR as an RNA-guided platform for sequence-specific control of gene expression, Cell, 152 (2013) 1173-1183.
[4] E. Schoger, L. Argyriou, W-H Zimmermann, L. Cyganek and L.C. Zelarayán, Generation of homozygous CRISPRa human induced pluripotent stem cell (hiPSC) lines for sustained endogenous gene activation, Stem Cell Research, 48:101944 (2020).
[5] R. Zufferey, J.E. Donello, D. Trono, T.J. Hope, Woodchuck hepatitis virus posttranscriptional regulatory element enhances expression of transgenes delivered by retroviral vectors, J Virol, 73 (1999) 2886-2892.

Table 1

Classification	Test	Result	Data
Morphology	Photography	Normal	Figure 1 panel E
Phenotype	Immunocytochemistry	Assess staining of pluripotency markers OCT4, TRA1-60	Figure 1 panel E
	Flow cytometry	Assess antigen levels & cell surface markers OCT4 = 97.46% (CRISPRi), = 96.22% (CRISPRi2)	Figure 1 panel E

		TRA1-60 = 92.14% (CRISPRi), = 84.37% (CRISPRi2)	
Genotype	SNP-based human microarray	Normal (Copy number events were reported if larger than 3.5×10^5 bps and 1×10^6 bps for loss of heterozygosity)	Figure 1 panel D and data available with authors
Identity	Microsatellite PCR (mPCR)	not performed	
	STR analysis	16 loci were tested with AmpFLSTR Identifiler Plus PCR Amplification Kit; 100% matched	Submitted in archive with journal
Mutation analysis (IF APPLICABLE)	Sequencing	Homozygous, insertion	Figure 1 panel B and C (Heterozygous insertion, data available with the authors)
	Southern Blot OR WGS	not performed	
Microbiology and virology	Mycoplasma	MycoALERT PLUS Mycoplasma Detection Kit (Lonza) Ratios <1 were considered mycoplasma free. Tested by bioluminescence Result: negative	not shown, available with author
Differentiation potential	Embryoid body formation OR Teratoma formation OR Scorecard OR Directed differentiation	Embryoid body formation, expression of AFP, α-SMA and βIII-Tubulin Tri-lineage directed differentiation, expression of PAX3, MAP2, TBXT, AFP	Figure 1 panel F and Supplementary Fig. 1 panel B and C
Donor screening (OPTIONAL)	HIV 1 + 2 Hepatitis B, Hepatitis C	N/A	
Genotype additional info (OPTIONAL)	Blood group genotyping	N/A	
	HLA tissue typing	N/A	

Table 2

Antibodies used for immunocytochemistry/flow-cytometry/immunoblotting			
	Antibody	**Dilution**	**Company Cat # and RRID**
Pluripotency Markers	Rabbit anti-OCT4	1:50	Abcam, Cat# 19857, RRID: AB_445175
	Mouse anti-TRA1-60-DyLight 650	1:50	Thermo Fisher Scientific, Cat# MA1-023-D650, RRID: AB_2536702
Differentiation Markers	Mouse anti-ACTA2	1:3,000	Sigma-Aldrich, Cat# A2547, RRID: AB_476701
	Rabbit anti-AFP	1:100	Agilent, Cat# A0008, RRID: AB_2650473
	Mouse anti-β-III-Tubulin	1:2,000	Covance, Cat# MMS-435P, RRID: AB_2313773
	Rabbit anti-TNNT2	1:200	Abcam, Cat# ab45932, RRID: AB_956386
Secondary antibodies	Goat anti-rabbit IgG-Alexa Fluor®488	1:250	Thermo Fisher Scientific, Cat# A11008, RRID: AB_143165
	Donkey anti-rabbit IgG Alexa Fluor 555	1:200	Thermo Fisher Scientific Cat# A-31572, RRID: AB_162543
	Donkey anti-mouse IgG Alexa Fluor 488	1:200	Thermo Fisher Scientific Cat# A-21202, RRID: AB_141607
Primary antibodies for immunoblots	Rabbit anti-Cas9	1:2,000	Diagenode, Cat# C15310258, RRID: AB_2715516
	Mouse anti-GAPDH	1:10,000	Proteintech, Cat# 60004-1-Ig, RRID: AB_2107436
Secondary antibodies for immunoblots	Rabbit anti-mouse-HRP	1:10,000	Dako, Cat# P0260, RRID: AB_2636929
	Goat anti-rabbit-HRP	1:5,000	Dako, Cat# P0448, RRID: RRID: AB_2617138
Control antibodies	Normal rabbit IgG	1:50	EMD Millipore, Cat# 12-370, RRID: AB_145841
	Normal mouse IgG	1:20	Santa Cruz, Cat# sc-2025, RRID: AB_737182
	Rabbit anti-mouse IgG-Alexa Fluor®633	1:250	Thermo Fisher Scientific, Cat# A-21052, RRID: AB_2535719

Primers		
	Target	**Forward/Reverse primer (5‘-3‘)**
Differentiation marker	*PAX3-fwd*	AGAAGCCGAACCACCTTCAC
	PAX3-rev	GGGTTGGAAGGAATCGTGCT
	MAP2-fwd	CCACCTAGAATTAAGGATCA

	MAP2-rev	GGCTTACTTTGCTTCTCTGA
	TBXT-fwd	AATTGGTCCAGCCTTGGAAT
	TBXT-rev	CGTTGCTCACAGACCACA
	AFP-fwd	ACTCCAGTAAACCCTGGTGTTG
	AFP-rev	GAAATCTGCAATGACAGCCTCA
Normalizing gene	*TBP-fwd*	GCACAGGAGCCAAGAGTGAA
	TBP-rev	TTGTTGGTGGGTGAGCACAA
RT qPCR	*dCas9KRAB fwd*	TCAGTCAATTACGGGGCTCT
	dCas9KRAB rev	CCCTGGTGAAGTCCACAAAC
	KLF15-fwd	AGCAAGGACTTGGATGCCTG
	KLF15-rev	AGGGCAGGTTCAAGTTGGAG
DNA genotyping & sequencing	*WT-AAVS1-fwd*	CGGAACTCTGCCCTCTAACG
	WT-AAVS1-rev	ATCCTCTCTGGCTCCATCGT
	TRANSGENE-AAVS1-fwd	CCGGACCACTTTGAGCTCTA
	TRANSGENE-AAVS1-rev	GGCTATGAACTAATGACCCCG
Cloning primers	*InFusion MluI-KRAB fwd*	CGTCGACTTGACGCGTCTGCGGCCGCTGGATCCGAT
	InFusion NheI-KRAB rev	CTCTGCCCTCGCTAGCTCCACTGCCTGTACA AACTTTGCGT
	AAVS1-InFusion-fwd	GACCGGTTCTATTGGCTCTAGAGGATCGAA
	AAVS1-InFusion-rev	CCGGTCCAGCCATTTCGATTTACTTGTACA
	AAVS1-WPRE fwd	AGCAATCGATTTAATTAACAATTGAATCAACCTCTGGA TTACAAAATTTG
	AAVS1-WPRE rev	CTTAATCGATGAATTAATTCCAGGCGGGGAG
	pGIPZ-MCS fwd	TCGAGGATATCATTTAAGGTACCTAAGCATTAATTAAG C
	pGIPZ-MCS rev	GGCCGCTTAATTAATGCTTAGGTACCTTAAATGATATC C
	KLF15-1-fwd	CACCGCGCCGCGAAGGCTCGCAGG

gRNA oligo-nucleotides	*KLF15-1-rev*	AAACCCTGCGAGCCTTCGCGGCGC
	KLF15-2-fwd	CACCGCGTGCGCGTCTGGCAGCTC
	KLF15-2-rev	AAACGAGCTGCCAGACGCGCACGC
	KLF15-3-fwd	CACCGGACCAGGCAGCGTGTTGGG
	KLF15-3-rev	AAACCCCAACACGCTGCCTGGTCC
	CT1-fwd	CACCGTCCAGCGGATAGAATGGCG
	CT1-rev	AAACCGCCATTCTATCCGCTGGAC
	CT2-fwd	CACCGGAGCGGTTTTGGATATTAG
	CT2-rev	AAACCTAATATCCAAAACCGCTCC
	CT3-fwd	CACCGTATGAGCGCGATGAAGGTG
	CT3-rev	AAACCACCTTCATCGCGCTCATAC
Off-target analysis	*Off-target-1-fwd*	TGAAGAAACAACCCGTTTCC
	Off-target-1-rev	TTCCCAGGAAACGATGAGAC
	Off-target-2-fwd	CCCTTGCTGAAGATCACACA
	Off-target-2-rev	CGTATGTTGCCCCCTACACT
	Off-target-3-fwd	GGCACAGAAGCATGAAGTGA
	Off-target-3-rev	CCTCCAGGTGCTGCTTACTC
	Off-target-4-fwd	TTTTCCCAGGAAACGATGAG
	Off-target-4-rev	GCTCCCAGCTCTCCCTAAGT
	Off-target-5-fwd	ATCAGCAGGGCCACTAGAGA
	Off-target-5-rev	AGCAAAGCTCCTCAAACCAA

Additional Files:

STR analysis

Supplementary Figure 1

Certificate Cell Line Authentication Test

Client Sample Name	TC1133,CRISPRi, 1.0 A #1	TC1133,CRISPRi, 1.0 B #9	TC1133,CRISPRi, 1.0CTR	TC1133,CRISPRi, 2.0 A, #5	TC1133,CRISPRi, 2.0 B #7
Sample Code	20_ZE_001650	20_ZE_001651	20_ZE_001652	20_ZE_001653	20_ZE_001654
D8S1179	13,14	13,14	13,14	13,14	13,14
D21S11	31.2,33.2	31.2,33.2	31.2,33.2	31.2,33.2	31.2,33.2
D7S820	10,11	10,11	10,11	10,11	10,11
CSF1PO	12,12	12,12	12,12	12,12	12,12
D3S1358	15,15	15,15	15,15	15,15	15,15
TH01	6,9.3	6,9.3	6,9.3	6,9.3	6,9.3
D13S317	9,11	9,11	9,11	9,11	9,11
D16S539	11,13	11,13	11,13	11,13	11,13
D2S1338	16,19	16,19	16,19	16,19	16,19
D19S433	13,16	13,16	13,16	13,16	13,16
vWA	16,16	16,16	16,16	16,16	16,16
TPOX	8,8	8,8	8,8	8,8	8,8
D18S51	14,14	14,14	14,14	14,14	14,14
AMEL	X,Y	X,Y	X,Y	X,Y	X,Y
D5S818	11,11	11,11	11,11	11,11	11,11
FGA	18,25	18,25	18,25	18,25	18,25
Database Name	LiPSC-GR1.1, LiPSC-GR1.2	LiPSC-GR1.1, LiPSC-GR1.2	LiPSC-GR1.1, LiPSC-GR1.2	LiPSC-GR1.1, LiPSC-GR1.2	LiPSC-GR1.1, LiPSC-GR1.2

STR analysis: The table shows the result of the cell line analysis for human induced pluripotent stem cells (hiPSC) **control**, **CRISPRi clone#1 and clone#9 and CRIPRi2 clone#7 and clone#5** and the comparison with the online database for cell line LiPSC-GR1.1 of the DSMZ (http://www.dsmz.de/de/service/services-human-and-animal-cell) and the Cellosaurus database (https://web.expasy.org/cellosaurus) showing a 100% matching.

Supplementary Figure 1

A Evaluation of potential *AAVS1* gRNA off-target sites

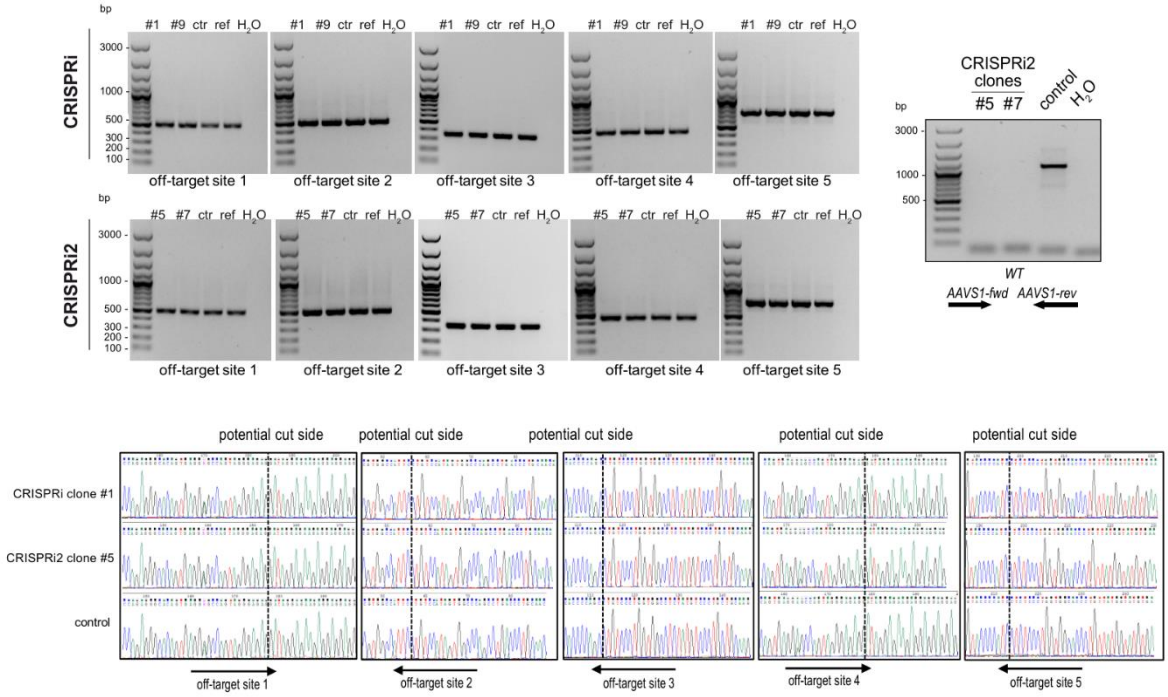

B Germ layer differentiation

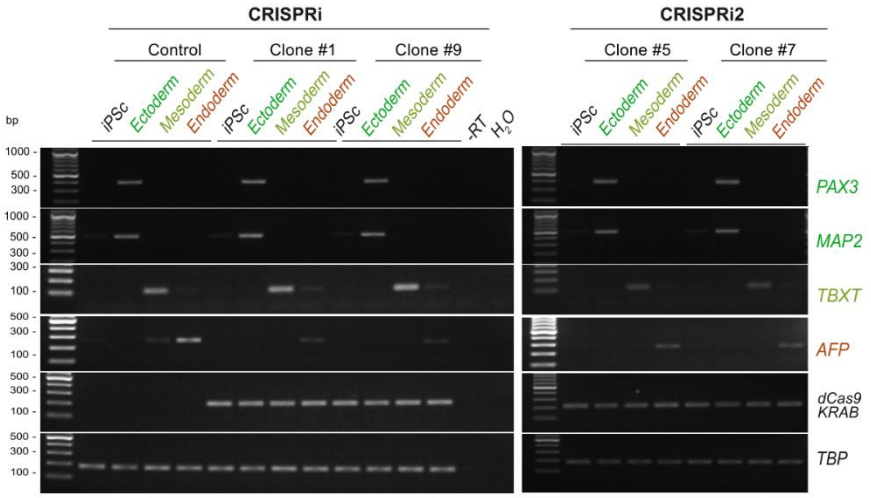

C Cardiomyocyte differentiation

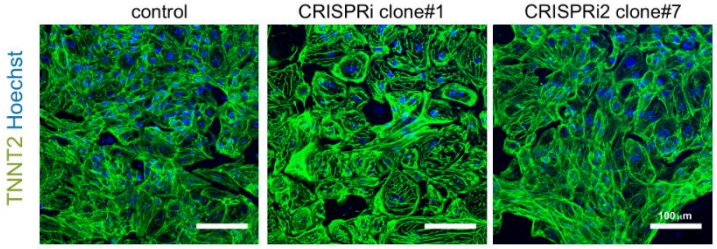

9. Chapter 5:

Enhanced endogenous gene activation in human induced pluripotent stem cells

"Establishment of a second generation homozygous CRISPRa human induced pluripotent stem cell (hiPSC) line for enhanced levels of endogenous gene activation"

Eric Schoger[1,2*], Wolfram-Hubertus Zimmermann[1,2,3,4,5], Lukas Cyganek[2,6] and Laura Cecilia Zelarayán[1,2*]

*corresponding authors

Affiliations:

[1] Institute of Pharmacology and Toxicology, University Medical Center Goettingen (UMG), Göttingen, Germany;

[2] DZHK (German Center for Cardiovascular Research), partner site Göttingen, Germany

[3]Cluster of Excellence "Multiscale Bioimaging: from Molecular Machines to Networks of Excitable Cells" (MBExC), University of Göttingen, Germany

[4] DZNE (German Center for Neurodegenerative Diseases), partner site Göttingen, Germany

[5] Fraunhofer Institute for Translational Medicine and Pharmacology (ITMP), Göttingen, Germany

[6] Clinic for Cardiology and Pneumology, University Medical Center Göttingen (UMG), Göttingen, Germany

Abstract: CRISPR/Cas9 technology based on nuclease inactive dCas9 and fused to the heterotrimeric VPR transcriptional activator is a powerful tool to enhance endogenous transcription by targeting defined genomic loci. We generated homozygous human induced pluripotent stem cell (hiPSC) lines carrying dCas9 fused to VPR along with a WPRE element at the *AAVS1* locus (CRISPRa2). We demonstrated pluripotency, genomic integrity and differentiation potential into all three germ layers. CRISPRa2 cells showed increased transgene expression and higher transcriptional induction in hiPSC-derived cardiomyocytes compared to a previously described CRISPRa line. Both lines allow studying endogenous transcriptional modulation with lower and higher transcript abundance.

Resource Table:

Unique stem cell line identifier	RUCDRi002-A-16 , RUCDRi002-A-17 https://hpscreg.eu/cell-line/RUCDRi002-A-15
Alternative name of stem cell line	TC-1133-CRISPRa2
Institution	Institute of Pharmacology and Toxicology, University Medical Center Goettingen, Germany
Contact information of distributor	Laura C. Zelarayán, laura.zelarayan@med.uni-goettingen.de Eric Schoger, eric.schoger@med.uni-goettingen.de
Type of cell line	Human induced pluripotent stem cell (hiPSC)
Origin	Human induced pluripotent stem cell (hiPSC) (LhiPSC-GR1.1), Accession: CVCL_RL65 (https://commonfund.nih.gov/stemcells/lines)
Additional origin info	Age: N/A Sex: male Ethnicity if known: N/A
Cell Source	Umbilical Cord Blood Cell (CD34+)
Method of reprogramming	Non-integrating, episomal
Associated disease	No disease was diagnosed
Type of Genetic Modification	Transgene generation *(overall structure, resistance, reported),*
Associated disease	*N.A*
Gene/locus	Targeted transgenesis in AAVS1. Integration: CRISPR/dCas9VPR/tdTomato, 19q13.3
Method of modification/site-specific nuclease used	Site-specific nuclease (SSN) CRISPR/Cas9
Site-specific nuclease (SSN) delivery method	RNP
All genetic material introduced into the cells	HDR donor vector *pAAVS1-CAG-dCas9VPR-WPRE*
Analysis of the nuclease-targeted allele status	Sequencing of the targeted allele and PCR for the untargeted allele
Method of the off-target nuclease activity surveillance	Targeted PCR/sequencing
Name of transgene	CRISPR/dCas9VPR/tdTomato/WPRE
Eukaryotic selective agent resistance (including inducible/gene expressing cell-specific)	N/A
Date archived/stock date	30th September 2020
Cell line repository/bank	Our cell line is stored in the Central Biobank of the University Medical Center Göttingen
Ethical/GMO work approvals	Reference number: 10/9/15
Addgene/public access repository recombinant DNA sources' disclaimers (if applicable)	N/A

Resource utility

The generated hiPSC-CRISPRa2 line was modified to allow for higher levels of dCas9VPR transgene expression as compared to previous described hiPSC-CRISPRa system. This modification results in increased transcriptional induction expanding the titrability of gene enhancement an can be applied to hiPSC-derived cells.

Resource Details

Several systems, based on modified nuclease inactive dCas9, have been developed. These systems allows transcriptional modulation with high levels of precision without altering the genetic information [1, 2]. We previously generated a hiPSC-CRISPRa-based system for enhancing single and multiplexed endogenous gene expression [3]. In order to expand CRISPR/Cas9 functions for transcriptional activation, we generated hiPSC-CRISPRa lines with increased activation efficiency.

A cassette containing dCas9 fused to heterotrimeric VPR transactivator consisting of VP64, p65, and RTA domains along with a tdTomato including the posttranscriptional regulatory element of woodchuck hepatitis virus (WPRE), to boost the transgene expression [4], under the control of the *CAG* promoter was inserted in the *AAVS1* human genomic locus of LhiPSC-GR1.1 (TC-1133) cells (Fig. 1A). Cells were selected by tdTomato expression and genotyped by PCR (Fig. 1B, primer binding shown in Fig. 1A, **black** primers amplified only the wild-type (WT) fragment; **green** primers amplified the inserted construct-*AAVS1* locus interface). Subsequently, two positive clones (CRISPRa2 #8 and #11) were expanded, analysed and cryopreserved. DNA sequencing data corroborated both, correct and homozygous knock-in transgene integration in the *AAVS1* locus in all lines (Fig. 1C). Clones that carried a unmodified WT locus were used as electroporated control (ctr) cells. The top five predicted off-targets were analyzed by PCR and subsequent Sanger sequencing. Control electroporated and non-electroporated (reference) lines were used for comparison. The analyzed sequences showed no editing event (Supplementary Fig. 1A). All lines tested negative for mycoplasma. SNP-based karyotyping demonstrated genomic integrity of CRISPRa2 as well as of control cells as compared to the reference line (Fig. 1D). Cell growth and morphology were comparable to controls (Fig. 1E*i*). Confocal microscopy (Fig. 1E*ii*) and Western blot (Fig. 1E*iv*) corroborated expression of tdTomato and dCas9 in CRISPRa2, respectively. CRISPRa2 showed higher transgene expression compared to previously described CRISPRa hiPSCs [3] (n=3 different passages). Pluripotency was assessed by immunofluorescence to analyze the expression of stemness marker OCT4 and TRA1-60 (Fig. 1E*iii*). Flow cytometry analysis confirmed 90% OCT4 and 99% TRA1-60 positive cells (Fig. 1E*v*). Spontaneous differentiation capacity into all three germ layers was tested by formation of embryoid bodies (EBs) and directed differentiation of CRISPRa2 lines. Immunofluorescence analysis confirmed expression of α-1-Feto-protein (AFP), β-III-Tubulin and α-Smooth Muscle Actin (ACTA2), further supporting endodermal, ectodermal and mesodermal fate, respectively (Fig. 1F). Analysis of transcript levels showed expression of Paired Box 3 (*PAX3*) and Microtubule-Associated Protein 2 (*MAP2*) indicating ectodermal differentiation, T-box transcription factor T (*TBXT*) indicating mesodermal fate and α-Feto-Protein (*AFP*) indicative of endodermal differentiation (Supplementary Fig. 1B). Furthermore, we investigated the suitability of the CRISPRa2 lines for generating cardiomyocytes by directed monolayer differentiation which resulted in spontaneously beating cells (data available by the authors) with robust α-Actinin 2 (ACTN2) and cardiac Troponin T (TNNT2) cardiomyocyte marker expression (Supplementary Fig. 1C). Finally, we validated the functionality of the CRISPRa2 cell lines by ascertaining the activation of *KLF15* expression. Three gRNAs were designed to the 5' upstream

region of *KLF15*, cloned into the corresponding vector for packaging into lentiviral particles and transduced side-by-side into CRISPRa [3], CRISPRa2, and control iPSC cardiomyocytes. *KLF15* transcriptional activation was observed in CRISPRa and CRISPRa2, compared to their respective parental lines transduced with a non-targeting (NT) gRNA. Importantly, gene activation was significantly more potent in CRISPRa2 than the induction achieved by the CRISPRa line [3]. Control cells did not show activation independent of the gRNAs transduced (Fig. 1G).

In summary, homozygous hiPSC-CRISPRa2 lines are pluripotent and can differentiate into all germ cell derivates. As proof-of-concept for the control of endogenous gene transcription targeting of the *KLF15* locus was demonstrated with higher transcript abundance compared to the previous hiPSC-CRISPRa1 version [3]. Controlling gene transcription in iPSC derivatives offers attractive possibilities for mechanistic studies and target validation.

Figure 1

A CRISPRa (dCas9VPR) cassette targeted in the *AAVS1* locus

B Genotyping

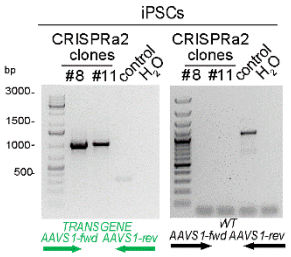

C Sequencing

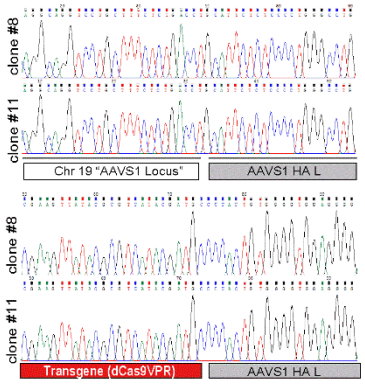

D SNP-based karyotype

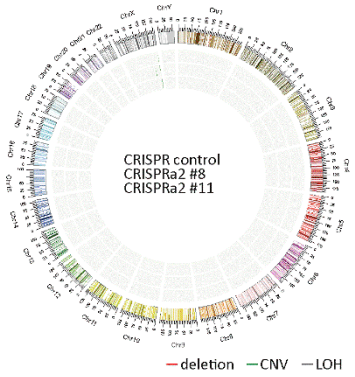

E Stemness & transgene expression

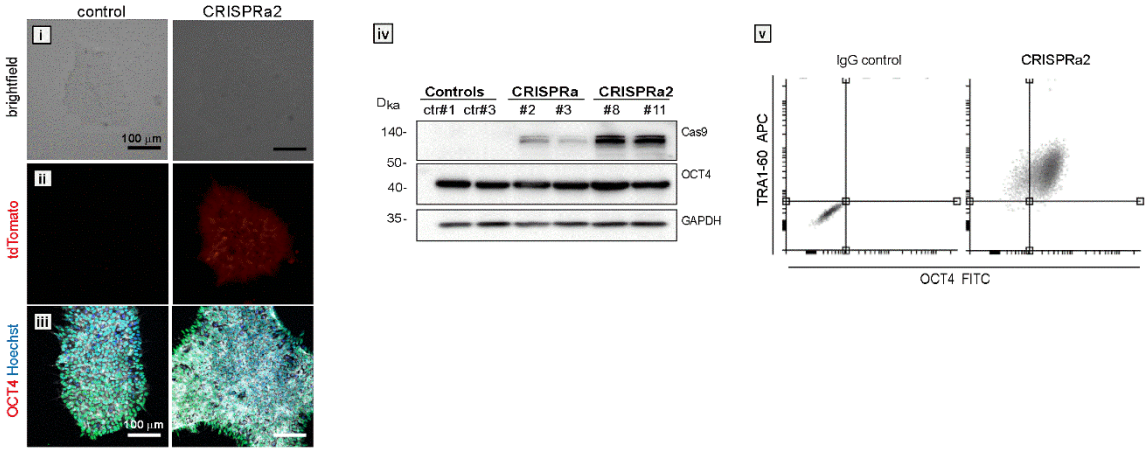

F Germ layer differentiation

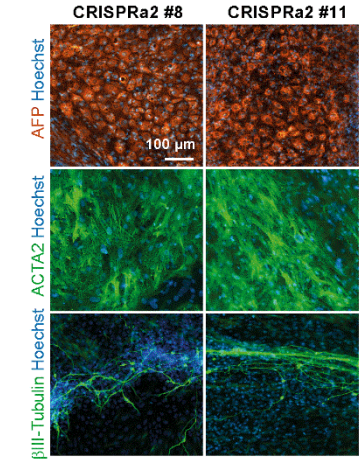

G Transcriptional activation

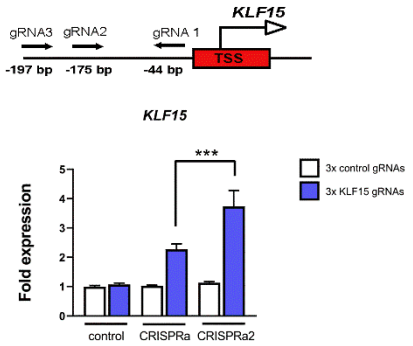

Materials and Methods

Cell lines and culture

Induced pluripotent stem cells (LiPSC-GR1.1 and derivates (Lonza, Wakersville, USA) were cultured on Matrigel (Corning) coated flasks in StemMACS iPS-Brew XF (Milteny Biotec) with daily media changes. Versene 1:5000 (Gibco) was used for passaging and cells were resuspended in StemMACS iPS-Brew XF with 5 µmol/L ROCK inhibitor Y27632 (Stemgent).

Molecular cloning of donor plasmid

The original pAAVS1-CAG-dCas9VPR-T2A-tdTomato sequence was reported before [2]. The CRISPRa2 construct was derived by removal of the bGH-polyA-EF1a-Puro cassette with PacI and KspAI (both Thermo Fisher Scientific) and the WPRE site was amplified from a pGIPZ construct (Horizon Discovery). Primers are listed in Table 2.

Gene targeting and clonal selection

Alt-R S.p. HiFi Cas9, tracrRNA and crRNA were used to target the AAVS1 safe harbor locus (5' GGGGCCACUAGGGACAGGAUGUUUUAGAGCUAUGCU 3') (IDT Integrated DNA Technologies) and electroporated together with the HDR donor plasmid into LiPSC-GR1.1 with a Neon Transfection System (Thermo Fisher Scientific).

Karyotyping

SNP-based human microarray using genomic DNA (QIAamp DNA Mini kit (Qiagen)) was performed with the Infinium Global Screening Array-24 v3.0 BeadChip and the iScan array scanner (Illumina). Digital karyotypes were analyzed in GenomeStudio v2.0 software (Illumina) with the CNVpartition 3.2.0 algorithm and default settings. Copy number events were reported if larger than 3.5×10^5 bps and 1×10^6 bps for loss of heterozygosity.

Genotyping and sequence analysis

RedExtract-N-Amp Tissue PCR Kit (Sigma Aldrich) was used for extraction and genotyping of iPSC clones. PCR products were Sanger-sequenced at Seqlab Goettingen. Primers are listed in Table 2.

RNA isolation and qPCR analysis

Total RNA was extracted with TRIzol reagent (Thermo Fisher Scientific). Complementary DNA was synthesized with Random Hexamers, dNTPs and M-MLV reverse transcriptase (all Promega). Takyon ROX SYBR 2x Master Mix dTTP Blue (Eurogentec) was used and reactions were performed on a 7900 HT Real Time Cycler (Applied Biosystems). Relative gene expression levels were determined based on standard curves comparisons and normalization to *TBP* expression. Primers are listed in Table 2. RT-PCR reactions were performed with 30 cycles for PAX3, MAP2, TBXT, AFP and dCas9VPR and with 32 cycles for AFP and TBP.

Cell authentication/ STR analysis

PCR-single-locus-technology was used for cell line authentication. 16 independent PCR-systems D8S1179, D21S11, D7S820, CSF1PO, D3S1358, TH01, D13S317, D16S539, D2S1338, AMEL, D5S818, FGA, D19S433, vWA, TPOX and D18S51 were investigated with AmpFLSTR Identifiler Plus PCR Amplification Kit.

Directed germ layer, embryoid body (EB) and cardiomyocytes differentiation

Directed germ line differentiation into ectodermal and endodermal cells was performed using the STEMdiff Trilineage Differentiation Kit (StemCell Technologies). Mesodermal cells were differentiated in basal medium (RPMI 1640 + GlutaMAX, 2% B27 supplement 200 µmol/L L-ascorbic acid, 1 mmol/L Na-pyruvate, 100 U/mL penicillin, 100 µg/mL streptomycin) supplemented with 9 ng/mL Activin A (Bio-Techne), 1 µmol/L CHIR99021 (Merck Chemicals GmbH), 5 ng/mL BMP4 (Bio-Techne), and 5 ng/mL FGF (Peprotech); subsequently, cardiomyocytes were differentiated in basal medium and 5 µmol/L IWP4 (ReproCELL) as described before (doi: 10.1161/CIRCULATIONAHA.116.024145). Cardiomyocytes were selected in RPMI, no glucose, 2.2mmol/L Na-lactate, 100 µmol/L β-mercaptoethanol, 100 U/mL penicillin, 100 µg/mL streptomycin. EBs were generated by mixing $5 \cdot 10^4$ iPSC and $2.5 \cdot 10^4$ mouse embryonic fibroblasts in a 96-well plate in hES medium (DMEM-F12, 15% KnockOut Serum Replacement, 1x MEM Non-Essential Amino Acids (Thermo Fisher Scientific), 50 µmol/L β-mercaptoethanol (Serva Electrophoresis) and 2 µmol/L Thiazovivin (Merck Millipore)). Cells were pelleted for 5 min at 250 xg and EBs were grown in suspension. From day 2 onwards, EBs were cultured in differentiation medium (IMDM with GlutaMAX, 20% Fetal Bovine Serum, 1x MEM Non-Essential Amino Acids (Thermo Fisher Scientific), 450 µmol/L 1-Thioglycerol (Sigma Aldrich)) until day 6. EBs were plated onto 0.1% gelatin-coated coverslips at day 8 and cultured for up to one month in differentiation medium with media changes every other day.

Immunoblotting

Protein lysates were quantified with ROTI Quant (Carl Roth). Proteins were separated by SDS-PAGE and transferred onto ROTI PVDF membranes (Carl Roth). Membranes were blocked and incubated with primary and secondary HRP-coupled antibodies in 5% milk. Membranes were exposed to femtoLUCENT Plus-HRP (G-Biosciences) and mages were taken with a ChemiDoc MP Imaging System (Bio-Rad). Antibodies are listed in table 2.

Immunocytochemistry

Cells were fixed with ROTI Histofix (Carl Roth), permeabilized in PBS, 0.2% BSA, 0.3% Triton X-100 and blocked in PBS, 5% BSA, 0.3% Triton X-100 before incubation with antibodies diluted in PBS, 0.2% BSA, 0.3% Triton X-100. Nuclei were stained with 10 µg/ml Hoechst (Thermo Fisher Scientific). Antibodies are listed in table 2.

Flow cytometry

Cells were fixed in ice-cold 70% ethanol and incubated with antibodies diluted in (PBS, 5% FCS, 1% BSA, 0.5% Triton X-100). Corresponding host organism IgGs served as control. Nuclei were stained with 10 µg/ml Hoechst (Thermo Fisher Scientific). Samples were analysed with a LSRII Flow Cytometer (BD Biosciences). Antibodies are listed in table 2.

CRISPRa-mediated gene activation

KLF15 gRNAs targeted to the *KLF15* promoter region or non-targeted gRNAs (NT) encoding oligonucleotides were cloned into triple gRNA expression vectors (TRISPR) as described before [5]. Guide RNA expression cassette was transferred into a modified pGIPZ (Horzion Discovery) construct for lentiviral particle generation in HEK293T cells transfected with pMD2.G, psPAX2 (both a gift from Didier Trono's Lab) and respective gRNA plasmid using TurboFect (Thermo Fisher Scientific). Lentiviral supernatants were used to transduce iPSC-cardiomyocytes and cells were cultured for 5 days post-transduction before proceeding with further analyses. Transcriptional changes are reported as fold-changes compared to corresponding cells transduced with NT gRNAs. Oligonucleotide sequences are listed in table 2.

Off-target analysis

Mismatch-based off-target prediction was conducted for all gRNAs using "Off-Spotter" (10.1186/s13062-015-0035-z). Top 5 predicted AAVS1 gRNA off-target sites (2-3 mismatches compared to on-target site sequence) were selected for examination of unintended edits. Off-target site primers are listed in Table 2.

Statistics

GraphPad Prism 8 was employed for statistical testing. Normal distribution analyses were performed with Shapiro-Wilk test, and for multiple group comparisons, one-way ANOVA with Bonferroni correction was used. Statistical significance was assumed if $p < 0.05$.

Acknowledgements

Generation of the GMP line LhiPSC-GR1.1 (TC1133 or RUCDRi002-A) was supported by the NIH Common Fund Regenerative Medicine Program, and reported in Stem Cell Reports (Baghbaderani et al. 2015, doi: 10.1016/j.stemcr.2015.08.015). The NIH Common Fund and the National Center for Advancing Translational Sciences (NCATS) are joint stewards of the LhiPSC-GR1.1 resource. The TC1133 line (Master Cell Bank Lot#: 50-001-21) was acquired by Repairon GmbH from the National Institute of Neurological Disorders and Stroke (NINDS) Human Cell and Data Repository (NHCDR) and processed to a GMP working cell bank (WCB). Post production cells from the WBC were kindly provided by Repairon to UMG for research use. We thank Yvonne Hintz, Kerstin Wenzel (Clinic for Cardiology and Pneumology, UMG), and Christina Weber (Institute of Pharmacology and Toxicology, UMG) for superb technical support. We acknowledge support by the Open Access Publication Funds of the Göttingen University. This work was supported by the DFG grant SFB1002 C07 and INF to LCZ; C04 to WHZ, S01 to LC/WHZ, the DZHK (German Center for Cardiovascular Research), and the Foundation Leducq.

References

[1] M.A. Mandegar, N. Huebsch, E.B. Frolov, E. Shin, A. Truong, M.P. Olvera, A.H. Chan, Y. Miyaoka, K. Holmes, C.I. Spencer, L.M. Judge, D.E. Gordon, T.V. Eskildsen, J.E. Villalta, M.A. Horlbeck, L.A. Gilbert, N.J. Krogan, S.P. Sheikh, J.S. Weissman, L.S. Qi, P.L. So, B.R. Conklin, CRISPR Interference

Efficiently Induces Specific and Reversible Gene Silencing in Human iPSCs, Cell Stem Cell, 18 (2016) 541-553.
[2] L.S. Qi, M.H. Larson, L.A. Gilbert, J.A. Doudna, J.S. Weissman, A.P. Arkin, W.A. Lim, Repurposing CRISPR as an RNA-guided platform for sequence-specific control of gene expression, Cell, 152 (2013) 1173-1183.
[3] E. Schoger, L. Argyriou, W.-H. Zimmermann, L. Cyganek, L.C. Zelarayán, Generation of homozygous CRISPRa human induced pluripotent stem cell (hiPSC) lines for sustained endogenous gene activation, Stem Cell Research, 48 (2020) 101944.
[4] R. Zufferey, J.E. Donello, D. Trono, T.J. Hope, Woodchuck hepatitis virus posttranscriptional regulatory element enhances expression of transgenes delivered by retroviral vectors, J Virol, 73 (1999) 2886-2892.
[5] E. Schoger, K.J. Carroll, L.M. Iyer, J. McAnally, W. Tan, N. Liu, C. Noack, O. Shomroni, G. Salinas, J. Gross, N. Herzog, S. Doroudgar, R. Bassel-Duby, W.H. Zimmermann, L.C. Zelarayan, CRISPR-Mediated Activation of Endogenous Gene Expression in the Postnatal Heart, Circ Res, (2019).

Table 1

Classification	Test	Result	Data
Morphology	Photography	Normal	Figure 1 panel E
Phenotype	Immunocytochemistry	Assess staining of pluripotency markers OCT4/TRA1-60	Figure 1 panel E
	Flow cytometry	Assess antigen levels & cell surface markers OCT4 = 90% TRA1-60 = 99%	Figure 1 panel E
Genotype	SNP-based human microarray	Normal (Copy number events were reported if larger than 3.5×10^5 bps and 1×10^6 bps for loss of heterozygosity)	Figure 1 panel D and data available with authors
Identity	Microsatellite PCR (mPCR)	not performed	
	STR analysis	16 loci were tested with AmpFLSTR Identifiler Plus PCR Amplification Kit; 100% matched	Submitted in archive with journal
Mutation analysis (IF APPLICABLE)	Sequencing	Homozygous, insertion	Figure 1 panel B and C (Heterozygous insertion, data available with the authors)
	Southern Blot OR WGS	not performed	

Microbiology and virology	Mycoplasma	MycoALERT PLUS Mycoplasma Detection Kit (Lonza) Ratios <1 were considered mycoplasma free. Tested by bioluminescence Result: negative	not shown, but available with author
Differentiation potential	Embryoid body formation OR Teratoma formation OR Scorecard OR Directed differentiation	Embryoid body formation, expression of AFP, α-SMA and βIII-Tubulin Tri-lineage directed differentiation, expression of PAX3, MAP2, TBXT, AFP	Figure 1 panel F and Supplementary Fig. 1B and C
Donor screening (OPTIONAL)	HIV 1 + 2 Hepatitis B, Hepatitis C	N/A	
Genotype additional info (OPTIONAL)	Blood group genotyping	N/A	
	HLA tissue typing	N/A	

Table 2

Antibodies used for immunocytochemistry/flow-cytometry/immunoblotting			
	Antibody	**Dilution**	**Company Cat # and RRID**
Pluri-potency Markers	Rabbit anti-OCT4	1:50	Abcam, Cat# 19857, RRID: AB_445175
	Mouse anti-TRA1-60-DyLight 650	1:50	Thermo Fisher Scientific, Cat# MA1-023-D650, RRID: AB_2536702
Differentia-tion Markers	Mouse anti-ACTA2	1:3,000	Sigma-Aldrich, Cat# A2547, RRID: AB_476701
	Rabbit anti-AFP	1:100	Agilent, Cat# A0008, RRID: AB_2650473
	Mouse anti-β-III-Tubulin	1:2,000	Covance, Cat# MMS-435P, RRID: AB_2313773
	Rabbit anti-TNNT2	1:200	Abcam, Cat# ab45932, RRID: AB_956386
Secondary antibodies	Goat anti-rabbit IgG-Alexa Fluor®488	1:250	Thermo Fisher Scientific, Cat# A11008, RRID: AB_143165
	Goat anti-mouse IgG-Alexa Fluor®488	1:250	Thermo Fisher Scientific, Cat# A11029, RRID: AB_138404

	Donkey anti-rabbit IgG Alexa Fluor 555	1:200	Thermo Fisher Scientific Cat# A-31572, RRID: AB_162543
	Donkey anti-mouse IgG Alexa Fluor 488	1:200	Thermo Fisher Scientific Cat# A-21202, RRID: AB_141607
Primary antibodies for immuno-blots	Rabbit anti-Cas9	1:2,000	Diagenode, Cat# C15310258, RRID: AB_2715516
	Mouse anti-GAPDH	1:10,000	Proteintech, Cat# 60004-1-Ig, RRID: AB_2107436
Secondary antibodies for immuno-blots	Rabbit anti-mouse-HRP	1:10,000	Dako, Cat# P0260, RRID: AB_2636929
	Goat anti-rabbit-HRP	1:5,000	Dako, Cat# P0448, RRID: RRID: AB_2617138
Control antibodies	Normal rabbit IgG	1:50	EMD Millipore, Cat# 12-370, RRID: AB_145841
	Normal mouse IgG	1:20	Santa Cruz, Cat# sc-2025, RRID: AB_737182
	Rabbit anti-mouse IgG-Alexa Fluor®633	1:250	Thermo Fisher Scientific, Cat# A-21052, RRID: AB_2535719
Primers			
	Target	**Forward/Reverse primer (5‘-3‘)**	
Differentia-tion marker	*PAX3-fwd*	AGAAGCCGAACCACCTTCAC	
	PAX3-rev	GGGTTGGAAGGAATCGTGCT	
	MAP2-fwd	CCACCTAGAATTAAGGATCA	
	MAP2-rev	GGCTTACTTTGCTTCTCTGA	
	TBXT-fwd	AATTGGTCCAGCCTTGGAAT	
	TBXT-rev	CGTTGCTCACAGACCACA	
	AFP-fwd	ACTCCAGTAAACCCTGGTGTTG	
	AFP-rev	GAAATCTGCAATGACAGCCTCA	
Normalizing gene	*TBP-fwd*	GCACAGGAGCCAAGAGTGAA	
	TBP-rev	TTGTTGGTGGGTGAGCACAA	
RT qPCR	*dCas9VPR-fwd*	GCCTCGCACCAACACCAAC	
	dCas9VPR-rev	GCCTCTTCCTTCTGGGGAATCAC	

	KLF15-fwd	TGCGCCAAGTTCAGCCGC
	KLF15-rev	GCGTGGCCTGGGACAATAGG
DNA genotyping & sequencing	*WT-AAVS1-fwd*	CGGAACTCTGCCCTCTAACG
	WT-AAVS1-rev	ATCCTCTCTGGCTCCATCGT
	TRANSGENE-AAVS1-fwd	CCGGACCACTTTGAGCTCTA
	TRANSGENE-AAVS1-rev	GGCTATGAACTAATGACCCCG
Cloning primers	*AAVS1-InFusion-fwd*	GACCGGTTCTATTGGCTCTAGAGGATCGAA
	AAVS1-InFusion-rev	CCGGTCCAGCCATTTCGATTTACTTGTACA
	AAVS1-WPRE fwd	AGCAATCGATTTAATTAACAATTGAATCAACCTCTGGATTACAAAATTTG
	AAVS1-WPRE rev	CTTAATCGATGAATTAATTCCAGGCGGGGAG
	pGIPZ-MCS fwd	TCGAGGATATCATTTAAGGTACCTAAGCATTAATTAAGC
	pGIPZ-MCS rev	GGCCGCTTAATTAATGCTTAGGTACCTTAAATGATATCC
	KLF15-1-fwd	CACCGCGCCGCGAAGGCTCGCAGG
	KLF15-1-rev	AAACCCTGCGAGCCTTCGCGGCGC
	KLF15-2-fwd	CACCGCGTGCGCGTCTGGCAGCTC
	KLF15-2-rev	AAACGAGCTGCCAGACGCGCACGC
	KLF15-3-fwd	CACCGGACCAGGCAGCGTGTTGGG
	KLF15-3-rev	AAACCCCAACACGCTGCCTGGTCC
gRNA oligo-nucleotides	*CT1-fwd*	CACCGTCCAGCGGATAGAATGGCG
	CT1-rev	AAACCGCCATTCTATCCGCTGGAC
	CT2-fwd	CACCGGAGCGGTTTTGGATATTAG
	CT2-rev	AAACCTAATATCCAAAACCGCTCC
	CT3-fwd	CACCGTATGAGCGCGATGAAGGTG
	CT3-rev	AAACCACCTTCATCGCGCTCATAC
	Off-target-1-fwd	TGAAGAAACAACCCGTTTCC
	Off-target-1-rev	TTCCCAGGAAACGATGAGAC

	Off-target-2-fwd	CCCTTGCTGAAGATCACACA
	Off-target-2-rev	CGTATGTTGCCCCCTACACT
	Off-target-3-fwd	GGCACAGAAGCATGAAGTGA
	Off-target-3-rev	CCTCCAGGTGCTGCTTACTC
Off-target analysis	*Off-target-4-fwd*	TTTTCCCAGGAAACGATGAG
	Off-target-4-rev	GCTCCCAGCTCTCCCTAAGT
	Off-target-5-fwd	ATCAGCAGGGCCACTAGAGA
	Off-target-5-rev	AGCAAAGCTCCTCAAACCAA

Additional Files:

STR analysis

Supplementary Figure 1

Certificate Cell Line Authentication Test

Client Sample Name	TC1133,CRISPRa2 2.0 A #8	TC1133,CRISPRa2 2.0 B #11	TC1133,CRISPRi, 1.0CTR
Sample Code	20_ZE_001655	20_ZE_001656	20_ZE_001652
D8S1179	13,14	13,14	13,14
D21S11	31.2,33.2	31.2,33.2	31.2,33.2
D7S820	10,11	10,11	10,11
CSF1PO	12,12	12,12	12,12
D3S1358	15,15	15,15	15,15
TH01	6,9.3	6,9.3	6,9.3
D13S317	9,11	9,11	9,11
D16S539	11,13	11,13	11,13
D2S1338	16,19	16,19	16,19
D19S433	13,16	13,16	13,16
vWA	16,16	16,16	16,16
TPOX	8,8	8,8	8,8
D18S51	14,14	14,14	14,14
AMEL	X,Y	X,Y	X,Y
D5S818	11,11	11,11	11,11
FGA	18,25	18,25	18,25
Database Name	LiPSC-GR1.1, LiPSC-GR1.2	LiPSC-GR1.1, LiPSC-GR1.2	LiPSC-GR1.1, LiPSC-GR1.2

STR analysis: The table shows the result of the cell line analysis for human induced pluripotent stem cells (hiPSC) **control** and **CRISPRa2 clone#8 and clone#11** and the comparison with the online database for cell line LiPSC-GR1.1 of the DSMZ (http://www.dsmz.de/de/service/services-human-and-animal-cell) and the Cellosaurus database (https://web.expasy.org/cellosaurus) showing a 100% matching.

Supplementary Figure 1

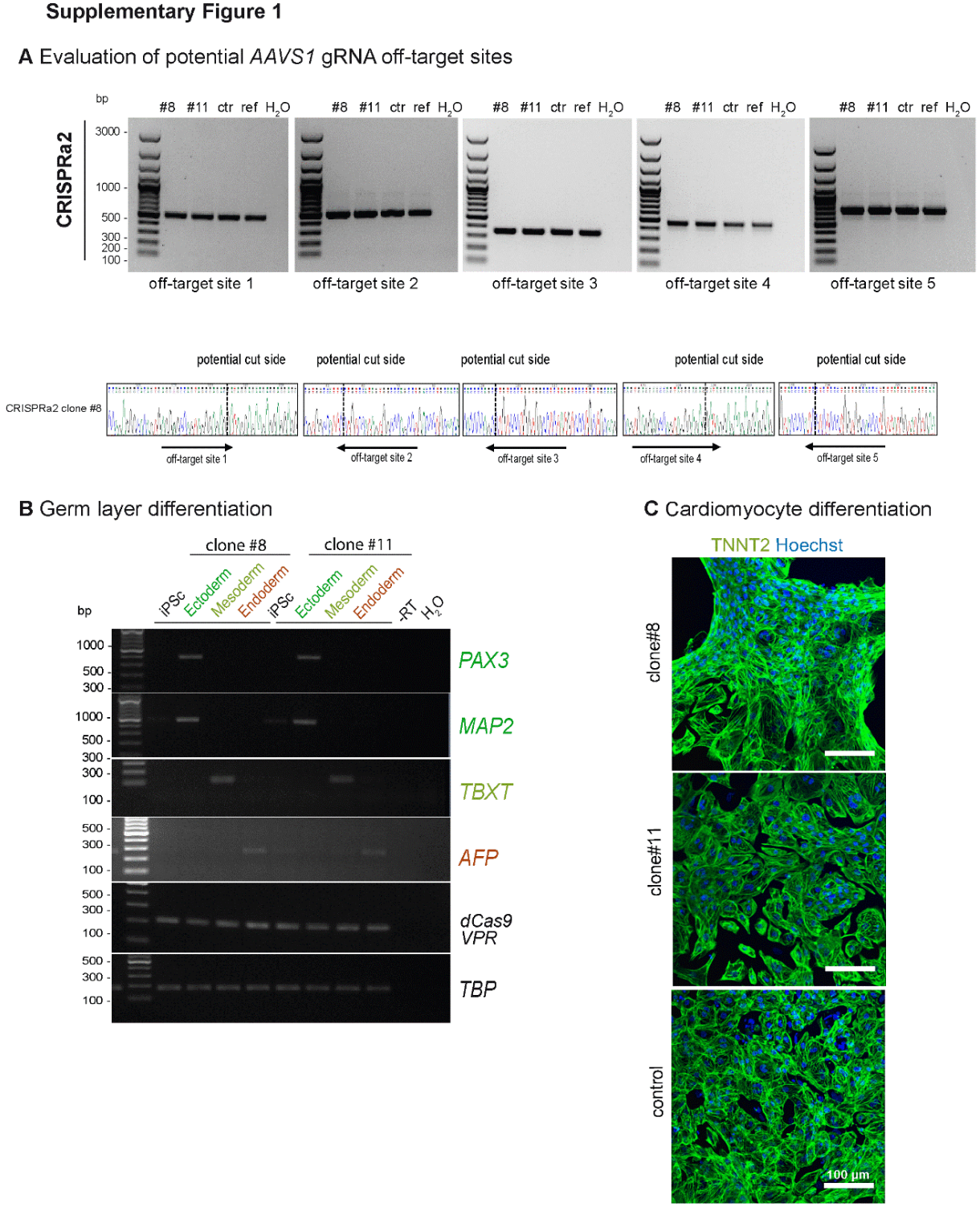

10. Chapter 6:

Fine-tuning guide RNA targeting rules for endogenous gene activation

Abstract

CRISPR-based synthetic gene modulation for endogenous gene activation (CRISPRa) is a powerful tool and was applied in multiple organisms and cell types. However, guidelines to effectively design gRNAs were scarce, making extensive experimental validations imperative. Here, empirical validation of gRNAs for 10 mouse and 5 human genes with the aim to induce endogenous gene activity was used to refine general gRNA design rules for CRISPRa applications. A target window of -100 bp (±50 bp) was identified for particularly amenable mammalian target genes. In contrast, gRNAs for target genes, which exhibited low activation potential in general, were extraordinarily ineffective when designed to this region. These findings contribute to a more comprehensive understanding of how synthetic transcription factors can be used effortlessly and reliably for a variety of basic and applied science questions. This modular data set will be a valuable basis for future targeted and unbiased gene activation approaches.

Introduction

Transcriptional modulation by programmable Cas9-related transcription factors was used for targeted gene activation and screening purposes. Scalable gene activation offered a valuable tool to decipher gene dose dependent functions. However, precise gene activity control in individual cells was difficult to achieve with conventional overexpression systems. CRISPR gene activation employed nuclease deficient Cas9 (dCas9) fused to transcriptional activators or epigenetic remodelers to be targeted to gene regulatory bodies within the genome to drive gene expression.[1] Multiple studies used this system for targeted gene activation or for unbiased screening approaches.[2,3] However, both applications required reliable design guidelines for individual gRNAs or, more importantly, for the generation of genome wide gRNA libraries. This was achieved previously by unbiased machine learning algorithms and revealed the distance of CRISPR-based transcription factors to transcriptional start sites (TSS) to be a major determinant for successful gene activation.[4] For instance, first steps towards control over endogenous gene activity in bacteria yielded in a preferential target site within -90 to -60 bp distance from the TSS.[5] *Drosophila melanogaster* genes were targeted with CRISPRa in a -400 bp distance from the TSS to successfully enhance endogenous gene expression.[6] For the human genome, a target window within -200 and +1 bp around the TSS were determined for effective gene activation.[7] These primordial rules were used in this work to design gRNAs for targeted gene activation. However, extensive empirical validation is still necessary for effective gene modulation. Thus, gRNA effectiveness prediction remains elusive and deserve further in-depth analyses to understand the genetic architecture amenable for such approaches. In this study, we aimed to compile in-house generated and curated datasets from CRISPRa gRNA validations to empirically determine optimal gRNA targeting windows for endogenous gene activation approaches.

Material and Methods

Cell culture

Neuro2a cells (#CCL-131, ATCC) or AAVpro HEK293T (#632273, TAKARA) cells were used to validate CRISPRa gRNAs in the mouse and the human genome, respectively. Cells were cultured in DMEM with 5% FCS, 100 U/mL penicillin and 100 µg/mL streptomycin (all Gibco). Cells were washed

with DPBS (Gibco) and passaged using 0.25% Trypsin (Gibco). $4 \cdot 10^5$ cells were seeded 16 h before transfection. Transfections were performed with 1 µg p-2xgRNA-based gRNA delivery plasmids along with 1 µg pPB-CAG-dCas9VPR-2A-tdTomato expression construct mixed in 200 µl MEM (Gibco) together with 4 µl Turbofect (Thermo Fisher Scientific) per reaction. Cells were harvested 48 h post-transfection for further analyses. Transfection success was controlled by examination of co-expressed reporter fluorescence (EGFP = gRNA expression construct and tdTomato = dCas9VPR expression constructs) with an Axiovert 200 fluorescence microscope and Axio (Carl Zeiss AG).

RNA extraction and quantitative polymerase chain reaction

Total RNA was isolated with NucleoSpin RNA (Macherey Nagel) columns according to manufacturer's protocol. RNA was transcribed into cDNA with MMLV-Reverse Transcriptase, dNTPs (both Promega) and Oligo dT20 (Eurofins Genomics). Quantitative polymerase chain reactions were performed with a final concentration of 0.3 µmol/L forward and reverse primers each (Eurofins Genomics) using Takyon ROX SYBR 2x Master Mix dTTP Blue (Eurogentec) on a 7900 HT Real Time Cycler (Applied Biosystems). Transcripts were calculated using standard curve comparisons and normalized to *18S* rRNA (Applied Biosystems), *Tbp* or *TBP* expression. Fold changes are reported with non-transfected cells as reference. All primers are listed in table 6.1. PCR products were Sanger sequenced (Microsynth Seqlab GmbH - Göttingen) to confirm amplicon identity.

Table 6.1. Primer sequences in chapter 6.

Gene	Primer	Primer sequence 5' → 3'	Species	Amplicon size
Hif1a	forward	CCTGCACTGAATCAAGAGGTTGC	mouse	110 bp
	reverse	CCATCAGAAGGACTTGCTGGCT		
Igfbp5	forward	AAGAAGCTGACCCAGTCCAA	mouse	201 bp
	reverse	GAATCCTTTGCGGTCACAGT		
Klf4	forward	GGCTCAGGTACCCCTCTCTC	mouse	397 bp
	reverse	TGGGTTAGCGAGTTGGAAAG		
Nos2	forward	CAGCTGGGCTGTACAAACCTT	mouse	95 bp
	reverse	CATTGGAAGTGAAGCGTTTCG		
Pou5f1	forward	ACATCGCCAATCAGCTTGG	mouse	51 bp
	reverse	AGAACCATACTCGAACCACATCC		
Rela	forward	TGACCCCTGTCCTCTCACATCCG	mouse	94 bp
	reverse	CAGCTCCCAGAGTTCCGGTT		
Rrbp1	forward	CAGCTGCCAATCAGGGTAAA	mouse	186 bp
	reverse	CCTTCTTCAGGGTTGCTTCC		
Shisa2	forward	TGCGACAACGACCGCCAGCAG	mouse	114 bp
	reverse	GAACACTGAGCCAACGATGA		
Shisa3	forward	CAGGGCAACTATCACGAGGG	mouse	189 bp
	reverse	GACATAGACAGGTTGCGCGG		
Tbp	forward	GCCTTCCACCTTATGCTCAG	mouse	250 bp
	reverse	TGTGTGGGTTGCTGAGATGT		
Tgfb2	forward	AGACGCTGTGCAGGAGTGG	mouse	96 bp
	reverse	TTATTAGACGGCACGAAGGT		
DLK1	forward	AGCACCTATGGGGCTGAATG	human	213 bp

	reverse	CCGAACATCTCTATCACAGAG		
IGFBP5	forward	TGCACCTGAGATGAGACAGG	human	136 bp
	reverse	GAATCCTTTGCGGTCACAAT		
KLF15	forward	TGCGCCAAGTTCAGCCGC	human	295 bp
	reverse	GCGTGGCCTGGGACAATAGG		
SHISA2	forward	CCTTCCCTCACACCAACAGT	human	170 bp
	reverse	TGAAGCCATCCAAAGGAATC		
SHISA3	forward	GGACGTGCAGGGCAACTACC	human	215 bp
	reverse	AGCCGACGATGAGAAAGGGG		
TBP	forward	GCACAGGAGCCAAGAGTGAA	human	176 bp
	reverse	TTGTTGGTGGGTGAGCACAA		

Analyses of gene activation potential and gRNA design

Transcriptional start sites were determined using data available at the Ensembl data base and at the eukaryotic promoter database (EPD). Single-nucleotide sequence assembly for analyses were performed with SerialCloner 2.6.1 (SerialBasics). Data was visualized with RStudio using the packages: knitr, ggplot2. Guide RNAs were designed with e-crisp (DKFZ - German Cancer Research Center).[8] Off-target predictions were performed with Off-Spotter (Computational Medicine Center - Thomas Jefferson University).[9] Selection criteria for gRNAs were: (1.) unique binding site with perfectly matched complementary sequence to the on target site, (2.) no less than two mismatches required for potential hybridization to any other location in the mouse or human genome, respectively, (3.) GC content between 40 - 90%, and (4.) 20 nucleotide gRNA length with the first (5') nucleotide being a guanine. The first nucleotide of *Igfbp5* gRNA A was exchanged to meet this requirement. Only the canonical 5' NGG 3' protospacer adjacent motive was considered for gRNA design and off-target predictions. Guide RNA encoding oligonucleotides (Eurofins Genomics) with suitable overhangs for insertion into the BbsI site in p-2xgRNA vectors were cloned as described before.[10] All gRNA sequences are listed in table 6.2.

Table 6.2. Guide RNA sequences in chapter 6.

Gene	gRNA	gRNA sequence 5' → 3'	DNA strand	Species	PAM sequence 5' → 3'
Hif1a	A	GAGGCGCTGAAGCAGCGGCA	-	mouse	GGG
	B	GAGCGGGCGCGCGCACCCCT	+		CGG
	C	GCGCGCGTTGGGTGCTGAGC	+		GGG
	D	GCGGGTTCCCGGAGAGCCAA	-		TGG
Igfbp5	A	GCCTGCGGGTTTCGAAGAGG	+	mouse	TGG
	B	GGAATGTACGGAAAGGGCTT	-		TGG
	C	GCTCTGTGTAGGGAGCGAAG	+		GGG
	D	GAGAGGCCTTCTAGACACGG	-		GGG
Klf4	A	GGCGGCCGCCGGCAGTTCCC	+	mouse	CGG
	B	GCTACCATGGCAACGCGCAG	+		TGG
	C	GCCCCCACTGCGCGTTGCCA	-		TGG
	D	GCCTGGCTGGCGTCACGGCC	+		TGG
	E	GCTCCAGCCCGCCAGCTGCC	+		TGG

	F	CGCGCGCCGCCACAGGGAGG	+		AGG
Nos2	A	GGAGGGGTATAAATACCTGA	+	mouse	TGG
	B	GCTAACTTGCACACCCAACT	+		GGG
	C	GACTCACTAGGGAGGGAGGC	-		TGG
	D	GCCAATATTCCAACACGCCC	-		AGG
Pou5f1	A	GGCACCCCGAGCCGGGGGCC	-	mouse	TGG
	B	GGGTGGAGGAGCAGAGCTGT	-		GGG
	C	GTGTCTTCCAGACGGAGGTT	-		GGG
	D	GACAGGACAACCCTTAGGAC	-		GGG
Rela	A	GCTCCGCAGCGCGGCTCGCT	-	mouse	CGG
	B	GCTCGGCTCCAGTCCCGGCC	+		AGG
	C	GCATGTGGCCCGTAGCACGC	+		GGG
	D	GCGAGCGTGCTGCATCCGAC	-		AGG
Rrbp1	D	GGGGCCGTTCGCCAGCTCCG	+	mouse	AGG
	E	GCAGGAGGCGGCGATCCCGG	+		CGG
	F	GATGAATGGCTGGTCCGGGT	+		GGG
	G	GCTAGTGAACCAATAGGAAG	+		AGG
	H	GTCAGAGGCCGGCAGAGTGG	+		CGG
	I	GCGACCATTGGCCAAAAAGG	-		AGG
	J	GCAACTCTCAGCTCTGCGCG	-		GGG
Shisa2	A	GAGGGCTTTCCCTCCGCCAG	-	mouse	GGG
	B	GGGCTACGAGTGTCCCCTGG	+		CGG
	C	GGGTGAACAGAACAGACAAG	-		TGG
	D	GTTTTAAGTCAGCCACGCCT	-		TGG
	E	GGAGAGTTGTCAGAGTAACT	+		CGG
	F	GATAGGGTTTGTGTTCGTCC	+		TGG
Shisa3	A	GGCGTCCCTTAAAAAGGCAG	-	mouse	AGG
	B	GCTCGCGCGGCGACCCCGGA	+		GGG
	C	GGGAGACGCGCGTGAACCTG	+		CGG
	D	GGGGTCACCGCCAAGGCCCG	+		GGG
	E	GCGCAAGTCCCCTCGTGAGC	+		TGG
	F	GAACGAATCCTCAGAATCGG	+		CGG
Tgfb2	A	GAAGGCAAACACGTGGTTTG	+	mouse	GGG
	B	GTTACTAAGACCACGAGCTC	-		TGG
	C	GGGGGACGGCCAGTAAGGGA	-		GGG
	D	GGCACGCACTCAACACAGGA	+		GGG
DLK1	E	GGTCGGGGGCGGCCCTGCGA	+	human	GGG
	F	GGCCCCGTGCGCACGGAGGC	+		GGG
	G	GCCCCGTGCGCACGGAGGCG	+		GGG
	H	GCGCTCTCCACCGCCGCTGC	-		CGG
IGFBP5	A	GACGCCTCTTACCTGTTCTG	+	human	CGG
	B	GGCGCTGTTCAGGGAGCGAA	+		GGG
	C	GCGCTGTTCAGAGGGGAGGA	+		GGG
	D	GCCCCTTTCTTACATTCCGG	+		GGG
KLF15	A	GCGCCGCGAAGGCTCGCAGG	-	human	AGG
	B	GACGCGCAGCGCGGGCCAAT	+		GGG
	C	GCTCAAGTCCGGGAGCCGCG	+		CGG

	D	GCGTGCGCGTCTGGCAGCTC	+		CGG
	E	GGACCAGGCAGCGTGTTGGG	+		GGG
	F	GCTGTCTCGCGGCGTCCACG	-		AGG
	G	GGGAACCGAGCTTTAGAAGC	+		CGG
	H	GTGATTGAGCGGGAAGCGCT	-		GGG
SHISA2	A	GACGAGGCCCGGGGGTCGCC	+	human	GGG
	B	GTCGTGGCCCCGGCGACCCC	-		CGG
	C	GGCGTCGCGGCAGAGGGGAG	+		TGG
	D	GGGGATGGCTTAGGAGCTCC	+		TGG
	E	GCCGGTGGCCCGGTCCCCTT	-		AGG
	F	GCACTCGCTGATGGAAATCT	-		CGG
SHISA3	A	GGACGCAGCTGGAAAGCGAA	-	human	GGG
	B	GCACTACGAGTTCCGCAGGC	-		CGG
	C	GCCGGCAGAGGCAGTTGCTG	-		GGG
	D	GCTATGAGCCGGGCGAAGGG	+		CGG
	E	GTTGGCAGCCCCGGGCGCTA	+		TGG
	F	GTTGGGACTCTGTGCGGCGC	+		TGG
	G	GGCTGAGCGGCCGCCTGTCT	+		GGG
	H	GGCCAAGTACAAACGGCCGC	-		GGG
NT	1	GTCCAGCGGATAGAATGGCG	N/A	N/A	N/A

Results

Targeting of gRNAs determines endogenous gene activation potential

A set of 3-8 gRNAs per gene were tested for endogenous gene activation in mouse (Neuro2A) and human cells (HEK293T) as predictive means for downstream applications in hiPSC-cardiomyocytes *in vitro*[11,12] and Myh6-dCas9VPR mice *in vivo*.[10] To this end, these validations yielded an in-house data set of 10 mouse and 5 human genes targeted for endogenous gene activation by CRISPR/dCas9VPR. The transcriptional activation was determined by quantitative PCR to compare fold change gene expression induction compared to untransfected cells, cells that were only transfected with the dCas9VPR plasmid or expressed dCas9VPR and a non-targeted gRNA (NT). A dependency of gene activation potential with respect to distance to the TSS was observed. The accurate identification of the TSS was previously suggested to be of critical importance and preferentially to be used from CAGEseq data (e.g. Eukaryotic Promoter Data Base (EPD)) instead of mRNAseq data (e.g. Ensembl Data base). Indeed, the adjustment to CAGEseq TSS allowed for the identification of gene induction potential patterns with a maximum at a ~ -100 bp distance from the TSS (Figure 6.1 A). Interestingly, by subdividing the datasets into high (H) activation potential- (at least 1 gRNA with >10-fold activation from baseline) and low (L) activation potential (all gRNAs with <10-fold activation from baseline), a maximum gene activation for H genes was observed when gRNAs were targeted to a -100 bp region upstream of the TSS. In contrast, gRNAs rendered specifically ineffective when targeted to this region of L genes (Figure 6.1 B). Importantly, the identified gRNA targeting window for murine genes was similar for human genes (Figure 6.1 C).

Figure 6.1

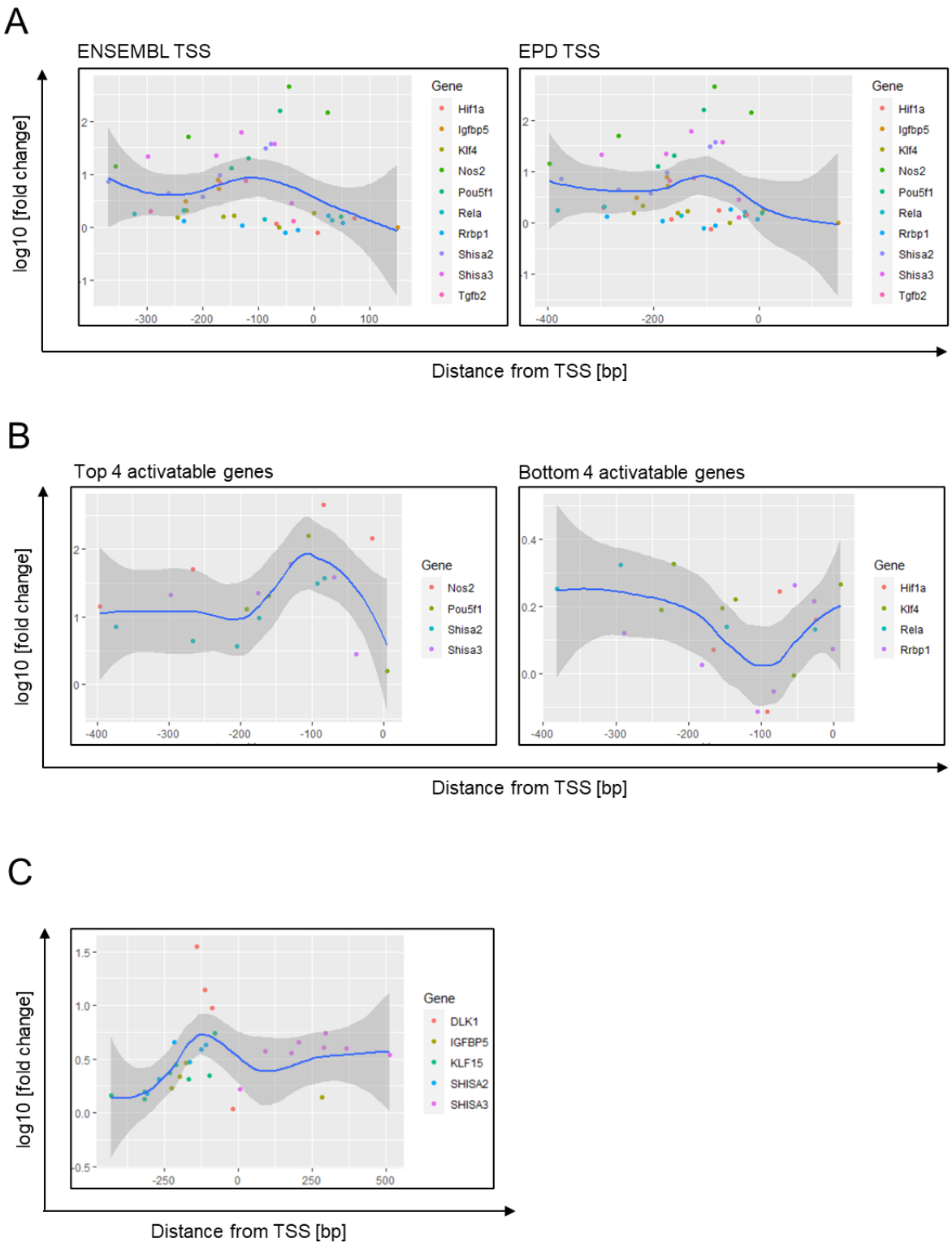

Figure 6.1. Endogenous gene expression efficiency is dependent on gRNA target site upstream of the transcriptional start site. A. Comparison of ENSEMBL and EPD databases determined TSS for 10 mouse genes targeted with 3-8 gRNAs per gene regarding gene activation potential. A target window of approximately -100 bp upstream of TSS was identified for most effective endogenous gene activation with dCas9VPR. Transcriptional fold change was compared to non-transfected cells (Neuro2a cells) and expression was normalized to 18S rRNA or *Tbp* expression. **B.** Subdivision of particularly potent gRNAs and gene candidates (top 4) and less effective gene candidates (bottom 4) revealed a distinct sensitivity to the -100 bp region upstream of the TSS. **C.** Similarly,

for 5 human genes the -100 bp upstream TSS region was found particularly susceptible for CRISPRa gRNA targeting. For the analyses of human target genes, the Eukaryotic Promoter database (EPD) TSS prediction was used. Depicted is the locally estimated scatterplot smoothing (LOESS) plotted with R package ggplot2. Data acquisition was supported by Niklas Bader, Janek Fischer, Kamal Hazzouri, and Laura Priesmeier, Institute of Pharmacology and Toxicology, University Medical Center Göttingen.

Discussion

Effective gRNA design is essential for robust targeted gene activation to be employed for multiplexed arrays as well as genome wide CRISPR gene activation-based screens. General rules for effective gRNA design were discussed before in multiple target organisms and revealed distinct optimal target window distances from the TSS.[13,14] Here, an optimal target window of -150 and -50 bp with a maximum at -100 bp was identified for a subset of genes, which were exceptionally amenable for endogenous gene activation with dCas9VPR. Transcription is controlled via the recruitment of transcription factors to gene regulatory sequences. Distal and proximal promoters are evolutionary conserved regions typically located upstream of the TSS and regulating baseline transcriptional activity. Notably, the identified region -100 bp upstream of target gene TSS is commonly characterized by localization of proximal promoter elements.[15–17] Additionally, Horlbeck at al. underscored the importance to take nucleosome position into account for gRNA/Cas9 targeting[4,18]; a feature, that prokaryotes, where the CRISPR/Cas9 system was derived from, are lacking. Specifically for *Streptococcus pyogenes* Cas9, gRNA length was reported to play a subordinate role for gRNA efficiency in dCas9VPR single target gene activation approaches.[19] GC-content was discussed as a potential determinant for gRNA effectiveness of CRISPRa approaches[14] however other studies did not confirm a correlation between stronger gene activation potential and increasing GC-content of gRNAs.[6] In general, we observed translatable gene activation from tested and selected gRNAs in validation experiments when applied in mouse and human cardiomyocytes, respectively. Importantly, baseline gene activity appeared to contribute to overall gene activation efficiency. This dependency was observed by others as well and needs to be taken into consideration at the stage of target gene selection for CRISPRa mediated transcription enhancement *a priori*.[20] The possible gene activation fold change between L and H genes differed by two orders of magnitude (on a base ten logarithmic scale), suggesting a switch-like mode of gene activation for H genes and a tune-like activatability of L genes. Further insight, specifically at single base pair resolution into the gene regulatory regions and structures of target gene regulatory regions is therefore necessary to improve gRNA designs especially for CRISPR-based transcriptional interventions. *Vice versa*, these novel tools harbor great potential for probing the genome in unprecedented detail to identify potential cell-type specific gene regulatory elements empirically. The presented modular data catalogue along with increasing knowledge about chromatin architecture will ultimately help to define targeting regions for CRISPR-based applications more precisely.

References (Chapter 6)

1. la Russa, M. F. & Qi, L. S. The New State of the Art: Cas9 for Gene Activation and Repression. *Molecular and Cellular Biology* **35**, 3800–3809 (2015).
2. Wang, G. *et al.* Multiplexed activation of endogenous genes by CRISPRa elicits potent antitumor immunity. *Nature Immunology* **20**, 1494–1505 (2019).
3. Bester, A. C. *et al.* An Integrated Genome-wide CRISPRa Approach to Functionalize lncRNAs in Drug Resistance. *Cell* **173**, 649-664.e20 (2018).
4. Horlbeck, M. A. *et al.* Compact and highly active next-generation libraries for CRISPR-mediated gene repression and activation. *eLife* **5**, 1–20 (2016).

5. Dong, C., Fontana, J., Patel, A., Carothers, J. M. & Zalatan, J. G. Synthetic CRISPR-Cas gene activators for transcriptional reprogramming in bacteria. *Nature Communications* **9**, (2018).

6. Lin, S., Ewen-Campen, B., Ni, X., Housden, B. E. & Perrimon, N. In Vivo Transcriptional Activation Using CRISPR/Cas9 in Drosophila. *Genetics* **201**, 433–442 (2015).

7. Konermann, S. *et al.* Genome-scale transcriptional activation by an engineered CRISPR-Cas9 complex. *Nature* **517**, 583–588 (2015).

8. Heigwer, F., Kerr, G. & Boutros, M. E-CRISP: Fast CRISPR target site identification. *Nature Methods* **11**, 122–123 (2014).

9. Pliatsika, V. & Rigoutsos, I. "Off-Spotter": Very fast and exhaustive enumeration of genomic lookalikes for designing CRISPR/Cas guide RNAs. *Biology Direct* **10**, 1–10 (2015).

10. Schoger, E. *et al.* CRISPR-Mediated Activation of Endogenous Gene Expression in the Postnatal Heart. *Circulation Research* **126**, 6–24 (2020).

11. Schoger, E., Argyriou, L., Zimmermann, W. H., Cyganek, L. & Zelarayán, L. C. Generation of homozygous CRISPRa human induced pluripotent stem cell (hiPSC) lines for sustained endogenous gene activation. *Stem Cell Research* **48**, 101944 (2020).

12. Schoger, E., Zimmermann, W.-H., Cyganek, L. & Cecilia Zelarayán, L. Establishment of a second generation homozygous CRISPRa human induced pluripotent stem cell (hiPSC) line for enhanced levels of endogenous gene activation. *Stem Cell Research* **56**, 102518 (2021).

13. Gilbert, L. A. *et al.* Genome-Scale CRISPR-Mediated Control of Gene Repression and Activation. *Cell* **159**, 647–661 (2014).

14. Mao, D. *et al.* Enhanced efficiency of flysam by optimization of sgrna parameters in drosophila. *G3: Genes, Genomes, Genetics* **10**, 4483–4488 (2020).

15. Petrovic, N. *et al.* Role of proximal promoter elements in regulation of renin gene transcription. *Journal of Biological Chemistry* **271**, 22499–22505 (1996).

16. Rowland, T. J., Bonham, A. J. & Cech, T. R. Allele-specific proximal promoter hypomethylation of the telomerase reverse transcriptase gene (TERT) associates with TERT expression in multiple cancers. *Molecular Oncology* **14**, 2358–2374 (2020).

17. Sun, D. *et al.* The proximal promoter region of the human vascular endothelial growth factor gene has a G-quadruplex structure that can be targeted by G-quadruplex-interactive agents. *Molecular Cancer Therapeutics* **7**, 880–889 (2008).

18. Horlbeck, M. A. *et al.* Nucleosomes impede Cas9 access to DNA in vivo and in vitro. *eLife* **5**, 1–21 (2016).

19. Kiani, S. *et al.* Cas9 gRNA engineering for genome editing, activation and repression. *Nature Methods* **12**, 1051–1054 (2015).

20. Strezoska, Ž. *et al.* CRISPR-mediated transcriptional activation with synthetic guide RNA. *Journal of Biotechnology* **319**, 25–35 (2020).

11. Chapter 7:

Re-activation of *Krüppel-like Factor 15* in stressed mouse and human cardiomyocytes

Abstract

Re-activation of homeostatic genes in diseased cardiomyocytes harbors the possibility to transcriptionally reprogram cardiomyocytes towards a healthy state, halting maladaptive remodeling and heart failure progression. The transcription factor *KLF15* maintains normal cardiomyocyte function in part via WNT/CTNNB1 signaling repression. *KLF15* transcript levels are decreased in the diseased human myocardium and, conversely, its down regulation or loss, resulted in heart failure progression. Therefore, I hypothesized that restoration of *KLF15* expression via CRISPR/Cas9 endogenous gene activation was sufficient to prevent maladaptive tissue remodeling in disease models including mouse cardiomyocytes *in vivo* and in human induced pluripotent stem cell derived cardiomyocyte (hiPSC-cardiomyocytes) *in vitro*. This hypothesis was tested using the established CRISPRa approach in mice *in vivo* and in human *in vitro* models. By viral delivery of gRNAs targeted to the mouse *Klf15* or human *KLF15* promoter region into CRISPRa cardiomyocytes, a re-normalization of *Klf15* transcript levels resulted in a blunted molecular and functional maladaptive cardiac remodeling response underscoring the role of *KLF15* in maintaining cardiomyocyte homeostasis. The transcriptional repression of *KLF15* was recapitulated in an engineered human myocardium (EHM) model and unraveled a TGFB1 mediated mechanism. Rescue of *KLF15* transcription in stressed EHM resulted in the prevention of the fetal sarcomeric protein alpha smooth muscle actin (ACTA2) expression suggesting attenuation of cardiomyocyte dedifferentiation, which normally follows upon hypertrophic stimulus, and ameliorated transcriptional remodeling.

Introduction

Cardiac remodeling and hypertrophy are the result of myocardial adaptation to stress signals and damage preceding heart failure progression. The adult heart is maintained in a cellular and molecular homeostasis by fine tuning of intra- and intercellular signaling cascades.[1–3] *KLF15* controls a variety of hypertrophy associated signaling pathways in the heart.[4] The role of *KLF15* to negatively control hypertrophic MEF2 and GATA4 signaling was described before.[5] Furthermore, protein-protein interaction with CTNNB1 and NLK indicated a regulatory role of WNT/CTNNB1 activity, which was confirmed in murine and human experimental disease models.[6,7] A lack of *KLF15* was associated with the decline of heart function in murine models[7] and in EHM with concomitant WNT/CTNNB1 signaling de-repression.[8] EHM was used as a surrogate of human heart tissue in a dish with advanced transcriptional and cardiomyocyte morphological features compared to 2D cardiomyocyte models including opportunities for cardiac disease modelling.[9] I specifically focused on *KLF15*'s role in repressing WNT/CTNNB1 signaling in cardiomyocytes as a potential candidate for cell-type specific therapeutic, transcriptional correction to prevent heart failure progression based on previous findings defining the fundamental biology of adult cardiomyocytes. To achieve this, I employed a second generation CRISPR/dCas9 gene activation system[10] to faithfully control *Klf15* expression *in vivo* and *in vitro*. Targeted *Klf15* activation with this system was described in cardiomyocytes of neonatal mice in frame of this study.[11] However, gene re-expression for the normalization of transcript levels in diseased cardiomyocytes of the adult heart and in stressed hiPSC-cardiomyocytes was not tested before.

Material and Methods

Mouse work

C57/BL6N mice expressing dCas9VPR under *Myh6* promoter control were bred and fed ad libitum and maintained in day/night cycles of 12 h. Genotyping was performed with the following primer pair: VPR fwd: 5' GCCTCGCACCAACACCAAC 3', VPR rev: 5' GCCTCTTCCTTCTGGGGAATCAC 3'. C57/BL6N *Klf15* knockout mice characterized by a LacZ cassette insertion in exon 2 of *Klf15* resulting in frameshift as described before.[6] The following primer pairs were used for genotyping: *Klf15* KO fwd: 5' ATCTGGACATTTGGCCACAG 3', *Klf15* KO rev: 5' CTCTTCGCTATTACGCCAGC 3' and *Klf15* WT fwd: 5' CTCAAAATGCACAAATGCAC 3', *Klf15* WT fwd: 5' ATACACTCGGGGGAGCAG 3'. These mice were crossed with Myh6-dCas9VPR mice to derive Myh6-dCas9VPR/Klf15KO mice. Four- to six-month-old Myh6-dCas9VPR or Myh6-dCas9VPR/Klf15KO mice were anesthetized with 0.5 mg/kg Medetomidin (cp-pharma), 5 mg/kg Midazolam (Roche) intraperitoneally, and $1 \cdot 10^{12}$ vg/mouse in saline were injected via the tail vein systemically. Tail vein injections were performed by Dr. Cheila Rocha, Mareike Jassyk, Petra Tucholla, and Federico Bleckwedel, Institute of Pharmacology and Toxicology, University Medical Center Göttingen. Pressure overload was induced by transverse aortic constriction surgery. Mice were anesthetized and analyzed with 0.5 mg/kg Medetomidin (cp-pharma), 5 mg/kg Midazolam (Roche), and 0.05 mg/kg Fentanyl (Rotexmedica) intraperitoneally as well as 5 mg/kg Carprofen (cp-pharma) subcutaneously immediately prior to surgery. The thoracic cavity was opened, and the aortic arch was dissected. Aortic constriction was performed by tying the aorta around a blunt-end 26G cannula. The same procedure without tying the node (sham) was performed as control. For antagonization, 2.5 mg/kg Atipamezol (cp-pharma) and 0.5 mg/kg Flumazenil (Inresa) were injected subcutaneously. Subsequent analgesia was implemented with 0.1 mg/kg Carprofen (cp-pharma) applied subcutaneously 6 h, 24 h, and 48 h post-intervention. Surgery was performed by Sarah Zafar, SFB1002 Service Unit. Animal work was approved by Niedersächsisches Landesamt für Verbraucherschutz und Lebensmittelsicherheit (Tierversuchsvorhaben AZ-G 15-1840 and AZ-G 33.9-42502-04-20/3434). Survival of groups was monitored over the entire experimental period and reported in the survival curve in Figure 7.2 H if 1.) a mouse spontaneously died or 2.) a mouse had to be euthanized because abort criteria defined in AZ-G 15-1840 or AZ-G 33.9-42502-04-20/3434 were fulfilled. Whole heart images were taken immediately after organ harvest with a Stereo Lumar.V12 stereomicroscope (Carl Zeiss).

Echocardiography

Mice were anaesthetized with Isoflurane (Isofluran CP 1 ml/ml, CP-Pharma) 2,5-4 v/v % in O2. Heart functional parameters and morphology were assessed by echocardiography using a VisualSonics Vevo 2100 Imaging System (Fujifilm) equipped with a 30 MHz MS-400 MicroScan transducer. Pressure gradients 3 days post-surgery were determined by pulse wave doppler echography with a 20 MHz MS-250 MicroScan transducer to assess successful aortic banding. Measurements were performed and imaging data was analyzed by Marcel Zoremba and Beate Knocke, SFB1002 Service Unit, who were blinded to surgery and treatment groups.

Fractional area shortening (FAS) was calculated with:

$$FAS = (area\text{-}s - area\text{-}d)/area\text{-}d \cdot 100$$

area-d: cross-sectional left ventricular myocardial area in diastole
area-s: cross-sectional left ventricular myocardial area in systole

Guide RNA design and cloning

Guide RNAs were designed and cloned into p2x-gRNA using the BpiI or Eco31I sites (both: FastDigest Enzymes, Thermo Fisher Scientific) and TRISPR constructs for *in vitro* validations and *in vivo* application as described before.[11] TRISPR triple gRNA expression cassettes were cloned into pGIPZ-based lentiviral constructs as described before.[12] Sequences for gRNAs are summarized in table 7.1.

Table 7.1. Guide RNA sequences in chapter 7.

Gene	gRNA	gRNA sequence 5' → 3'	DNA strand	Species	PAM sequence 5' → 3'
Klf15	A	GGGACTCTGCGGGCTTTCAG	+	mouse	TGG
	B	GTGCAGATCCACGAAGAGAC	+		CGG
	C	GACACGGTCCCTACTAGATC	+		GGG
KLF15	A	GCGCCGCGAAGGCTCGCAGG	-	human	AGG
	B	GACGCGCAGCGCGGGCCAAT	+		GGG
	C	GCTCAAGTCCGGGAGCCGCG	+		CGG
	D	GCGTGCGCGTCTGGCAGCTC	+		CGG
	E	GGACCAGGCAGCGTGTTGGG	+		GGG
	F	GCTGTCTCGCGGCGTCCACG	-		AGG
	G	GGGAACCGAGCTTTAGAAGC	+		CGG
	H	GTGATTGAGCGGGAAGCGCT	-		GGG
NT	1	GTCCAGCGGATAGAATGGCG	N/A	N/A	N/A
NT	2	GGAGCGGTTTTGGATATTAG	N/A	N/A	N/A
NT	3	GTATGAGCGCGATGAAGGTG	N/A	N/A	N/A

RNA extraction and reverse transcriptase quantitative polymerase chain reaction

RNA was extracted using TRIzol (Thermo Fisher Scientific) according to manufacturer's protocol. Co-precipitant GlycoBlue (Thermo Fisher Scientific) was used for RNA pellet visualization. Complementary DNA (cDNA) was synthesized with MMLV-Reverse Transcriptase, Hexamers (both Promega) or Oligo dT20 (Eurofins Genomics). For quantitative PCR, 1:3, 1:5 or 1:10 diluted cDNA was combined with Takyon No ROX SYBR 2X MasterMix blue dTTP (Eurogentec), primers (listed in table 7.2) in a final concentration of 0.3 µmol/L. PCR reactions were performed in triplicates. The following cycler program was used for quantitative PCR (qPCR) reactions in a 7900 HT Fast Real-Time PCR System (Applied Biosystems). Results were analyzed by standard curve comparisons and transcripts were normalized to *Tbp* (mouse) or *TBP* (human) expression, respectively.

Table 7.2. Primer sequences in chapter 7.

Gene	Primer	Primer sequence 5' → 3'	Species	Amplicon size
Klf15	forward	CAACTCATCTGAGCGGGAA	mouse	143 bp
	reverse	CAAGAGCAGCCACCTCAAG		
Nppb	forward	AAGTCCTAGCCAGTCTCCAGAGC	mouse	268 bp
	reverse	CTTCAGTGCGTTACAGCCCAAAC		
Shisa3	forward	CAGGGCAACTATCACGAGGG	mouse	189 bp
	reverse	GACATAGACAGGTTGCGCGG		
Cd44	forward	CAGCCAGTGACAGGTTCCAT	mouse	319 bp
	reverse	TGCTCAGGGCCAACTTCATT		
Tbp	forward	GCCTTCCACCTTATGCTCAG	mouse	250 bp
	reverse	TGTGTGGGTTGCTGAGATGT		
KLF15	forward	AGCAAGGACTTGGATGCCTG	human	337 bp
	reverse	AGGGCAGGTTCAAGTTGGAG		
ACTA2	forward	GGAAAAGATCTGGCACCACTC	human	196 bp
	reverse	GCGTCCAGAGGCATAGAGAG		
TBP	forward	GCACAGGAGCCAAGAGTGAA	human	176 bp
	reverse	TTGTTGGTGGGTGAGCACAA		

Cytosolic and nuclear protein separation

Tissue was minced in Hypotonic Buffer (10 mmol/L KCl, 10 mmol/L HEPES, 2 mmol/L $MgCl_2$, 100 µmol/L EDTA, 1 mmol/L DTT) including PhosSTOP (Sigma Aldrich) and cOmplete Mini Protease Inhibitor (Sigma Aldrich) and cells were lysed for 15 min on ice. 10 v/v % Igepal CA-630 was added and tissue was incubated on ice for 5 min. Nuclei were pelleted by centrifugation at 1,500 xg at 4 °C for 5 min and cytosolic protein containing supernatant was collected. Nuclei pellets were washed with Hypotonic Buffer before lysis in Hypertonic Buffer (300 mmol/L NaCl, 50 mmol/L KCl, 50 mmol/L HEPES, 100 µmol/L EDTA, 1 mmol/L DTT, 10 v/v % Glycerol) for 25 min on ice. 10 v/v % Igepal CA-630 was added and further incubated on ice for 5 min. After centrifugation at 16,000 xg at 4°C for 5 min, nuclear protein lysates were collected.

Protein sample preparation and immunoblotting

Tissues and cells were lysed in Lysis Buffer (350 mM NaCl, 20 mM HEPES, 1 mmol/L $MgCl_2 \cdot 6\ H_2O$, 0.5 mmol/L EDTA, 0.1 mmol/L EGTA, 1 v/v % Igepal CA-630, 20 v/v % glycerol) including PhosSTOP (Sigma Aldrich) and cOmplete Mini Protease Inhibitor (Sigma Aldrich) and homogenized with a Tissue Lyser II (Qiagen). Protein content was quantified with RotiQuant (Carl Roth). Protein samples were prepared with 4x Sample Buffer (100 mmol/L TRIS-HCl, 0.025 v/v % bromophenol blue, 8 w/v % SDS, 10 v/v % glycerol, 10 v/v % β-mercaptoethanol). Electrophoresis was performed in Electrophoresis Buffer (25 mmol/L TRIS ultrapure, 190 mmol/L Glycine, 0.1 w/v % SDS) on discontinuous SDS-polyacrylamide gels to separate 5 µg - 20 µg of total protein/ sample at 110 V for 1.5 h. Proteins were transferred onto PVDF membranes in Transfer Buffer (25 mmol/L TRIS ultrapure, 190 mmol/L Glycine, 20 v/v % methanol) at 100 V and 4 °C for 2.5 h. Membranes were blocked in 5% non-fat dried milk (AppliChem) in TBST (20 mmol/L Tris ultrapure, 150 mmol/L NaCl, 0.1 v/v % Tween (Carl Roth), pH 7.6). Antibodies (summarized in table 7.3) were applied for 16 h diluted in 5 v/w % non-fat dried milk or 5 v/w % bovine serum albumin (Carl Roth) in TBST at 4 °C. Membranes were washed thrice in TBST and incubated with secondary antibodies for 2 h at room temperature.

Bands were detected using the femtoLUCENT PLUS-HRP Kit (G-Biosciences) and a ChemiDoc MP Imaging System with Image Lab Version 5.1 (both BioRad).

Table 7.3. Primary and secondary antibodies chapter 7.

Antibody	Manufacturer	Catalogue Number	Host organism	Dilution (IB)	Dilution (IF)
Anti-ACTA2	Sigma Aldrich	A2547	mouse	1:1 000	1:200
Anti-ACTN2	Sigma Aldrich	A7811	mouse	1:2 000	-
Anti-BZW2	Sigma Aldrich	HPA022813	rabbit	1:1 000	-
Anti-Cas9	Diagenode	C15310258-100	rabbit	1:1 000	-
Anti-CTNNB1	BD Transduction	610153	mouse	1:2 000	-
Anti-S675-P-CTNNB1	Cell Signaling	4176	rabbit	1:1 000	-
Anti-GAPDH	Proteintech	60004-1-Ig	mouse	1:50 000	-
Anti-Lamin A/C	Santa Cruz Biotechnology	sc-6215	goat	1:1 000	-
Anti-TCF7L2	EMD Millipore	17-10109	mouse	1:500	-
Anti-TNNT2	Abcam	ab45932	rabbit	1:2 000	1:200
Anti-TurboGFP	Thermo Fisher Scientific	PA5-22688	rabbit	1:5 000	-
Anti-goat-HRP	Dako	P0449	rabbit	1:2 0000	-
Anti-mouse HRP	Dako	P0260	rabbit	1:10 000	-
Anti-rabbit HRP	Dako	P0448	goat	1: 5 000	-
Alexa Fluor 488 anti-rabbit	Thermo Fisher Scientific	A-11008	goat	-	1:400
Alexa Fluor 555 anti-mouse	Thermo Fisher Scientific	A-21424	goat	-	1:400

Single cell isolation and single cell transcriptomics

Mouse hearts were canulated via the ascending aorta with a 18G blunt-end needle and retrogradely perfused with Perfusion Buffer (150 mmol/L NaCl, 5 mmol/L HEPES, 5.4 mmol/L KCl, 10 mmol/L glucose, 2 mmol/L Na-pyruvate, 1.2 mmol/L $MgCl_2 \cdot 6\ H_2O$, 10 mmol/L taurine, 12.38 mmol/L 2,3-butanedione monoxime, pH 7.35). Hearts were enzymatically digested with Digestion Buffer (210 µg/ml Liberase DH (Roche), 25 µmol/L $CaCl_2$ in Perfusion Buffer) for 10 min at 37 °C, minced into tissue pieces, homogenized by pipetting with a 10 ml serological pipette to yield a single cell suspension of rod-shaped cells. Debris was removed by washing with Exchange Buffer (0.5 w/v % bovine serum albumin, 200 µmol/L $CaCl_2$ in Perfusion Buffer) and gravitational settling of tissue pieces for 1 min. Samples were prepared, processed, and analyzed for single cell transcriptomics at the Next Generation Sequencing Facility, Institute of Human Genetics, University Medical Center Göttingen. Briefly, cells were distributed on 5,184 nanowell chips ICELL8 250v Chip (ICELL8 System, Takara Bio). Single alive cells were identified using Hoechst 33342 and propidium iodide staining (NucBlue Cell Stain Reagent, Thermo Fisher Scientific) and the CellSelect Software (Takara Bio). Complementary DNA synthesis was performed by oligo-dT priming in a one-step RT-PCR reaction. P5 indexing primers, Terra Polymerase and Reaction Buffer were added for library preparation. Transposase enzyme and reaction buffer (Tn5 mixture) were added to each well. P7indexing primers were dispensed to wells. Final libraries were amplified and pooled as they are extracted from the chip. Pooled libraries were

purified, and size selected with Agencourt AMPureXP magnetic beads (Beckman Coulter) to obtain an average library size of 500 bp. A typical yield for a library comprised of ~1300 cells was 15 nmol/L. Libraries were sequenced with a HiSeq4000 (Illumina) to obtain on average ~$3 \cdot 10^5$ reads per cell (single-end, 50 bp). Raw sequencing files (bcl-files) were converted into a single fastq file using Illumina bcl2fastq software (v2.20.0.422) for each platform. Each fastq file was demultiplexed and analyzed using the Cogent NGS analysis pipeline (CogentAP) from Takara Bio (v1.0). In brief, "cogent demux" wrapper function was used to allocate the reads to the cells based on the cell barcodes provided in the well-list files. Subsequently, "cogent analyze" wrapper function performed read trimming with cutadapt (Martin, M. Cutadapt removes adapter sequences from high-throughput sequencing reads. EMBnet.journal 17, 10 (2011)) (version 3.2), genome alignment to Homo sapiens genome GRCm38 using STAR (version 2.7.7a),[13] read counting for exonic, genomic and mitochondrial regions using featureCounts (version 2.0.1)[14] and utilizing Mus musculus gene annotation version 102 from ENSEMBL and generating a gene matrix (https://www.ensembl.org/Homo_sapiens/Info/Index) with number of reads expressed for each cell in each gene. Raw gene matrices underwent quality control (QC) filtering for cells and genes using the following parameters: (a) for cells, only those with at least 10000 reads associated to at least 300 different genes, and (b) for genes, only those containing at least 100 reads mapped to them from at least 3 different cells.

In addition to the association of cells based on their sample identity, an unsupervised clustering known as K-nearest neighbor (KNN) graph and Louvain community detection was used to determine how cells cluster independently of their sample association but based on their genetic profiles. For this, the R package FNN version 1.1.3 (Alina Beygelzimer, Sham Kakadet, John Langford, Sunil Arya, David Mount and Shengqiao Li (2019). FNN: Fast Nearest Neighbor Search Algorithms and Applications. R package version 1.1.3. https://CRAN.R-project.org/package=FNN) was used the KNN algorithm to define 100 centers which cells could associate to based on their multi-dimensional proximity to them, and the R package igraph version 1.2.6 (Csardi G, Nepusz T: The igraph software package for complex network research, InterJournal, Complex Systems 1695. 2006. https://igraph.org) used the Louvain community detection to reduce the number of neighbors by merging nearby ones until a certain point of convergence.

For single cell imaging, glass cover slips were coated with Matrigel (Corning) for 1 h at 37 °C. Cells were distributed in Exchange Buffer and seeded on prepared cover slips. Cells attached within 30 min at room temperature. Live cell imaging was performed on an Axio Imager M2 with ZEN software (Carl Zeiss).

Human induced pluripotent stem cell derived cardiomyocytes and lentiviral transduction

Previously described stem cell lines TC1133-CRISPRa[15] and TC1133-CRISPRa2[16] were maintained in StemMACS Brew XF on Matrigel (Corning) coated tissue culture flasks with media changes daily. Cells were passaged using Versene (Gibco) and re-seeded with ROCK inhibitor Y-27632 (Stemgent) at 5 µmol/L final concentration. When cells reached a confluency of 70%, mesoderm was induced with basal medium (RPMI 1640 + GlutaMAX, 1 mmol/L sodium pyruvate (Gibco), 200 µmol/L L-ascorbic acid, 100 U/mL penicillin and 100 µg/mL streptomycin (Gibco), 2% B27 supplement (Thermo Fisher Scientific)) supplemented with 1 µmol/L CHIR99021 (Merck Chemicals GmbH), 5 ng/mL BMP4 (Bio-Techne), 5 ng/mL FGF-2 (Peprotech), 9 ng/mL Activin-A (Bio-Techne) for three days. Cardiomyocyte differentiation was initiated with base medium supplemented with 5 µmol/L IWP4 (ReproCELL Europe Ltd.) and implemented for nine days. The cardiomyocyte population was metabolically selected for five days in RPMI 1640, no glucose, 2.2 mmol/L Na-lactate, 100 µmol/L β-mercaptoethanol (Gibco), 100 U/mL penicillin and 100 µg/mL streptomycin (Gibco). Cells were detached using StemPro Accutase

Cell Dissociation Reagent (Gibco) (30 min) and Versene (Gibco) (5 min) at room temperature and reseeded on Matrigel coated flasks in base medium supplemented with 5 µM ROCK inhibitor Y-27632 (Stemgent). Medium was changed after 24 hours to base medium and was subsequently changed every other day. Cardiomyocytes were metabolically purified again for five days as described above before proceeding to downstream applications. Lentiviral particles were harvested from $3 \cdot 10^6$ seeded HEK293T (TAKARA) in T75 flasks transfected with 1.23 µg pMD2, 2.27 µg psPAX2 (both plasmids are a kind gift from the Didier Trono laboratory), and 3.5 µg pGIPZ-based gRNA transfer plasmid mixed in 700 µl MEM (Gibco) and 14 µl Turbofect (Thermo Fisher Scientific). Media (DMEM supplemented with 10 v/v % fetal bovine serum 100 U/mL penicillin and 100 µg/mL streptomycin) was discarded 24 h post-transfection and then harvested for three subsequent days. Cells and cell debris were removed by centrifugation for 5 min at 300 xg and 4 °C. Lentiviral supernatants were stored at -80 °C before further use. $5 \cdot 10^5$ - $1 \cdot 10^6$ cardiomyocytes/well were distributed in a 12 well multi-well plate and exposed to lentiviral supernatants three days after seeding. Media was changed the next day and changed every other day subsequently. Fluorescence reporter signal (tdTomato, indicating dCas9VPR expression or TurboGFP, indicating lentiviral transduction and gRNA expression) were checked with an Axiovert 200 fluorescence microscope and AxioVision software (both Carl Zeiss).

EHM casting and culture

EHM were generated as described previously.[17] Briefly, hiPSC-cardiomyocytes were replated and re-selected for 5 days after initial differentiation and primary metabolic selection and detached with Accutase (30 min) and Versene (Gibco) (5 min) and resuspended in basal medium (RPMI, 1 mM sodium pyruvate, ascorbic acid, 100 U/mL penicillin and 100 µg/mL streptomycin, B27 supplement) supplemented with 5 µmol/L Y27632 ROCK inhibitor (Stemgent). Human foreskin fibroblasts (ATCC #SCRC-1041) were cultured in DMEM supplemented with 10 v/v % fetal calve serum (Gibco) and 1% were detached with Tryple (Gibco) and resuspended in basal medium. Cells were counted with a Neubauer chamber and combined to yield a mix of with 2x sterile RPMI (Thermo Fisher Scientific, #51800-035), Bovine Collagen Type I (Collagen Solutions LLC) and neutralized with 0.1 N NaOH, all prepared on ice. Each EHM contained $3.85 \cdot 10^5$ hiPSC-cardiomyocytes and $1.65 \cdot 10^5$ human foreskin fibroblasts. Tissues were cast into a 48 EHM multi-well plate (myriamed GmbH) and EHM medium with TGFB1 (Peprotech) was added 1 h after casting. Cells were fed daily with EHM medium (Iscove's minimal essential medium (MEM) with GlutaMAX Supplement, 1 v/v % MEM non-essential amino acids, 100 U/mL penicillin and 100 µg/mL streptomycin (all Gibco), 10 ng/mL FGF-2 (Peprotech), 5 ng/mL $VEGF_{165}$ (Peprotech), 100 ng/mL IGF-1 (Peprotech), 2 v/v % B27 minus insulin supplement (Thermo Fisher Scientific), 300 µmol/L L-ascorbic acid) and 5 ng/mL TGFB1 for the initial three days and subsequently with EHM medium for two weeks. For mechanical stress induction experiments, tissues were cultured in MEM α-based EHM medium (MEM α, GlutaMAX Supplement, no nucleosides, Gibco #32561037), 1 v/v % MEM non-essential amino acids, 100 U/mL penicillin and 100 µg/mL streptomycin (all Gibco), 10 ng/mL FGF-2 (Peprotech), 5 ng/mL $VEGF_{165}$ (Peprotech), 100 ng/mL IGF-1 (Peprotech), 2 v/v % B27 minus insulin supplement (Thermo Fisher Scientific) for two weeks before transfer to metal pole (fix) stretchers and subsequent cultivation for an additional week. Spontaneous contraction of EHM was monitored by fluorescence pole displacement measurements (myriamed GmbH).

Rheology measurements

Material properties of EHM were assessed by destructive tensile strength measurements with a RSA-G2 rheometer (TA Instruments) at 37 °C in DPBS (Gibco). Force values (F[mN]) were measured under constant linear stretch of tissues at 0.03 mm/s. Tissue dimensions were assessed with a Stereo Lumar.V12 stereomicroscope (Carl Zeiss) and cross-sectional area (CSA [mm^2]) was used to calculate stress (S[kPa]):

$S = N/CSA$

Stress-strain curves were derived by plotting the calculated stress against strain. The slope of the elastic region (=Young's modulus) of the stress-strain curve was derived by linear regression using GraphPad Prism8 (GraphPad Software, Inc.).

EHM contraction analyses in isolated organ bath apparatus

EHM contractility was determined with an isolated organ bath apparatus (IOA - 5301, Fa. Föhr Medical Instruments GmbH, Seeheim/Ober-Beerbach) under isometric contractions in Tyrode Buffer (120 mmol/L NaCl, 1 mmol/L $MgCl_2$, 0.2 mmol/L $CaCl_2$ 5.4 mmol/L KCl, 22.6 mmol/L $NaHCO_3$, 4.2 mmol/L NaH_2PO_4, 5.6 mmol/L glucose and 0.56 mmol/L L-ascorbic acid) at 37 °C and 5% CO_2 / 95 % O_2 and stretched according to Frank-Starling-Mechanism to exert maximum force at 1.8 mmol/L Ca^{2+} and electrical pacing at 1.5 Hz and 5 ms square pulses of 200 mA. Ca^{2+} response was measured by increasing concentration in 0.4 mmol/L steps and 1.5 Hz and 5 ms square pulses of 200 mA electrical pacing. Response to adrenergic stimulus was tested with 1 µmol/L isoprenaline at Ca^{2+} EC_{50} and electrical pacing at 1.5 Hz and 5 ms square pulses of 200 mA.

Histology

Tissues were fixed with 4% paraformaldehyde (ROTI Histofix, Carl Roth) for 16 h at 4 °C. Tissues were stored in 70% ethanol/DPBS and embedded in paraffin blocks. Paraffin section (4 µm thickness) were cut, rehydrated in an ethanol dilution series, and stained with Picro-Sirius Red (abcam) according to manufacturer's protocol. FITC coupled wheat germ agglutin (Sigma Aldrich) staining was performed on rehydrated paraffin sections and nuclei were counterstained with 10 µg/ml Hoechst 33342 (Thermo Fisher Scientific). Images were taken with an Axio Imager M2 with ZEN software (Carl Zeiss).

Fluorescence immunocytochemistry

Cells grown on glass cover slides were fixed with 4% paraformaldehyde (ROTI Histofix, Carl Roth) for 15 min at room temperature, washed with PBS (Gibco) and permeabilized with Permeabilization Buffer (0.2% w/v BSA (Carl Roth), 0.3% v/v Triton X-100 (AppliChem) in PBS). Cells were blocked in Blocking Buffer (5 w/v % BSA, 0.1 v/v % Triton X-100 in PBS) and probed with primary and secondary antibodies listed in table 7.3 diluted in Antibody Buffer (2 w/v % BSA, 0.1 v/v % Triton X-100 in PBS) for 16 h at 4 °C and for 2 h at room temperature, respectively. Nuclei were stained with 10 µg/ml Hoechst 33342 (Thermo Fisher Scientific) for 10 min at room temperature. Cover slips were mounted on Superfrost Plus Glass Slides (Thermo Fisher Scientific) with Fluoromount G (Thermo Fisher Scientific). Images were taken with a LSM710 confocal microscope and ZEN software (Carl Zeiss).

Flow cytometry

Cells were rinsed with PBS and centrifuged for 5 min at 300 xg at room-temperature. Nuclei were counterstained with 10 µg/ml Hoechst 33342 (Thermo Fisher Scientific) for 10 min at room temperature and cells were washed again with PBS before analyses. For ACTN2 flow cytometry, hiPSC-cardiomyocytes were fixed in ice-cold 70% ethanol, permeabilized and blocked with DPBS with 5% FCS, 1% BSA and 0.5% Triton X-100 and incubated with anti-ACTN2 (Sigma Aldrich, #A7811, dilution: 1:5,000) followed by secondary antibody incubation (Alexa Fluor 488 anti-mouse, Thermo Fisher Scientific #A-11001, dilution: 1:400). Nuclei were stained with 10 µg/ml Hoechst 33342 (Thermo Fisher Scientific) for 10 min at room temperature. Cells (10,000 events per sample) were analyzed with a BD LSR II Flow Cytometer and BD FACSDiva Software (both Becton Dickinson) or Flowing Software 2.5.1 (Turku Centre for Biotechnology, University of Turku, Finland).

Nanostring transcript analyses

Hybridization-based, parallel transcript analyses were performed with 60 ng total RNA using a NanoString nCounter platform and analyzed with nSolver 4.0 software (NanoString Technologies, Inc.). Threshold for gene expression analyses was set to >50 transcript counts across all samples. Expression was normalized to *TNNT2* expression or *TBP* expression as indicated.

Statistics

GraphPad Prism 8 and GraphPad Prism 9 (GraphPad Software, Inc.) were used for statistical analyses. Statistical significance for two-group comparisons were evaluated by unpaired students t-tests. Multiple groups comparisons were evaluated by one-way ANOVA and Bonferroni, Tukey or Dunnett's correction or two-way ANOVA with Benjamini-Krieger-Yekutieli correction with a false discovery rate of Q = 0.05 or Tukey correction. Mantel-Cox log-rank test was performed for survival curve comparisons. Data sets were checked for normal distribution of data points by Shapiro-Wilk normality test and ROUT outlier test with Q = 1% was performed. Statistical significance was assumed if $p < 0.05$ or $q < 0.05$.

Results

Guide RNA delivery for activation of *Krüppel-like factor 15* in the adult mouse heart

Delivery of gRNAs was effective for transduction of cardiomyocytes *in vivo* by systemic AAV9 application in neonatal mice for gene editing and endogenous gene activation purposes.[11,18] However, it was unclear whether this application strategy could be used effectively to transduce murine cardiomyocytes later in postnatal life, especially aiming for endogenous gene activation with CRISPR/dCas9VPR. AAV9 delivery of gRNAs by systemic injection in adult mice was tested in a pilot study with respect to *Klf15* induction in the adult heart. As a proof of concept, six-month-old Myh6-dCas9VPR mice (high dCas9VPR expressing mouse line[11]) were injected with $1 \cdot 10^{12}$ vg/mouse AAV9 encoding TRISPR *Klf15* constructs via the tail vein. Of note, dCas9VPR expression was unchanged over the entire life span and specifically expressed in cardiomyocytes without affecting cardiac function up to 16 months of age (Figure 7.1 A and B). Hearts were checked for fluorescence reporter expression two to eight weeks post-injection, which revealed homogenous delivery of AAV9 cargo based on EGFP expression, co-expressed from the gRNA expression construct, in the entire ventricular myocardium (Figure 7.1 B). *Klf15* transcript elevation was confirmed two and eight weeks post-AAV delivery by

qPCR and showed a 1.7-fold increase compared to saline injected wild-type controls after eight weeks (Figure 7.1 C). I concluded, that the chosen viral dose of $1 \cdot 10^{12}$ vg/mouse was sufficient to robustly transduce ventricular cardiomyocytes *in vivo* in an adult murine experimental setting and for activating *Klf15* levels to a physiologically relevant degree.

Figure 7.1

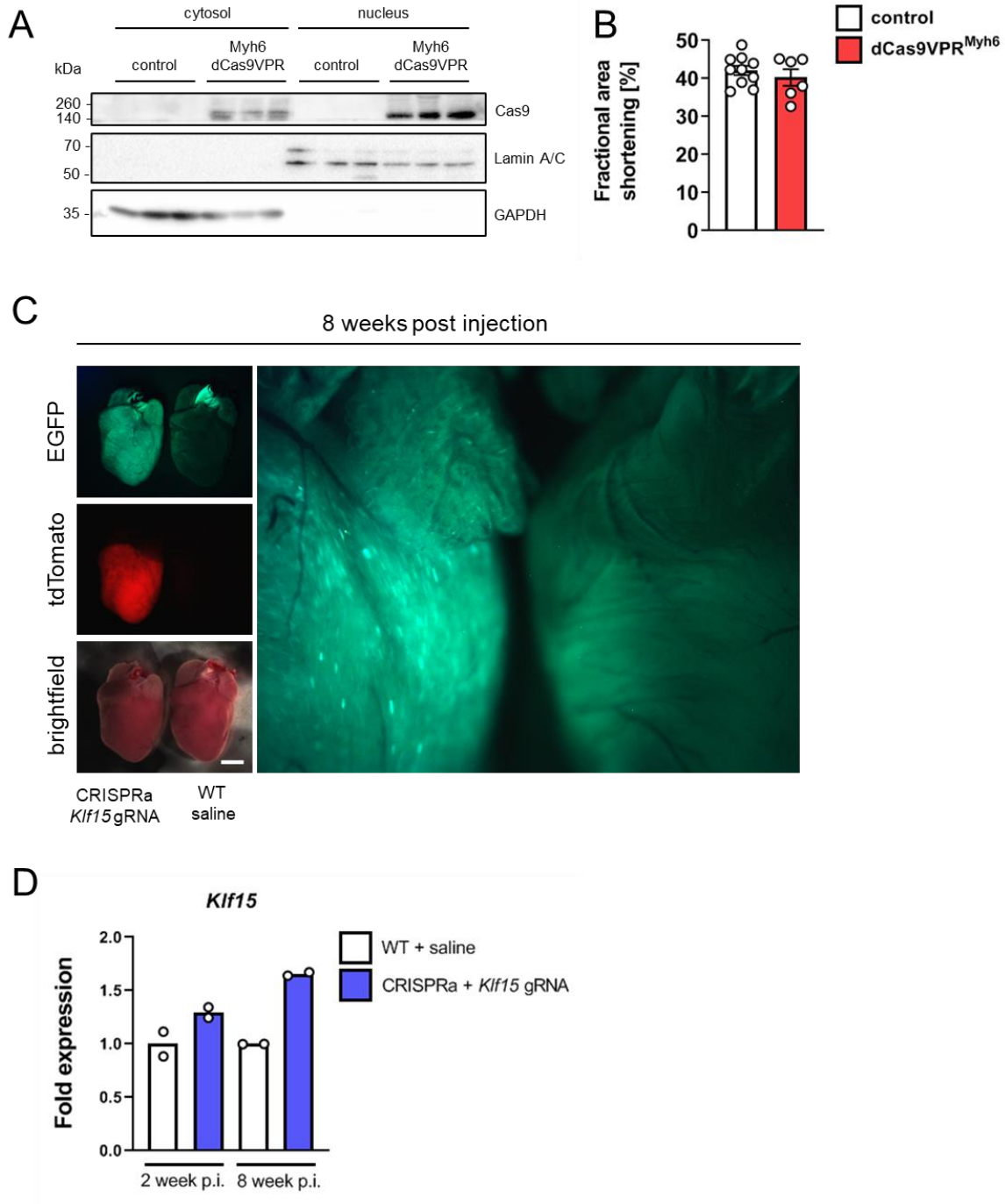

Figure 7.1. CRISPRa for transcriptional activity control in the adult mouse heart. A. Expression of dCas9VPR was confirmed in adult mice (at six to eight months of age) with an enrichment in the nuclear fraction in heart tissue as expected. Non-transgenic mice were used as controls. GAPDH (cytosol fraction) and Lamin A/C (nuclear fraction) were used as loading controls. n = 3 per group. **B.** Echocardiography of over one year old Myh6-dCas9VPR mice (high line) did not show significantly different heart function as evaluated by fractional area

shortening, indicating innocuous dCas9VPR expression in the heart. n ≥ 6 per group. Depicted is the mean ± SEM. Student's t-test was performed to test for statistical significance. **C.** Myh6-dCas9VPR (CRISPRa) mice were tail-vein injected with 1×10^{12} vg/mouse (AAV9 TRISPR *Klf15*) at six months of age. After eight weeks, gRNA delivery (*Klf15* gRNA) was confirmed by co-expressed EGFP. Non-transgenic mice (WT) injected with saline served as control. **D.** Transcriptional activation of *Klf15* was confirmed two weeks and eight weeks post injection (p.i.). n = 2 per group. Depicted is the mean.

Restoration of *KLF15* transcription prevents cardiomyocyte hypertrophy upon pressure overload

Having confirmed gRNA delivery to adult cardiomyocytes, I next aimed to restore *Klf15* expression in failing cardiomyocytes. Myh6-dCas9VPR mice (high line) were injected with AAV9 *Klf15* gRNAs (CRISPRa-*Klf15*), AAV9 non-targeted gRNAs (CRISPRa-NT) or saline and subjected to transverse aortic constriction (TAC) or sham surgery (Figure 7.2 A). AAV9 delivered gRNA construct transduction was monitored by EGFP expression while dCas9VPR expression was confirmed, represented by tdTomato expression, to be similar in sham and TAC groups. TAC CRISPRa-saline and CRISPRa-NT hearts showed increased cardiac size and dilation as expected. In contrast, TAC CRISPRa-*Klf15* hearts were less dilated. Additionally, TAC Myh6-dCas9VPR/Klf15KO mice injected with *Klf15* gRNAs showed increased cardiac dilation compared to mice with intact *Klf15* alleles (Figure 7.2 B) and served as additional controls. This was accompanied by reduced cardiomyocyte cross-sectional area indicating reduced cardiomyocyte hypertrophy as well as reduced interstitial collagen deposition overall indicating a halted cardiac remodeling response of the myocardium to pressure overload upon dCas9VPR mediated *Klf15* activation (Figure 7.2 C and D). Transcript analyses confirmed a re-normalization of *Klf15* transcript levels in TAC-CRISPRa-*Klf15* hearts, similar to physiological baseline sham-saline or sham-NT-CRISPRa expression levels (Figure 7.2 E). *Nppb* expression, a hallmark of cardiomyocyte stress, as well as *Shisa3* expression, elevated in response to *Klf15* loss[7], was overall increased in TAC groups with a tendency for lower expression in TAC hearts with restored *Klf15* expression. WNT/CTNNB1 target gene *Cd44* expression[19] was elevated in the TAC NT gRNA group and showed a tendency to be less expressed in the TAC *Klf15* gRNA group (Figure 7.2 F). *Klf15* transcriptional restoration was accompanied by increased overall survival compared to saline and NT gRNA groups. Interestingly, *Klf15* gRNA TAC Myh6-dCas9VPR/Klf15KO mice, were particularly sensitive to pressure overload (Figure 7.2 G). The halted cardiac hypertrophy upon *Klf15* restoration was additionally supported by reduced heart weight to tibia length or body weight ratios of TAC *Klf15* gRNA hearts compared to TAC NT gRNA hearts (Figure 7.2 H). Fractional area shortening decreased over the time-course of eight weeks in CRISPRa-NT TAC hearts while functional decline was reduced in CRISPRa-*Klf15* mice. Sham-surgery groups served as controls and heart function was unchanged at baseline in CRISPRa-NT, CRISPRa-*Klf15* as well as saline injected mice, indicating innocuous expression of dCas9VPR, gRNAs and AAV9 transduction in adult cardiomyocytes (Figure 7.3 A). Posterior and anterior wall thickness as assessed by echocardiography were increased in all TAC groups however, left ventricular inner diameter was significantly increased in TAC NT gRNA but unchanged in TAC *Klf15* gRNA hearts (Figure 7.3 B). Importantly, a similar induced pressure overload between groups was assessed by doppler echography confirming a comparable stress trigger among groups (Figure 7.3 C). To gain a detailed understanding of cell-type specific transcriptional programming upon *Klf15* re-activation, single cells were isolated from sham and TAC CRISPRa mice transduced with NT gRNA or *Klf15* gRNA. A high proportion of tdTomato and EGFP positive cells was confirmed indicating effective delivery and expression strategy of CRISPRa components (Figure 7.4 A). With these cells, single cell transcriptome analyses were performed. All cardiac cell types including different cardiomyocyte populations (CM1-4) were identified in these hearts. A distinct population of cardiomyocytes (CM4) characterized by expression of typical cardiomyocyte stress genes (among others *Nppa*, *Acta2* and *Myh7*) in TAC NT gRNA hearts compared to sham control was identified as diseased cardiomyocytes. This (CM4)

population was markedly reduced in TAC *Klf15* gRNA hearts which overall resembled a transcriptional profile closer to sham controls at single cell resolution (Figure 7.4 B).

Figure 7.2

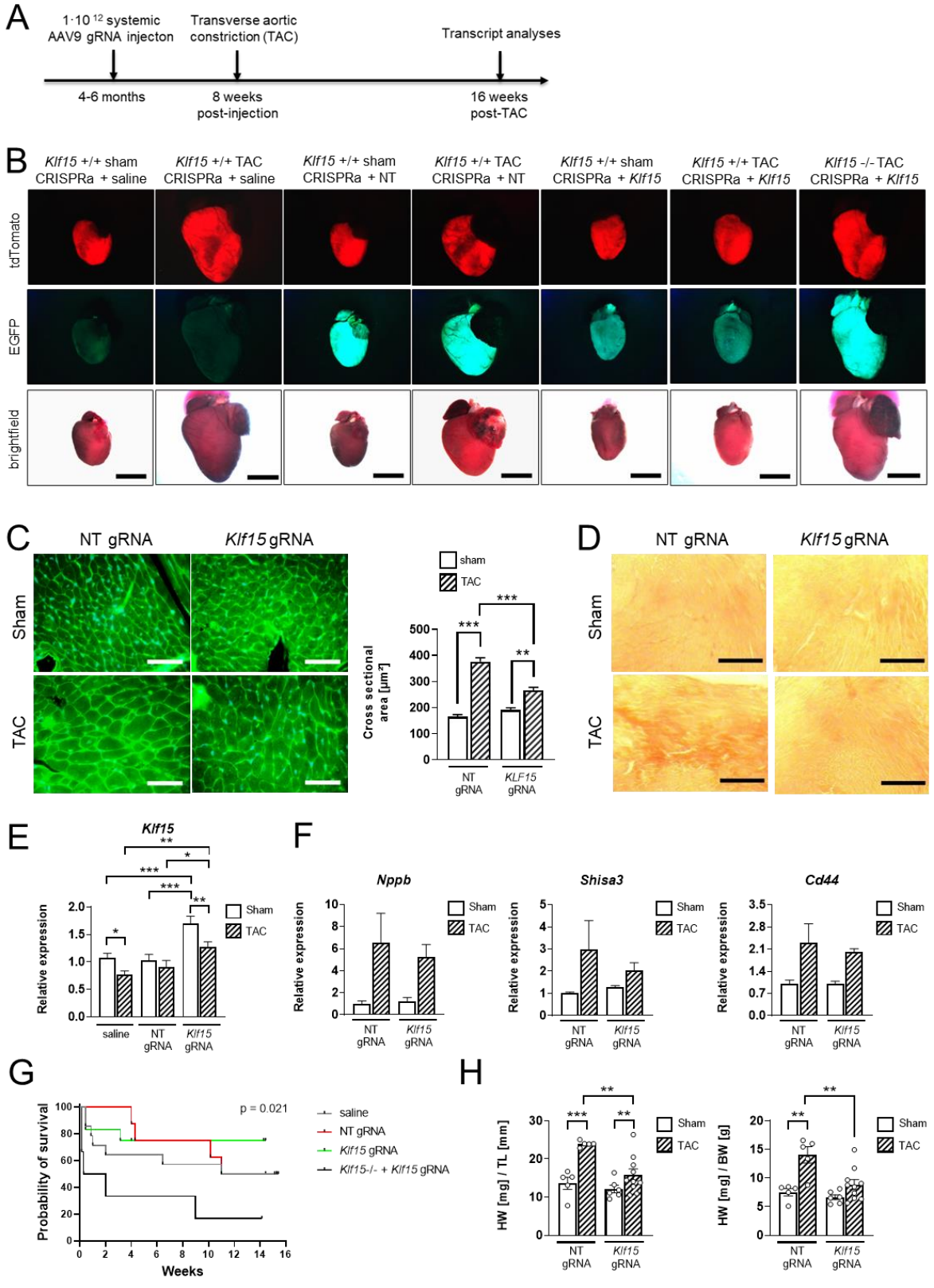

Figure 7.2. Transcriptional restoration of *Krüppel-like factor 15* in the stressed murine heart. A. Schematic overview of experimental set up. Adult mice were systemically injected with AAV9 carrying TRISPR *Klf15* or

NT gRNA constructs. TAC surgery was performed eight weeks post injection. Survival and cardiac function were assessed over 16 weeks before hearts were harvested for cellular and molecular downstream analyses. **B.** Representative whole heart live images showing robust expression of dCas9VPR (tdTomato) and AAV9 delivered gRNA expression constructs (EGFP). Sham surgery hearts were similar in size while TAC saline and NT gRNA hearts were enlarged. Notably, TAC *Klf15* gRNA hearts were less dilated. TAC *Klf15*-/- *Klf15* gRNA hearts served as control and were massively dilated. **C.** WGA-FITC membrane staining revealed reduced cardiomyocyte hypertrophy in TAC *Klf15* gRNA compared to TAC NT gRNA. $n \geq 40$ cardiomyocytes from two to three hearts per group. Depicted is the mean ± SEM. Two-way ANOVA and Tukey correction was performed to test for statistical significance. ***$p < 0.001$. **D.** Picro-Sirius Red staining of tissue sections showed reduced fibrosis in TAC *Klf15* gRNA hearts compared to TAC NT gRNA. **E.** *Klf15* expression was reduced in TAC groups however TAC *Klf15* gRNA *Klf15* mRNA levels were restored comparable to sham NT gRNA or saline. n = 7 (sham saline), n = 8 (TAC saline), n = 8 (sham NT gRNA), n = 5 (TAC NT gRNA), n = 6 (sham *Klf15* gRNA), n = 9 (TAC *Klf15* gRNA). Depicted is the mean ± SEM. Two-way ANOVA and Benjamini-Hochberg-Yekutieli . *$q < 0.05$; **$q < 0.01$; ***$q < 0.001$. **F.** Whole ventricular transcript analyses of cardiomyocyte stress marker *Nppb* as well as WNT-response targets *Shisa3* and *Cd44* were similar between groups as evaluated by qPCR. Depicted is the mean ± SEM. Two-way ANOVA and Tukey correction was performed to test for statistical significance. **G.** Increased survival was observed in TAC *Klf15* gRNA groups compared to TAC saline and TAC NT gRNA groups. Notably, *Klf15*-/- VPR+ mice injected with AAV9 *Klf15* gRNAs and subjected to TAC surgery served as control and were particularly sensitive to pressure overload stress. Statistical significance for differences between curves was tested by Mantel-Cox log-rank test. **H.** Heart weight (HW) was reduced in TAC *Klf15* gRNA compared to TAC NT gRNA normalized to tibia length (TL) or body weight (BW). n = 5 (sham NT gRNA), n = 5 (TAC NT gRNA), n = 6 (sham *Klf15* gRNA), n = 9 (TAC *Klf15* gRNA). Depicted is the mean ± SEM. Two-way ANOVA and Tukey correction was performed to test for statistical significance. **$p < 0.01$.

Figure 7.3

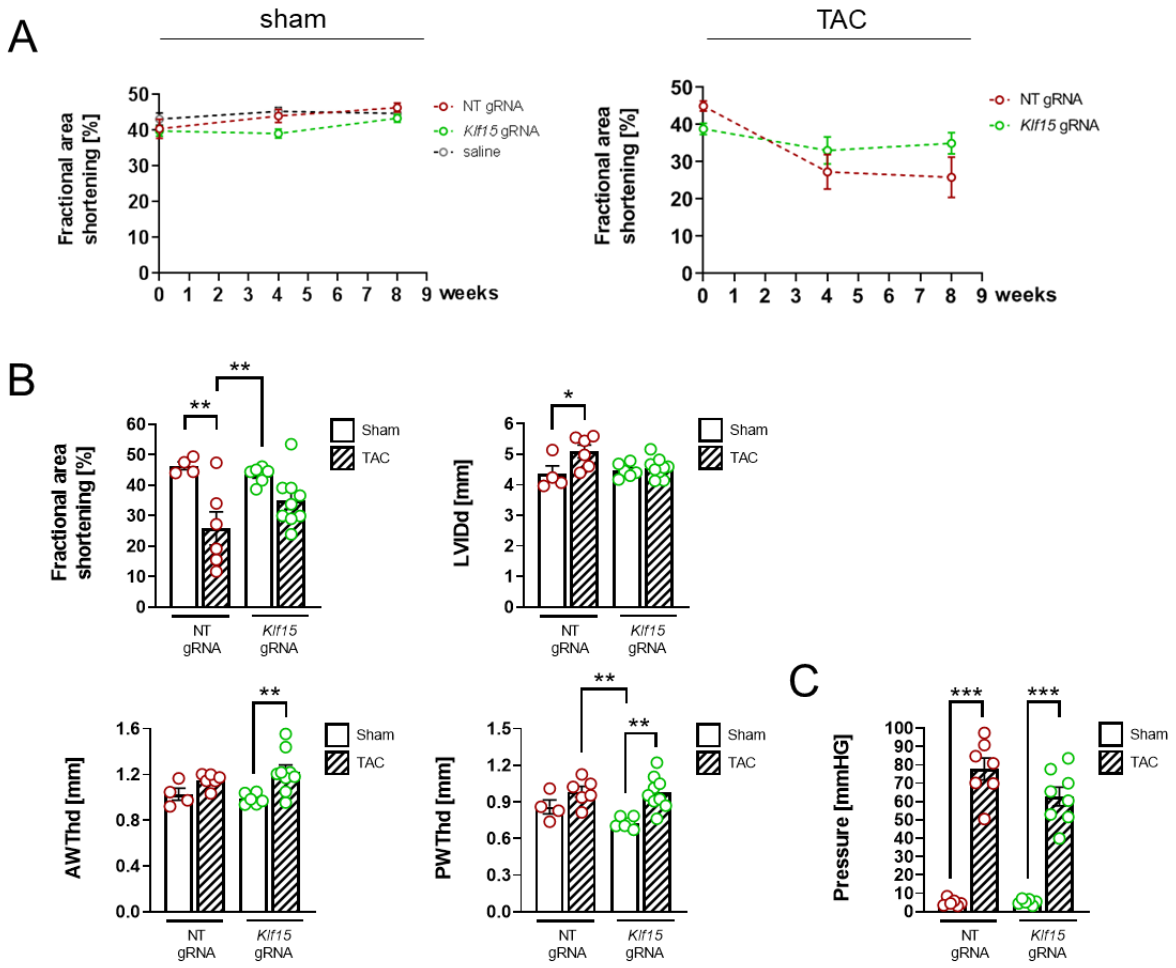

Figure 7.3. Heart function decline was reduced in *Klf15* restored animals. A. Fractional area shortening was comparable between sham *Klf15*, NT gRNA and saline groups. TAC *Klf15* gRNA showed a tendency for improved cardiac function upon pressure overload compared to TAC NT gRNA. **B.** Data from eight weeks echocardiography post-surgery showed reduced fractional area shortening, increased left ventricular inner diameter in diastole (LVIDd) in TAC NT gRNA while fractional area shortening reduction was less pronounced and LVIDd was unchanged in TAC *Klf15* gRNA compared to respective sham groups. Anterior and posterior wall thickness in diastole (AWThd and PWThd) were elevated in both TAC NT and *Klf15* gRNA groups and reached statistical significance in the TAC *Klf15* gRNA group compared to sham. n = 4 (sham NT gRNA), n = 6 (TAC NT gRNA), n = 6 (sham *Klf15* gRNA), n = 9 (TAC *Klf15* gRNA). Depicted is the mean ± SEM. Two-way ANOVA and Tukey correction were used to test for statistical significance. *p < 0.05; **p < 0.01. **C.** Gradient measurements three days post-surgery confirmed successful and comparable pressure overload induction in TAC NT and *Klf15* gRNA groups. n = 4 (sham NT gRNA), n = 6 (TAC NT gRNA), n = 4 (sham *Klf15* gRNA), n = 7 (TAC *Klf15* gRNA). Depicted is the mean ± SEM. Two-way ANOVA and Tukey correction was used to test for statistical significance. ***p < 0.001.

Figure 7.4

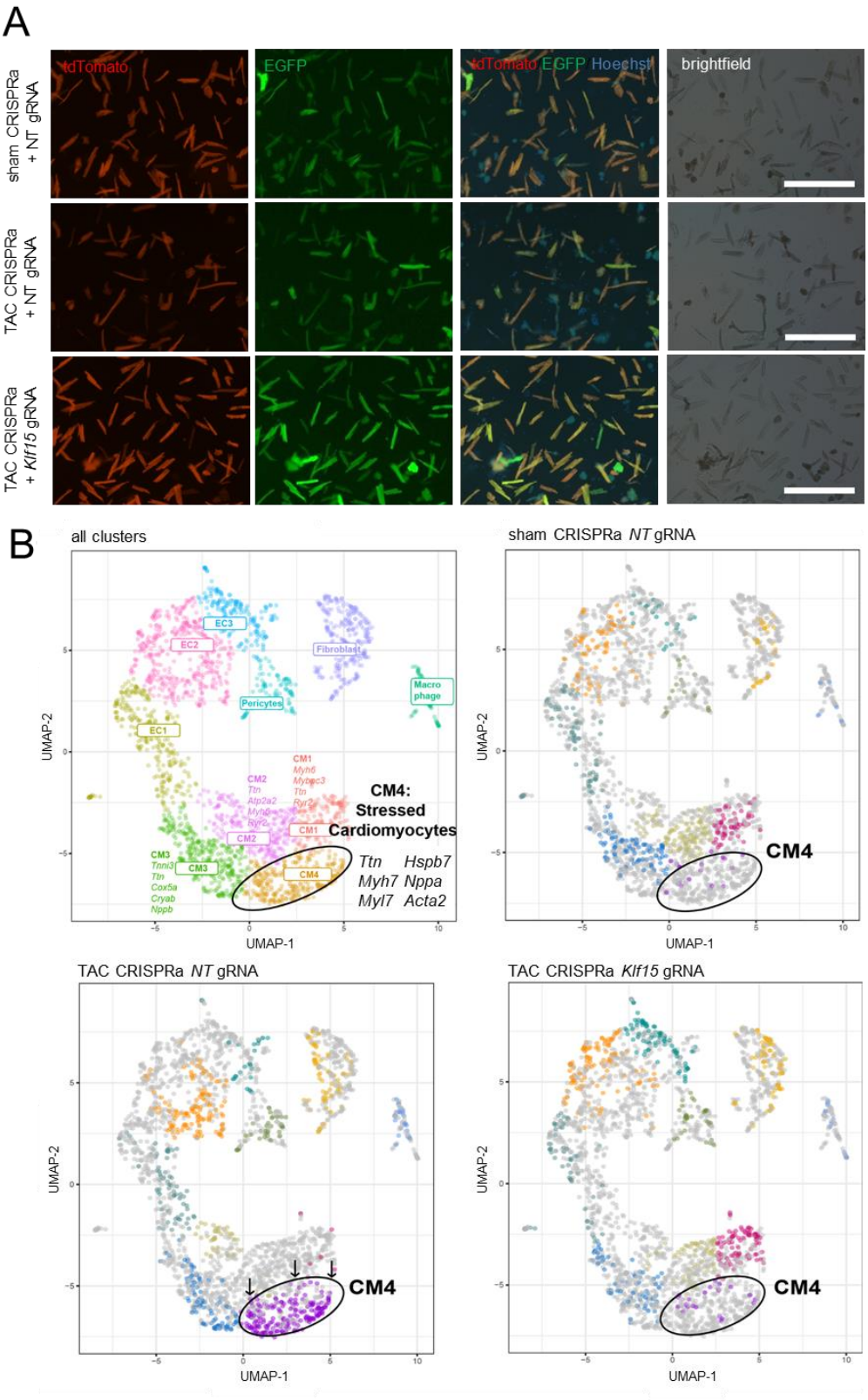

Figure 7.4. Single cell isolations from CRISPRa *Klf15* hearts. A. Representative images of sham NT gRNA, TAC NT and *Klf15* gRNA cardiomyocytes 4 weeks post-surgery. Expression of dCas9VPR (tdTomato) and gRNA constructs (EGFP) was confirmed in the vast majority of isolated rod-shaped cardiomyocytes subjected to single-cell transcriptome analyses. Scale bar = 100 µm. **B.** UMAP clustering depicting cardiomyocyte transcriptome profile similarities. Cardiomyocyte cluster 4 (CM4) represented diseased cardiomyocyte expression profile, which

was observed in TAC NT-gRNA and which was reduced in TAC *Klf15*-gRNA similar to a sham NT-gRNA heart. n = 1 (sham NT gRNA), n = 2 (TAC NT gRNA), n = 1 (TAC *Klf15* gRNA).

Endogenous gene activation in engineered human myocardium

To translate these findings into human cardiomyocytes, I aimed to generate EHM[9] comprising CRISPRa, CRISPRa2 (similar to the high line dCas9VPR mouse model) or control hiPSC-cardiomyocytes mixed with human foreskin fibroblasts embedded in a collagen matrix and cultured on flexible silicone poles, allowing spontaneous, auxotonic contractions. Guide RNAs targeted to the *KLF15* 5' upstream transcriptional start site region (Figure 7.5 A) were tested first in HEK293T cells and the most effective single gRNAs (A, D, and E) were selected for further use (Figure 7.5 B). Single gRNA (A) and multiple gRNAs (A, D, and E) were tested for endogenous gene activation in hiPSC-cardiomyocytes from two independent CRISPRa clones (CRISPRa #2 and #3). Elevated *KLF15* mRNA levels were confirmed upon single gRNA use, which was enhanced by combined triple gRNA delivery compared to isogenic control cells and NT gRNA groups (Figure 7.5 C). Importantly, similar transduction efficiencies were ensured to eliminate gRNA delivery efficiency as a potential biasing factor for gene activation (Figure 7.5 D). Cardiomyocyte purity was morphologically checked and exemplarily tested by flow cytometry confirming >90% ACTN2 positive cells from cardiomyocyte differentiations post-metabolic selection and unaffected by dCas9VPR transgene expression (Figure 7.5 E). For experiments in 3D cultures, CRISPRa and CRISPRa2 hiPSC-cardiomyocytes were transduced with lentiviral particles five to seven days before tissue casting (Figure 7.6 A), expressing *KLF15* gRNAs or NT gRNAs along with a TurboGFP reporter. Macroscopic inspection showed observable contraction of these tissues typically within seven days post-casting. Homogenous and robust expression of dCas9VPR based on tdTomato co-expressed reporter as well as gRNAs based on TurboGFP expression was confirmed over a time course of at least four weeks in all tissues generated (Figure 7.6 B and C). Transcript analyses confirmed *KLF15* activation in four-week cultured EHM compared to controls (Figure 7.6 D). Contractility of tissues was monitored by non-paced flexible pole deflection. Peak force of contraction was comparable between dCas9VPR expressing tissues, tissues expressing gRNAs (NT or *KLF15*) and non-transduced, non-transgenic tissues indicating innocuous expression of CRISPRa components and delivery of gRNAs via lentiviral particles to cardiomyocytes in line with the *in vivo* findings (Figure 7.6 E). These data suggested sustained CRISPRa activity in cardiomyocytes with concomitant long-term endogenous gene activation potential without aberrant functional effects on tissues.

Figure 7.5

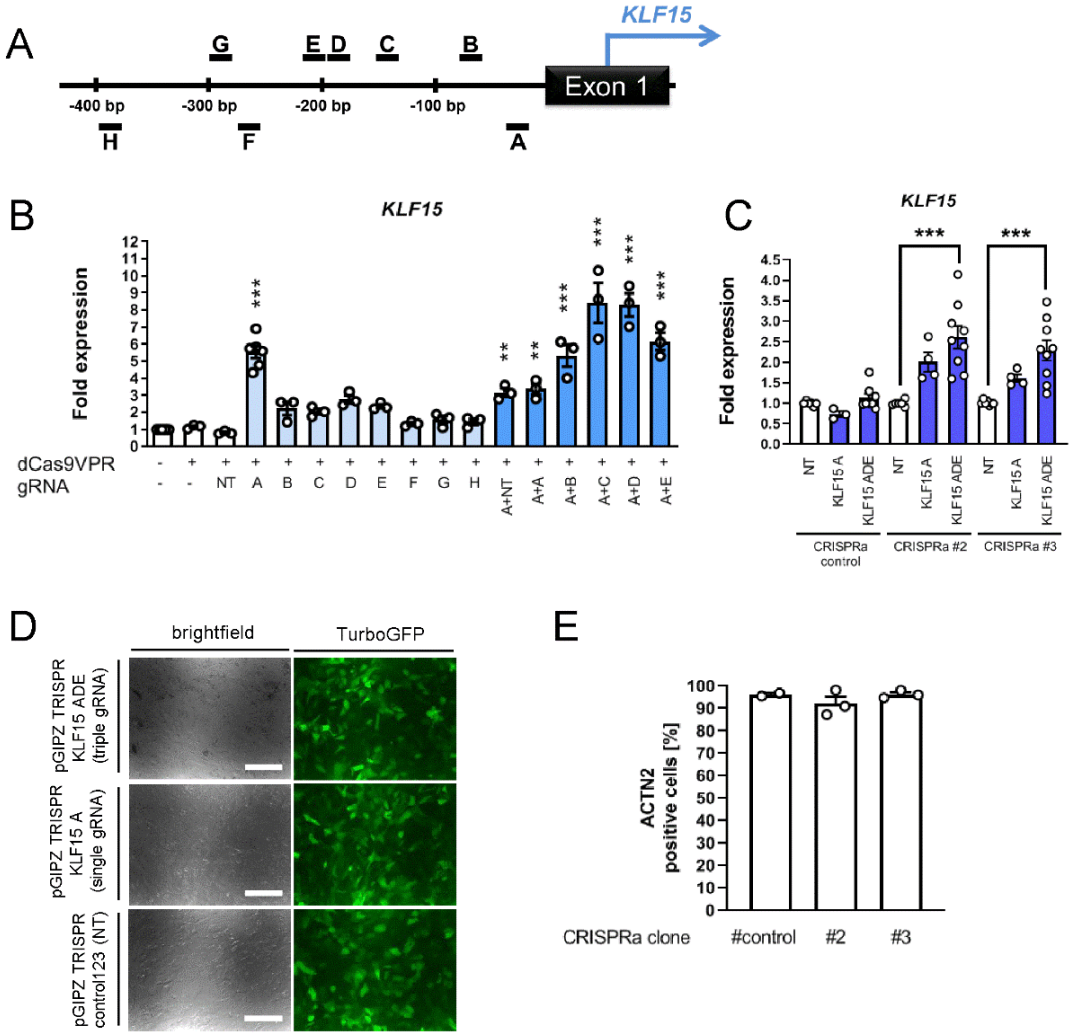

Figure 7.5. Endogenous gene activation of *Krüppel-like factor 15* in hiPSC-derived cardiomyocytes. A. Guide RNA targeting scheme with relative distances to the *KLF15* transcriptional start site. **B.** Individual gRNA testing in HEK293T cells with transient dCas9VPR and gRNA expression. Cells were harvested 48 h post-transfection for *KLF15* transcript analyses by qPCR. n = 3-6 per group. Depicted is the mean ± SEM. One-way ANOVA and Bonferroni correction. **p < 0.01; ***p < 0.001 compared to all control groups (white bars). Combination of two gRNAs overall increased gene activation potential. For downstream experiments, gRNAs A, D, and E were selected. **C.** Endogenous *KLF15* activation in hiPSC-cardiomyocytes derived from two independent CRISPRa hiPSC cell lines revealed increased *KLF15* transcript levels with single gRNA use and enhanced gene activation when three gRNAs were employed. NT gRNA transduced respective CRISPRa hiPSC-cardiomyocytes and a non-transgenic parental cell line served as controls. n = 3-9 per group. Depicted is the mean ± SEM. One-way ANOVA and Bonferroni correction. ***p < 0.001. **D.** Transduction of gRNA expression constructs was monitored by TurboGFP expression co-encoded in the lentiviral pGIPZ-TRISPR gRNA expression constructs. Representative fluorescence images confirmed similar transduction efficiencies for hiPSC-cardiomyocytes used or transcript analyses in C. **E.** Representative flow cytometry results from CRISPRa and control hiPSC indicating a high cardiomyocyte fraction with > 90% ACTN2 positive cells independent of dCas9VPR expression. n = 2-3 analyses from independent hiPSC passages and hiPSC-cardiomyocytes differentiations per group. Depicted is the mean ± SEM if applicable.

Figure 7.6

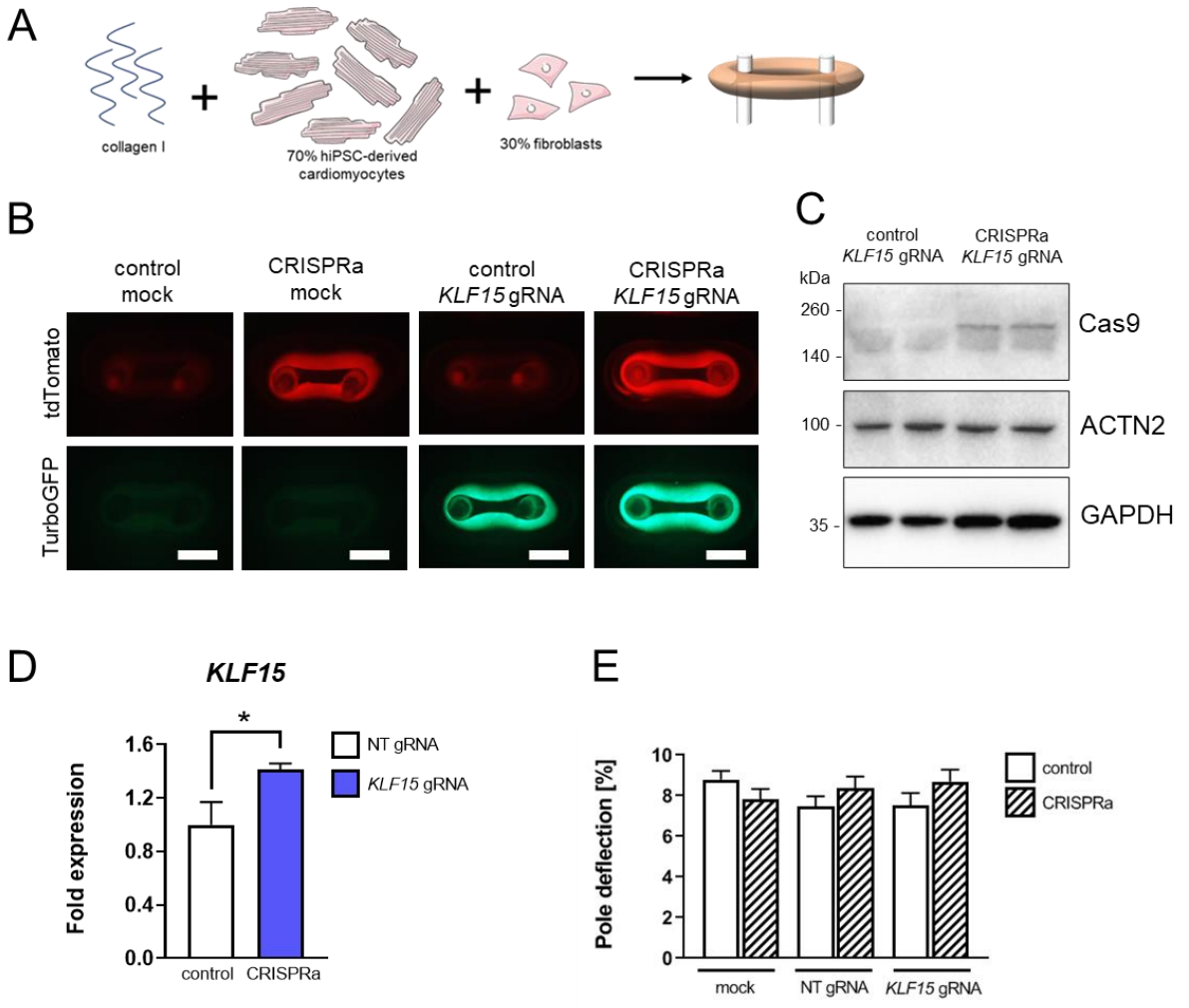

Figure 7.6. CRISPRa in engineered human myocardium. A. Hydrogel containing hiPSC-cardiomyocytes (CRISPRa or control), human foreskin fibroblasts and bovine collagen I is cast in ring shaped and cultured in 48-well multi-well plate with flexible silicone poles to allow auxotonic tissue contractions. **B.** Representative fluorescence images EHM containing CRISPRa hiPSC-cardiomyocytes (tdTomato+) and/or *KLF15* gRNA transduced hiPSC-cardiomyocytes (TurboGFP+). Images were taken 1-week post-casting and maintained robust reporter expression for the entire culture period of four weeks. Scale bar = 2 mm. **C.** Expression of dCas9VPR was confirmed in EHM four weeks after casting by immunoblotting. ACTN2 (cardiomyocyte fraction) and GAPDH (all cells) served as loading controls. **D.** Elevated *KLF15* transcript levels in CRISPRa EHM expressing *KLF15* gRNAs were confirmed. n ≥ 7 per group. **E.** Non-paced pole deflection was used to compare contractility of EHM and was not affected by dCas9VPR expression or gRNA transduction, irrespective of NT or *KLF15* gRNA delivery. n = 36-45 per group from six independent hiPSC-cardiomyocytes differentiations and three independent casting sessions. Depicted is the mean ± SEM. Student's t-test (D) or Two-way ANOVA and Tukey *post-hoc* test (E) was performed to test for statistical significance.

Restoration of *KLF15* levels in engineered human myocardium upon mechanical stress

Next, I aimed to elucidate the transcriptional loss of *KLF15* in engineered human myocardium. To mimic sustained pressure overload, tissues were transferred to non-flexible (fix) poles for forced isometric contractions over a time course of seven days (Figure 7.7 A and B). EHM cultured on flexible poles (flex), allowing auxotonic contractions, served as "healthy" controls. As a first line evaluation of

tissue stress induction by the choice of respective culture condition, EHM were subjected to rheological analyses to determine viscoelastic properties of tissues as described before.[20,21] An increased tissue stiffness as well as reduced elasticity was observed when EHM were cultured on fixed poles compared to flexible poles indicating fibrotic remodeling and stress induction (Figure 7.7 C and D). This condition was accompanied by decreased *KLF15* similar to the *in vivo* pressure overload hearts. Importantly, this transcriptional loss was abrogated in CRISPRa tissues expressing *KLF15* gRNAs, confirming the effective transcriptional restoration of *KLF15* expression by CRISPR/dCas9VPR endogenous gene activation as shown *in vivo* (Figure 7.7 E). In response to this stress condition, *ACTA2* mRNA levels, normally elevated in stressed cardiomyocytes *in vivo*, were elevated in this experimental *in vitro* stress model. However, *KLF15* re-expression reduced the *ACTA2* elevation response (Figure 7.7 F). Protein analyses revealed unchanged CTNNB1 levels and activated serin-675 phosphorylated CTNNB1 levels among all groups indicating no upstream WNT/CTNNB1 activity induction as well as unchanged TCF7L2 and BZW2 protein levels. A significant increase of ACTA2 protein levels in fix (stressed) NT gRNA (control) EHM was observed compared to flex (healthy) NT gRNA EHM but not in fix *KLF15* EHM compared to flex EHM. This is underpinning the relevance of transcriptional activation of *ACTA2* upon stress induction and the correction of its expression under halted hiPSC-cardiomyocyte remodeling response upon *KLF15* transcriptional re-activation (Figure 7.7 G). Importantly, this data was normalized to ACTN2 protein levels to take cardiomyocyte proportions in each EHM into account. Transcript analyses indicated a cardiomyocyte stress response confirming increased *ACTA2* expression, as well as a *MYH7*/*MYH6* switch, increased expression of adrenergic receptors (*ADRB1* and *ADRB2*) (Figure 7.8 A) in fix-stressed EHM. Focusing on WNT-signaling components and potential target candidates, unchanged *CTNNB1* transcript levels were found while target genes *TCF7L2* and *SOX4* showed a tendency toward increased mRNA levels in fix-stressed EHM. Expression of SHISA family members *SHISA2* and *SHISA3* were found to be increased in fix-stressed EHM in line with *in vivo* findings upon WNT-signaling activity[7] (Figure 7.8 B). Signs of cardiomyocyte remodeling were apparent by elevated mRNA levels of *PDGFA*, *NR2F2* (*COUP-TFII*) and *HEY1*. Non-myocyte activation was observed by expression of *VIM*, EMCN and *FLK1*. Interestingly, VEGFA expression was significantly increased in *KLF15* fix-stressed EHM compared to NT fix-stressed EHM while *BMP4* as well as *HEY2* expression were reduced indicating a *KLF15* mediated transcriptional control upon stress (Figure 7.8 C). The expression of selected normalizing genes (*TNNT2*, *POL2RA*, and *GAPDH*) were unchanged (Figure 7.8 D). EHM under flex and fix culture conditions appeared morphologically similar and expressed CRISPRa components robustly (Figure 7.9 A). Functionally, contractility as well as Ca^{2+} EC_{50} of fix-EHM was moderately reduced while response to adrenergic stress was similar between groups indicating early onset of sarcomere remodeling and loss as well as disturbed calcium homeostasis (Figure 7.9 B and C). Importantly, TurboGFP positive cell content (representing gRNA construct transduced cells) were similar between NT gRNA and *KLF15* gRNA groups as assessed by live cell flow cytometry with hiPSC-cardiomyocytes intended for EHM casting (Figure 7.9 D). Overall, a stress model which mimicked the *KLF15* repression in human cardiomyocytes was established along with indications of cellular dedifferentiation. Furthermore, *KLF15* transcriptional restoration was sufficient to partially abolish this cardiomyocyte stress response upon tissue stress induction.

Figure 7.7

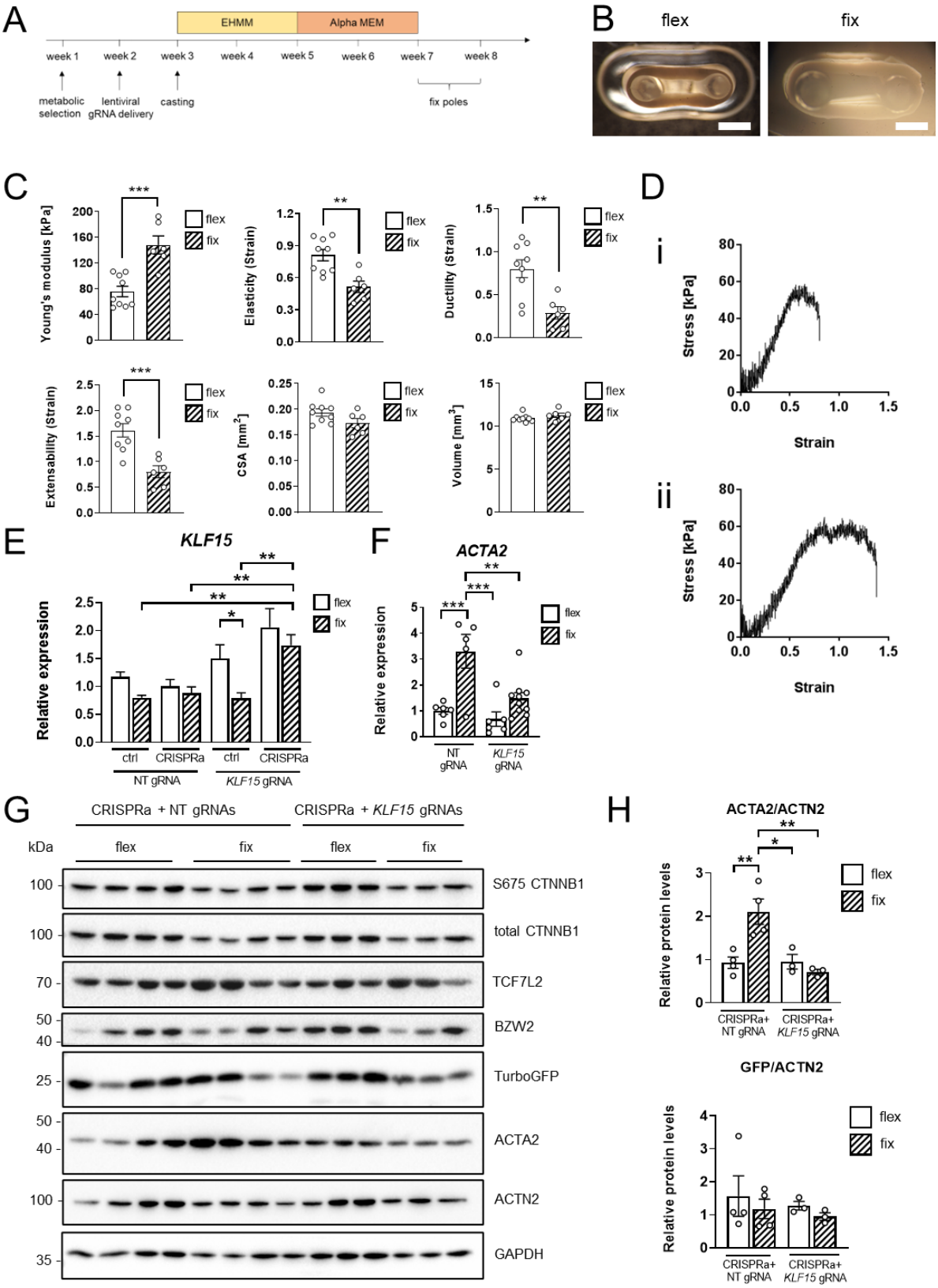

Figure 7.7. Myocardial stress modeling in engineered human myocardium. A. Experimental time course of hiPSC-cardiomyocytes transduction, tissue casting, culture and stress modeling on non-flexible (fix) poles. **B.** Representative whole-tissue images of EHM cultured on flexible silicone poles (flex) and non-flexible metal poles (fix). Scale bar = 2 mm. **C.** Rheology analyses were performed to determine tissue material property effects of

EHM cultured on fix and flex conditions. Fix-EHM showed an increased Young's modulus as well as reduced elasticity, ductility and extensibility indicating overall increased tissue stiffness and brittleness. These data suggested a fibrotic remodeling of these tissues overall validating the stress induction. **D.** Representative stress-strain curves for (i) flex-EHM and (ii) fix-EHM which were used to determine parameters in (C). n = 6-9 per group from four independent hiPSC-cardiomyocyte differentiations and two independent casting sessions and experiments. Depicted is the mean ± SEM. Student's t-test was performed for statistical analyses. **p < 0.01; ***p < 0.001. Rheology experiments were performed and analyzed by Dr. Gabriela L. Santos. **E.** *KLF15* expression was reduced in fix-EHM compared to flex-EHM but *KLF15* mRNA levels in fix *KLF15* gRNA EHM were comparable to control flex-EHM indicating transcriptional restoration by CRISPRa. n = 7-15 per group from six independent hiPSC-cardiomyocytes differentiations and three independent casting sessions and experiments. Depicted is the mean ± SEM. One-way ANOVA and Benjamini-Hochberg-Yekutieli correction was used to test for statistical significance. *q < 0.05; **q < 0.01. **F.** *ACTA2* expression was increased in fix-EHM compared to flex-EHM. Importantly, *KLF15* restoration reduced the *ACTA2* response in fix-EHM. Depicted is the mean ± SEM. Two-way ANOVA and Tukey correction were performed to check for statistical significance. **p < 0.01; ***p < 0.001. **G.** Immunoblotting indicated increased ACTA2 expression in fix-NT gRNA EHM compared to flex-NT gRNA EHM. This was abrogated in fix *KLF15* gRNA EHM. **H.** Densitometry analyses for ACTA2 and TurboGFP expression. Protein levels were normalized to ACTN2 expression representing the hiPSC-cardiomyocyte fraction. n = 3-4 per group from four independent hiPSC-cardiomyocyte differentiations and two independent casting sessions and experiments. Depicted is the mean ± SEM. Two-way ANOVA and Tukey correction. *p < 0.01; **p < 0.01.

Figure 7.8

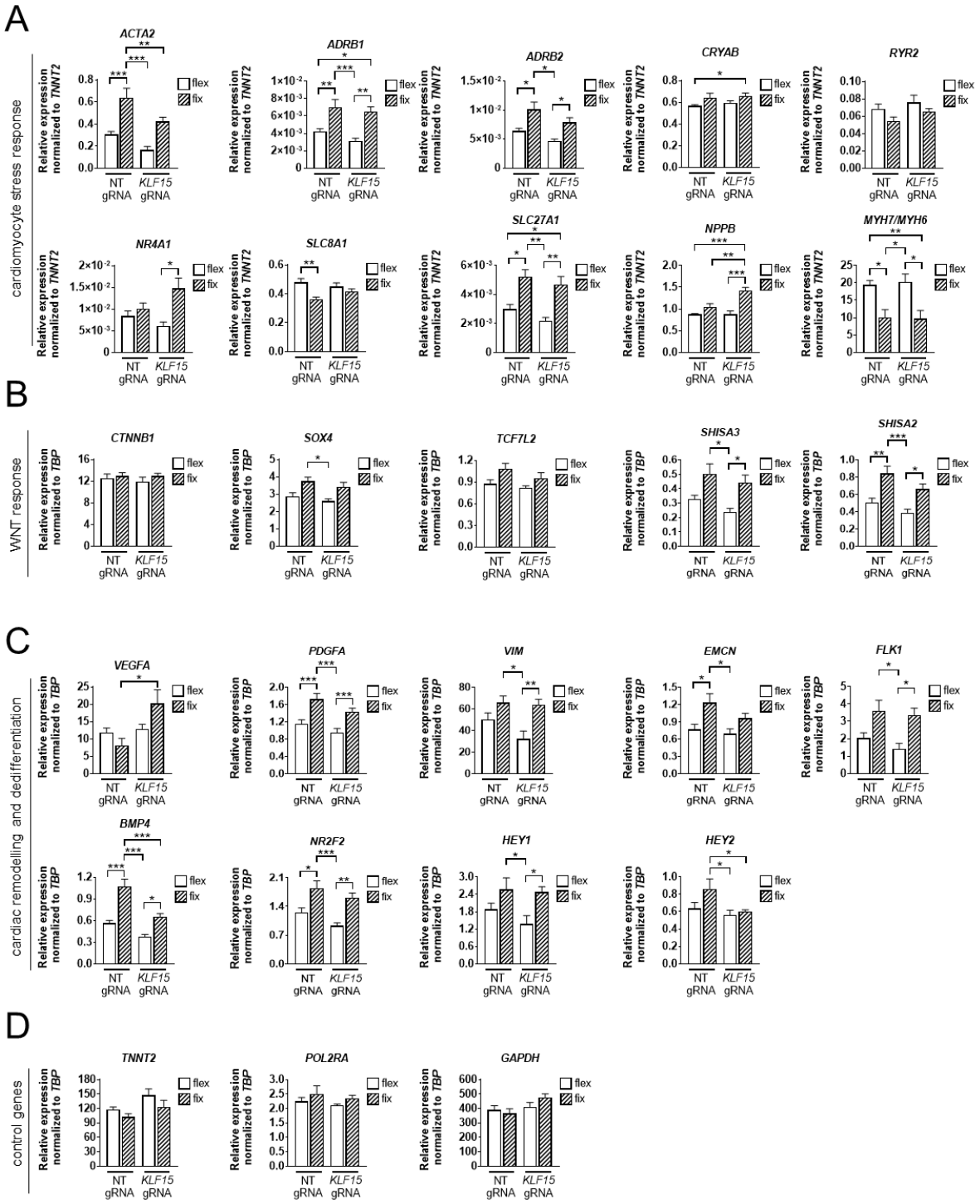

Figure 7.8. Cardiomyocyte remodeling in stressed EHM is reduced upon *KLF15* transcriptional restoration. **A.** Nanostring transcript analyses were performed to determine transcriptional changes of stressed EHM. *ACTA2* as well as expression of β-adrenergic receptors (*ADRB1* and *ADRB2*) were increased in fix EHM suggesting a dedifferentiation and stress-response upon mechanical stress. *ACTA2* expression was however reduced in fix EHM re-expressing *KLF15* compared to NT control. Transcript counts were normalized to *TNNT2* expression to account for the cardiomyocyte population exclusively. **B.** Putative WNT signaling targets *SOX4* and *TCF7L2* expression showed a tendency to increase in fix EHM while *CTNNB1* expression was unchanged. WNT-signaling regulators *SHISA2* and *SHISA3* expression were increased. **C.** Expression of *PDGFA*, *EMCN*, *FLK1*, *NR2F2* and *HEY1* were increased in fix-EHM. Expression of *BMP4* and *HEY2* were increased in NT gRNA fix-EHM but significantly lower in *KLF15* gRNA fix-EHM. **D.** Additional control genes normalized to *TBP* expression used for transcript

count normalization are depicted and were similar between groups. n = 6-9 per group from four independent hiPSC-cardiomyocyte differentiations and two independent casting sessions and experiments. Depicted is the mean ± SEM. Two-way ANOVA and Tukey correction was used to test for statistical significance. *p < 0.05; **p < 0.01; ***p < 0.001. Nanostring data were acquired by Laura Priesmeier, Institute of Pharmacology and Toxicology, University Medical Center Göttingen.

Figure 7.9

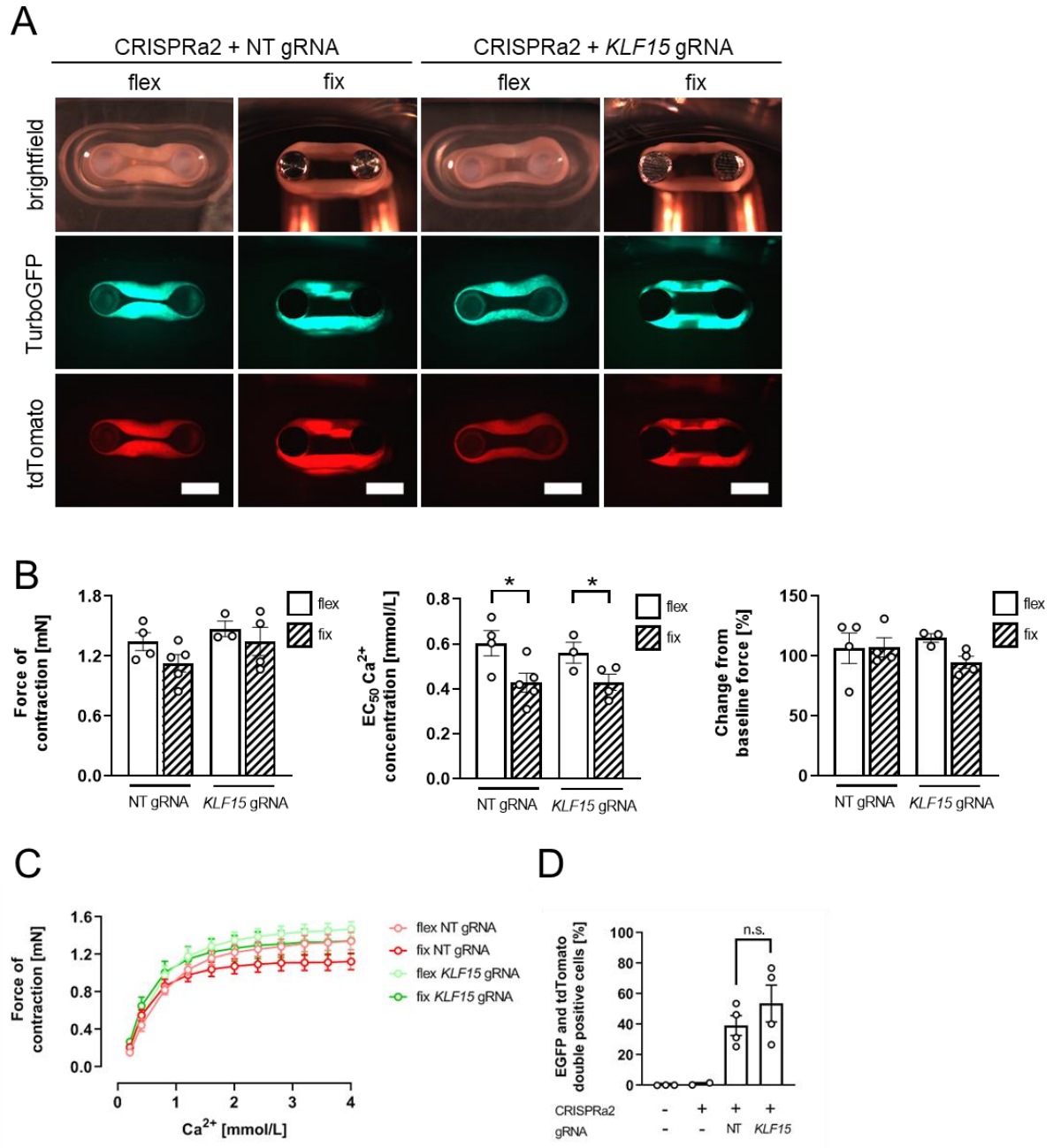

Figure 7.9. Functional assessment of stressed EHM upon putative *KLF15* restoration. A. Representative live EHM images cultured for 7 days on flexible (flex) or fixed (fix) poles to model tissue stress. CRISPRa component expression (tdTomato = dCas9VPR; TurboGFP = gRNAs) was robust over the entire experimental time course and comparable between *KLF15* and NT gRNA groups. Scale bar = 2 mm. **B.** Isolated organ bath contraction experiments were performed and showed a tendency for reduced maximum force of contraction as well as a reduced Ca^{2+} EC_{50} of fix-EHM compared to flex-EHM. Response to isoprenaline was unchanged between culture conditions. Depicted is the mean ± SEM. Statistical significance was tested with two-way ANOVA and Tukey

correction. $p < 0.05$. **C.** Force-Ca^{2+} concentration response curves showed a modest reduction of fix-EHM compared to flex-EHM while *KLF15* gRNA fix-EHM showed comparable maximum force of contraction as NT gRNA flex-EHM. n = 3-5 EHM per group from two independent tissue casting sessions and two hiPSC-cardiomyocyte differentiations. **D.** The mean number of EGFP positive cells, indicating the gRNA expressing population, used for EHM generation were between 40 - 50% and similar between NT gRNA and *KLF15* gRNA groups. n = 2-4 analyses from two independent experiments. Depicted is the mean ± SEM. Statistical significance was tested with one-way ANOVA and Tukey correction. n.s. = not significant. Organ bath contraction experiments were performed by Laura Priesmeier, Institute of Pharmacology and Toxicology, University Medical Center Göttingen.

TGFβ signaling mediates *KLF15* transcriptional repression in hiPSC-cardiomyocytes

To further elucidate on the upstream mechanism of *KLF15* repression in stressed EHM, I aimed to provoke a cardiomyocyte stress response triggered by TGFB1 signaling, which was reported to directly inhibit *KLF15* expression via a p38/MAPK mediated signaling in fibroblasts *in vitro*.[22] To test if TGFB1 affected *KLF15* expression specifically in cardiomyocytes, a TGFB1 dose-response titration with concomitant *KLF15* transcript analysis in hiPSC-cardiomyocytes was performed. ACTA2 expression was increased in hiPSC-cardiomyocytes exposed to 10 pmol/L TGFB1 (Figure 7.10 A) while TGFB1 repressed *KLF15* expression in a dose-dependent manner (Figure 7.10 B). ACTA2 co-localized with TNNT2 expressing cells, indicating cardiomyocyte dedifferentiation upon TGFB1-stimulus (Figure 7.10 C). Notably, this experiment was repeated in human foreskin fibroblasts and revealed a dose dependent *KLF15* sensitivity to TGFB1 exposure in these cells likewise, suggesting a common response to *KLF15* repression mediated via TGFB1 stimulus. ACTA2 was not expressed in human foreskin fibroblasts irrespective of TGFB1 stimulation (not detectable by immunoblotting) further validating a cardiomyocyte-specific TGFB1-mediated stress response. Increasing CTNNB1 and active phospho-S675-CTNNB1 protein levels were found upon TGFB1 exposure in human foreskin fibroblasts indicating a distinctly different TGFB1 response compared to hiPSC-cardiomyocytes (Figure 7.10 D and E). Next, I used CRISPRa2 hiPSC-cardiomyocytes to test the impact of putative *KLF15* gene activation upon TGFB1 exposure. ACTA2 protein levels increased with increasing TGFB1 concentrations as expected but were lower in *KLF15* gRNA transduced hiPSC-cardiomyocytes compared to NT gRNA transduced cells (Figure 7.11 A). In summary, this indicated a TGFβ-mediated stress reaction responsible for *KLF15* transcriptional repression and cardiomyocyte remodeling *in vitro*. This response may be halted by transcriptional restoration of *KLF15* via targeted CRISPR/dCas9VPR gene activation.

Figure 7.10

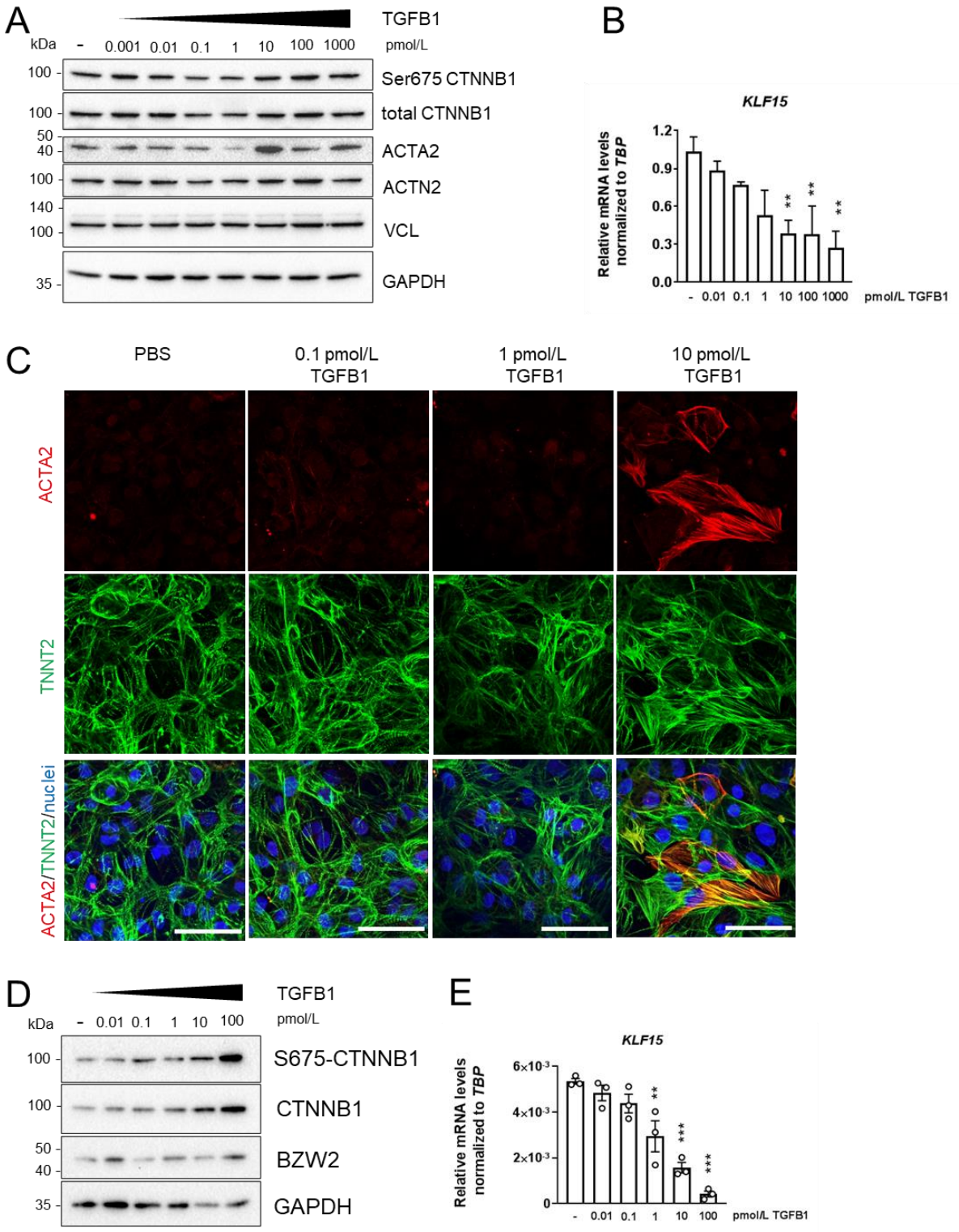

Figure 7.10. The *KLF15* transcriptional repression can be mimicked in hiPSC-cardiomyocytes with TGFB1 stimulation resulting in increased ACTA2 protein levels. A. Human induced pluripotent stem cell derived cardiomyocytes were exposed to indicated final concentrations of TGFB1 for seven days with increased ACTA2 expression at 10 pmol/L or higher. Protein levels of CTNNB1 and phosphorylated (stabilized) Ser675-CTNNB1 were unchanged. ACTN2 protein levels were similar upon TGFB1 exposure indicating unchanged cardiomyocyte content. VCL and GAPDH served as loading control. **B.** TGFB1 dependent *KLF15* repression in hiPSC-derived cardiomyocytes. **C.** Immunofluorescence staining of hiPSC-cardiomyocytes exposed to TGFB1 revealed a co-localization of TNNT2 (green) expressing cells with ACTA2 (red) expression at 10 pmol/L after seven days but

not at lower TGFB1 concentrations indicating a hiPSC-cardiomyocytes response to TGFB1 stimulation. Hoechst33342 was used to counterstain nuclei (blue). Scale bar = 50 µm. **D.** TGFB1 exposure in human foreskin fibroblasts revealed a dose dependent increase of Ser675-phosphorylated and total CTNNB1 protein levels. KLF15 and CTNNB1 interaction partner BZW2 protein levels were unchanged. **E.** *KLF15* expression was repressed in a dose dependent manner in human foreskin fibroblasts evaluated by qPCR analyses. qPCRs: n = 3-6 in (B) and n = 3 in (E). Depicted is the mean ± SEM. One-way ANOVA and Dunnett's post hoc test were used to determine statistically significant differences between treatment groups and untreated cells. **p < 0.01; ***p < 0.001. Rosa Kim, Institute of Pharmacology and Toxicology, University Medical Center Göttingen contributed to qPCR and immunofluorescence experiments.

Figure 7.11

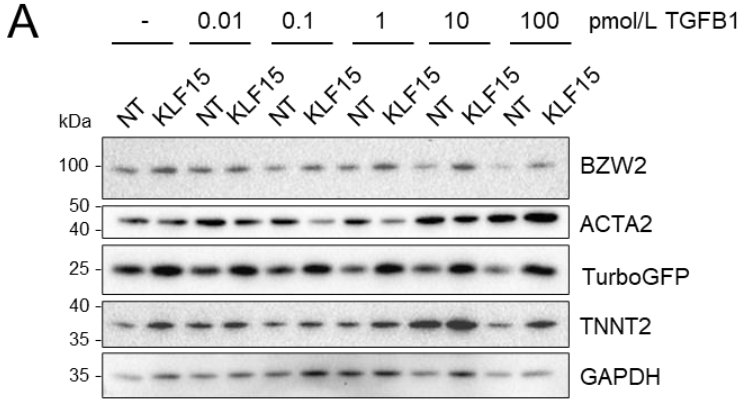

Figure 7.11. *KLF15* restoration limits ACTA2 expression upon TGFB1 stimulus in hiPSC-cardiomyocytes. A. Human induced pluripotent stem cell derived cardiomyocytes (CRISPRa2 and isogenic control) were transduced with lentiviral particles for *KLF15* gRNA delivery (KLF15) and compared to non-targeted gRNA (NT) upon TGFB1 stimuli at indicated concentrations for 7 days. ACTA2 levels were increased upon TGFB1 stimulus but lower in CRISPRa *KLF15* groups compared to NT. BZW2 protein levels appeared to decrease in high TGFB1 concentration groups (>10 pmol/L) which was not observed in *KLF15* gRNA hiPSC-cardiomyocytes. TNNT2 protein levels were similar upon TGFB1 exposure indicating unchanged cardiomyocyte content. GAPDH served as loading control.

Discussion

Cardiomyocyte hypertrophy is a hallmark of heart failure progression. An intricate interplay of molecular signaling pathways controls cardiomyocyte size and adaptation to stress signals.[23] *Krüppel-like factor 15* was described to play a regulatory role in cardiomyocyte metabolic and hypertrophic response to neurohumoral and mechanical stress.[24] I aimed to expand our insight into *KLF15* transcriptional dynamics in disease conditions. In agreement with previous studies, I observed transcriptional reduction of *KLF15* upon pressure overload[25] in mouse and human cardiomyocytes and used precision transcriptome editing tools to restore its transcriptional activity. This was accompanied by an overall improvement of cardiac function and a reduced cardiomyocyte remodeling response *in vivo* and *in vitro*. Making use of EHM as a model for human myocardium-like tissue in a dish, I additionally mimicked the transcriptional *KLF15* repression *in vitro* offering insight into human pathophysiology processes.

Previous attempts to re-express *Klf15* in the diseased rodent heart showed improved cardiac function and reduced fibrosis overall highlighting the promising potential therapeutic value of *Klf15* re-expression.[25,26] However, these studies mostly relied on transgenic mouse models. Leenders et al. used AAV9 to deliver the *Klf15* open reading frame to cardiomyocytes of an Angiotensin II induced cardiac hypertrophy murine model and observed a reduced cardiomyocyte hypertrophic response and less cardiac fibrosis[4] in line with the findings in this study. Notably, AAV9 injections were performed eight weeks prior Angiotensin II stimulation, similar to the experimental strategy in this study to ensure robust *Klf15* expression at the onset of the hypertrophic stimulus. From a therapeutic point of view, future studies should therefore clarify if *Klf15* re-expression is capable of reverting cardiac remodeling post-stress induction or if restoration of *Klf15* merely halts further disease progression.

Disease modelling with stem cell-derived cardiomyocyte models were challenged by the relative immaturity of the cells and short-term stress induction incapable of fully reflecting chronic progressive disease dynamics as well as multicellular and interorgan effects.[27] However, typical cardiomyocyte transcriptional responses upon stress were reported in embryonic and induced pluripotent stem cell derived cardiomyocytes upon adrenergic stress.[28,29] Tissue models were reported to yield increased cardiomyocyte maturity, allowing enhanced modelling of pathophysiologic states of the adult mammalian myocardium upon neurohumoral stress.[9,30,31] Furthermore, these models were harnessed for tissue damage studies by cryoinjuries.[32] Here, a forced isometric contraction model with 3D engineered human myocardium was chosen to compare findings with the pressure overload situation in mouse TAC models. Strikingly, the *KLF15* transcriptional decrease upon stress induction was comparable to previously reported loss of *KLF15* expression[7,33] and the *in vivo* data. Importantly, this system is suitable for studying cardiomyocyte biology and was therefore used in this work, as the focus was to further elucidate the *KLF15* transcriptional dynamics specifically in cardiomyocytes. However, discrepancies between organotypic transcriptional response upon stress induction in EHM compared to the *in vivo* model demand an involvement of 1.) increasing cell-composition complexity and 2.) further tissue maturation in culture. For instance, optimized culture media[34] as well as mechanical[35] and electrical cues[36] were proposed to increase tissue maturity allowing approximation to patient-relevant disease states. While the chosen *in vitro* disease model reflected an overall tissue response with increased stiffness, suggesting a fibrotic remodeling within EHM upon mechanical stress, in depth histological and molecular analyses are required to fully establish the disease model. This may be accompanied by using primary cardiac fibroblasts as shown before[20] or by iPSC-derived stromal cells[37] for refining the cellular composition of these tissues. A moderate reduction in maximum force development was observed with fix-EHM compared to flex-EHM upon *KLF15* restoration. Thus, a prolonged tissue culture period should be tested to further provoke disease progression, potentially allowing insights into human, stage-specific disease states.

Mechanistically, I found a TGFB1 mediated transcriptional loss of *KLF15* in hiPSC-cardiomyocytes and human foreskin fibroblasts. Previously, *KLF15* transcriptional repression was reported in fibroblasts mediated by p38/MAPK signalling.[22] However, I found a TGFB1 dose dependent reduction of *KLF15* mRNA levels in hiPSC-cardiomyocytes likewise, suggesting a common cellular response in cardiomyocytes and fibroblasts with concomitant transcriptional repression of *KLF15*. Interestingly, TGFB1 exposure induced *ACTA2* expression in iPSC-cardiomyocytes, which was not expressed in human foreskin fibroblasts, regardless of TGFB1 presence, suggesting a cardiomyocyte-specific response to TGFB1 signaling. ACTA2 expression in cardiomyocytes is a hallmark of immature cardiomyocytes and was described as an early response upon myocardial remodeling and cardiomyocyte hypertrophy.[38] Interestingly, restoration of *KLF15* levels in stressed tissues and in TGFB1 challenged hiPSC-cardiomyocytes reduced *ACTA2* expression, indicating a blunted response to hypertrophic stress signals. Additionally, TGFβ signaling target *BMP4* in hiPSC-cardiomyocytes[39] was increased in mechanically stressed EHM. However, the expression of *BMP4* was significantly reduced in EHM with

restored *KLF15* expression in stress condition, further corroborating the role of *KLF15* to impede disease signaling transmission. It remains to be clarified if this implies an overall reduced long-term cardiomyocyte remodeling and prevention of further disease progression. This should be investigated in prolonged culture conditions and advanced media compositions[40] as described before, allowing for pathophysiological conditions reminiscent of the adult *in vivo* myocardial milieu. Moreover, further *in vivo* analyses will corroborate the pathophysiological meaning of these findings. The contribution of distinct cell types with loss of *KLF15* transcriptional activity and their restoration with CRISPRa should be addressed in future studies and may benefit from single cell transcriptomics, which we harnessed in this study to evaluate the *in vivo* restoration of *Klf15* expression at single cell resolution. Along with this, the established protocols for single cell transcriptomics from adult murine myocardial cells are the basis for further understanding the cell-type specific implications of *Klf15* re-expression, particularly in the light of WNT/CTNNB1 regulation along with the transcriptional correction of stressed cardiomyocytes upon *Klf15* gRNA delivery. Recent observations showed that altered single cell transcriptomic profiles in the human diseased heart reversed towards a normal state with improved organ function.[41] This is motivating to develop approaches based on synthetic transcription control, targeting gene regulatory networks to correct transcriptional programs of diseased cardiomyocytes as presented in this study.

In this part of the study, I could readily restore *KLF15* expression levels in the diseased murine and human myocardium *in vivo* and *in vitro* to baseline levels, which was in part sufficient to prevent cardiomyocyte transcriptional remodeling and functional decline. These data suggested a promising opportunity for targeted *KLF15* re-normalization as a therapeutic option for heart failure treatment, specifically with nuclease-free CRISPR/Cas9 transcriptional modulation.

References (Chapter 7)

1. Brade, T., Männer, J. & Kühl, M. The role of Wnt signalling in cardiac development and tissue remodelling in the mature heart. **72**, 198–209 (2006).

2. Wang, J., Liu, S., Heallen, T. & Martin, J. F. The Hippo pathway in the heart: pivotal roles in development, disease, and regeneration. *Nature Reviews Cardiology* **15**, 672–684 (2018).

3. MacGrogan, D., Münch, J. & de la Pompa, J. L. Notch and interacting signalling pathways in cardiac development, disease, and regeneration. *Nature Reviews Cardiology* **15**, 685–704 (2018).

4. Leenders, J. J. *et al.* Repression of Cardiac Hypertrophy by KLF15: Underlying Mechanisms and Therapeutic Implications. *PLoS ONE* **7**, e36754 (2012).

5. Fisch, S. *et al.* Kruppel-like factor 15 is a regulator of cardiomyocyte hypertrophy. *Proceedings of the National Academy of Sciences of the United States of America* **104**, 7074–9 (2007).

6. Noack, C. *et al.* Krueppel-like factor 15 regulates Wnt/β-catenin transcription and controls cardiac progenitor cell fate in the postnatal heart. *EMBO Molecular Medicine* **4**, 992–1007 (2012).

7. Noack, C. *et al.* KLF15-Wnt–Dependent Cardiac Reprogramming Up-Regulates SHISA3 in the Mammalian Heart. *Journal of the American College of Cardiology* **74**, 1804–1819 (2019).

8. Noack, C., Haupt, L. P., Zimmermann, W. H., Streckfuss-Bömeke, K. & Zelarayán, L. C. Generation of a KLF15 homozygous knockout human embryonic stem cell line using paired CRISPR/Cas9n, and human cardiomyocytes derivation. *Stem Cell Research* **23**, 127–131 (2017).

9. Tiburcy, M. *et al.* Defined engineered human myocardium with advanced maturation for applications in heart failure modeling and repair. *Circulation* **135**, 1832–1847 (2017).

10. Chavez, A. *et al.* Highly efficient Cas9-mediated transcriptional programming. *Nature Methods* **12**, 326–328 (2015).

11. Schoger, E. *et al.* CRISPR-Mediated Activation of Endogenous Gene Expression in the Postnatal Heart. *Circulation Research* **126**, 6–24 (2020).

12. Schoger, E., Zimmermann, W.-H., Cyganek, L. & Zelarayán, L. C. Establishment of two homozygous CRISPR interference (CRISPRi) knock-in human induced pluripotent stem cell (hiPSC) lines for titratable endogenous gene repression. *Stem Cell Research* **55**, 102473 (2021).

13. Dobin, A. *et al.* STAR: ultrafast universal RNA-seq aligner. *Bioinformatics* **29**, 15–21 (2013).

14. Liao, Y., Smyth, G. K. & Shi, W. featureCounts: an efficient general purpose program for assigning sequence reads to genomic features. *Bioinformatics* **30**, 923–930 (2014).

15. Schoger, E., Argyriou, L., Zimmermann, W. H., Cyganek, L. & Zelarayán, L. C. Generation of homozygous CRISPRa human induced pluripotent stem cell (hiPSC) lines for sustained endogenous gene activation. *Stem Cell Research* **48**, 101944 (2020).

16. Schoger, E., Zimmermann, W.-H., Cyganek, L. & Cecilia Zelarayán, L. Establishment of a second generation homozygous CRISPRa human induced pluripotent stem cell (hiPSC) line for enhanced levels of endogenous gene activation. *Stem Cell Research* **56**, 102518 (2021).

17. Tiburcy, M., Meyer, T., Liaw, N. Y. & Zimmermann, W. H. Generation of Engineered Human Myocardium in a Multi-well Format. *STAR Protocols* **1**, 100032 (2020).

18. Carroll, K. J. *et al.* A mouse model for adult cardiac-specific gene deletion with CRISPR/Cas9. *Proceedings of the National Academy of Sciences* **113**, 201523918 (2015).

19. Foulquier, S. *et al.* WNT Signaling in Cardiac and Vascular Disease. *Pharmacological Reviews* **70**, 68–141 (2018).

20. Santos, G. L., Hartmann, S., Zimmermann, W. H., Ridley, A. & Lutz, S. Inhibition of Rho-associated kinases suppresses cardiac myofibroblast function in engineered connective and heart muscle tissues. *Journal of Molecular and Cellular Cardiology* **134**, 13–28 (2019).

21. Santos, G. L. *et al.* Fibroblast Derived Human Engineered Connective Tissue for Screening Applications. *J Vis Exp* **174** (2021).

22. Wang, B. *et al.* The Kruppel-like factor KLF15 inhibits connective tissue growth factor (CTGF) expression in cardiac fibroblasts. *Journal of Molecular and Cellular Cardiology* **45**, 193–197 (2008).

23. Heineke, J. & Molkentin, J. D. Regulation of cardiac hypertrophy by intracellular signalling pathways. *Nature Reviews Molecular Cell Biology* **7**, 589–600 (2006).

24. Pollak, N. M., Hoffman, M., Goldberg, I. J. & Drosatos, K. Krüppel-Like Factors: Crippling and Uncrippling Metabolic Pathways. *JACC: Basic to Translational Science* **3**, 132–156 (2018).

25. Zou, S. F. *et al.* KLF15 is a protective regulatory factor of heart failure induced by pressure overload. *Molecular Medicine Reports* **21**, 1336–1345 (2020).

26. Gao, L., Guo, Y., Liu, X., Shang, D. & Du, Y. KLF15 protects against isoproterenol-induced cardiac hypertrophy via regulation of cell death and inhibition of Akt/mTOR signaling. *Biochemical and Biophysical Research Communications* **487**, 22–27 (2017).

27. Ahmed, R. E., Anzai, T., Chanthra, N. & Uosaki, H. A Brief Review of Current Maturation Methods for Human Induced Pluripotent Stem Cells-Derived Cardiomyocytes. *Frontiers in Cell and Developmental Biology* **8**, 1–9 (2020).

28. Borchert, T. *et al.* Catecholamine-Dependent β-Adrenergic Signaling in a Pluripotent Stem Cell Model of Takotsubo Cardiomyopathy. *Journal of the American College of Cardiology* **70**, 975–991 (2017).

29. Földes, G. *et al.* Aberrant α-adrenergic hypertrophic response in Cardiomyocytes from human induced pluripotent cells. *Stem Cell Reports* **3**, 905–914 (2014).

30. Tiburcy, M. & Zimmermann, W. H. Modeling myocardial growth and hypertrophy in engineered heart muscle. *Trends in Cardiovascular Medicine* **24**, 7–13 (2014).

31. Tiburcy, M. *et al.* Terminal differentiation, advanced organotypic maturation, and modeling of hypertrophic growth in engineered heart tissue. *Circulation Research* **109**, 1105–1114 (2011).

32. del Campo, C. V. *et al.* Regenerative potential of epicardium-derived extracellular vesicles mediated by conserved miRNA transfer. *Cardiovascular Research* **44**, (2021).

33. Haldar, S. M. *et al.* Klf15 Deficiency Is a Molecular Link Between Heart Failure and Aortic Aneurysm Formation. *Science Translational Medicine* **2**, 26ra26-26ra26 (2010).

34. Batho, C. A. P., Mills, R. J. & Hudson, J. E. Metabolic Regulation of Human Pluripotent Stem Cell-Derived Cardiomyocyte Maturation. *Current Cardiology Reports* **22**, (2020).

35. Bliley, J. M. *et al.* Dynamic loading of human engineered heart tissue enhances contractile function and drives a desmosome-linked disease phenotype. *Science Translational Medicine* **13**, eabd1817 (2021).

36. Ronaldson-Bouchard, K. *et al.* Engineering of human cardiac muscle electromechanically matured to an adult-like phenotype. *Nature Protocols* **14**, 2781–2817 (2019).

37. Iyer, D. *et al.* Robust derivation of epicardium and its differentiated smooth muscle cell progeny from human pluripotent stem cells. *Development* **143**, 904 (2015).

38. Kern, S., Feng, H. Z., Wei, H., Cala, S. & Jin, J. P. Up-regulation of alpha-smooth muscle actin in cardiomyocytes from non-hypertrophic and non-failing transgenic mouse hearts expressing N-terminal truncated cardiac troponin I. *FEBS Open Bio* **4**, 11–17 (2014).

39. Churko, J. M. *et al.* Defining human cardiac transcription factor hierarchies using integrated single-cell heterogeneity analysis. *Nature Communications* **9**, (2018).

40. Knight, W. E. *et al.* Maturation of Pluripotent Stem Cell-Derived Cardiomyocytes Enables Modeling of Human Hypertrophic Cardiomyopathy. *Stem Cell Reports* **16**, 519–533 (2021).

41. Wang, L. *et al.* Single-cell reconstruction of the adult human heart during heart failure and recovery reveals the cellular landscape underlying cardiac function. *Nature Cell Biology* **22**, 108–119 (2020).

12. General Discussion

Despite major advances to define treatment options for heart failure management[1], therapeutic concepts causatively preventing disease progression are not yet optimal. The advent of precision genome and transcriptome editing offered new possibilities to dissect gene programs and functions in basic cardiovascular research, including gene activity modulation. However, the concept of targeted endogenous transcriptional modulation, allowing tailoring of gene-specific activity in postnatal cardiomyocytes, was not available at the onset of this work. The present studies shed light on the fundamental biology of diseased cardiomyocytes as well as contributed to the cardiovascular research field with different models for endogenous gene activation. This included a mouse model that allows for transcriptional activation in *Myh6* expressing cells *in vivo* as well as human induced pluripotent stem cell lines, which were used in this work to modulate gene expression in derived cardiomyocytes but can be employed for other cell types and research areas as well. These models were established with the main purpose of controlling endogenous gene activity of *Krüppel-like factor 15* in mouse and human cardiomyocytes, which was characterized as a part of a multiprotein complex controlling the evolutionary conserved nuclear WNT/CTNNB1 activity. Consequently, modulation of *KLF15* during disease was tested as a therapeutic proof-of-concept using the established models within this work.

5.1 Transcriptional modulation by CRISPR gene activation in the heart *in vivo*

Efficient *in vivo* transcription regulation mediated by CRISPRa systems was demonstrated in the brain, liver, kidney, and skeletal muscle[2–4], however a model for the heart was missing. Within this study, a transgenic mouse model expressing enzymatically inactive Cas9 fused to transcriptional activators was designed with the aim to gain full control over endogenous gene activity in cardiomyocytes *in vivo*. The utility of this model was validated with systemically delivered gRNAs targeted to the 5' upstream region of genes of interest by viral vectors for transcriptional activation, specifically in the postnatal heart. Effective *in vivo* CRISPR components expression and delivery was achieved in earlier reports of efficient CRISPR/Cas9 applications for gene editing purposes in the postnatal mouse heart along with delivery of gRNAs into cardiomyocytes via AAV9. Carroll et al. and Johansen et al. generated mouse models for cardiomyocyte-specific, enzymatically active Cas9 expressing mice for gene editing in the postnatal heart with single and dual gRNA delivery in neonatal postnatal day four in mice. Cas9 expression driven by *Myh6* promoter control was robust and homogenous based on both, tdTomato and EGFP, reporter fluorescence indicating expression of dCas9VPR and gRNA expression vectors, respectively. This was sufficient to induce cardiomyopathy phenotypes by insertion/deletion mutations (indels) in the *Myh6* open reading frame.[5,6] Guo et al. delivered Cas9 and gRNAs by AAV9 systemically in newborn mice (postnatal day 0) and observed up to 80% cardiomyocytes expressing both components.[7] This was in line with systemic gRNA delivery by AAV9 for CRISPR-based gene activation in this study, where I observed up to 71.11±5.46% cardiomyocyte viral transduction efficiency eight weeks post-AAV injection, when AAV9 were injected at postnatal day four. Importantly, this transduction efficiency resulted in robust expression of CRISPR components with concomitant transcriptional as well as protein translation enhancement of the targeted *Mef2d* locus. This was sufficient to reproduce a cardiomyopathy phenotype induced by increased *Mef2d* steady state protein levels, which was however phenotypically less pronounced when compared to standard transgenic mice overexpressing *Mef2d*. Kim et al. reported a gene dose dependent cardiomyopathy severity with a correlation of *MEF2D* expression levels with both, cardiac function as well as molecular signatures of myocardial stress and fibrosis.[8] CRISPRa mediated *Mef2d* activation was comparable to the hypertrophic phenotype generally observed in MEF2 factor overexpressing murine models with cardiomyocyte hypertrophy, increased fibrosis and progressive loss of myocardial function.[9] In this

study, I additionally investigated the titratability of endogenous gene activation by making use of distinct dCas9VPR expression levels *in vitro* and *in vivo* as well as by using single and multiple gRNAs. Enhanced endogenous gene activation potential corresponded to the dCas9VPR expression, namely high expressing dCas9VPR hearts (high line) allowed for increased transcriptional activation as compared to low expressing hearts (low line). The use of multiple gRNAs targeted to the same gene yielded enhanced gene activation when compared to single gRNA use, in line with previous reports.[10] These data indicated the potential of the model to test gene dose dependency at different levels using the same mouse model. Importantly, classical overexpression of *Mef2d* by transient cDNA transfection resulted in aberrant localization in the cytosol, which was prevented by titrating expression levels using CRISPRa-mediated endogenous gene activation.[11] This highlights the demand for an imperative understanding of the physiological/dynamic range of gene expression and its function.

In terms of gene activation, several *in vitro* and *in vivo* studies reported effectiveness of endogenous gene expression induction across species, cell types and individual genes. The first *in vivo* study employing *Drosophila melanogaster* as a model organism induced *wnt* expression resulting in wing disc abnormalities consequently suggesting gene activation to functionally relevant levels.[12] The pursue for tissue-specific gene activation approaches by engineered transcription factor systems led to the successful adaptation of the concept in eukaryotes for liver, brain, kidney, and muscle cells.[13] For instance, murine hepatocytes were targeted for endogenous gene activation demonstrated by mice expressing the SunTag system along with hemodynamic gRNA delivery.[14] Making use of first generation CRISPR activation using dCas9VP64 to normalize a *Sim1* haploinsufficiency causing obesity was sufficient to rescue the phenotype. Induction of *Sim1* expression was achieved in transgenic mice expressing *Streptococcus pyogenes* dCas9VP64 ubiquitously and via AAV-mediated injection of *Staphylococcus aureus* dCas9VP64 together with gRNAs targeting the *Sim1* or *Mc4r* promoter or enhancer region in the target tissue. This resulted in normalization of *Sim1* and *Mc4r* transcript levels and phenotypic reversal of *Sim1* and *Mc4r* haploinsufficiencies, respectively. Interestingly, the authors used ubiquitously expressed dCas9VP64, however *Sim1* activation was exclusively observed in the hypothalamus and was sufficient for phenotype correction, indicating a context-specific susceptibility for endogenous gene activation.[15] Multiplexed gene activation in neurons *in vivo* was achieved by AAV mediated target tissue-specific injection[16] and was applied to rescue an epilepsy phenotype by *Kcna1* or *Scn1a* activation.[4,17] Liao et al. employed a SAM based CRISPR activation mouse model and demonstrated restoration of skeletal muscle function by activation of *Utrn* (*Utrophin*) in a model for Duchenne muscular dystrophy, activation of *Kl* (*Klotho*) in a kidney injury model and by activating *Pdx1* to reprogram hepatocytes into insulin producing cells resulting in reduced hyperglycemia in a streptozotocin-induced diabetes model.[2] Additionally, a kidney-specific epigenetic modifier with dCas9TET3 fusion proteins to induce gene activity was shown by Xu et al.[18] These studies highlighted the applicability of CRISPR-based gene activation in *in vivo* settings to model pathophysiological processes and to rescue disease phenotypes with unprecedented precision. They also demonstrated first proof-of-concept applications for CRISPR gene activation modulation based therapeutical approaches.

For endogenous gene activation in the murine heart, I aimed for cell type-specific expression of dCas9VPR together with AAV9 mediated gRNA delivery. This combination guaranteed cardiomyocyte-restricted gene activation despite transducibility of skeletal muscle, kidney, and liver cells by AAV9[19] with potential gene activation in these off-target tissues. The expression of dCas9VPR in cardiomyocytes did not reveal any adverse phenotypic consequences in terms of cardiac function and gene expression signature based on echocardiography and genome-wide transcriptome data, respectively.[11] By tackling the *KLF15* repression in heart failure progression in this study, I could add a transcriptional restoration approach specifically for cardiomyocytes to the list of amenable cell-types and targets using an endogenous gene modulation strategy *in vivo*. This targeting approach was accompanied by a re-normalization of cardiomyocyte transcriptional profiles at single cell resolution as

well as with functional improvement and overall increased survival upon sustained pressure overload, highlighting the robustness of the approach.

Most of the discussed studies used AAV-based gRNA delivery as a standard tool for *in vivo* nucleotide delivery. This is ideal for clinical translation as gene therapy strategies emerged due to a low cancerogenic potential and long-term expressional stability by episomal expression in host cells.[20,21] Using the same delivery strategy in this study, I observed long term expression of the fluorescence EGFP reporter, co-expressed with gRNAs, delivered by AAV9 as reported before in non-dividing cells such as cardiomyocytes and neurons.[22,23] This robust expression was accompanied with long-term gene activation for at least eight weeks post-delivery as tested for *Mef2d* activation, suggesting constitutive expression of gRNAs from AAV vectors in target cells without endogenous silencing of the expression cassette. Effectiveness of AAV9 mediated gene delivery is however challenged due to limited packaging capacity (~ 4.7 kbp)[24], pre-immunization against AAV particles[25] and high virus titers necessary for postnatal *in vivo* use in larger organisms.[26] Alternative delivery strategies are in focus of current efforts such as lipid nanoparticles (LNP), which will have to meet several requirements to prove applicability including target cell type specificity as well as effective cargo delivery to the nucleus of target cells. The first clinical application with CRISPR/Cas9 gene editing for the treatment of Transthyretin amyloidosis made use of mRNA encoding Cas9 and a single gRNA delivered via LNP.[27] The delivery of ribonucleotides, proteins and small molecules either via intramyocardial injections or systemic application for cargo delivery in infarcted hearts was described before and harbors the potential for viral-free CRISPR/Cas9 delivery for therapeutic purposes.[28] A considerable difference between gene editing and transcriptional editing is the requirement for Cas9 to be constantly present in the nucleus of target cells. While for gene editing purposes, a single cut event may suffice to correct a mutation with lifelong benefits,[29] dCas9 effectors need to be readily available to constitutively modulate gene expression. This may constitute a hurdle when mRNA based Cas9 delivery is considered. Hence, vector-based approaches are attractive alternatives to guarantee episomal and long-term cargo expression. Smaller Cas9-protein family members are currently under investigation for potential use in all-in-one gene/transcriptome editing AAV vectors for clinical use. *Neisseria meningitidis* Cas9 (NmeCas9)[30], *Staphylococcus aureus* Cas9 (SaCas9)[31], *Staphylococcus auricularis* Cas9 (SauriCas9)[32] and *Staphylococcus lugdunensis* SlugCas9[33] are considerably smaller than the widely used *Streptococcus pyogenes Cas9* (SpyCas9) with the potential for single-Cas9-gRNA vector applications allowing dense packaging of Cas9, gRNA and target cell type-specific promoters. Initial steps towards compact Cas9 variants used as synthetic transcription factors were taken, however these concepts lack tissue-specificity and *in vivo* testing to date.[34]

The delivery of foreign nucleotides via viral vectors inherently poses risks for pre-existing immunity as well as innate and adaptive immune system responses.[35,36] The microbial derived Cas9 proteins may harbor an immunogenic potential with anti-Cas9 antibodies detectable in human serum.[37] Reports about Cas9 and AAV mediated humoral responses are reported[38] and preformed Cas9 antibodies triggered a T-cell response with concomitant cytotoxicity and diminished gene editing efficiencies.[25] Altogether, these findings may compromise direct translation of viral vector transduced CRISPR-based therapeutics. Transient immunomodulation may therefore be considered for clinically relevant and therapeutic CRISPR/Cas9 applications and deserve further evaluation in late preclinical studies.[39]

5.2 Specificity of CRISPR-based transcriptional modulation

In this work the specificity of CRISPRa was assessed by genome-wide chromatin immunoprecipitation of dCas9VPR with murine heart tissue *in vivo* as well as gRNA dependent and independent DNA-association was investigated. This analysis revealed limited unspecific dCas9VPR associated off-target activation in both gRNA-dependent conditions and when gRNAs were absent. Although, dCas9 was found bound to several genomic regions, it did not result in unspecific gene activation. On-target association of dCas9VPR was observed in both cases, at the promoter region of *Mef2d* and *Klf15*, respectively, with several 10-folds higher chromatin enrichment compared to background signal. The 3D structure of the genome adds another layer of complexity to the identification of potential off-target sites especially considering shared promoter and co-regulatory regions, which cannot exclude the possibility that potential off-target sites may in fact be co-regulatory regions. For instance, secondary target gene induction was investigated in earlier studies in the context of potential off-target activity with dCas9VPR, which were reported to be low.[12] CRISPR off-target validation was approached with enzymatically inactive Cas9 employing DNA-dCas9 association studies.[40,41] While genome wide off-target editing events are a major concern for gene editing applications[42], high specificity of dCas9-DNA association and limited off-target binding events were shown *in vitro*[41] in line with the results of this work *in vivo*.[11] CRISPR/Cas9 approaches for gene activity regulation rely on the permanent presence of dCas9-gRNA complexes to recruit the transcriptional machinery. In this work, a narrow window of 100 base pairs upstream of the TSS was identified for effective transcriptional modulation of most mouse and human genes tested. This outlines a self-limiting feature of the system, which reduces the probability of unintended gene activation regulation, but also making accurate target site selection imperative. This is in line with previous attempts to identify effective target windows for CRISPRa-mediated probing of gene regulatory regions.[43] Furthermore, I observed a dCas9VPR expression level dependency with respect to gene induction potential. This suggested that dCas9VPR affinity and kinetics determine efficiency and therefore safety of endogenous gene activation approaches. This implies that accurate gRNA design and off-target predictions are a pre-requisite for the safe use of CRISPR-based applications. This was addressed and implemented in these studies by *in silico* mismatch-based off-target predictions in the process of gRNA selection for endogenous gene activation of multiple individual mouse and human target sites. Overall, this allowed me to benchmark protocols for faithful gRNA design and validation specifically for CRISPR/dCas9VPR mediated gene activation studies.

Tissue-specific and temporal control over Cas9 activity in general is an actively debated topic in the field of genome editing.[44] CRISPR/Cas9 off-switches are of major interest to gain precise control over Cas9 activity.[45] Inducible-Cas9 variants were proposed to gain spatiotemporal control over Cas9 activity.[46] Anti-CRISPR systems were first discovered as an evasion mechanism of bacteriophages to counteract CRISPR/Cas9 immunity of bacteria and were proposed as a tool to limit Cas9 activity in both gene editing and transcriptional modulation approaches.[47] For gene expression modulation purposes, anti-CRISPR peptides mediating Cas9 - DNA binding or Cas9 - crRNA interaction prevention, such as AcrII3C, AcrIIA2 or AcrII2C, may be suitable for improved Cas9 activity control.[48] These advances offer an ideal platform for further development of safer CRISPR/dCas9-based approaches, ultimately aiming for clinical translation.

5.3 Efficiency of transcriptional modulation

CRISPR gene activation approaches relied on the recruitment of dCas9 fusion proteins to the TSS of genes of interest. I observed distance dependent activation potency peaking at -100 bp from the 5' TSS of tested gRNAs for mouse and human genes. In prokaryotes, the effective target sites for endogenous gene activation were empirically determined to be -100 to -60 bp upstream of the TSS[49] and studies in

mammalian cells found an optimal gRNA target window for CRISPR gene activation upstream of the TSS between -400 bp to -50 bp.[43] The consistency of target windows described in these studies across species suggested a physical proximity of dCas9 synthetic transcription factors to intended target genes to be necessary for successful gene activation. A systematic approach to decipher general rules for gRNA targeting was available by Horlbeck et al. using machine learning algorithms to generate genome wide CRISPRa (and CRISPRi) gRNA libraries. Top influencing factors for efficient gRNA design for transcriptional modulation included the distance from the TSS under consideration of nucleosome positioning.[50,51] Further detailed analyses of the genome wide nucleosome distribution of target cells are therefore necessary to define general rules for gene activation/repression targeting windows particularly in mammalian cells. Implementation of single cell Assay for Transposase Accessible Chromatin (ATAC) sequencing data sets for target cells[52] are therefore a valuable resource in future studies to further define effective dCas9VPR target sites. Aside from promoter region targeting, enhancer targeting by CRISPRa was successfully harnessed.[53] However, the limited information about putative enhancer features makes this application challenging. Additionally, the activation of long non-coding RNAs (lncRNA) was demonstrated, however this requires further insight into lncRNA expression control, which were so far not defined to a systematic extent.[54] In this study, I used enzymatically inactive Cas9 fused to VPR, a strong transcriptional activation system.[55] A major advantage of dCas9VPR was its relatively low complexity consisting of a dCas9 protein fused to transcriptional activation domains with a dCas9:transactivator ratio of 1:1 and the use of a classical gRNA design in contrast to the SunTag system, relying on extensive antibody chains, and the SAM approaches, using modified gRNAs, while maintaining comparable gene activation robustness[56] and was therefore selected in this work. It is worth mentioning, that the design of dCas9VPR based tools was compatible with modified gRNAs used with the SAM approach to further enhance transcriptional activation if desired. The Cas9 variant independence of the SAM system was demonstrated *in vivo* using enzymatically active Cas9 before.[2] In this work, I used single or multiple gRNAs to target dCas9VPR to their respective target sites, making use of Type 3 Pol III promoter sequences (U6, H1 and 7SK) to transcribe gRNAs as described before for gene editing purposes *in vivo* across mammalian species.[39,57] Synergistic effects were reported for gene activation and inhibition approaches upon combined gRNA application, which were confirmed testing combinations of gRNAs in four independent cell lines (C2C12 mouse myoblasts, 10T1/2 mouse fibroblasts, Neuro2a mouse glioblastoma cells and HEK293T human embryonic kidney cells) as well as in hiPSC-cardiomyocytes.[58] The delivery of multiple gRNAs per cell became a focus of CRISPR/Cas9 approaches for simultaneous multiplexed gene editing or gene expression regulation. Initial concerns of transcriptional activation potency drop upon multiplexing could not be confirmed[56] and were not observed in this work either. This may be explained by the overall abundance of ribonucleoprotein (RNP) complexes expressed in relation to targeted alleles per cell when single or few loci are targeted. The expansion of gRNA expression cassettes for simultaneous targeting of multiple genes of interest is currently compromised by packaging size limitations intended for viral delivery strategies especially when individual gRNA expression cassettes are used. Strategies for tandem encoded gRNAs, which make the repetition of promoter sequences obsolete, are therefore under development, but remain to be adapted for mammalian CRISPR-based applications.[59]

Furthermore, the present studies contributed transgenic human cell lines to effectively use CRISPR-based gene modulation *in vitro*. CRISPRa and CRISPRi hiPSC lines which harbor the potential for endogenous gene activity control in a variety of hiPSC-derived cell types were generated and validated. The expression of enzymatically inactive Cas9 effector fusion proteins did not affect pluripotency of hiPSC in line with previous observations.[60] The versatility of similar hiPSC-derived tools was demonstrated by using CRISPRa-mediated *Amyloid-beta precursor protein* (*APP*) overexpression to model early onset Alzheimer's disease like pathology in trisomy 21.[61] Additionally, cellular reprogramming of fibroblasts to pluripotent cells[62] and conversion of fibroblasts to neurons[63] as well as

to cardiomyocytes[64] was demonstrated indicating functionally relevant levels of gene program induction to (re-)determine cell fates *in vitro*.[65]

The developed CRISPRa[66,67] and CRISPRi[68] hiPSC cell lines in this study are based on integration of dCas9VPR or dCas9KRAB at the *AAVS1* site on human chromosome 19, which was identified as a locus for AAV genome integration and extensively used for transgene integration especially in hiPSC cell lines. Described as a so called "safe harbor locus", this strategy gained popularity despite encoding for the protein phosphatase 1 regulatory subunit 12C (*PPP1R12C*) which expression was abolished by targeted integration at this site.[69] To this end, no consensus on truly safe innocuous integration of transgenes in host genomes was agreed upon.[70] Within this study, no evidence was found for unwanted effects by the homozygous loss of *PPP1R12C* and simultaneous integration of dCas9 effectors with respect to 1.) hiPSC pluripotency and potential for derivation of cells from all three germ layers, 2.) derivation of spontaneously beating cardiomyocytes as well as functional assessment of derived EHM. This was in agreement with previously generated cell lines when transgenes were expressed from the *AAVS1* locus.[71,72] However, caution needs to be taken, when signaling pathways involving the *PPP1R12C* gene product are investiagted.[73] The use of the ubiquitous CAG promoter within these cell lines to drive dCas9VPR or dCas9KRAB expression, respectively, renders these cell lines as valuable tools for a broad range of applications for gene activity control in hiPSC-derived cell types and systems, which are not limited to cardiovascular research. However, potential transgenic cell line-specific behavioral deviation from isogenic controls, as used as control groups in this work, should be monitored in future studies, considering transgene integration site and dCas9 expression especially when so far uncharacterized derived cell types are investigated.

5.4 The role of *Krüppel-like factor 15* in heart failure

Efficiency and safety of endogenous gene modulation by CRISPR/dCas9 synthetic transcription factors were reviewed offering a precision tool to govern endogenous transcriptional activity for a variety of applications.[74] Within the scope of my work, I aimed to use this tool to readily restore the expression of a pathophysiologically lost transcription factor. An exquisite example for testing this concept was the transcriptional re-activation of *Krüppel-like factor 15* in heart failure progression. *KLF15* was expressed in cardiomyocytes and fibroblasts in the adult heart and was known to be transcriptionally repressed in heart failure.[75] The loss of *KLF15* expression in diseased hearts was ranging between 20% to 60% reduction of transcript levels depending of the experimental model.[76,77] *KLF15* repressed CTGF expression in cardiac fibroblasts overall exerting an anti-fibrotic role and its expression was diminished upon TGFB1 treatment.[78] Similarly, I observed *KLF15* transcriptional loss in hiPSC-cardiomyocytes *in vitro* upon TGFB1 stimulus, which was accompanied by cardiomyocyte dedifferentiation demonstrated by fetal gene re-expression as well as in mechanically stressed EHM accompanied by fibrotic remodeling. *KLF15* restoration partially reduced this transcriptomic switch, indicating the specific role of *KLF15* in human cardiomyocytes upon stress and demonstrating its relevance in pathological conditions.

To further highlight the relevance of *KLF15* in human cardiac disease, a recent study identified a family carrying heterozygous mutations in the *KLF15* open reading frame associated with atrial and ventricular arrythmias and hypertrophic cardiomyopathy phenotype.[79] This suggested a key regulatory function of *KLF15* for cardiomyocyte hypertrophy development in human pathophysiology. Mechanistically, *KLF15* was downstream linked to mTOR/AKT signaling as well as suppression of cardiac hypertrophy signaling by SRF family proteins including MRTF-A, MRTF-B as well as MEF2 family members, GATA4 and MYOCD overall exerting cell growth inhibiting processes.[75,80,81] Consistent with the observations that *Klf15* was regulated in cardiac disease progression, I observed reduced levels of *Klf15*

in dCas9VPR pressure overload challenged mice compared to sham controls, while this transcriptional loss was abolished in CRISPRa *Klf15* gRNAs expressing hearts upon stress. This was in line with previous results by Zou et al. who used a transgenic mouse model for cardiomyocyte-specific *Klf15* overexpression and observed a reduced functional decline as well as reduced interstitial fibrosis upon aortic banding.[82] However, posttranscriptional regulation of *Klf15* expression levels mediated by miRNA candidates were reported[83–85] and need to be considered, when effective expression restoration is intended. *Klf15* expression was controlled by miR-137-3p upon ischemia reperfusion[83] as well as by miR-133 regulating *Glut4* mediated glucose uptake in cardiomyocytes.[84] Moreover, *KLF15* was also linked to the regulation of lipid metabolism control in cardiomyocytes[86], altogether suggesting a central function in controlling the myocardial energy supply. This is in agreement with *KLF15*'s known dynamic gene expression in a circadian rhythm-controlled and feeding and fasting-controlled manner in the heart.[86,87] These studies suggested a significant posttranscriptional fine-tuning as well as highly dynamic nature of *KLF15* levels in the normal and diseased heart. *Klf15* was previously linked to regulate WNT/CTNNB1 activity specifically in the heart. Mechanistically, KLF15 interaction with CTNNB1, TCF7L2 and NLK, all part of the nuclear WNT/CTNNB1 complex, was shown.[88] Genetic deletion of *KLF15* resulted in a hypertrophic cardiomyopathy with cardiac-specific de-repression of the WNT/CTNNB1 pathway suggesting a tissue-specific role of *KLF15* to repress WNT/CTNNB1 signalling.[76] Further interactions of *KLF15* activity with the canonical WNT pathway were demonstrated by co-operative transcriptional regulation of *LRP5* by *KLF15* and *SP1*.[89] Taking these described functions into account, *Klf15* levels were rescued in a cardiomyocyte-specific manner in this study by targeted CRISPR-based gene activation with the goal to re-repress aberrantly active WNT/CTNNB1 signaling in the failing heart. These findings highlight the dynamic role of *KLF15* as a central integrator within the complex network of signaling pathways to control cardiomyocyte metabolism and growth. Full control over *KLF15* activity may therefore be an attractive target for therapeutic interventions upon cardiac remodeling. *KLF15* modulation by CRISPR/dCas9VPR demonstrated transcriptional control of *KLF15* within the dynamic range of physiological and pathophysiological conditions and is therefore an adequate tool to steer *KLF15* activity.

5.5 Re-establishment of *KLF15* and the nuclear WNT/CTNNB1 protein complex

The re-establishment of transcriptionally lost transcription factors upon cardiac remodeling requires an in-depth understanding of the regulatory processes within a given multiprotein complex to modulate gene program activity with high precision and effectiveness. KLF15 showed strong repressive actions on WNT signaling in heart muscle[88] but neither CTNNB1 nor KLF15 are cardiomyocyte-specific factors. Therefore, further cell-specific interaction partners were investigated to elucidate the nuclear WNT/CTNNB1 responsive complex in cardiomyocytes.[90] In this context, BZW2 was identified as an interaction partner of KLF15 and CTNNB1.[91] A myocyte enriched abundance conserved among species rendered it a potential candidate for tissue-specific co-regulation of the WNT/CTNNB1 pathway. Expression of BZW2 was reported in neuronal tissue, somites, limbs and hearts in rodent embryos[91] while expression of BZW2 was enriched in muscle tissue, including the heart, in the adult organism.[92] However, its role in muscle tissue was not investigated before. Tissues under tumor-pathological conditions were associated with increased BZW2, and its homologue BZW1 protein levels.[93] Moreover, we confirmed the potential of heterodimerization of BZW2 and BZW1 *in vitro*. Mechanistically, a role of BZW2 was reported in modulating mTOR/AKT and ERK/MAPK signalling[94] suggesting a broad role in the complex network of cellular signaling cascades possibly in part via its role in protein translation regulation.[95] The functional characterization, potentially in frame of WNT/CTNNB1 signaling, remains to be determined, especially in cardiomyocytes. In this work, a late onset cardiomyopathy phenotype manifested in a global *BZW2* knockout mouse model indicating a role as a

cardiac homeostasis maintaining factor. It is tempting to speculate that BZW2 may serve as a scaffold to recruit KLF15 and CTNNB1 to exert local integration and transmission of a variety of cascade signals. The multifaceted roles of the WNT/CTNNB1 pathway were shown to mediate a downstream time- and context-dependent transcriptional modulation.[96] TCF7L2 occupancy differences in postnatal heart development and pathological remodeling were reported before and indeed hinted towards a gene regulatory framework controlling WNT signaling output in a larger context of cell growth and metabolism control.[97] The multiprotein containing *WNT enhanceosome* controls WNT downstream transcriptional activity in the nucleus[98,99] and potentially shapes the WNT/CTNNB1 related transcriptional landscape in a tissue-specific manner, which may be entangled with the identified CTNNB1/KLF15/BZW2 complex. Interestingly, intracellular CTNNB1 mislocalization by loss of EMD resulted in increased WNT-downstream target gene expression, suggesting a WNT-ligand independent mode of action and downstream mechanisms limiting CTNNB1 signaling activity in homeostatic cardiomyocytes.[100,101] A potential regulation of CTNNB1 dependent but WNT independent activity was reported before, underscoring the relevance of non-linear signaling and potential cross-talk with other pathways especially, but not exclusively, in the heart.[102] Several inhibitors of WNT/CTNNB1 signaling were known and anti-hypertrophic effects upon myocardial stress were demonstrated. For instance, PORCN inhibitors were capable to inhibit WNT ligand maturation and therefore prevented aberrant WNT/CTNNB1 signaling upon myocardial infarction.[103] However, these endogenous and exogenous inhibitors of the pathway lacked tissue and cell type specificity, therefore tempering their therapeutic value.

Having established the tools necessary to interfere with gene expression in a titratable and physiologically meaningful manner, complex signaling pathway crosstalk and co-mediated effects can now be elucidated. The unique and plausible possibility to use these systems for multiplexed gene activation or repression allows us to understand genetic programs in health and disease uncaging our view of cellular behavior away from linear isolated gene and signaling cascade effects. As BZW2 was involved in a variety of cellular signal cascades[94], it appears appealing to broaden our view to understand intercommunication of signaling pathways and cooperative total output. Focusing on WNT/CTNNB1 as a central, well described signaling cascade controlling cardiac homeostasis, interactions with other pathways, cooperatively fine-tuning gene expression profiles, are under investigation. Interaction points of YAP/TAZ signaling with the TGFβ/BMP as well as WNT/CTNNB1 were identified.[104] The results of this work indeed hinted towards a complex regulatory network of factors, which was provoked by TGFB1 mediated *KLF15* transcriptional loss in hiPSC-cardiomyocytes resulting in a *BMP4* expression increase and a reduced *VEGFA* expression. The restoration of *KLF15* conversely inhibited the *BMP4* expressional response which resulted in increased *VEGFA* expression. Importantly, *BMP4* was described as a regulator of *VEGFA* expression in the cardiovascular system[105] and in heart development.[106] This should be further elucidated to clarify cause and effect as well as to decipher signaling hierarchies and potential pathway crosstalk in health and disease conditions. These interactions of evolutionary conserved signaling cascades may underlie transient regulation within the cardiac remodeling process and deserve further detailed analysis in a time-dependent as well as disease model-dependent manner. This can be tackled now by employing targeted multiplexed CRISPR/dCas9VPR gene modulation with the tools established and defined in this work. Overall, this will lead to an improved understanding of intracellular molecular networks and target identification for precision therapeutics development.

Conclusions

In this work, I demonstrated the feasibility of CRISPR-based approaches for gene activity modulation in murine and human cardiomyocytes. As a proof-of-concept, I triggered a hypertrophic cardiomyopathy in the adult mouse heart by *Mef2d* activation and restored *Klf15* transcription in stressed cardiomyocytes in the failing mouse heart. I translated the model into hiPSC and hiPSC-derived cardiomyocytes as well as in a surrogate 3D model of human myocardium to investigate the titratability of the gene activation approach. I also contributed to defining the optimal target site within the 5' TSS region for endogenous gene activation purposes. Based on these results, I aimed to re-establish the WNT/CTNNB1 protein complex, necessary for normal cardiac tissue homeostasis. Having established effective gRNAs for both, mouse *Klf15* and human *KLF15*, I achieved transcriptional control over *KLF15* as one of the complex components and identified the interaction interface with BZW2 as a molecular, cell-specific interaction partner. These findings allow to validate novel therapeutic targets with emphasis on normalization of transcriptional activity in diseased hearts to reprogram cardiomyocytes into a homeostatic state with the potential to prevent heart failure progression. The established mouse model and cell lines are currently used world-wide to elucidate a variety of aspects in cardiovascular basic research and beyond. Overall, this work contributed to the advancement of knowledge and feasibility for a novel generation of therapeutics in heart failure treatment. Perspectively, the combination of powerful single cell transcriptomics and the bioinformatic assessment to elucidate regulatory networks along with the here established concept of CRISPR-based synthetic control of transcription will allow the steering of gene expression profiles in specific subpopulations of the diseased heart in order to detour a cell towards a physiological state and prevent organ deterioration in a multifactorial, disease and patient-specific manner (Discussion figure 1).

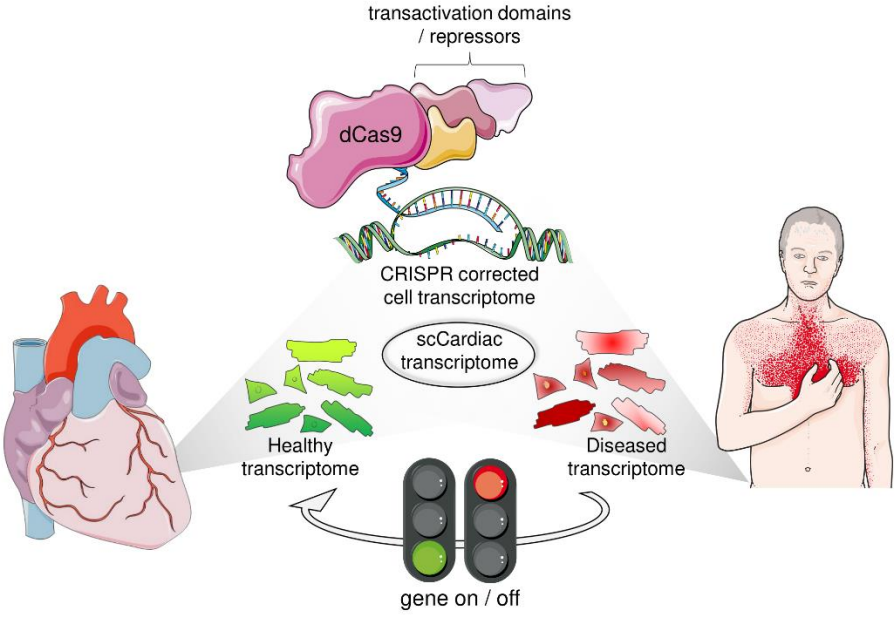

Discussion figure 1: Perspective for single cell transcriptomics and cell type-specific transcriptome editing with CRISPR/dCas9. Advanced single-cell transcriptome sequencing techniques are available to define disease expression profiles of cardiac cells. CRISPR-based transcription modulation allows for precise tuning of gene activities with the aim to re-install a normal, healthy gene expression profile. Illustration was made with Servier Medical Art and was prepared for a review article submission (unpublished).

Literature (General Discussion)

1. Zannad, F. *et al.* SGLT2 inhibitors in patients with heart failure with reduced ejection fraction: a meta-analysis of the EMPEROR-Reduced and DAPA-HF trials. *The Lancet* **396**, 819–829 (2020).

2. Liao, H. K. *et al.* In Vivo Target Gene Activation via CRISPR/Cas9-Mediated Trans-epigenetic Modulation. *Cell* **171**, 1495-1507.e15 (2017).

3. Lau, C.-H., Ho, J. W.-T., Lo, P. K. & Tin, C. Targeted Transgene Activation in the Brain Tissue by Systemic Delivery of Engineered AAV1 Expressing CRISPRa. *Mol Ther Nucleic Acids* **16**, 637–649 (2019).

4. Colasante, G. *et al.* In vivo CRISPRa decreases seizures and rescues cognitive deficits in a rodent model of epilepsy. *Brain* **143**, 891–905 (2020).

5. Carroll, K. J. *et al.* A mouse model for adult cardiac-specific gene deletion with CRISPR/Cas9. *Proceedings of the National Academy of Sciences* **113**, 201523918 (2015).

6. Johansen, A. K. *et al.* Postnatal Cardiac Gene Editing Using CRISPR/Cas9 With AAV9-Mediated Delivery of Short Guide RNAs Results in Mosaic Gene Disruption. *Circ Res* **121**, 1168–1181 (2017).

7. Guo, Y. *et al.* Analysis of Cardiac Myocyte Maturation Using CASAAV, a Platform for Rapid Dissection of Cardiac Myocyte Gene Function in Vivo. *Circ Res* **120**, 1874–1888 (2017).

8. Kim, Y. *et al.* The MEF2D transcription factor mediates stress-dependent cardiac remodeling in mice. *Journal of Clinical Investigation* **118**, 124–132 (2008).

9. Xu, J. *et al.* Myocyte enhancer factors 2A and 2C induce dilated cardiomyopathy in transgenic mice. *Journal of Biological Chemistry* **281**, 9152–9162 (2006).

10. Cheng, A. W. *et al.* Multiplexed activation of endogenous genes by {CRISPR-on,} an {RNA-guided} transcriptional activator system. *Cell Res* **23**, 1163–1171 (2013).

11. Schoger, E. *et al.* CRISPR-Mediated Activation of Endogenous Gene Expression in the Postnatal Heart. *Circ Res* **126**, 6–24 (2020).

12. Lin, S., Ewen-Campen, B., Ni, X., Housden, B. E. & Perrimon, N. In Vivo Transcriptional Activation Using CRISPR/Cas9 in Drosophila. *Genetics* **201**, 433–442 (2015).

13. Lek, A., Ma, K., Woodman, K. G. & Lek, M. Nuclease-Deficient Clustered Regularly Interspaced Short Palindromic Repeat-Based Approaches for in Vitro and in Vivo Gene Activation. *Hum Gene Ther* **32**, 260–274 (2021).

14. Wangensteen, K. J. *et al.* Combinatorial genetics in liver repopulation and carcinogenesis with a in vivo CRISPR activation platform. *Hepatology* **68**, 663–676 (2018).

15. Matharu, N. *et al.* CRISPR-mediated activation of a promoter or enhancer rescues obesity caused by haploinsufficiency. *Science* **363**, (2019).

16. Zhou, H. *et al.* In vivo simultaneous transcriptional activation of multiple genes in the brain using CRISPR–dCas9-activator transgenic mice. *Nat Neurosci* **21**, 440–446 (2018).

17. Yamagata, T. *et al.* CRISPR/dCas9-based Scn1a gene activation in inhibitory neurons ameliorates epileptic and behavioral phenotypes of Dravet syndrome model mice. *Neurobiol Dis* **141**, 104954 (2020).

18. Xu, X. *et al.* High-fidelity CRISPR/Cas9- based gene-specific hydroxymethylation rescues gene expression and attenuates renal fibrosis. *Nat Commun* **9**, (2018).

19. Zincarelli, C., Soltys, S., Rengo, G. & Rabinowitz, J. E. Analysis of AAV Serotypes 1–9 Mediated Gene Expression and Tropism in Mice After Systemic Injection. *Molecular Therapy* **16**, 1073–1080 (2008).

20. Choi, V. W., McCarty, D. M. & Samulski, R. J. Host Cell DNA Repair Pathways in Adeno-Associated Viral Genome Processing. *J Virol* **80**, 10346–10356 (2006).

21. Naso, M. F., Tomkowicz, B., Perry, W. L. & Strohl, W. R. Adeno-Associated Virus (AAV) as a Vector for Gene Therapy. *BioDrugs* **31**, 317–334 (2017).

22. Prasad, K. M. R., Xu, Y., Yang, Z., Acton, S. T. & French, B. A. Robust cardiomyocyte-specific gene expression following systemic injection of AAV: In vivo gene delivery follows a Poisson distribution. *Gene Ther* **18**, 43–52 (2011).

23. Aschauer, D. F., Kreuz, S. & Rumpel, S. Analysis of Transduction Efficiency, Tropism and Axonal Transport of AAV Serotypes 1, 2, 5, 6, 8 and 9 in the Mouse Brain. *PLoS One* **8**, 1–16 (2013).

24. Dong, J., Fan, P. & Frizzell, R. A. Quantitative analysis of the packaging capacity of recombinant adeno-associated virus. *Hum Gene Ther* **7**, 2101–2112 (1996).

25. Li, A. *et al.* AAV-CRISPR Gene Editing Is Negated by Pre-existing Immunity to Cas9. *Molecular Therapy* **28**, 1432–1441 (2020).

26. Pleger, S. T. *et al.* Cardiac AAV9-S100A1 gene therapy rescues post-ischemic heart failure in a preclinical large animal model. *Sci Transl Med* **3**, (2011).

27. Cullis, P. R. & Hope, M. J. Lipid Nanoparticle Systems for Enabling Gene Therapies. *Molecular Therapy* **25**, 1467–1475 (2017).

28. Fan, C. *et al.* Nanoparticle-Mediated Drug Delivery for Treatment of Ischemic Heart Disease. *Front Bioeng Biotechnol* **8**, 1–13 (2020).

29. Deng, H.-X. *et al.* Efficacy and long-term safety of CRISPR/Cas9 genome editing in the SOD1-linked mouse models of ALS. *Commun Biol* **4**, 396 (2021).

30. Amrani, N. *et al.* NmeCas9 is an intrinsically high-fidelity genome-editing platform Jin-Soo Kim. *Genome Biol* **19**, 1–25 (2018).

31. Ran, F. A. *et al.* In vivo genome editing using Staphylococcus aureus Cas9. *Nature* **520**, 186–191 (2015).

32. Hu, Z. *et al.* A compact cas9 ortholog from staphylococcus auricularis (sauricas9) expands the DNA targeting scope. *PLoS Biol* **18**, 1–18 (2020).

33. Hu, Z. *et al.* Discovery and engineering of small SlugCas9 with broad targeting range and high specificity and activity. *Nucleic Acids Res* **49**, 4008–4019 (2021).

34. Ma, D., Peng, S., Huang, W., Cai, Z. & Xie, Z. Rational Design of Mini-Cas9 for Transcriptional Activation. *ACS Synth Biol* **7**, 978–985 (2018).

35. Martino, A. T. & Markusic, D. M. Immune Response Mechanisms against AAV Vectors in Animal Models. *Mol Ther Methods Clin Dev* **17**, 198–208 (2020).

36. Verdera, H. C., Kuranda, K. & Mingozzi, F. AAV Vector Immunogenicity in Humans: A Long Journey to Successful Gene Transfer. *Molecular Therapy* **28**, 723–746 (2020).

37. Charlesworth, C. T. *et al.* Identification of preexisting adaptive immunity to Cas9 proteins in humans. *Nat Med* **25**, 249–254 (2019).

38. Chew, W. L. *et al.* A multifunctional AAV-CRISPR-Cas9 and its host response. *Nat Methods* **13**, 868–874 (2016).

39. Amoasii, L. *et al.* Gene editing restores dystrophin expression in a canine model of duchenne muscular dystrophy. *Science (1979)* **51**, 1–6 (2018).

40. Wu, X. *et al.* Genome-wide binding of the CRISPR endonuclease Cas9 in mammalian cells. *Nat Biotechnol* **32**, 670–676 (2014).

41. O'Geen, H., Henry, I. M., Bhakta, M. S., Meckler, J. F. & Segal, D. J. A genome-wide analysis of Cas9 binding specificity using ChIP-seq and targeted sequence capture. *Nucleic Acids Res* **43**, 3389–3404 (2015).

42. Zhang, X.-H., Tee, L. Y., Wang, X.-G., Huang, Q.-S. & Yang, S.-H. Off-target Effects in CRISPR/Cas9-mediated Genome Engineering. *Mol Ther Nucleic Acids* **4**, e264 (2015).

43. Gilbert, L. A. *et al.* Genome-Scale CRISPR-Mediated Control of Gene Repression and Activation. *Cell* **159**, 647–661 (2014).

44. Dominguez, A. A., Lim, W. A. & Qi, L. S. Beyond editing: repurposing CRISPR–Cas9 for precision genome regulation and interrogation. *Nat Rev Mol Cell Biol* **17**, 5–15 (2015).

45. Carlson-Stevermer, J. *et al.* CRISPRoff enables spatio-temporal control of CRISPR editing. *Nat Commun* **11**, 1–7 (2020).

46. Shao, J. *et al.* Synthetic far-red light-mediated CRISPR-dCas9 device for inducing functional neuronal differentiation. *Proc Natl Acad Sci U S A* **115**, E6722–E6730 (2018).

47. Pawluk, A., Davidson, A. R. & Maxwell, K. L. Anti-CRISPR: discovery, mechanism and function. *Nat Rev Microbiol* **16**, 12–17 (2018).

48. Kim, Y. *et al.* Anti-CRISPR AcrIIC3 discriminates between Cas9 orthologs via targeting the variable surface of the HNH nuclease domain. *FEBS Journal* **286**, 4661–4674 (2019).

49. Dong, C., Fontana, J., Patel, A., Carothers, J. M. & Zalatan, J. G. Synthetic CRISPR-Cas gene activators for transcriptional reprogramming in bacteria. *Nat Commun* **9**, (2018).

50. Horlbeck, M. A. *et al.* Nucleosomes impede Cas9 access to DNA in vivo and in vitro. *Elife* **5**, 1–21 (2016).

51. Horlbeck, M. A. *et al.* Compact and highly active next-generation libraries for CRISPR-mediated gene repression and activation. *Elife* **5**, 1–20 (2016).

52. Jia, G. *et al.* Single cell RNA-seq and ATAC-seq analysis of cardiac progenitor cell transition states and lineage settlement. *Nat Commun* **9**, (2018).

53. Dai, Z. *et al.* Inducible CRISPRa screen identifies putative enhancers. *J Genet Genomics* **48**, 917-927 (2021).

54. Goyal, A. *et al.* Challenges of CRISPR/Cas9 applications for long non-coding RNA genes. *Nucleic Acids Res* **45**, e12 (2016).

55. Chavez, A. *et al.* Highly efficient Cas9-mediated transcriptional programming. *Nat Methods* **12**, 326–328 (2015).

56. Chavez, A. *et al.* Comparison of Cas9 activators in multiple species. *Nat Methods* **13**, 563–567 (2016).

57. Long, C. *et al.* Postnatal genome editing partially restores dystrophin expression in a mouse model of muscular dystrophy. *Science* **351**, 400–403 (2016).

58. Cheng, A. W. *et al.* Multiplexed activation of endogenous genes by CRISPR-on, an RNA-guided transcriptional activator system. *Cell Res* **23**, 1163–71 (2013).

59. Zhang, Y. *et al.* A gRNA-tRNA array for CRISPR-Cas9 based rapid multiplexed genome editing in Saccharomyces cerevisiae. *Nat Commun* **10**, 1–10 (2019).

60. Hazelbaker, D. Z. *et al.* A multiplexed gRNA piggyBac transposon system facilitates efficient induction of CRISPRi and CRISPRa in human pluripotent stem cells. *Sci Rep* **10**, 1–10 (2020).

61. Ovchinnikov, D. A., Korn, O., Virshup, I., Wells, C. A. & Wolvetang, E. J. The Impact of APP on Alzheimer-like Pathogenesis and Gene Expression in Down Syndrome iPSC-Derived Neurons. *Stem Cell Reports* **11**, (2018).

62. Weltner, J. *et al.* Human pluripotent reprogramming with CRISPR activators. *Nat Commun* **9**, 1–12 (2018).

63. Liu, Y. *et al.* CRISPR Activation Screens Systematically Identify Factors that Drive Neuronal Fate and Reprogramming. *Cell Stem Cell* **23**, 758-771.e8 (2018).

64. Wang, J. *et al.* Lineage reprogramming of fibroblasts into induced cardiac progenitor cells by CRISPR/Cas9-based transcriptional activators. *Acta Pharm Sin B* **10**, 313–326 (2020).

65. Baumann, V. & Stricker, S. H. Seeking fate—CRISPRa screens reveal new neural lineage and reprogramming factors. *Stem Cell Investig* **6**, 30–30 (2019).

66. Schoger, E., Argyriou, L., Zimmermann, W. H., Cyganek, L. & Zelarayán, L. C. Generation of homozygous CRISPRa human induced pluripotent stem cell (hiPSC) lines for sustained endogenous gene activation. *Stem Cell Res* **48**, 101944 (2020).

67. Schoger, E., Zimmermann, W.-H., Cyganek, L. & Cecilia Zelarayán, L. Establishment of a second generation homozygous CRISPRa human induced pluripotent stem cell (hiPSC) line for enhanced levels of endogenous gene activation. *Stem Cell Res* **56**, 102518 (2021).

68. Schoger, E., Zimmermann, W.-H., Cyganek, L. & Zelarayán, L. C. Establishment of two homozygous CRISPR interference (CRISPRi) knock-in human induced pluripotent stem cell (hiPSC) lines for titratable endogenous gene repression. *Stem Cell Res* **55**, 102473 (2021).

69. Oceguera-Yanez, F. *et al.* Engineering the AAVS1 locus for consistent and scalable transgene expression in human iPSCs and their differentiated derivatives. *Methods* **101**, 43–55 (2016).

70. Papapetrou, E. P. & Schambach, A. Gene insertion into genomic safe harbors for human gene therapy. *Molecular Therapy* **24**, 678–684 (2016).

71. Sun, Y. H. *et al.* Human induced pluripotent stem cell line with genetically encoded fluorescent voltage indicator generated via CRISPR for action potential assessment post-cardiogenesis. *Stem Cells* **38**, 90–101 (2020).

72. Castaño, J. *et al.* Generation and characterization of a human iPSC cell line expressing inducible Cas9 in the "safe harbor" AAVS1 locus. *Stem Cell Res* **21**, 137–140 (2017).

73. Robitaille, A. M. & Hall, M. N. Ramping up mitosis: An AMPKα2-regulated signaling network promotes mitotic progression. *Mol Cell* **45**, 8–9 (2012).

74. Vora, S., Tuttle, M., Cheng, J. & Church, G. Next stop for the CRISPR revolution: RNA-guided epigenetic regulators. *FEBS Journal* **283**, 3181–3193 (2016).

75. Fisch, S. *et al.* Kruppel-like factor 15 is a regulator of cardiomyocyte hypertrophy. *Proc Natl Acad Sci U S A* **104**, 7074–9 (2007).

76. Noack, C. *et al.* KLF15-Wnt–Dependent Cardiac Reprogramming Up-Regulates SHISA3 in the Mammalian Heart. *J Am Coll Cardiol* **74**, 1804–1819 (2019).

77. Haldar, S. M. *et al.* Klf15 Deficiency Is a Molecular Link Between Heart Failure and Aortic Aneurysm Formation. *Sci Transl Med* **2**, 26ra26-26ra26 (2010).

78. Wang, B. *et al.* The Kruppel-like factor KLF15 inhibits connective tissue growth factor (CTGF) expression in cardiac fibroblasts. *J Mol Cell Cardiol* **45**, 193–197 (2008).

79. Li, N. *et al.* KLF15 Loss-of-Function Mutation Underlying Atrial Fibrillation as well as Ventricular Arrhythmias and Cardiomyopathy. *Genes (Basel)* **12**, 408 (2021).

80. Shimizu, N. *et al.* Crosstalk between glucocorticoid receptor and nutritional sensor mTOR in skeletal muscle. *Cell Metab* **13**, 170–182 (2011).

81. Leenders, J. J. *et al.* Repression of Cardiac Hypertrophy by KLF15: Underlying Mechanisms and Therapeutic Implications. *PLoS One* **7**, e36754 (2012).

82. Zou, S. F. *et al.* KLF15 is a protective regulatory factor of heart failure induced by pressure overload. *Mol Med Rep* **21**, 1336–1345 (2020).

83. Zhao, T., Qiu, Z. & Gao, Y. MiR-137-3p exacerbates the ischemia-reperfusion injured cardiomyocyte apoptosis by targeting KLF15. *Naunyn Schmiedebergs Arch Pharmacol* **393**, 1013–1024 (2020).

84. Horie, T. *et al.* MicroRNA-133 regulates the expression of GLUT4 by targeting KLF15 and is involved in metabolic control in cardiac myocytes. *Biochem Biophys Res Commun* **389**, 315–320 (2009).

85. Carè, A. *et al.* MicroRNA-133 controls cardiac hypertrophy. *Nat Med* **13**, 613–618 (2007).

86. Prosdocimo, D. A. *et al.* KLF15 and PPAR α Cooperate to Regulate Cardiomyocyte Lipid Gene Expression and Oxidation. *PPAR Res* **2015**, 1–10 (2015).

87. Zhang, L. *et al.* KLF15 Establishes the Landscape of Diurnal Expression in the Heart Report KLF15 Establishes the Landscape of Diurnal Expression in the Heart. *CellReports* **13**, 2368–2375 (2015).

88. Noack, C. *et al.* Krueppel-like factor 15 regulates Wnt/β-catenin transcription and controls cardiac progenitor cell fate in the postnatal heart. *EMBO Mol Med* **4**, 992–1007 (2012).

89. Li, J. *et al.* Sp1 and KLF15 regulate basal transcription of the human LRP5 gene. *BMC Genet* **11**, 6–13 (2010).

90. Renger, A. *et al.* The four and a half LIM-domain 2 controls early cardiac cell commitment and expansion via regulating β-catenin-dependent transcription. *Stem Cells* **31**, 928–940 (2013).

91. Chebbok, E. Basic leucine zipper and W2 domain- containing protein 2 (BZW2) : A novel cardiac WNT component. *Georg-August-Universität Göttingen - Molekulare Medizin* (2015).

92. Nishinaka, N. *et al.* Identification of the novel developmentally regulated gene, Bdm2, which is highly expressed in fetal rat brain. *Brain Res Dev Brain Res* **120**, 57–64 (2000).

93. Li, S. *et al.* BZW1, a novel proliferation regulator that promotes growth of salivary muocepodermoid carcinoma. *Cancer Lett* **284**, 86–94 (2009).

94. Huang, L., Chen, S., Fan, H., Ai, F. & Sheng, W. BZW2 promotes the malignant progression of colorectal cancer via activating the ERK/MAPK pathway. *J Cell Physiol* **235**, 4834–4842 (2020).

95. Singh, C. R. *et al.* Mechanisms of translational regulation by a human eIF5-mimic protein. *Nucleic Acids Res* **39**, 8314–8328 (2011).

96. Röhrs, S. *et al.* Chronological expression of Wnt target genes Ccnd1, Myc, Cdkn1a, Tfrc, Plf1 and Ramp3. *Cell Biol Int* **33**, 501–508 (2009).

97. Iyer, L. M. *et al.* A context-specific cardiac β-catenin and GATA4 interaction influences TCF7L2 occupancy and remodels chromatin driving disease progression in the adult heart. *Nucleic Acids Res* **46**, 2850–2867 (2018).

98. van Tienen, L. M., Mieszczanek, J., Fiedler, M., Rutherford, T. J. & Bienz, M. Constitutive scaffolding of multiple Wnt enhanceosome components by legless/BCL9. *Elife* **6**, 1–23 (2017).

99. Flack, J. E., Mieszczanek, J., Novcic, N. & Bienz, M. Wnt-Dependent Inactivation of the Groucho/TLE Co-repressor by the HECT E3 Ubiquitin Ligase Hyd/UBR5. *Mol Cell* **67**, 181-193.e5 (2017).

100. Wheeler, M. A., Warley, A. & Ellis, J. A. Identification of an emerin – b -catenin complex in the heart important for intercalated disc architecture and b -catenin localisation. *Cellular and Molecular Life Sciences* **67**, 781–796 (2010).

101. Stubenvoll, A., Rice, M., Wietelmann, A., Wheeler, M. & Braun, T. Attenuation of wnt/??-catenin activity reverses enhanced generation of cardiomyocytes and cardiac defects caused by the loss of emerin. *Hum Mol Genet* **24**, 802–813 (2015).

102. Haq, S. *et al.* Stabilization of beta-catenin by a Wnt-independent mechanism regulates cardiomyocyte growth. *Proc Natl Acad Sci U S A* **100**, 4610–5 (2003).

103. Moon, J. *et al.* Blockade to pathological remodeling of infarcted heart tissue using a porcupine antagonist. *Proceedings of the National Academy of Sciences* **114**, 1649–1654 (2017).

104. Chen, X., Yuan, W., Li, Y., Luo, J. & Hou, N. Role of Hippo-YAP1/TAZ pathway and its crosstalk in cardiac biology. *Int J Biol Sci* **16**, 2454–2463 (2020).

105. Valdimarsdottir, G. *et al.* Stimulation of Id1 expression by bone morphogenetic protein is sufficient and necessary for bone morphogenetic protein-induced activation of endothelial cells. *Circulation* **106**, 2263–2270 (2002).

106. Bai, Y. *et al.* Bmp signaling represses Vegfa to promote outflow tract cushion development. *Development* **140**, 3395–3402 (2013).